AE 6200: Aeroelasticity

Class Notes[1]

Dewey H. Hodges, Professor
G. Alvin Pierce, Professor Emeritus
Olivier A. Bauchau, Professor
and
Marilyn J. Smith, Associate Professor
The Daniel Guggenheim School of Aerospace Engineering
Georgia Institute of Technology, Atlanta, Georgia

Dear Student:

Reproduction of copyrighted material, without prior permission of the copyright owner, particularly in an educational setting, is an issue of concern for the academic community. Unfortunately, the impropriety of much unauthorized copying is all too often overlooked by users in an educational setting.

Although copying all or part of a work without obtaining permission may appear to be an easy and convenient solution to an immediate problem, such unauthorized copying can frequently violate the rights of the author or publisher of the copyrighted work, and be directly contrary to the academic mission to *teach respect* for ideas and for the intellectual property that expresses those ideas.

With that in mind, Georgia Tech has sought permission and paid royalties where applicable for all materials enclosed. The price of your class notes reflects those necessary costs.

Contents

1 INTRODUCTION **1**

2 REVIEW OF FOUNDATIONS OF MECHANICS **7**

2.1 Uniform Beam Torsional Dynamics 7

2.1.1 Equation of Motion 7

2.1.2 Boundary Conditions 10

2.1.3 Example Solutions for Mode Shapes and Frequencies 13

2.2 Uniform Beam Bending Dynamics 20

2.2.1 Equation of Motion 20

2.2.2 General Solutions 25

2.2.3 Boundary Conditions 26

2.2.4 Example solution for clamped-free beam 30

2.3 Orthogonality of Mode Shapes 32

2.3.1 Using Orthogonality 35

2.3.2 Example: response due to given initial shape 37

2.4 Principle of Virtual Work 38

2.5 Hamilton's Principle 39

2.6 Lagrange's Equations 40

2.6.1 Generalized Force 40

2.6.2 Example calculation of generalized force 42

2.7 Ritz's Method 43

2.7.1 Example: The Ritz Method Using Clamped-Free Modes 46

2.7.2 Example: The Ritz Method Using a Simple Power Series 48

2.8 Galerkin's Method 51

2.8.1 Example: Galerkin's Method for a Beam in Bending 53

2.8.2 Example: Galerkin's Method for a Beam in Bending Using an Alternative Form of the Equation of Motion 54

3 OPERATOR NOTATION **57**

3.1 Structural operators 57

3.2 Aerodynamic operators 64

3.3 Inertial operators 67
3.4 Summary 67

4 STATIC AEROELASTICITY 69
4.1 Rigid Wind-Tunnel Models on Flexible Supports 69
4.1.1 Wall-Mounted Model 70
4.1.2 Sting-Mounted Model 75
4.1.3 Strut-Mounted Model 77
4.1.4 Wall-Mounted Model for Application to Aileron Reversal 78
4.2 Uniform Lifting Surface 81
4.2.1 Equilibrium Equation 82
4.2.2 Torsional Divergence 85
4.2.3 Airload Distribution 88
4.2.4 Sweep Effects 92
4.2.5 Effect of Drag on Divergence of Slender Wings 112
4.3 Nonuniform Lifting Surfaces 118
4.3.1 Unswept Wings Attached to a Frame 118
4.3.2 Effect of Weight and Load Factor 121
4.4 Complete Aircraft 122
4.4.1 Aircraft with Unswept Wings 122
4.4.2 Aircraft with Swept Wings 125
4.4.3 Aileron Reversal 127
4.5 Treatment of Low-Aspect-Ratio Wings 134
4.5.1 Aerodynamic Operator 134
4.5.2 Structural Operator 136
4.6 Epilogue 140

5 DYNAMIC AEROELASTICITY 149
5.1 Dynamic Stability 150
5.2 Panel Flutter 158
5.3 Aeroelastic Stability Characteristics 161
5.3.1 Overview of Typical Aeroelastic System Equations 163
5.3.2 Analytical and Numerical Solution Methods 168
5.4 Aeroelastic Analysis of a Typical Section 170
5.4.1 Stability Based on Steady-flow Aerodynamics 173
5.4.2 Stability Based on Quasi-Steady Aerodynamics 177
5.4.3 Motivation for Better Aerodynamic Theory 178
5.5 Classical Flutter Analysis 180
5.5.1 One-Degree-of-Freedom Flutter 181
5.5.2 Two-Degree-of-Freedom Flutter 184
5.6 Engineering Solutions for Flutter 186

5.6.1 The k Method . . . 187
5.6.2 The p-k Method . . . 189
5.7 Unsteady Aerodynamics . . . 192
5.7.1 Theodorsen's Unsteady Thin-Airfoil Theory . . . 196
5.7.2 Finite-State Unsteady Thin-Airfoil Theory of Peters et al. . . . 197
5.7.3 Alternative Unsteady Thin-Airfoil Theory . . . 206
5.8 Flutter Prediction via Assumed Modes . . . 207
5.9 Flutter of an Aircraft with Unswept Wings . . . 213
5.10 Flutter Boundary Characteristics . . . 224
5.11 Dynamic Response and Transient Stresses . . . 230
5.11.1 Landing Gear . . . 231
5.11.2 Unrestrained Elastic Airplane . . . 248
5.11.3 Gust Response . . . 251
5.12 Epilogue . . . 254

BIBLIOGRAPHY **263**

APPENDIX A: LAGRANGE'S EQUATION **265**
A.1 Introduction . . . 265
A.2 Degrees of Freedom . . . 265
A.3 Generalized Coordinates . . . 266
A.4 Lagrange's Equations . . . 266
A.5 Lagrange's Equations for Conservative Systems . . . 270
A.6 Lagrange's Equations for Nonconservative Systems . . . 273

List of Figures

1.1 Schematic of the field of aeroelasticity 3

2.1 Beam undergoing torsional deformation 8
2.2 Cross-sectional slice of beam undergoing torsional deformation 8
2.3 Clamped end of a beam 11
2.4 Free end of a beam 11
2.5 Elastically restrained end of a beam 12
2.6 Inertially restrained end of a beam 12
2.7 Schematic of clamped-free beam undergoing torsion 13
2.8 First three mode shapes for clamped-free beam vibrating in torsion 16
2.9 Schematic of free-free beam undergoing torsion 16
2.10 First three elastic mode shapes for free-free beam vibrating in torsion 19
2.11 Schematic of torsion problem with spring 20
2.12 Plot of the lowest values of α_i versus ζ for a clamped-spring-restrained beam in torsion 21
2.13 First three mode shapes for clamped-spring-restrained beam in torsion, $\zeta = 1$ 22
2.14 Schematic of beam for bending dynamics 23
2.15 Schematic of differential beam segment 23
2.16 Schematic of pinned end condition 27
2.17 Schematic of sliding end condition 27
2.18 Schematic of translational spring end conditions 28
2.19 Schematic of rotational spring end conditions 29
2.20 Schematic of translational mass end conditions 30
2.21 Schematic of rotational inertia end conditions 30
2.22 Schematic of clamped-free beam 30
2.23 First three free-vibration mode shapes of a clamped-free beam in bending . . 33
2.24 Initial shape of plucked string 37
2.25 Concentrated force acting on beam 42
2.26 Distributed force $F(x,t)$ acting on beam 42

3.1 Schematic of a spring element undergoing a force F through a displacement x 57

3.2 Schematic of internal twisting moment at x for unit applied twisting moment at η . . . 59
3.3 Schematic of a tapered beam with internal torques discretized . . . 60
3.4 Schematic of a tapered beam with distributed external torque . . . 62

4.1 Planform view of a rigid wind-tunnel model on a torsionally elastic support . 70
4.2 Airfoil for wind-tunnel model . . . 71
4.3 Relative change in lift due to aeroelastic effect . . . 73
4.4 Plot of $1/\theta$ versus $1/q$ . . . 74
4.5 Schematic of a sting-mounted wind-tunnel model . . . 75
4.6 Detailed view of the cantilevered beam . . . 75
4.7 Detailed view of the sting-mounted wing . . . 76
4.8 Schematic of strut-supported wind-tunnel model . . . 77
4.9 Cross section of strut-supported wind-tunnel model . . . 78
4.10 Schematic of the airfoil section of a flapped two-dimensional wing in a wind tunnel . . . 79
4.11 Uniform unswept cantilevered lifting surface . . . 83
4.12 Cross section of spanwise uniform lifting surface . . . 84
4.13 Plot of tip twist angle for wing versus $\overline{q}$ for $\alpha_{\mathrm{r}} + \overline{\alpha}_{\mathrm{r}} = 1^\circ$ . . . 87
4.14 Rigid and elastic wing lift distributions holding α_{r} constant . . . 90
4.15 Rigid and elastic wing lift distributions holding total lift constant . . . 91
4.16 Schematic of swept wing (positive Λ) . . . 93
4.17 Divergence dynamic pressure versus Λ . . . 96
4.18 Lift distribution for positive, zero, and negative Λ . . . 97
4.19 τ_D versus β_D for coupled bending-torsion divergence; solid lines (exact solution) and dashed line (Eq. 4.93) . . . 103
4.20 τ_D versus r for coupled bending-torsion divergence; solid lines (exact solution) and dashed lines (Eq. 4.96 and $\tau_D = -27r^2/4$ in fourth quadrant) . . . 104
4.21 τ_D versus r for coupled bending-torsion divergence; solid lines (exact solution) and dashed lines (Eq. 4.96) . . . 105
4.22 Normalized divergence dynamic pressure for an elastically uncoupled, swept wing with $GJ/EI = 1.0$ and $e/\ell = 0.02$ . . . 106
4.23 Normalized divergence dynamic pressure for an elastically uncoupled, swept wing with $GJ/EI = 0.2$ and $e/\ell = 0.02$ . . . 107
4.24 Normalized divergence dynamic pressure for an elastically uncoupled, swept wing with $e = 0.05\,\ell$ and $GJ/EI = 0.2$: exact solution (solid line) and closed-form approximate solution (dashed line) . . . 108
4.25 Normalized divergence dynamic pressure for an elastically coupled, swept wing with $GJ/EI = 0.2$ and $e/\ell = 0.02$; $\kappa = -0.4$ (dots and dashes), $\kappa = 0$ (solid lines), $\kappa = 0.4$ (dashed lines) . . . 113

4.26 Sweep angle for which divergence dynamic pressure is infinite for a wing with $GJ/EI = 0.5$; solid line is for $e/\ell = 0.01$; dashed line is for $e/\ell = 0.04$ 114
4.27 Sweep angle for which divergence dynamic pressure is infinite for a wing with $e/\ell = 0.02$; solid line is for $GJ/EI = 1.0$; dashed line is for $GJ/EI = 0.25$ . . 114
4.28 Schematic of nonuniform wing attached to fuselage 119
4.29 Cross section of nonuniform wing at station i 119
4.30 Schematic of complete aircraft 123
4.31 Schematic of aircraft tail airfoil section 123
4.32 Schematic of a rolling aircraft 128
4.33 Wing section with aileron 129
4.34 Wing section with aileron as a part of length 131
4.35 Typical variation of nondimensional roll rate versus aircraft speed U 132
4.36 Typical variation of the components of the rolling moment versus aircraft speed U 133
4.37 Schematic of delta-winged aircraft showing differential area of lifting surface 137
4.38 Schematic of local deformation and the angle of attack 138

5.1 Schematic of beam undergoing compressive axial follower force 151
5.2 Exact solution for imaginary part of nondimensional eigenvalue s versus nondimensional force f for Beck's column 155
5.3 Exact solution for real part of nondimensional eigenvalue s versus nondimensional force f for Beck's column 156
5.4 Approximate solution for imaginary part of nondimensional eigenvalue s versus nondimensional force f for Beck's column 157
5.5 Approximate solution for real part of nondimensional eigenvalue s versus nondimensional force f for Beck's column 157
5.6 Imaginary part of nondimensional eigenvalue s versus M_∞ for $\overline{a} = 1$, $\overline{b} = 0.1$, and $\mu = 5$. 161
5.7 Real part of nondimensional eigenvalue s versus M_∞ for $\overline{a} = 1$, $\overline{b} = 0.1$, and $\mu = 5$ (note that there is a root very near the zero axis shown in more detail in Fig. 5.8) 162
5.8 Closeup of the real part of the critical nondimensional eigenvalue s versus M_∞ for $\overline{a} = 1$, $\overline{b} = 0.1$, and $\mu = 5$. 162
5.9 Closeup of the critical nondimensional eigenvalue s versus M_∞ for $\overline{a} = 1$, $\overline{b} = 0.1$, and $\mu = 5$; the left end of the curve is for $M_\infty = 1.7$ and the right end for $M_\infty = 5.0$. 163
5.10 Behavior of typical mode amplitude when $\Omega_k \neq 0$ 167
5.11 Schematic showing geometry of the wing section with pitch and plunge spring restraints 172
5.12 Plot of the modal frequency versus V for $a = -1/5$, $e = -1/10$, $\mu = 20$, $r^2 = 6/25$, and $\sigma = 2/5$ (steady-flow theory) 175

5.13 Plot of the modal damping versus V for $a = -1/5$, $e = -1/10$, $\mu = 20$, $r^2 = 6/25$, and $\sigma = 2/5$ (steady-flow theory) 176
5.14 Plot of $\Im(s)$, the modal frequency, versus V for $a = -1/5$, $e = -1/10$, $\mu = 20$, $r^2 = 6/25$, and $\sigma = 2/5$ (quasi-steady theory) 178
5.15 Plot of $\Re(s)$, the modal damping, versus V for $a = -1/5$, $e = -1/10$, $\mu = 20$, $r^2 = 6/25$, and $\sigma = 2/5$ (quasi-steady theory) 179
5.16 Schematic of the airfoil of a two-dimensional wing that is spring-restrained in pitch 182
5.17 Comparison between p and k methods of flutter analysis for a twin-jet transport airplane [from Hassig (1971) Fig. 1, used by permission] 193
5.18 Comparison between p and p-k methods of flutter analysis for a twin-jet transport airplane [from Hassig (1971) Fig. 2, used by permission] 194
5.19 Comparison between p-k and k methods of flutter analysis for a horizontal stabilizer with elevator [from Hassig (1971) Fig. 3, used by permission] . . . 195
5.20 Plot of the real and imaginary parts of $C(k)$ for k varying from zero, where $C(k) = 1$, to unity 198
5.21 Plot of the real and imaginary parts of $C(k)$ versus $1/k$ 199
5.22 Schematic showing geometry of the zero-lift line, relative wind, and lift directions 200
5.23 Plot of the modal frequency versus $U/(b\omega_\theta)$ for $a = -1/5$, $e = -1/10$, $\mu = 20$, $r^2 = 6/25$, and $\sigma = 2/5$; solid lines: p method, aerodynamics of Peters et al.; dashed lines: steady flow aerodynamics 204
5.24 Plot of the modal damping versus $U/(b\omega_\theta)$ for $a = -1/5$, $e = -1/10$, $\mu = 20$, $r^2 = 6/25$, and $\sigma = 2/5$; solid lines: p method, aerodynamics of Peters et al.; dashed lines: steady flow aerodynamics 205
5.25 Wagner function 207
5.26 Cross section of spanwise uniform lifting surface 208
5.27 Schematic of aircraft for flutter analysis 213
5.28 Nominal increase in flutter speed with sweep back 219
5.29 Top view of a nacelle on a wing 219
5.30 Side view of a nacelle on a wing 220
5.31 Flutter speed versus position along wing 221
5.32 Flutter speed versus fore/aft position 222
5.33 Typical behavior of g for bending, torsion, and aileron modes 224
5.34 Plot of dimensionless flutter speed versus mass ratio for the case $\sigma = 1/\sqrt{10}$, $r = 1/2$, $x_\theta = 0$, and $a = -3/10$ 225
5.35 Plot of dimensionless flutter speed versus frequency ratio for the case $\mu = 3$, $r = 1/2$ and $a = -1/5$ where the solid line is for $x_\theta = 0.2$ and the dashed line is for $x_\theta = 0.1$ 227
5.36 Plot of dimensionless flutter speed versus e for the case $\mu = 10$, $\sigma = 1/\sqrt{2}$, and $r = 1/2$; the solid line is for $a = 0$ and the dashed line is for $a = 0.2$ . . . 228
5.37 Flight envelope for typical Mach 2 fighter 230

5.38 Schematic of flexible landing gear undergoing time-dependent force 231
5.39 Normalized displacement $v(\ell, \tau)$ for the response of a landing gear to a quasi-static sinusoidal pulse with $\Omega = 0.5\omega_1$; one mode (dashes), two modes (solid line) 234
5.40 Normalized displacement $v(\ell, \tau)$ for the response of a landing gear to a dynamic sinusoidal pulse with $\Omega = 10\omega_1$; two modes (dashes), three modes (solid line) 235
5.41 Normalized displacement $v(\ell, \tau)$ for the response of a landing gear to a quasi-impulsive sinusoidal pulse with $\Omega = 25\omega_1$; two modes (dashes), three modes (solid line) 235
5.42 Modal displacement method approximation (i.e. by differentiation of mode shape) of root bending moment on strut subjected to a quasi-static sinusoidal pulse with $\Omega = 0.5\omega_1$; one mode (dashed line), two modes (solid line) 236
5.43 Modal displacement method approximation (i.e. by differentiation of mode shape) of root bending moment on strut subjected to a quasi-static sinusoidal pulse with $\Omega = 0.5\omega_1$; four-mode result (dashed line), five-mode result (solid line) 237
5.44 Modal displacement method approximation (i.e. by differentiation of mode shape) of root bending moment on strut subjected to a dynamic sinusoidal pulse with $\Omega = 10\omega_1$; one mode (dashed line), two modes (solid line) 238
5.45 Modal displacement method approximation (i.e. by differentiation of mode shape) of root bending moment on strut subjected to a dynamic sinusoidal pulse with $\Omega = 10\omega_1$; four modes (dashed line), five modes (solid line) 239
5.46 Modal displacement method approximation (i.e. by differentiation of mode shape) of root bending moment on strut subjected to a quasi-impulsive sinusoidal pulse with $\Omega = 25\omega_1$; one mode (dashed line), two modes (solid line) . 240
5.47 Modal displacement method approximation (i.e. by differentiation of mode shape) of root bending moment on strut subjected to a quasi-impulsive sinusoidal pulse with $\Omega = 25\omega_1$; four modes (dashed line), five modes (solid line) 241
5.48 Force summation method approximation of root bending moment on strut subjected to a quasi-static sinusoidal pulse with $\Omega = 0.5\omega_1$; one mode (dashed line), two modes (solid line) 243
5.49 Force summation method method approximation of root bending moment on strut subjected to a dynamic sinusoidal pulse with $\Omega = 10\omega_1$; three modes (dashed line), four modes (solid line) 244
5.50 Force summation method method approximation of root bending moment on strut subjected to a quasi-impulsive sinusoidal pulse with $\Omega = 25\omega_1$; four modes (dashed line), five modes (solid line) 245
5.51 Plot of $\omega_{1,2}/\omega_\theta$ versus $U/(b\omega_\theta)$ using the k method and Theodorsen aerodynamics with $a = -1/5$, $e = -1/10$, $\mu = 20$, $r^2 = 6/25$, and $\sigma = 2/5$ 258

5.52 Plot of g versus $U/(b\omega_\theta)$ using the k method and Theodorsen aerodynamics with $a = -1/5$, $e = -1/10$, $\mu = 20$, $r^2 = 6/25$, and $\sigma = 2/5$ 258
5.53 Plot of estimated value of $\Omega_{1,2}/\omega_\theta$ versus $U/(b\omega_\theta)$ using the p-k method with Theodorsen aerodynamics (symbols) and the p method with the aerodynamics of Peters et al. (lines) for $a = -1/5$, $e = -1/10$, $\mu = 20$, $r^2 = 6/25$, and $\sigma = 2/5$260
5.54 Plot of estimated value of $\Gamma_{1,2}/\omega_\theta$ versus $U/(b\omega_\theta)$ using the p-k method with Theodorsen aerodynamics (symbols) and the p method with the aerodynamics of Peters et al. (lines) for $a = -1/5$, $e = -1/10$, $\mu = 20$, $r^2 = 6/25$, and $\sigma = 2/5$261
A.1 Schematic for the mechanical system of Example 4 272
A.2 Schematic for mechanical system of Example 6 273

List of Tables

2.1 Values of $\alpha_i \ell$, $(2i-1)\pi/2$, and β_i for i=1,...,5 for the clamped-free beam . . 32

2.2 Approximate values of $\omega_1 \sqrt{\frac{m\ell^4}{EI}}$ for clamped-free beam with tip mass of $\mu m \ell$ using n clamped-free modes of Section 2.2.4, Eq. (2.93) 48

2.3 Approximate values of $\omega_2 \sqrt{\frac{m\ell^4}{EI}}$ for clamped-free beam with tip mass of $\mu m \ell$ using n clamped-free modes of Section 2.2.4, Eq. (2.93) 49

2.4 Approximate values of $\omega_1 \sqrt{\frac{m\ell^4}{EI}}$ for clamped-free beam with tip mass of $\mu m \ell$ using n polynomial functions 50

2.5 Approximate values of $\omega_2 \sqrt{\frac{m\ell^4}{EI}}$ for clamped-free beam with tip mass of $\mu m \ell$ using n polynomial functions 50

2.6 Approximate values of $\omega_i \sqrt{\frac{m\ell^4}{EI}}$ for i=1, 2, and 3, for a clamped-free beam using n polynomial functions 54

2.7 Approximate values of $\omega_i \sqrt{\frac{m\ell^4}{EI}}$ for i=1, 2, and 3, for a clamped-free beam using n terms of a power series with a reduced-order equation of motion . . . 55

5.1 Types of motion and stability characteristics for various values of Γ_k and Ω_k 168

5.2 Variation of mass ratio for typical vehicle types 226

Chapter 1

INTRODUCTION

Aeroelasticity is the study of static and dynamic behavior of structural elements in a flowing fluid. Aeroelasticity in aerospace engineering is chiefly concerned with the interaction between the deformation of an elastic structure in an airstream and the resulting aerodynamic force. Aeroelastic phenomena can be observed on a daily basis in nature. Such everyday occurrences as the swaying of trees in the wind, the buzzing sound emanating from one's nose when he blows it too hard, and the humming sound Venetian blinds make in the wind are all aeroelastic. In physiology, the flow of blood in flexible blood vessels is aeroelastic. Aeroelastic phenomena must be taken into account in many problems in engineering outside aeronautical engineering. These include, for example, mechanical engineering problems involving the flow of fluid in flexible piping systems and the "pogo effect" in rocket fuel lines in which structural vibrations contribute to inlet valve disturbances, which are in turn amplified by the fuel pump and produce fluctuations in the thrust. These fluctuations contribute to the structural vibration, and so on it goes. Aeroelasticity is also of interest in civil engineering (wind-induced motion of suspension bridges and high-rise buildings), nuclear engineering (flutter of nuclear reactor hardware), and biomedical engineering (blood flow in flexible blood vessels).

The most general aeroelastic phenomena include dynamics, but static aeroelastic phenomena are also quite important. Aeroelastic phenomena can result in dangerous static and dynamic deformations and instabilities and, thus, have very important practical consequences in many areas of technology. Especially when one is concerned with the design of modern aircraft and space vehicles, both of which are characterized by the demand for extremely lightweight structures, the solution of many aeroelasticity problems is a basic requirement for achieving an operationally reliable and structurally optimal system. Aeroelastic phenomena can also play an important role in turbomachinery, civil engineering structures, wind energy converters, and even in the sound generation of musical instruments.

Aeroelastic problems may be roughly classified into the categories of response and stability. Although stability problems are the principal focus of the material presented herein, this is not because response problems are any less important. Rather, because the amplitude

of deformation is indeterminate in linear stability problems, one may consider an exclusively linear treatment and still manage to solve many practical problems. However, because the amplitude is important in response problems, one is far more likely to need to be concerned with nonlinear behavior when attempting to solve them. Although nonlinear equations come closer to representing reality, analytical solution of nonlinear equations can be problematic.

The interdisciplinary nature of the field can be best illustrated by Fig. 1.1, which depicts the interaction of the three disciplines of aerodynamics, dynamics, and elasticity. Classical aerodynamic theories provide a prediction of the forces acting on a body of a given shape. Elasticity provides a prediction of the shape of an elastic body under a given load. Dynamics introduces the effects of inertial forces. With the knowledge of elementary aerodynamics, dynamics, and elasticity, the student is in a position to look at problems in which two or more of these phenomena interact. Two of those areas of interaction are the fields of flight mechanics and structural dynamics, to which separate courses in aerospace engineering are generally dedicated.

These notes will consider the two remaining areas of interaction, namely, interactions between aerodynamics and elasticity (static aeroelasticity), and among all three (dynamic aeroelasticity). Because of their importance to aerospace system design, these are appropriate for study in an aeronautics/aeronautical engineering curriculum. In aeroelasticity one finds that the loads depend on the deformation (aerodynamics), and the deformation depends on the loads (structural mechanics/dynamics); thus one has a coupled problem. Consequently, prior study of all three constituent disciplines is necessary before a study in aeroelasticity can be undertaken. Moreover, a study in structural dynamics can be helpful to develop concepts that are useful in solving aeroelasticity problems, such as the modal representation.

It is of interest to note that aeroelastic phenomena have played a major role throughout the history of powered flight. The Wright brothers utilized controlled warping of the wings on their Wright Flyer in 1903 to achieve lateral control. This was essential to their success in achieving powered flight because the aircraft was laterally unstable owing to the significant anhedral of the wings. Earlier in 1903 Samuel Langley made two attempts to achieve powered flight from the top of a houseboat on the Potomac River. His efforts resulted in catastrophic failure of the wings caused by their being overly flexible and overloaded. Such aeroelastic phenomena, including torsional divergence, were major factors in the predominance of the biplane design until the early 1930s when "stressed skin" metallic structural configurations were introduced to provide adequate torsional stiffness for monoplanes.

The first recorded and documented case of flutter in an aircraft occurred in 1916. The Handley Page O/400 bomber experienced violent tail oscillations as the result of the lack of a torsion rod connection between the port and starboard elevators, an absolute design requirement of today. The incident involved a dynamic twisting of the fuselage to as much as 45 degrees in conjunction with an antisymmetric flapping of the elevators. Catastrophic failures due to aircraft flutter became a major design concern during the First World War and remain so today. R. A. Frazer and W. J. Duncan at the National Physical Laboratory

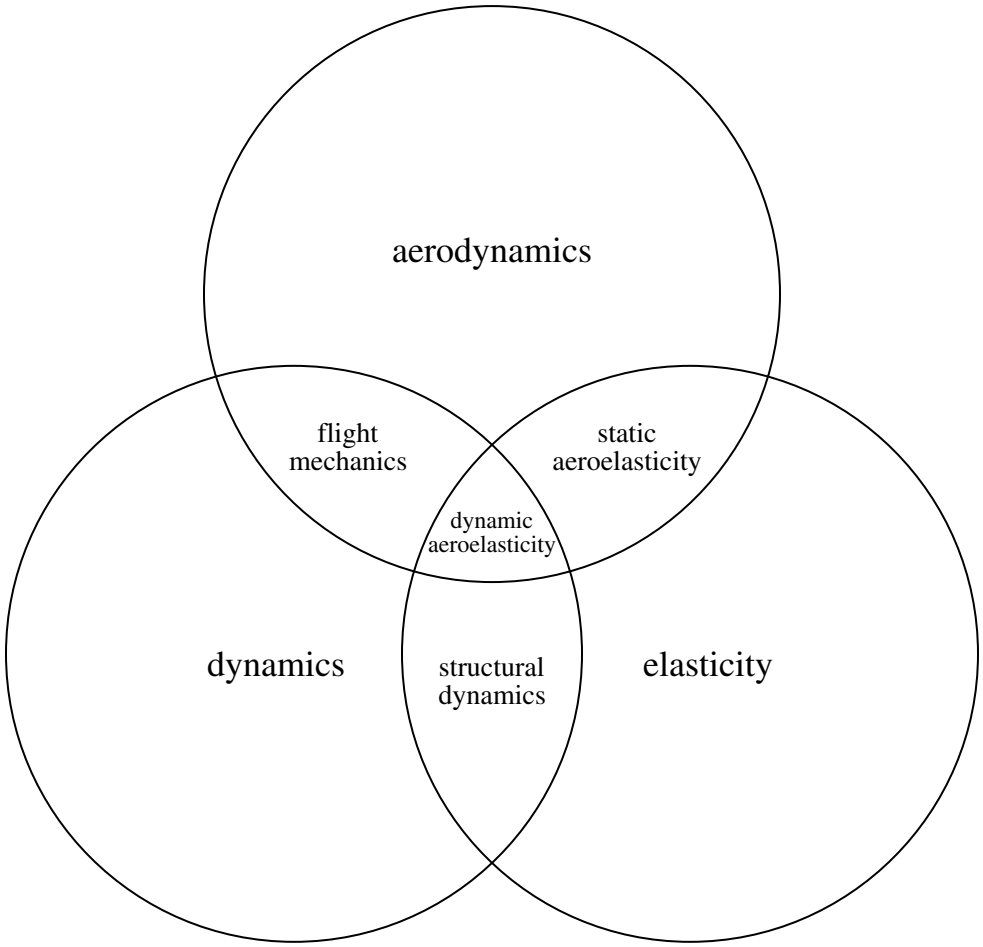

Figure 1.1: Schematic of the field of aeroelasticity

in England compiled a classic document on this subject entitled "The Flutter of Aeroplane Wings" as R&M 1155 in August 1928. This small document (about 200 pages) became known as "The Flutter Bible." Their treatment for the analysis and prevention of the flutter problem laid the groundwork for the techniques in use today.

Another major aircraft design concern that may be classified as a static aeroelastic phenomenon was experienced in 1927 by the Bristol Bagshot, a twin-engine, high-aspect-ratio English aircraft. As the speed was increased the aileron effectiveness decreased to zero and then became negative. This loss and reversal of aileron control is commonly known today as aileron reversal. The incident was successfully analyzed and design criteria were developed for its prevention by Roxbee Cox and Pugsley at the Royal Aircraft Establishment in the early 1930s. Although aileron reversal does not generally lead to a catastrophic failure, it can be quite dangerous and is thus an essential design concern. It is of interest to note that during this period of the early 1930s it was Roxbee Cox and Pugsley who proposed the name "aeroelasticity" to describe these phenomena, which are the subject of this text.

In the design of aerospace vehicles, aeroelastic phenomena can result in a full spectrum of behavior from the near benign to the catastrophic. At the near benign end of the spectrum one finds passenger and pilot discomfort. One moves from there to steady-state and transient vibrations that slowly cause the aircraft structure to suffer fatigue damage at the microscopic level. At the catastrophic end, there are aeroelastic instabilities that can quickly destroy an aircraft and result in loss of human life without warning. Aeroelastic problems that need to be addressed by the aerospace system designer can be mainly static in nature, meaning that inertial forces do not play a significant role, or they can be strongly influenced by inertial forces. Although not the case in general, the analysis of some aeroelastic phenomena can be undertaken by means of small deformation theories. Aeroelastic phenomena may strongly affect the performance of an aircraft, positively or negatively. They may also determine whether its control surfaces perform their intended functions well, poorly, or even in the exact opposite manner of that which they are intended to do. It is clear then that all these studies have very important practical consequences in many areas of aerospace technology. The design of modern aircraft and space vehicles is characterized by the demand for extremely lightweight structures. Therefore, the solution of many aeroelastic problems is a basic requirement for achieving an operationally reliable and structurally optimal system. Aeroelastic phenomena also play an important role in turbomachinery, in wind energy converters, and even in the sound generation of musical instruments.

The most commonly posed problems for the aeroelastician are stability problems. Although the elastic moduli of a given structural member are independent of the speed of the aircraft, the aerodynamic forces strongly depend on it. It is therefore not difficult to imagine scenarios in which the aerodynamic forces "overpower" the elastic restoring forces. When this occurs in such a way that inertial forces have little effect, we refer to this as a static aeroelastic instability – or "divergence." In contrast, when the inertial forces are important, the resulting dynamic instability is called "flutter." Both divergence and flutter can be catastrophic, leading to sudden destruction of the vehicle. Thus, it is vital for aircraft

designers to know how to design lifting surfaces that are free of such problems. In addition to lifting surfaces, compressor blades and thin panels can experience flutter. The latter is primarily a problem at high Mach number. Most of the treatment of aeroelasticity in this text is concerned with stability problems.

Much of the rest of the field of aeroelasticity involves a study of the response of aircraft in flight. Static aeroelastic response problems constitute a special case in which inertial forces do not contribute and in which one may need to predict the lift developed by an aircraft of given configuration at a specified angle of attack, or determine the maximum load factor such an aircraft can sustain. Also, problems of control effectiveness and aileron reversal fall under this category. When inertial forces are important, one may need to know how the aircraft reacts in turbulence or in gusts. Another important phenomenon is buffeting, which is characterized by transient vibration induced by wakes behind wings, nacelles, or other components of the aircraft.

Most of the above are treatable within the context of a linear analysis. Mathematically, linear aeroelastic response and stability problems are complementary. That is, instabilities are predictable from examining the situations under which homogeneous equations possess nontrivial solutions. Response problems, however, are generally based on solution of nonhomogeneous equations. When the system goes unstable, a solution to the nonhomogeneous equations ceases to exist, while the homogeneous equations and boundary conditions associated with a stable conguration have no nontrivial solution

Sometimes the use of linear theory may limit the amount and accuracy of information that can be extracted from an analysis. For example, unlike the predictions from linear analyses, in real aircraft it is possible for self-excited oscillations to develop, even at speeds less than the flutter speed. Moreover, large disturbances can bump a system that is predicted to be stable by linear analyses into a state of large oscillatory motion. Both situations can lead to steady-state periodic oscillations for the entire system called limit-cycle oscillations. In such situations, there can be fatigue problems leading to concerns about the life of certain components of the aircraft as well as passenger comfort and pilot endurance. To capture such behavior in an analysis, the aircraft must be treated as a nonlinear system. Although of great practical importance, nonlinear analyses are beyond the scope of these notes.

Chapter 4 treats *static aeroelasticity*. Therein we concern ourselves with static instabilities, steady airloads, and control effectiveness problems. Again, we begin with simple systems, such as elastically restrained rigid wings. We move up to wings in torsion and finish the chapter with a treatment of swept wings undergoing elastically coupled bending and torsion deformation. Finally, Chapter 5 treats *aeroelastic flutter*, which is associated with dynamic aeroelastic instabilities due to the mutual interaction of aerodynamic, elastic and inertial forces. A generic lifting surface analysis is first presented, and this is followed by illustrative treatments involving simple "typical section models." Engineering solution methods for flutter are discussed, followed by a brief presentation of unsteady aerodynamic theories, both classical and modern. The chapter culminates with an application of the modal representation to the flutter analysis of flexible wings and a discussion of the flutter

boundary characteristics of conventional aircraft. It is important to note that central to our study in these last two chapters are the phenomena of divergence and flutter, which typically result in catastrophic failure of the lifting surface and may lead to subsequent destruction of the flight vehicle.

A list of references is included, along with an appendix in which Lagrange's equations are derived and illustrated.

Chapter 2

REVIEW OF FOUNDATIONS OF MECHANICS

2.1 Uniform Beam Torsional Dynamics

We now consider the dynamics of beam torsional deformation. The beam has many of the characteristics of typical aeronautical structures. Indeed, high-aspect-ratio wings and helicopter rotor blades are frequently idealized as beams, especially in preliminary design. Even for low-aspect-ratio wings, although a plate model is more realistic, the bending and torsional deformation can be approximated by use of beam theory with adjusted stiffness coefficients.

In an effort to retain a level of simplicity that promotes tractability, the torsional rigidity of St. Venant theory, denoted GJ, will be taken as given. For homogeneous and isotropic beams, G denotes the shear modulus and J is a constant that depends only on the geometry of the cross section. For such beams J can be determined by solving a boundary-value problem over the cross-sectional area, which requires finding the cross-sectional warping caused by torsion. Although analytical solutions for this problem are available for some simple cross-sectional geometries, solving for the cross-sectional warping and torsional stiffness is not a trivial exercise in general. For nonhomogeneous, anisotropic beams one may also use the symbol GJ to denote an effective torsional rigidity, which can be determined by solving a far more involved boundary-value problem over the cross-sectional area.

2.1.1 Equation of Motion

The beam will be considered initially to have nonuniform properties along the x-axis, which is chosen to coincide with the elastic axis for the beam. In our idealized model for beams, this axis is assumed to be straight and, by definition, corresponds to the locus of the cross-sectional shear centers. This choice of x-axis structurally uncouples torsion and transverse displacements caused by bending for isotropic beams. For composite beams, this choice

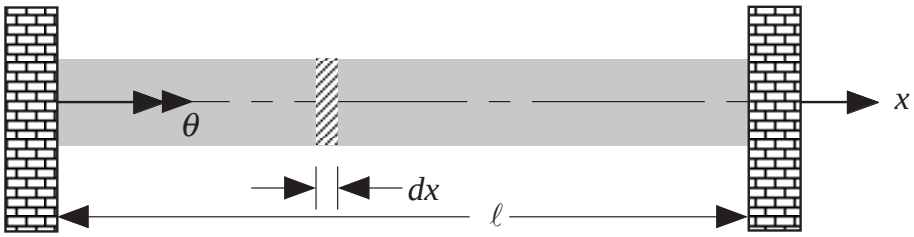

Figure 2.1: Beam undergoing torsional deformation

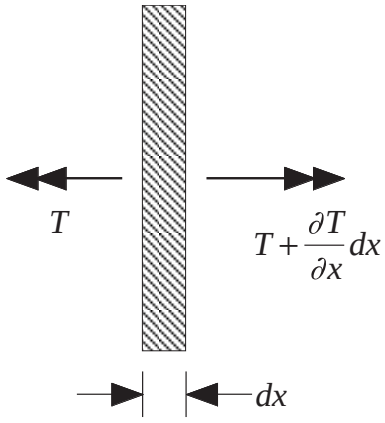

Figure 2.2: Cross-sectional slice of beam undergoing torsional deformation

of x-axis uncouples torsion and transverse shear deformation, but torsion and transverse displacements may remain coupled depending on whether the beam has bending-torsion coupling. For a further simplification, we assume that cross-sectional mass centroids lie along the elastic axis, in which case transverse motions due to bending are inertially uncoupled from torsional motion. The elastic twisting deflection, θ, will be positive in a right-handed sense about this axis as illustrated in Fig. 2.1. In contrast, the twisting moment, denoted by T, is the structural torque, i.e., the resultant moment of the tractions on a cross-sectional face about the elastic axis. Recall that an outward-directed normal on the positive x face is directed to the right, whereas an outward-directed normal on the negative x face is directed to the left. Thus, the direction of a positive torque tends to rotate the positive x face in a direction that is positive in the right-hand sense and the negative x face in a direction that is negative in the right-hand sense, as depicted in Fig. 2.1. This will affect the boundary conditions, as noted below.

Letting $\rho I_p dx$ be the polar mass moment of inertia about the x-axis of the differential beam segment in Fig. 2.2, one can obtain the equation of motion by equating the resultant twisting moment on both faces of the segment to the rate of change of the segment's angular momentum about the elastic axis. This yields

$$T + \frac{\partial T}{\partial x} dx - T = \rho I_p dx \frac{\partial^2 \theta}{\partial t^2} \tag{2.1}$$

or

$$\frac{\partial T}{\partial x} = \rho I_p \frac{\partial^2 \theta}{\partial t^2} \tag{2.2}$$

where

$$\rho I_p = \int_{\mathcal{A}} \rho \left(y^2 + z^2 \right) d\mathcal{A} \tag{2.3}$$

Here $\mathcal{A}$ is the cross section of the beam, y and z are cross-sectional Cartesian coordinates, and ρ is the mass density of the beam. When ρ is constant over the cross section, then I_p is the area polar moment of inertia per unit length. When ρ varies over the cross section, one may interpret ρI_p as the mass polar moment of inertia for the cross section.

The twisting moment can be written in terms of the twist rate and the Saint-Venant torsional rigidity as

$$T = GJ \frac{\partial \theta}{\partial x} \tag{2.4}$$

Substituting these expressions into Eq. (2.2) one obtains the partial differential equation of motion for the nonuniform beam given by

$$\frac{\partial}{\partial x} \left(GJ \frac{\partial \theta}{\partial x} \right) = \rho I_p \frac{\partial^2 \theta}{\partial t^2} \tag{2.5}$$

For the special case of uniform beams this relation simplifies to the one-dimensional wave equation

$$\frac{GJ}{\rho I_p} \frac{\partial^2 \theta}{\partial x^2} = \frac{\partial^2 \theta}{\partial t^2} \tag{2.6}$$

Other than the constants that multiply the second partial derivatives, this is the same equation that governed the dynamic behavior of the string. Thus, all the previously discussed properties of standing and traveling waves will exist here as well. However, as will be discussed in detail below, there are more interesting possibilities for the boundary conditions.

To establish these properties the separation of variables method will be applied as

$$\theta(x,t) = X(x)Y(t) \tag{2.7}$$

which, when substituted into the wave equation, yields

$$\frac{X''}{X} = \frac{\rho I_p}{GJ}\frac{\ddot{Y}}{Y} \tag{2.8}$$

Since the dependencies on x and t have been separated across the equality, each side must equal a constant, say $-\alpha^2$, so that

$$\frac{X''}{X} = \frac{\rho I_p}{GJ}\frac{\ddot{Y}}{Y} = -\alpha^2 \tag{2.9}$$

Two ordinary differential equations then follow from this, namely,

$$\begin{aligned} X''(x) + \alpha^2 X(x) &= 0 \\ \ddot{Y}(t) + \alpha^2 \frac{GJ}{\rho I_p} Y(t) &= 0 \end{aligned} \tag{2.10}$$

(Note the similarity with the equations of motion for a vibrating string.) For $\alpha \neq 0$, Eqs. (2.10) have solutions that can be written as

$$\begin{aligned} X(x) &= A\sin(\alpha x) + B\cos(\alpha x) \\ Y(t) &= C\sin\left(\sqrt{\frac{GJ}{\rho I_p}}\alpha t\right) + D\cos\left(\sqrt{\frac{GJ}{\rho I_p}}\alpha t\right) \end{aligned} \tag{2.11}$$

To complete the solution the constants A and B can be determined from the boundary conditions at the ends of the beam, and C and D can be found as a function of the initial beam deflection and rate of deflection. The special case of $\alpha = 0$ is very important and will be addressed in more detail in Section 2.1.3.

2.1.2 Boundary Conditions

There are four different boundary conditions that can be imposed at the ends of the beam for determination of the constants A and B. For any given beam only one boundary condition is required at each end.

Figure 2.3: Clamped end of a beam

Figure 2.4: Free end of a beam

Clamped end

In this case (see Fig. 2.3) the end of the beam is assumed to be "built-in" or "cantilevered" at a wall. As a consequence there will be no rotation due to elastic twist at the beam end, and the boundary condition is

$$\theta(\ell, t) = 0 = X(\ell)Y(t) \tag{2.12}$$

which is identically satisfied when

$$X(\ell) = 0 \tag{2.13}$$

Free end

When the end of the beam is free (see Fig. 2.4) there are no external loads acting on the beam. Therefore the twisting moment at the end must be zero.

$$T(\ell, t) = GJ\frac{\partial\,\theta}{\partial x}(\ell, t) = 0 \tag{2.14}$$

or, for uniform beams

$$\frac{\partial\theta}{\partial x}(\ell, t) = X'(\ell)Y(t) = 0 \tag{2.15}$$

Thus, the specific condition to be satisfied is

$$X'(\ell) = 0 \tag{2.16}$$

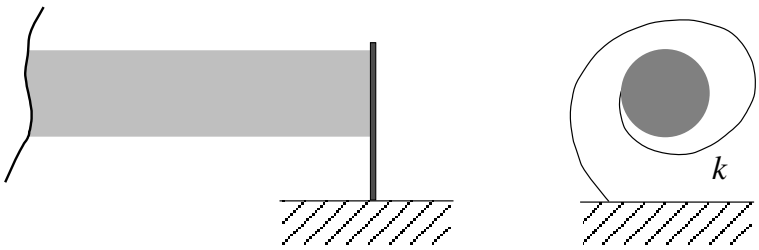

Figure 2.5: Elastically restrained end of a beam

Figure 2.6: Inertially restrained end of a beam

Elastic constraint

An elastic constraint (see Fig. 2.5) can be treated as a linearly elastic torsional spring attached to the end of the beam. The twisting moment at the beam end must be equal and opposite to the spring reaction for any finite deflection of the end so that

$$\begin{aligned} T(\ell,t) &= GJ\frac{\partial\theta}{\partial x}(\ell,t) \\ &= -k\theta(\ell,t) \end{aligned} \tag{2.17}$$

where k is the spring constant. Thus,

$$GJX'(\ell)Y(t) = -kX(\ell)Y(t) \tag{2.18}$$

which requires that

$$GJX'(\ell) = -kX(\ell) \tag{2.19}$$

The reader should verify that the same type of boundary condition at the other end would yield

$$GJX'(0) = kX(0) \tag{2.20}$$

where the sign change comes about by virtue of the switch in direction noted above for a positive twisting moment.

Figure 2.7: Schematic of clamped-free beam undergoing torsion

Inertial constraint

Here we consider a beam with a rigid body attached to its right end (see Fig. 2.6). This rigid body has a mass moment of inertia about the beam elastic axis denoted by I_c, which contributes a concentrated rotational inertia effect. The twisting moment at the beam end must be equal and opposite to the inertial reaction of the concentrated inertia for any finite angular acceleration of the end. Therefore,

$$T(\ell,t) = GJ\frac{\partial\theta}{\partial x}(\ell,t) = -I_c\frac{\partial^2\theta}{\partial t^2}(\ell,t) \tag{2.21}$$

so that

$$GJX'(\ell)Y(t) = -I_cX(\ell)\ddot{Y}(t) \tag{2.22}$$

From the functional form of $Y(t)$ as established from the separation procedure, it can be noted that

$$\ddot{Y}(t) = -\alpha^2\frac{GJ}{\rho I_p}Y(t) \tag{2.23}$$

Substitution into the preceding condition yields

$$GJX'(\ell)Y(t) = \alpha^2\frac{GJ}{\rho I_p}I_cX(\ell)Y(t) \tag{2.24}$$

which requires that

$$\rho I_pX'(\ell) = \alpha^2I_cX(\ell) \tag{2.25}$$

As above, the reader should verify that the same type of boundary condition at the other end would yield

$$\rho I_pX'(0) = -\alpha^2I_cX(0) \tag{2.26}$$

2.1.3 Example Solutions for Mode Shapes and Frequencies

In this section we consider several examples of the calculation of natural frequencies and mode shapes of vibrating beams in torsion. We begin with the clamped-free case. Next,

we consider the free-free case, illustrating the concept of the rigid-body mode. Finally, we consider a case that requires numerical solution of the transcendental characteristic equation, a beam clamped at its root and restrained with a rotational spring at its tip.

Example solution for clamped-free beam

To illustrate the application of these boundary conditions, consider the case of a uniform beam that is clamped at $x = 0$ and free at $x = \ell$, as shown in Fig. 2.7. The boundary conditions for this case are

$$X(0) = X'(\ell) = 0 \tag{2.27}$$

Recall that the general solution was previously determined as

$$\theta(x,t) = X(x)Y(t) \tag{2.28}$$

where X and Y are given in Eqs. (2.11). For $\alpha \neq 0$ the first of those equations has the solution

$$X(x) = A\sin(\alpha x) + B\cos(\alpha x) \tag{2.29}$$

It is apparent that the boundary conditions lead to the following:

$$\begin{aligned} X(0) = 0 \text{ requires } & B = 0 \\ X'(\ell) = 0 \text{ requires } & A\alpha\cos(\alpha\ell) = 0 \end{aligned} \tag{2.30}$$

If $A = 0$ a trivial solution will be obtained, such that the deflection will be identically zero. Since $\alpha \neq 0$, a nontrivial solution requires that

$$\cos(\alpha\ell) = 0 \tag{2.31}$$

This is called the "characteristic equation," the solutions of which consist of a denumerably infinite set called the "eigenvalues" and are given by

$$\alpha_i\ell = \frac{(2i-1)\pi}{2} \qquad (i = 1, 2, \ldots) \tag{2.32}$$

The $Y(t)$ portion of the general solution can be observed to have the form of simple harmonic motion, as indicated in Eq. (2.23), so that the natural frequency is

$$\omega = \alpha\sqrt{\frac{GJ}{\rho I_p}} \tag{2.33}$$

Since α can have only specific values, the frequencies will also take on specific numerical values given by

$$\omega_i = \alpha_i\sqrt{\frac{GJ}{\rho I_p}} = \frac{(2i-1)\pi}{2\ell}\sqrt{\frac{GJ}{\rho I_p}} \tag{2.34}$$

These are the natural frequencies of the beam. Associated with each frequency is a "mode shape" as determined from the x-dependent portion of the general solution. The mode shapes (or eigenfunctions) can be written as

$$\phi_i(x) = \sin(\alpha_i x) = \sin\left[\frac{(2i-1)\pi x}{2\ell}\right] \tag{2.35}$$

or any constant times $\phi_i(x)$. The first three of these mode shapes are plotted in Fig. 2.8. The zero derivative at the free end is indicative of the vanishing twisting moment at the free end.

Example solution for free-free beam

A second example, which exhibits both elastic motion as described above and motion as a rigid body, is the case of a beam that is free at both ends as shown in Fig. 2.9. The boundary conditions are

$$X'(0) = X'(\ell) = 0 \tag{2.36}$$

From the general solution for $X(x)$ in Eqs. (2.11), one finds that for $\alpha \neq 0$

$$X'(x) = A\alpha\cos(\alpha x) - B\alpha\sin(\alpha x) \tag{2.37}$$

Thus, the condition at $x = 0$ requires that

$$A\alpha = 0 \tag{2.38}$$

For $A = 0$ the condition at $x = \ell$ requires that

$$\sin(\alpha\ell) = 0 \tag{2.39}$$

since a null solution ($\theta \equiv 0$) is obtained if $B = 0$. This characteristic equation is satisfied by

$$\alpha_i\ell = i\pi \qquad (i = 1, 2, \ldots) \tag{2.40}$$

and the corresponding natural frequencies become

$$\omega_i = \frac{i\pi}{\ell}\sqrt{\frac{GJ}{\rho I_p}} \tag{2.41}$$

The associated mode shapes are determined from the corresponding $X(x)$ as

$$\phi_i(x) = \cos(\alpha_i x) = \cos\left(\frac{i\pi x}{\ell}\right) \tag{2.42}$$

These frequencies and mode shapes describe the normal mode of vibration for the elastic degrees of freedom of the free-free beam in torsion.

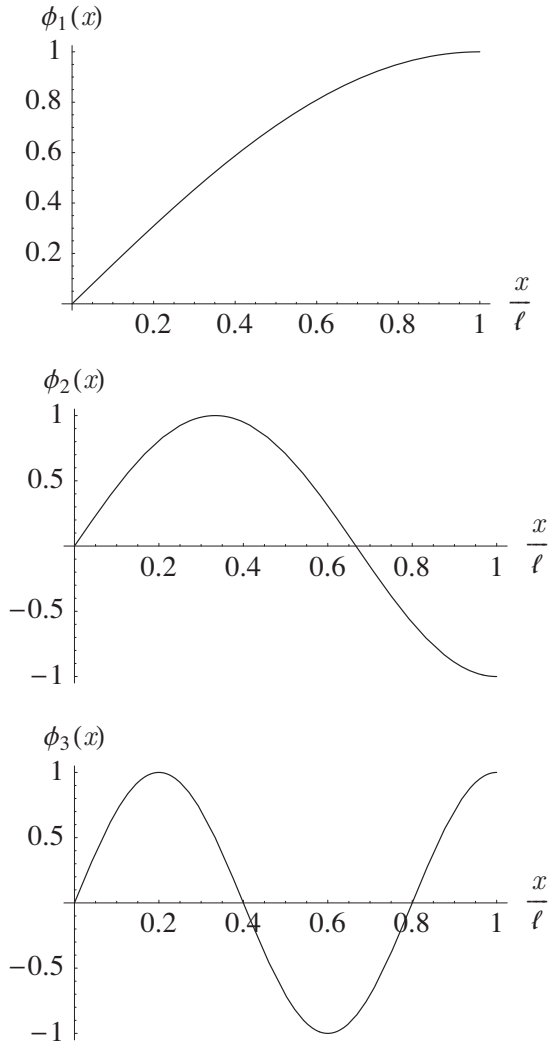

Figure 2.8: First three mode shapes for clamped-free beam vibrating in torsion

Figure 2.9: Schematic of free-free beam undergoing torsion

Now, if in the above analysis the separation constant, α, is taken as zero, then the governing ordinary differential equations are changed to

$$\frac{X''}{X} = \frac{\rho I_p}{GJ}\frac{\ddot{Y}}{Y} = 0 \tag{2.43}$$

or

$$X''(x) = 0 \text{ and } \ddot{Y}(t) = 0 \tag{2.44}$$

The general solutions to these equations can be written as

$$\begin{aligned} X(x) =& ax + b \\ Y(t) =& ct + d \end{aligned} \tag{2.45}$$

The arbitrary constants, a and b, in the spatially dependent portion of the solution can again be determined from the boundary conditions. For the present case of the free-free beam the conditions are

$$\begin{aligned} X'(0) = 0 \text{ requires } a = 0 \\ X'(\ell) = 0 \text{ requires } a = 0 \end{aligned} \tag{2.46}$$

Because both conditions are satisfied without imposing any restrictions on the constant b, this constant can be anything, which implies that the torsional deflection can be nontrivial for $\alpha = 0$. From $X(x)$ with $a = 0$ it is apparent that the corresponding value of θ will be independent of the coordinate x. This means that this motion for $\alpha = 0$ is a "rigid-body" rotation of the beam.

The time-dependent solution for this motion, $Y(t)$, is also different from that obtained for the elastic motion. Primarily it can be noted that the motion is not oscillatory; thus, the rigid-body natural frequency is zero. The arbitrary constants, c and d, can be obtained from the initial values of the rigid-body orientation and angular velocity. To summarize the complete solution for the free-free beam in torsion, a set of generalized coordinates can be defined by

$$\theta(x,t) = \sum_{i=0}^{\infty} \phi_i(x)\xi_i(t) \tag{2.47}$$

where

$$\begin{aligned} \phi_0 =& 1 \\ \phi_i =& \cos\left(\frac{i\pi x}{\ell}\right) \qquad (i = 1, 2, \ldots) \end{aligned} \tag{2.48}$$

The first three elastic mode shapes are plotted in Fig. 2.10. The zero derivative at both ends is indicative of the vanishing twisting moment there. The natural frequencies associated with these mode shapes are

$$\begin{aligned} \omega_0 =& 0 \\ \omega_i =& \frac{i\pi}{\ell}\sqrt{\frac{GJ}{\rho I_p}} \qquad (i = 1, 2, \ldots) \end{aligned} \tag{2.49}$$

It may be noted that the rigid-body generalized coordinate, $\xi_0(t)$, represents the radian measure of the rigid-body rotation of the beam about the x-axis.

Note that a quick way to verify the existence of a rigid-body mode is to substitute $\omega = 0$ and $X =$ a constant into the differential equation and boundary conditions for X. A rigid-body mode exists if and only if all are satisfied.

Example solution for clamped-spring-restrained beam

A final example for beam torsion is given by the system in Fig. 2.11. The beam is clamped at the root ($x = 0$) end, and the other end is restrained with a rotational spring having spring constant $k = \zeta GJ/\ell$ where ζ is a dimensionless parameter. The boundary conditions on X are thus

$$\begin{aligned} X(0) &= 0 \\ GJX'(\ell) &= -kX(\ell) = -\frac{GJ}{\ell}\zeta X(\ell) \end{aligned} \tag{2.50}$$

When these boundary conditions are substituted into the general solution found in Eqs. (2.11), one sees that the first condition requires that $B = 0$; the second condition, along with the requirement for a nontrivial solution, leads to

$$\zeta \tan(\alpha\ell) + \alpha\ell = 0 \tag{2.51}$$

This transcendental equation has a denumerably infinite set of roots that cannot be found in closed form. However, as many of these roots as desired can be found using numerical procedures found in commercially available software packages such as Mathematica,™ Maple,™ or MATLAB.™ These roots of Eq. (2.51) will be functions of ζ, and the first four such roots are plotted versus ζ in Fig. 2.12. Denoting these roots by α_i, with i=1, 2, ..., one obtains the corresponding natural frequencies

$$\omega_i = \alpha_i \sqrt{\frac{GJ}{\rho I_p}} \qquad (i=1,\ 2,\ \ldots) \tag{2.52}$$

From the plots (and from Eq. 2.51) we note that as ζ tends toward zero, α_1 tends toward $\pi/2$, which means that the fundamental natural frequency is

$$\omega_1 = \frac{\pi}{2\ell}\sqrt{\frac{GJ}{\rho I_p}} \qquad (\zeta \to 0) \tag{2.53}$$

which is the natural frequency of a clamped-free beam in torsion (as shown above). One can also show that as ζ tends to infinity, α_1 tends toward π so that the fundamental natural frequency is

$$\omega_1 = \frac{\pi}{\ell}\sqrt{\frac{GJ}{\rho I_p}} \qquad (\zeta \to \infty) \tag{2.54}$$

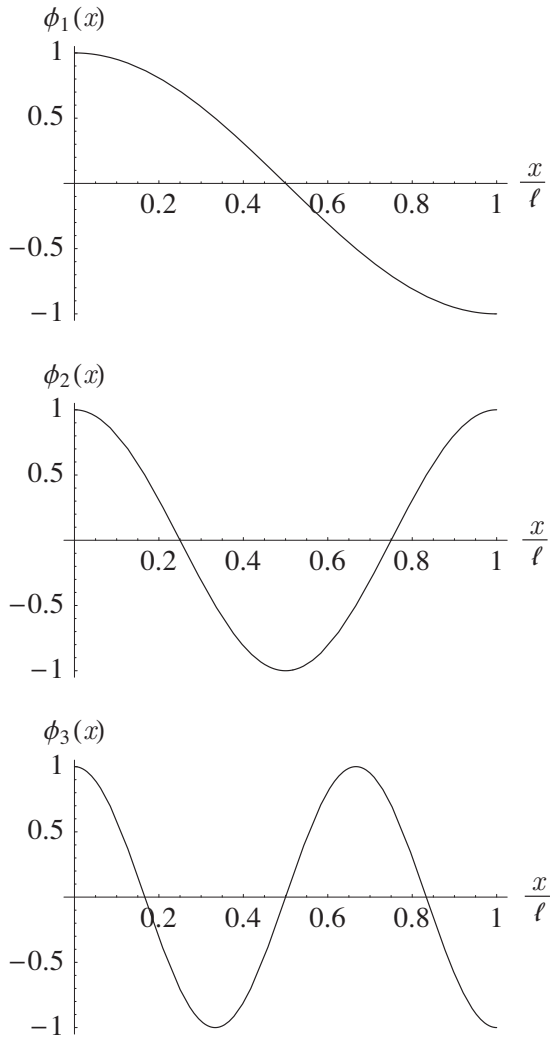

Figure 2.10: First three elastic mode shapes for free-free beam vibrating in torsion

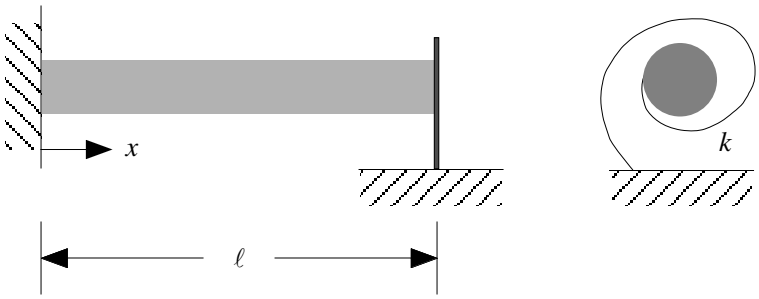

Figure 2.11: Schematic of torsion problem with spring

which is the natural frequency of a clamped-clamped beam in torsion. The determination of the natural frequencies of a clamped-clamped beam in torsion is left as an exercise for the reader.

To obtain the corresponding mode shapes, one takes the solutions for α_i and substitutes back into X, recalling that we can arbitrarily set $A = 1$ and that $B = 0$. The resulting mode shape is

$$\phi_i = \sin(\alpha_i x) \qquad (i=1,\ 2,\ \ldots) \tag{2.55}$$

The first three modes for $\zeta = 1$ are shown in Fig. 2.13. As expected, neither the twist angle nor its derivative are equal to zero at the tip.

2.2 Uniform Beam Bending Dynamics

The free vibration of a beam in transverse bending motion is often referred to as transverse vibration. This type of motion differs from the transverse string dynamics and beam torsional dynamics in that the governing equations of motion are of a different mathematical form. Although these equations are different, their solutions are obtained in a similar manner and exhibit similar physical characteristics. It should also be observed that, whereas most aerospace structures will experience combined or simultaneous bending and torsional dynamic behavior, we have here chosen certain configuration variables to uncouple these types of motion.

2.2.1 Equation of Motion

As in the case of torsion the beam will initially be treated as having nonuniform properties along the x-axis. The x-axis will be taken as the line of the individual cross-sectional neutral axes associated with pure bending in and normal to the plane of the diagram in Fig. 2.14. For simplicity, however, we will only consider uncoupled bending in the x-y plane, thus excluding initially twisted beams from the development. The bending deflections are denoted by $v(x, t)$

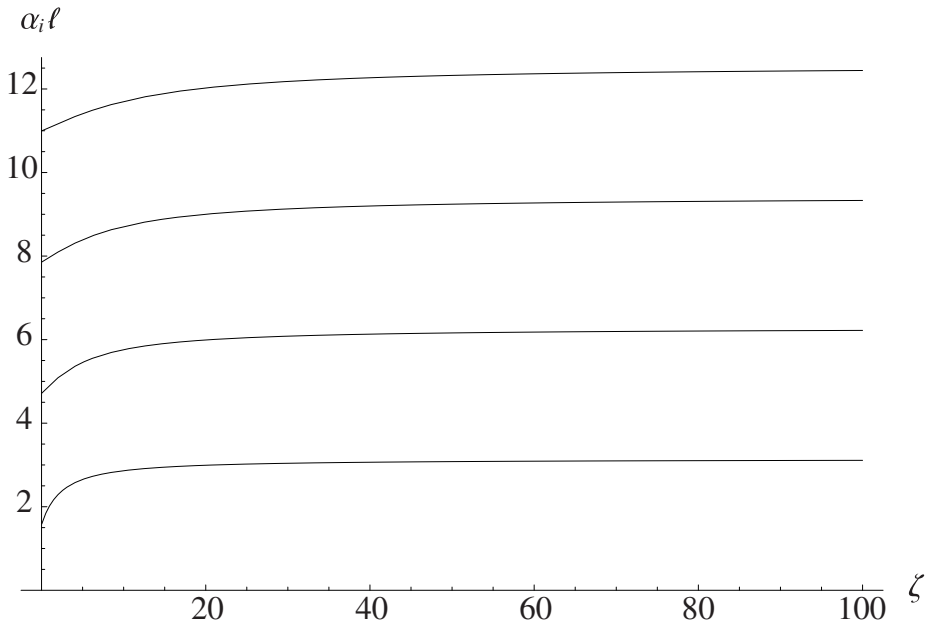

Figure 2.12: Plot of the lowest values of α_i versus ζ for a clamped-spring-restrained beam in torsion

in the y direction. The x-axis is presumed to be straight, thus excluding initially curved beams. We will continue to assume for now that the properties of the beam allow the x-axis to be chosen so that bending and torsion are both structurally and inertially uncoupled. Finally, the transverse beam displacement, v, will be presumed small to permit a linearly elastic representation of the deformation.

A free-body diagram for the differential beam segment shown in Fig. 2.15 includes the shear force, V, and the bending moment, M. Recall from our earlier discussion on torsion that an outward-directed normal on the positive x face is directed to the right, and an outward-directed normal is directed to the left on the negative x face. By this convention, V is the resultant of the transverse shear stresses in the positive y direction (upward in Fig. 2.15) on a positive x cross section face and in the negative y direction on a negative x cross section face. In other words, a positive shear force tends to displace the positive x face upward and the negative x face downward, as depicted in Fig. 2.15. The bending moment, M is the moment of the longitudinal stresses about a line parallel to the z-axis (out of the paper in Fig. 2.15) at the intersection between the cross-sectional plane and the neutral surface. Thus, a positive bending moment tends to rotate the positive x face positively about the z-axis (in the right-handed sense) and the negative x face negatively about the z-axis. This will affect the boundary conditions, as noted below. The distributed loading (with units of force per unit length) is denoted by q. The equation of motion for transverse beam displacements can be obtained by setting the resultant force on the segment equal to

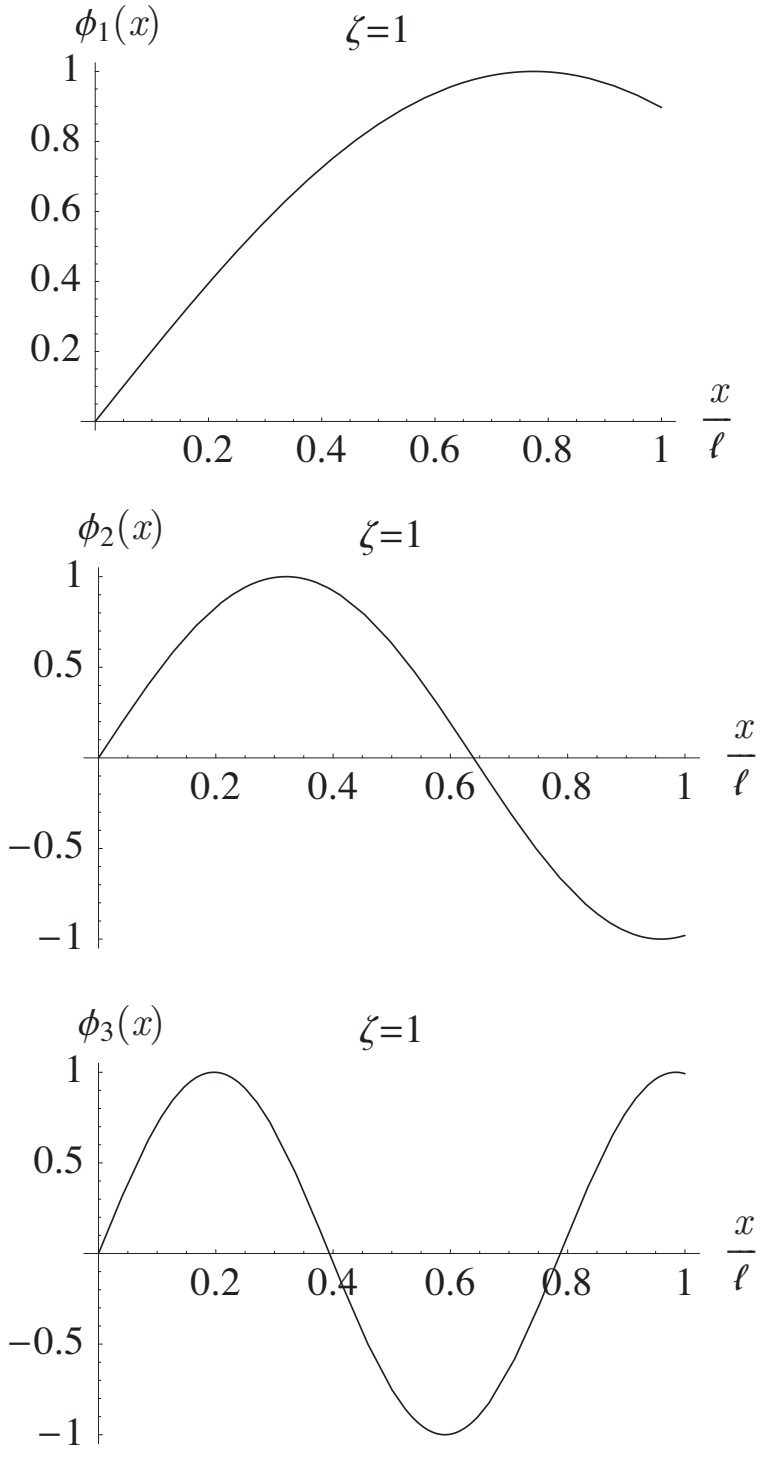

Figure 2.13: First three mode shapes for clamped-spring-restrained beam in torsion, $\zeta = 1$

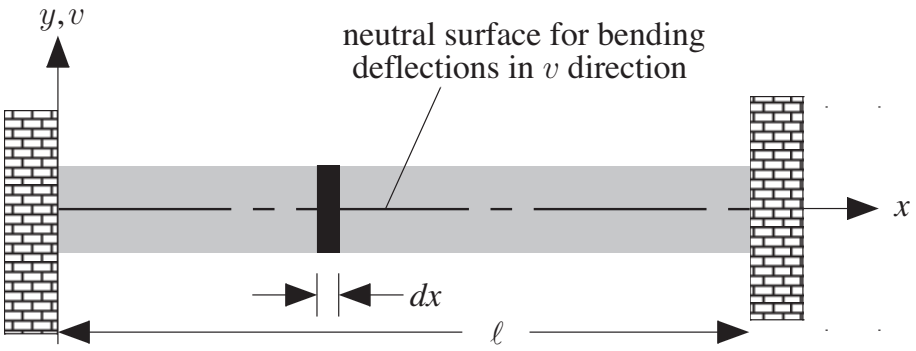

Figure 2.14: Schematic of beam for bending dynamics

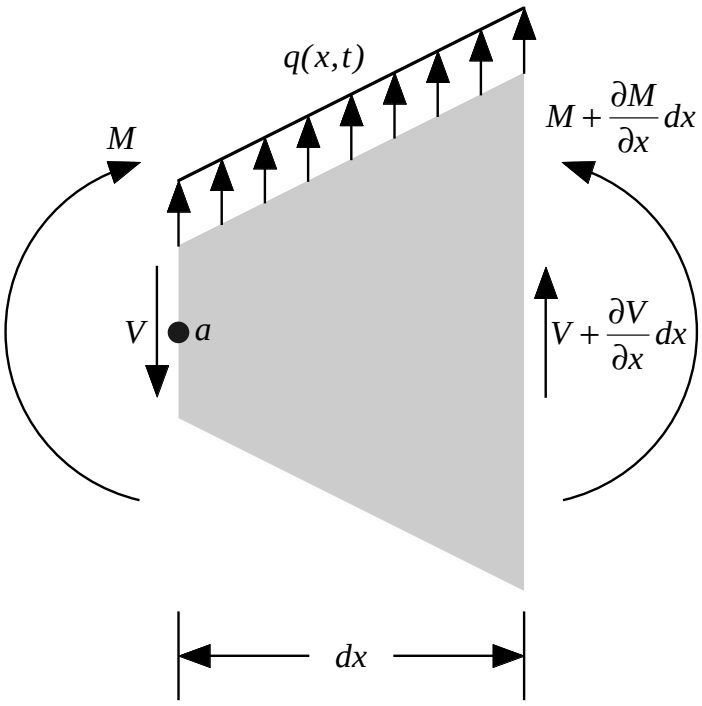

Figure 2.15: Schematic of differential beam segment

its mass times its acceleration, which yields

$$q(x,t)dx - V + \left(V + \frac{\partial V}{\partial x}dx\right) = m\,dx\frac{\partial^2 v}{\partial t^2} \tag{2.56}$$

and leads to

$$-\frac{\partial V}{\partial x} + m\frac{\partial^2 v}{\partial t^2} = q(x,t) \tag{2.57}$$

where $m = \rho A$ is the mass per unit length, ρ is the material density and A is the cross-sectional area. We must also consider the moment equation. We note here that the cross-sectional rotational inertia (about an axis normal to the page) will be ignored because it has a small effect. Taking a counterclockwise moment as positive, we sum the moments about the point a to obtain

$$-M + \left(M + \frac{\partial M}{\partial x}dx\right) + \left(V + \frac{\partial V}{\partial x}dx\right)dx - \frac{1}{2}m\frac{\partial^2 v}{\partial t^2}dx^2 = 0 \tag{2.58}$$

which, after we neglect the higher-order differentials (i.e., higher powers of dx), becomes

$$\frac{\partial M}{\partial x} + V = 0 \tag{2.59}$$

Recall that the bending moment is proportional to the local curvature and so

$$M = EI\frac{\partial^2 v}{\partial x^2} \tag{2.60}$$

where EI may be regarded as the effective bending stiffness of the beam at a particular cross section. For homogeneous and isotropic beams, E is Young's modulus and I is the cross-sectional area moment of inertia about the z-axis for a particular cross section. Substitution of Eq. (2.60) into Eq. (2.59) and of the resulting equation into Eq. (2.57) yields the partial differential equation of motion for a nonuniform beam as

$$\frac{\partial^2}{\partial x^2}\left(EI\frac{\partial^2 v}{\partial x^2}\right) + m\frac{\partial^2 v}{\partial t^2} = q(x,t) \tag{2.61}$$

In the following sections, we will be treating the special case of free vibration for which $q(x,t) = 0$. Also, for simplicity we will specialize the equations for the case of spanwise uniformity of all properties, for which the parameter a can be defined as a constant such that

$$a^4 = \frac{EI}{m} \tag{2.62}$$

to simplify the equation of motion to

$$a^4\frac{\partial^4 v}{\partial x^4} + \frac{\partial^2 v}{\partial t^2} = 0 \tag{2.63}$$

2.2.2 General Solutions

A solution to the equation of motion for transverse beam vibrations can be obtained by a separation of the independent variables. This separation will be denoted as

$$v(x,t) = X(x)Y(t) \tag{2.64}$$

which when substituted into the equation of motion yields

$$\frac{X''''}{X} = -\frac{1}{a^4}\frac{\ddot{Y}}{Y} \tag{2.65}$$

Since the dependencies on x and t have been separated across the equality, each side must equal a constant, say α^4. The resulting ordinary differential equations then become

$$\begin{aligned} X'''' - \alpha^4 X &= 0 \\ \ddot{Y} + a^4\alpha^4 Y &= 0 \end{aligned} \tag{2.66}$$

For $\alpha \neq 0$, the general solution to the second (the time-dependent) equation can be written as in the cases for the string and beam torsion, namely

$$Y(t) = A\sin(\omega t) + B\cos(\omega t) \tag{2.67}$$

where it is clear from the second of Eqs. (2.66)

$$\omega = \alpha^2 a^2 = \alpha^2\sqrt{\frac{EI}{m}} = (\alpha\ell)^2\sqrt{\frac{EI}{m\ell^4}} \tag{2.68}$$

For $\alpha \neq 0$, the general solution to the spatially dependent equation can be obtained by presuming a solution of the form

$$X(x) = \exp(\lambda x) \tag{2.69}$$

Substitution of this assumed form into the fourth-order differential equation for $X(x)$ yields

$$\lambda^4 - \alpha^4 = 0 \tag{2.70}$$

which can be factored to

$$(\lambda - i\alpha)(\lambda + i\alpha)(\lambda - \alpha)(\lambda + \alpha) \tag{2.71}$$

which indicates a general solution of the form

$$X(x) = C_1\exp(i\alpha x) + C_2\exp(-i\alpha x) + C_3\exp(\alpha x) + C_4\exp(-\alpha x) \tag{2.72}$$

Rewriting the exponential functions as trigonometric and hyperbolic sine and cosine functions yields an alternative form of the general solution as

$$X(x) = D_1\sin(\alpha x) + D_2\cos(\alpha x) + D_3\sinh(\alpha x) + D_4\cosh(\alpha x) \tag{2.73}$$

Eventual determination of the constants D_i (i =1, 2, 3, and 4) and α will require specification of appropriate boundary conditions. To facilitate this procedure this last solution form can be rearranged to provide in some cases a slight advantage in the algebra, so that

$$\begin{aligned} X(x) =& E_1[\sin(\alpha x) + \sinh(\alpha x)] + E_2[\sin(\alpha x) - \sinh(\alpha x)] \\ &+ E_3[\cos(\alpha x) + \cosh(\alpha x)] + E_4[\cos(\alpha x) - \cosh(\alpha x)] \end{aligned} \tag{2.74}$$

To complete the solution the constants A and B can be determined from the initial deflection and rate of deflection of the beam. The remaining constants, C_i, D_i, or E_i (i = 1, 2, 3, and 4), can be evaluated from the boundary conditions, which must be imposed at each end of the beam. The very important special case of $\alpha = 0$ is connected with rigid-body modes.

2.2.3 Boundary Conditions

For the beam bending problem it is necessary to impose two boundary conditions at each end of the beam. A boundary condition can be any linear, homogeneous relation involving the beam deflection and one or more of its partial derivatives. Although it is not a mathematical requirement, the particular combination of conditions to be specified at a beam end should represent a physically realizable constraint. The various derivatives of the beam deflection can be associated with particular beam states at any arbitrary point along the beam. There are four such states of practical interest:

1. Deflection = $v(x,t) = X(x)Y(t)$
2. Slope = $\frac{\partial v}{\partial x}(x,t) = X'(x)Y(t)$
3. Bending Moment = $M(x,t) = EI\frac{\partial^2 v}{\partial x^2}(x,t) = EIX''(x)Y(t)$
4. Shear = $V(x,t) = -EI\frac{\partial^3 v}{\partial x^3}(x,t) = -EIX'''(x)Y(t)$

It should be noted when relating these beam states that the positive convention for deflection and slope is the same at both ends of the beam. In contrast, the shear and bending moment sign conventions differ at opposite beam ends as illustrated by the free-body differential beam element used to obtain the equation of motion shown in Fig. 2.15.

The most common conditions that can occur at the beam ends involve vanishing pairs of individual states. Typical of such conditions are the following classical configurations:

- Simply-supported, hinged or pinned end, which indicates zero deflection and bending moment, is denoted by the triangular symbol in Fig. 2.16 and has $v(\ell,t) = M(\ell,t) = 0$ so that $X(\ell) = X''(\ell) = 0$.
- Cantilever or built-in end, which implies zero deflection and slope, is illustrated in Fig. 2.3 and has $v(\ell,t) = \frac{\partial v}{\partial x}(\ell,t) = 0$ so that $X(\ell) = X'(\ell) = 0$.

Figure 2.16: Schematic of pinned end condition

Figure 2.17: Schematic of sliding end condition

- Free end, which corresponds to zero bending moment and shear, is illustrated in Fig. 2.4 and has $M(\ell, t) = V(\ell, t) = 0$ so that $X''(\ell) = X'''(\ell) = 0$.

- Sliding end, which corresponds to zero shear and slope, is illustrated in Fig. 2.17 and has $\frac{\partial v}{\partial x}(\ell, t) = V(\ell, t) = 0$ so that $X'(\ell) = X'''(\ell) = 0$.

All of these conditions can occur in the same form at $x = 0$.

In addition to these zero-state conditions, the boundary conditions can correspond to linear constraint reactions associated with elastic and inertial elements. These types of conditions were previously observed for the torsional dynamics of beams. They may occur alone or in conjunction with others. The boundary conditions associated with these constraint reactions are of four basic types:

1. translational elastic constraint,

2. rotational elastic constraint,

3. translational inertia constraint, and

4. rotational inertia constraint.

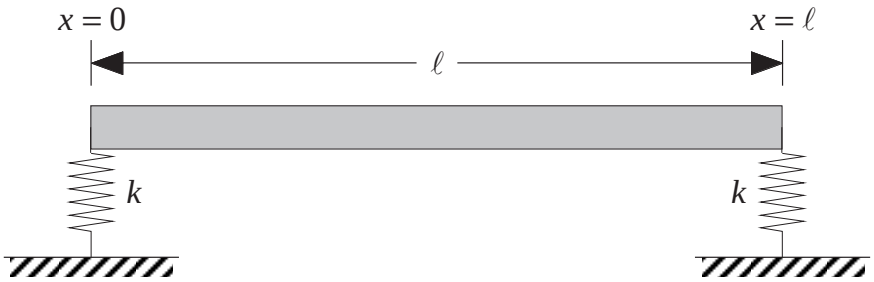

Figure 2.18: Schematic of translational spring end conditions

Translational elastic constraint

A translational elastic constraint corresponds to a spring reaction force that is equated to the shear force, as shown in Fig. 2.18. At the left end

$$EI\frac{\partial^3 v}{\partial x^3}(0,t) = -kv(0,t) \qquad \rightarrow \qquad EIX'''(0) = -kX(0) \tag{2.75}$$

At the right end

$$EI\frac{\partial^3 v}{\partial x^3}(\ell,t) = kv(\ell,t) \qquad \rightarrow \qquad EIX'''(\ell) = kX(\ell) \tag{2.76}$$

As previously observed, it is seen here that the constraint relations differ in sign at opposite beam ends. It should also be noted that the above conditions must be augmented by one additional condition at each end, since two are required. As illustrated in Fig. 2.18, in this instance the second condition would be zero bending moment.

Rotational elastic constraint

The rotational elastic constraint corresponds to a spring reaction moment that is equated to the bending moment. This is illustrated in Fig. 2.19. At the left end

$$EI\frac{\partial^2 v}{\partial x^2}(0,t) = k\frac{\partial v}{\partial x}(0,t) \qquad \rightarrow \qquad EIX''(0) = kX'(0) \tag{2.77}$$

At the right end

$$EI\frac{\partial^2 v}{\partial x^2}(\ell,t) = -k\frac{\partial v}{\partial x}(\ell,t) \qquad \rightarrow \qquad EIX''(\ell) = -kX'(\ell) \tag{2.78}$$

As in the previous case the signs differ and one more condition is required at each end.

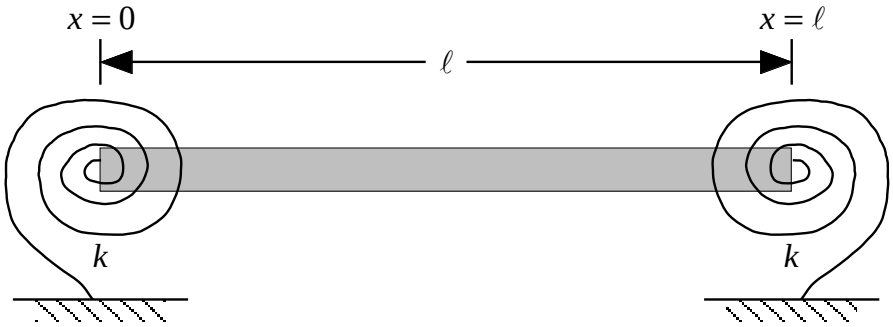

Figure 2.19: Schematic of rotational spring end conditions

Translational inertia constraint

The translational inertia constraint corresponds to the inertial reaction force associated with the translational acceleration of a rigid body or particle of mass m_c attached to the end for the beam, as illustrated in Fig. 2.20. This force is equated to the shear. At the left end

$$EI\frac{\partial^3 v}{\partial x^3}(0,t) = -m_c\frac{\partial^2 v}{\partial t^2}(0,t) \tag{2.79}$$

From the previously given general solution

$$\frac{\partial^2 v}{\partial t^2} = X(x)\ddot{Y}(t) = -\omega^2 X(x)Y(t) = -\omega^2 v = -a^4\alpha^4 v \tag{2.80}$$

and so the boundary condition can now be written as

$$EI\frac{\partial^3 v}{\partial x^3}(0,t) = m_c a^4\alpha^4 v(0,t) \qquad \rightarrow \qquad EIX'''(0) = m_c a^4\alpha^4 X(0) \tag{2.81}$$

At the right end the sign is changed as the result of the shear convention to yield

$$EIX'''(\ell) = -m_c a^4\alpha^4 X(\ell) \tag{2.82}$$

The above conditions must be augmented by one additional condition at each end, since two are required. As illustrated in Fig. 2.20, in this instance the second condition would be zero bending moment.

Rotational inertia constraint

The rotational inertia constraint corresponds to the inertial reaction moment associated with the rotational acceleration of a rigid body attached to the end of the beam, as shown in Fig. 2.21. This moment is equated to the bending moment. At the left end

$$EI\frac{\partial^2 v}{\partial x^2}(0,t) = I_c\frac{\partial^3 v}{\partial x\partial^2 t}(0,t) = -I_c a^4\alpha^4\frac{\partial v}{\partial x}(0,t) \tag{2.83}$$

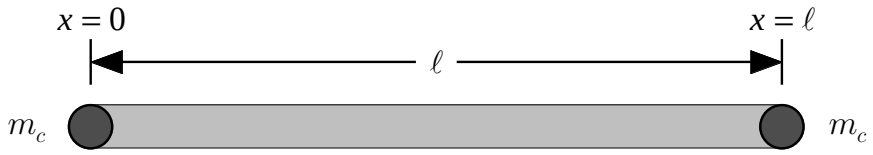

Figure 2.20: Schematic of translational mass end conditions

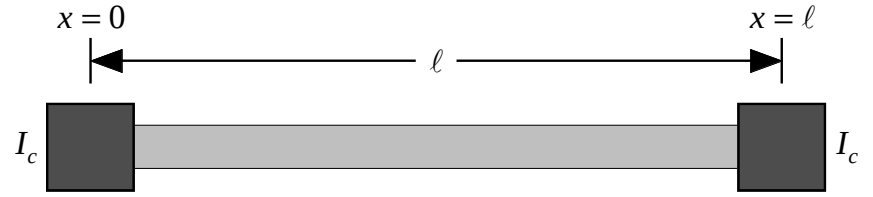

Figure 2.21: Schematic of rotational inertia end conditions

and so the boundary condition can now be written as

$$EIX''(0) = -I_c a^4 \alpha^4 X'(0) \tag{2.84}$$

At the right end the sign is changed as the result of the bending moment sign convention to yield

$$EIX''(\ell) = I_c a^4 \alpha^4 X'(\ell) \tag{2.85}$$

We note here that when the attached mass is idealized as a particle, then $I_c = 0$; and the moment boundary condition reduces to be the same as indicated above for the translational mass, that is, the bending moment is zero.

2.2.4 Example solution for clamped-free beam

Consider the clamped-free beam as shown in Fig. 2.22, the boundary conditions of which reduce to conditions on X given by

$$X(0) = X'(0) = X''(\ell) = X'''(\ell) = 0 \tag{2.86}$$

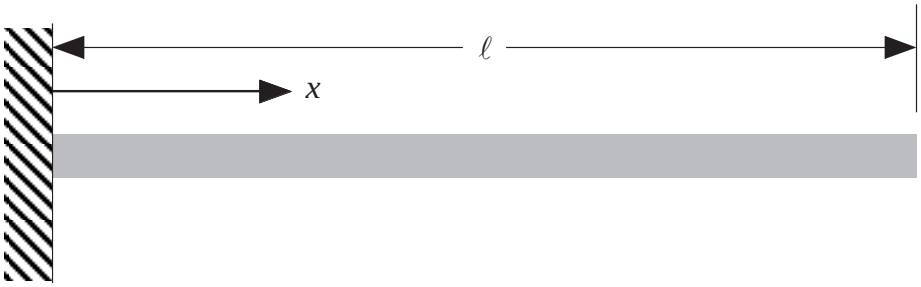

Figure 2.22: Schematic of clamped-free beam

As with the previous example, one can show that this problem exhibits no nontrivial solution for the case of $\alpha = 0$. Thus, we use the form of the general solution in Eqs. (2.74) for which $\alpha \neq 0$. Along with the first two boundary conditions, this yields

$$\begin{aligned} X(0) = 0 &\rightarrow E_3 = 0 \\ X'(0) = 0 &\rightarrow E_1 = 0 \end{aligned} \tag{2.87}$$

The remaining boundary conditions yield two homogeneous, algebraic equations which may be reduced to the form

$$\begin{bmatrix} \sinh(\alpha\ell) + \sin(\alpha\ell) & \cosh(\alpha\ell) + \cos(\alpha\ell) \\ \cosh(\alpha\ell) + \cos(\alpha\ell) & \sinh(\alpha\ell) - \sin(\alpha\ell) \end{bmatrix} \begin{Bmatrix} E_2 \\ E_4 \end{Bmatrix} = \begin{Bmatrix} 0 \\ 0 \end{Bmatrix} \tag{2.88}$$

It can be verified by applying Cramer's method for their solution that a nontrivial solution only exists if the determinant of the coefficients is equal to zero. This is typical of all nontrivial solutions to homogeneous, linear, algebraic equations, and here yields

$$\sinh^2(\alpha\ell) - \sin^2(\alpha\ell) - [\cosh(\alpha\ell) + \cos(\alpha\ell)]^2 = 0 \tag{2.89}$$

or, noting the identities

$$\begin{aligned} \sin^2(\alpha\ell) + \cos^2(\alpha\ell) &= 1 \\ \cosh^2(\alpha\ell) - \sinh^2(\alpha\ell) &= 1 \end{aligned} \tag{2.90}$$

one obtains the characteristic equation as simply

$$\cos(\alpha\ell)\cosh(\alpha\ell) + 1 = 0 \tag{2.91}$$

One cannot extract a closed-form exact solution for this transcendental equation. However, numerical solutions are easily obtained. Most numerical solution procedures require initial estimates of the solution in order for the procedure to converge. Since $\cosh(\alpha\ell)$ becomes large as its argument becomes large, one can argue that at least the larger roots will be close to those of $\cos(\alpha\ell) = 0$, or $\alpha_i\ell = (2i-1)\pi/2$. Indeed, the use of these values as initial estimates yields a set of numerical values that approach the initial estimates ever more closely as i becomes large. The values of $\alpha_i\ell$ (dimensionless quantities) are listed in Table 2.1. To six places, all values of $\alpha_i\ell$ for $i \geq 5$ are equal to $(2i-1)\pi/2$. The corresponding natural frequencies are given by

$$\omega_i = \alpha_i^2\sqrt{\frac{EI}{m}} = (\alpha_i\ell)^2\sqrt{\frac{EI}{m\ell^4}} \tag{2.92}$$

To obtain the mode shapes, one substitutes the values in Table 2.1 back into either of Eqs. (2.88). The resulting equation for the i^{th} mode has one arbitrary constant remaining (either E_{2i} or E_{4i} can be kept), which can be set equal to any number desired so as to normalize the resulting mode shape ϕ_i in some convenient way. For example, normalizing the solution by $-E_{4i}$, which is equivalent to setting $E_{4i} = -1$, one can show that

$$\phi_i = \cosh(\alpha_i x) - \cos(\alpha_i x) - \beta_i[\sinh(\alpha_i x) - \sin(\alpha_i x)] \tag{2.93}$$

i	$\alpha_i\ell$	$(2i-1)\pi/2$	β_i
1	1.87510	1.57080	0.734096
2	4.69409	4.71239	1.01847
3	7.85476	7.85398	0.999224
4	10.9955	10.9956	1.00003
5	14.1372	14.1372	0.999999

Table 2.1: Values of $\alpha_i\ell$, $(2i-1)\pi/2$, and β_i for i=1,...,5 for the clamped-free beam

where

$$\beta_i = -\frac{E_{2i}}{E_{4i}} = \frac{\cosh(\alpha_i\ell) + \cos(\alpha_i\ell)}{\sinh(\alpha_i\ell) + \sin(\alpha_i\ell)} \tag{2.94}$$

and

$$\begin{aligned} \int_0^\ell \phi_i^2 dx &= \ell \\ \phi_i(\ell) &= 2(-1)^{i+1} \end{aligned} \tag{2.95}$$

The values of β_i are also tabulated in Table 2.1. The first three mode shapes are depicted in Fig. 2.23. Note that the higher the mode number is, the more crossings of the zero displacement line occur.

2.3 Orthogonality of Mode Shapes

A most significant property of the mode shapes previously discussed is that they form a set of orthogonal mathematical functions. If the system is nonuniform then the mode shapes are orthogonal with respect to some inertial weighting function, such as the mass or sectional mass moment inertia distribution. For the string, the equation of motion for which is

$$T\frac{\partial^2 v}{\partial x^2} = m\frac{\partial^2 v}{\partial t^2} \tag{2.96}$$

the condition of functional orthogonality can be described analytically as

$$\begin{aligned} \int_0^\ell m\phi_i(x)\phi_j(x)\, dx &= 0 \qquad (i \neq j) \\ &\neq 0 \qquad (i = j) \end{aligned} \tag{2.97}$$

where $\phi_i(x)$ is the mode shape. To prove that the mode shapes obtained for the uniform string problem are orthogonal, an individual modal contribution given by

$$v_i(x,t) = \phi_i(x)\xi_i(t) \tag{2.98}$$

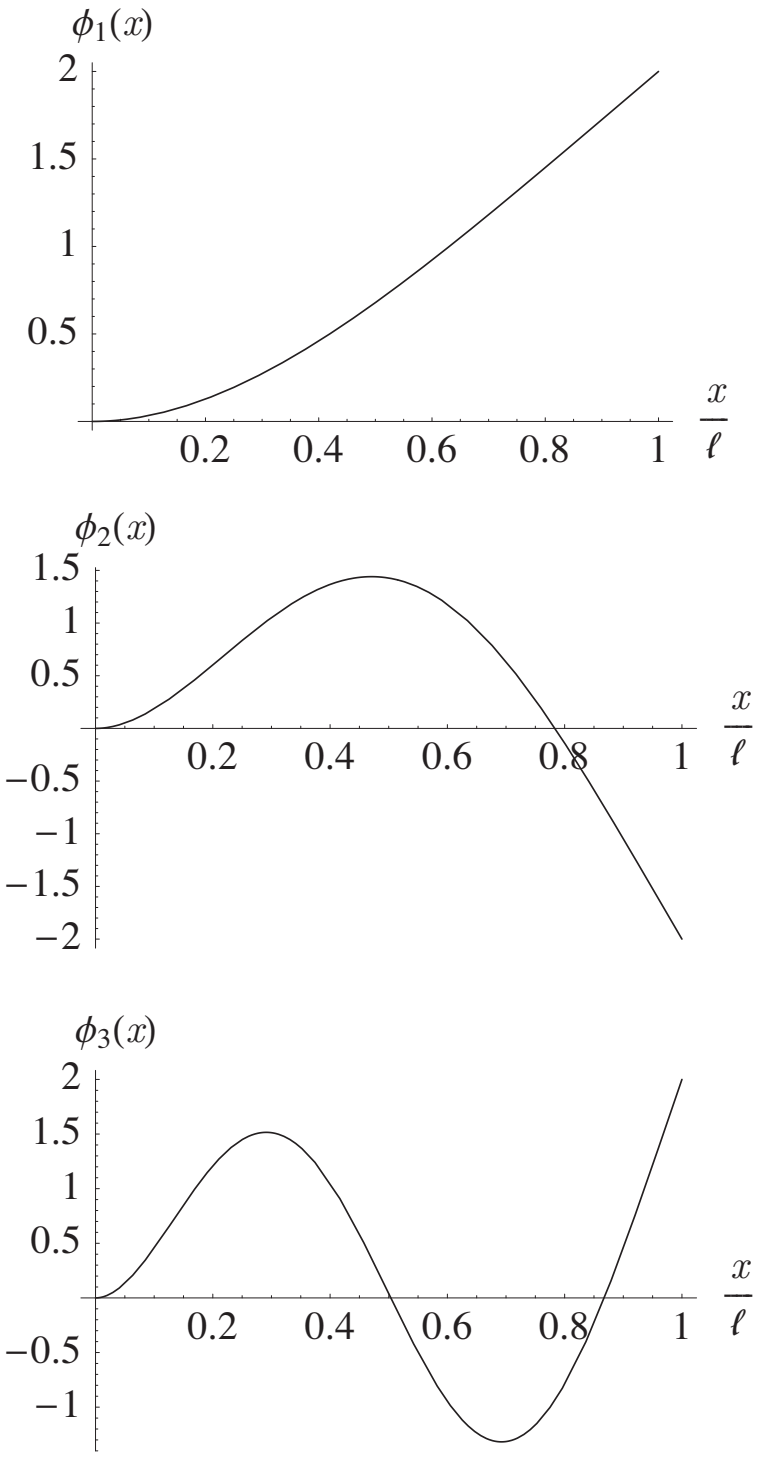

Figure 2.23: First three free-vibration mode shapes of a clamped-free beam in bending

is substituted into the governing differential equation (wave equation) to obtain

$$T\frac{\partial^2 v_i}{\partial x^2} = m\frac{\partial^2 v_i}{\partial t^2} \tag{2.99}$$

Because the generalized coordinate is a simple harmonic function for the homogeneous solution, then

$$\ddot{\xi}_i = -\omega_i^2\, \xi_i \tag{2.100}$$

and the wave equation becomes

$$T\phi_i''(x)\xi_i(t) = -m\phi_i(x)\omega_i^2\xi_i(t) \tag{2.101}$$

so that

$$T\phi_i''(x) = -m\phi_i(x)\omega_i^2 \tag{2.102}$$

If this procedure is repeated by substituting the j^{th} modal contribution into the wave equation, a similar result

$$T\phi_j''(x) = -m\phi_j(x)\omega_j^2 \tag{2.103}$$

is obtained. After multiplying Eq. (2.102) by ϕ_j and Eq. (2.103) by ϕ_i, subtracting, and integrating the result over the length of the string, we obtain

$$\left(\omega_i^2 - \omega_j^2\right) m \int_0^\ell \phi_i(x)\phi_j(x)dx = T\int_0^\ell \left[\phi_i(x)\phi_j''(x) - \phi_i''(x)\phi_j(x)\right] dx \tag{2.104}$$

The integral on the right-hand side can be integrated by parts using

$$\int_a^b udv = uv\Big|_a^b - \int_a^b vdu \tag{2.105}$$

by letting

$$\begin{aligned} u &= \phi_i \qquad du = \phi_i' dx \\ v &= \phi_j' \qquad dv = \phi_j'' dx \end{aligned} \tag{2.106}$$

for the first term and

$$\begin{aligned} u &= \phi_j \qquad du = \phi_j' dx \\ v &= \phi_i' \qquad dv = \phi_i'' dx \end{aligned} \tag{2.107}$$

for the second term. The result becomes

$$\begin{aligned} &\left(\omega_i^2 - \omega_j^2\right) m \int_0^\ell \phi_i(x)\phi_j(x)dx \\ &\quad = T\left(\phi_i\phi_j' - \phi_i'\phi_j\right)\Big|_0^\ell - T\int_0^\ell (\phi_i'\phi_j' - \phi_i'\phi_j')dx = 0 \end{aligned} \tag{2.108}$$

Note that the right-hand side is zero because ϕ_i is zero at both ends by virtue of the original boundary conditions. It may now be concluded that $\omega_i \neq \omega_j$ when $i \neq j$, so that

$$m \int_0^\ell \phi_i(x)\phi_j(x)dx = 0 \tag{2.109}$$

However, when $i = j$

$$m \int_0^\ell \phi_i^2(x)dx = M_i \tag{2.110}$$

This integral value, M_i, is called the "generalized mass" of the i^{th} mode. These relations thus demonstrate that the mode shapes for the string, which is fixed at both ends, form an orthogonal set of functions.

The above development is for a string of constant mass per unit length and constant tension force. It is important to note that it can readily be generalized for nonuniform mass per unit length. In more involved developments for beam bending and torsional deformation, the structural stiffnesses, which are analogous to the tension force in the string problem, may also be nonuniform along the span. Although these quantities may not be taken outside the integrals in such cases, the rest of the development remains quite similar.

2.3.1 Using Orthogonality

The property of orthogonality is very useful in many aspects of structural dynamics analysis. As an illustration, consider the so-called homogeneous initial condition problem for the string, the equation of motion for which is Eq. (2.96). In this case there are no external loads on the string, but it is presumed to have an initial deflection shape and an initial velocity distribution. Let these initial conditions be represented as

$$\begin{aligned} v(x,0) &= f(x) \\ \frac{\partial v}{\partial t}(x,0) &= g(x) \end{aligned} \tag{2.111}$$

where it should be noted that both $f(x)$ and $g(x)$ must certainly be compatible with the boundary conditions.

Using the solution, given as

$$\begin{aligned} v(x,t) &= \sum_{i=1}^{\infty} v_i(x,t) \\ &= \sum_{i=1}^{\infty} \sin\left(\frac{i\pi x}{\ell}\right)\left[E_i \sin\left(\sqrt{\frac{T}{m}}\frac{i\pi t}{\ell}\right) + F_i \cos\left(\sqrt{\frac{T}{m}}\frac{i\pi t}{\ell}\right)\right] \end{aligned} \tag{2.112}$$

these initial conditions can be written in terms of modal representation as

$$\begin{aligned} v(x,0) &= \sum_{i=1}^{\infty} F_i \sin\left(\frac{i\pi x}{\ell}\right) = f(x) \\ \frac{\partial v}{\partial t}(x,0) &= \sum_{i=1}^{\infty} \frac{E_i i\pi}{\ell}\sqrt{\frac{T}{m}} \sin\left(\frac{i\pi x}{\ell}\right) = g(x) \end{aligned} \tag{2.113}$$

Both of these relations will be multiplied by $\sin(j\pi x/\ell)$ and integrated over the length of the string, yielding

$$\begin{aligned} \int_0^{\ell} f(x) \sin\left(\frac{j\pi x}{\ell}\right) dx &= \sum_{i=1}^{\infty} F_i \int_0^{\ell} \sin\left(\frac{i\pi x}{\ell}\right) \sin\left(\frac{j\pi x}{\ell}\right) dx \\ &= F_j \int_0^{\ell} \sin^2\left(\frac{j\pi x}{\ell}\right) dx \\ &= \frac{F_j \ell}{2} \end{aligned} \tag{2.114}$$

The above evaluation has made use of the orthogonality property of the mode shapes, which causes every term in the infinite sum to be zero except where $i = j$. The initial velocity relation can be reduced in the same manner, so that

$$\begin{aligned} \int_0^{\ell} g(x) \sin\left(\frac{j\pi x}{\ell}\right) dx &= \sum_{i=1}^{\infty} \frac{E_i i\pi}{\ell}\sqrt{\frac{T}{m}} \int_0^{\ell} \sin\left(\frac{i\pi x}{\ell}\right) \sin\left(\frac{j\pi x}{\ell}\right) dx \\ &= \frac{E_j j\pi}{\ell}\sqrt{\frac{T}{m}} \int_0^{\ell} \sin^2\left(\frac{j\pi x}{\ell}\right) dx \\ &= \frac{E_j j\pi}{2}\sqrt{\frac{T}{m}} \end{aligned} \tag{2.115}$$

This treatment of the initial conditions permits a direct evaluation of the unknown constants (E_i and F_i) in the modal representation of the total string displacement; that is,

$$\begin{aligned} E_i &= \frac{2}{i\pi}\sqrt{\frac{m}{T}} \int_0^{\ell} g(x) \sin\left(\frac{i\pi x}{\ell}\right) dx \\ F_i &= \frac{2}{\ell} \int_0^{\ell} f(x) \sin\left(\frac{i\pi x}{\ell}\right) dx \end{aligned} \tag{2.116}$$

Thus, for the prescribed initial conditions given by $f(x)$ and $g(x)$, the resulting string displacement can be described as

$$v(x,t) = \sum_{i=1}^{\infty} \sin\left(\frac{i\pi x}{\ell}\right) \left[E_i \sin(\omega_i t) + F_i \cos(\omega_i t)\right] \tag{2.117}$$

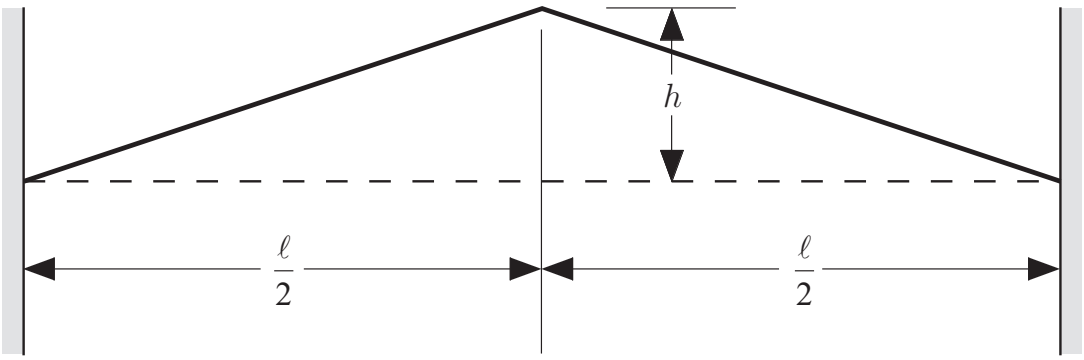

Figure 2.24: Initial shape of plucked string

2.3.2 Example: response due to given initial shape

To further illustrate this procedure consider the case of the plucked string with zero initial velocity. Let the initial shape be as shown in Fig. 2.24. If we assume the initial velocity to be zero, then $g(x) = 0$ and $E_i = 0$ for all i. The string displacement becomes

$$v(x,t) = \sum_{i=1}^{\infty} F_i \sin\left(\frac{i\pi x}{\ell}\right) \cos(\omega_i t) \tag{2.118}$$

To evaluate the constants, F_i, the initial string shape will be written as

$$\begin{array}{rll} f(x) = & 2h\left(\frac{x}{\ell}\right) & 0 \le x \le \frac{\ell}{2} \\ = & 2h\left(1 - \frac{x}{\ell}\right) & \frac{\ell}{2} \le x \le \ell \end{array} \tag{2.119}$$

Substituting this function into the preceding integral yields

$$\begin{aligned} F_i &= \frac{4h}{\ell^2}\left[\int_0^{\frac{\ell}{2}} x \sin\left(\frac{i\pi x}{\ell}\right) dx + \int_{\frac{\ell}{2}}^{\ell} (\ell - x) \sin\left(\frac{i\pi x}{\ell}\right) dx\right] \\ &= \frac{8h}{(i\pi)^2} \sin\left(\frac{i\pi}{2}\right) \end{aligned} \tag{2.120}$$

It may be noted that $\sin(i\pi/2)$ is zero for all even values of the index and that it is either positive or negative one for the odd values. If desired these constants can be written as

$$F_i = \begin{cases} \frac{8h}{(i\pi)^2}(-1)^{\frac{i-1}{2}} & (i \text{ odd}) \\ 0 & (i \text{ even}) \end{cases} \tag{2.121}$$

The fact that $F_i = 0$ for all even values of i is indicative of the symmetry of the initial string displacement about the midpoint. That is, since the initial shape is symmetric about $x = \ell/2$,

no antisymmetric modes of vibration are excited thereby. The total string displacement becomes

$$v(x,t) = \frac{8h}{\pi^2} \sum_{i=1,3,\ldots}^{\infty} \frac{(-1)^{\frac{i-1}{2}}}{i^2} \sin\left(\frac{i\pi x}{\ell}\right) \cos(\omega_i t) \tag{2.122}$$

where

$$\omega_i = \frac{i\pi}{\ell}\sqrt{\frac{T}{m}} \tag{2.123}$$

It should be noted from this solution that the modal contributions to the total displacement significantly decrease as the mode number (the index i) increases. This can be observed from the dependence of F_i on i. This is characteristic of almost all structural dynamics response problems and thus permits a truncation of the infinite sum to a finite number of the lower-order modes. It also should be noted that the above solution indicates that the string will vibrate forever, with the string returning to its initial shape periodically. In real systems there are always dissipative phenomena that cause the motion to die out in time. This will be considered when we deal with aeroelastic flutter in Chapter 5.

2.4 Principle of Virtual Work

The principle of virtual work provides an alternative for the Newtonian method for deriving equations of equilibrium and boundary conditions. Consider a system with strain energy U. The system is in equilibrium if and only if

$$\delta U = \overline{\delta W} \tag{2.124}$$

where δU is the variation of the strain energy and $\overline{\delta W}$ is the work done by all external forces through a virtual displacement of the configuration. Virtual displacements are any displacements that satisfy all the constraints on the system. The line over $\overline{\delta W}$ indicates that the virtual work is not the variation of any functional. Instead it can be found as the dot product of applied forces and virtual displacements.

For a discrete system, the configuration of which is described at any instant in time by n generalized coordinates $\xi_1(t)$, $\xi_2(t)$, $\ldots$, $\xi_n(t)$, the variation of U is defined as

$$\delta U \equiv \sum_{i=1}^{n} \frac{\partial U}{\partial \xi_i} \delta\xi_i \tag{2.125}$$

where $\delta\xi_i$ is an increment in ξ_i. The virtual work of applied loads is often represented as

$$\overline{\delta W} \equiv \sum_{i=1}^{n} \Xi_i \delta\xi_i \tag{2.126}$$

where Ξ_i is the generalized force associated with the i^{th} displacement.

2.5 Hamilton's Principle

The principle of virtual work, when the virtual work includes the work done by inertial loads through a virtual displacement, also applies to dynamical systems. However, it is more common to use Hamilton's principle in such situations. Hamilton's principle is an alternative to the Newtonian method for finding equations of motion and boundary conditions. Hamilton's principle in its most general form, usually referred to as Hamilton's extended principle, can be written as

$$\int_{t_1}^{t_2} \left[\delta(T-U) + \overline{\delta W}\right] dt = 0 \tag{2.127}$$

where T is the kinetic energy of the system, t is time, and t_1 and t_2 are arbitrary, fixed times.

For example, the equations of motion for the free vibration of a clamped-free beam in bending can be derived by Hamilton's principle as follows. First, the strain energy can be written as

$$U = \frac{1}{2}\int_0^\ell EI\left(\frac{\partial^2 v}{\partial x^2}\right)^2 dx \tag{2.128}$$

and the kinetic energy is

$$T = \frac{1}{2}\int_0^\ell m\left(\frac{\partial v}{\partial t}\right)^2 dx \tag{2.129}$$

where, as before, EI is the bending stiffness, m is the mass per unit length, v is the displacement of the reference line, and x is the axial coordinate. For this case the external forces are zero. Thus, Hamilton's principle gives

$$\int_{t_1}^{t_2}\int_0^\ell \left(m\frac{\partial v}{\partial t}\frac{\partial \delta v}{\partial t} - EI\frac{\partial^2 v}{\partial x^2}\frac{\partial^2 \delta v}{\partial x^2}\right) dx dt = 0 \tag{2.130}$$

We first integrate by parts in time, so that

$$m\frac{\partial v}{\partial t}\delta v\Big|_{t_1}^{t_2} - \int_{t_1}^{t_2}\int_0^\ell \left(m\frac{\partial^2 v}{\partial t^2}\delta v + EI\frac{\partial^2 v}{\partial x^2}\frac{\partial^2 \delta v}{\partial x^2}\right) dx dt = 0 \tag{2.131}$$

The first term vanishes by virtue of a choice for virtual displacements, which vanish at both t_1 and t_2. The remaining integral can be simplified because the time integral is no longer needed, so that

$$\int_0^\ell \left(m\frac{\partial^2 v}{\partial t^2}\delta v + EI\frac{\partial^2 v}{\partial x^2}\frac{\partial^2 \delta v}{\partial x^2}\right) dx = 0 \tag{2.132}$$

This equation is now a statement of the principle of virtual work for dynamic equilibrium of the vibrating beam at any instant in time. We can now integrate the last term by parts twice, yielding,

$$EI\frac{\partial^2 v}{\partial x^2}\frac{\partial \delta v}{\partial x}\Big|_0^\ell - \frac{\partial}{\partial x}\left(EI\frac{\partial^2 v}{\partial x^2}\right)\delta v\Big|_0^\ell + \int_0^\ell \left(m\frac{\partial^2 v}{\partial t^2} + EI\frac{\partial^4 v}{\partial x^4}\right)\delta v dx = 0 \tag{2.133}$$

By virtue of the arbitrariness of the virtual displacement δv over the interior and at a boundary that is not constrained, all three terms must vanish. Constraints on the displacement or rotation affect δv or $\partial \delta v / \partial x$ at the ends. If there is an absence of either type of constraint at the beam ends, one then has "natural" boundary conditions on shear or bending moment, respectively. The integral must vanish, and on account of the arbitrariness of δv, the integrand must vanish at all points on the interior of the beam.

As an example, consider the clamped-free case, for which $v(0,t) = \partial v(0,t)/\partial x = 0$. Thus, because δv and $\partial \delta v(0,t)/\partial x = 0$ must be constrained in the same way, the trailing terms in Eq. (2.133)

$$EI \frac{\partial^2 v}{\partial x^2} \frac{\partial \delta v}{\partial x} \bigg|_0^\ell \tag{2.134}$$

and

$$\frac{\partial}{\partial x} \left(EI \frac{\partial^2 v}{\partial x^2} \right) \delta v \bigg|_0^\ell \tag{2.135}$$

both vanish at $x = 0$. At $x = \ell$ those quantities are not constrained. Therefore,

$$EI \frac{\partial^2 v}{\partial x^2}(\ell, t) = 0 \tag{2.136}$$

and

$$\frac{\partial}{\partial x} \left(EI \frac{\partial^2 v}{\partial x^2} \right) (\ell, t) = 0 \tag{2.137}$$

This methodology is especially useful when there are springs and/or masses attached to the beam, as there is far less chance of making a sign error than with the Newtonian method.

2.6 Lagrange's Equations

One can easily deduce Lagrange's equations from either the virtual work principle or from Hamilton's Principle. They can be written as

$$\frac{d}{dt} \left(\frac{\partial L}{\partial \dot{\xi}_i} \right) - \frac{\partial L}{\partial \xi_i} = \Xi_i \qquad\qquad i = 1, 2, \ldots, n \tag{2.138}$$

Lagrange's equation provides an alternative method of derivation for discrete systems vis a vis the Newtonian method. It is also the basis for the application of the Ritz method when the energy is given approximately.

2.6.1 Generalized Force

The generalized force, $\Xi_i(t)$, which appears on the right-hand side of the generalized equations of motion, represents the effective loading associated with all forces and moments not

accounted for in P, which includes any nonconservative forces and moments. These forces and moments are most commonly identified as externally applied loads, which may or may not be a function of modal response. They will also include any dissipative loads such as those from dampers. To determine the contribution of distributed loads, denoted by $F(x,t)$, the virtual work will be computed as

$$\overline{\delta W} = \int_0^\ell F(x,t)\delta v(x,t)dx \tag{2.139}$$

The term $\delta v(x,t)$ represents the virtual displacement, which can be written in terms of the generalized coordinates and mode shapes as

$$\delta v(x,t) = \sum_{i=1}^{\infty} \phi_i(x)\delta\xi_i(t) \tag{2.140}$$

where $\delta\xi_i(t)$ is an arbitrary increment in the i^{th} generalized coordinate. Thus, the virtual work becomes

$$\begin{aligned} \overline{\delta W} &= \int_0^\ell \sum_{i=1}^{\infty} F\phi_i\delta\xi_i dx \\ &= \sum_{i=1}^{\infty} \delta\xi_i \int_0^\ell F\phi_i dx \end{aligned} \tag{2.141}$$

Identifying the generalized force as

$$\Xi_i(t) = \int_0^\ell F(x,t)\phi_i(x)dx \tag{2.142}$$

one finds that the virtual work reduces to

$$\overline{\delta W} = \sum_{i=1}^{\infty} \Xi_i \ \delta\xi_i \tag{2.143}$$

The loading $F(x,t)$ in the above development is a distributed load with units of force per unit length. If instead this loading is concentrated at one or more points say as $F_c(t)$ with units of force acting at $x = x_c$ as shown in Fig. 2.25, then its functional representation must include the Dirac delta function, $\delta(x - x_c)$, which is similar to the impulse function in the time domain. In this case the distributed load can be written as

$$F(x,t) = F_c(t)\delta(x - x_c) \tag{2.144}$$

It may be recalled that the Dirac delta function can be thought of as the limiting case of a rectangular shape with area held constant and equal to unity as its width goes to zero.

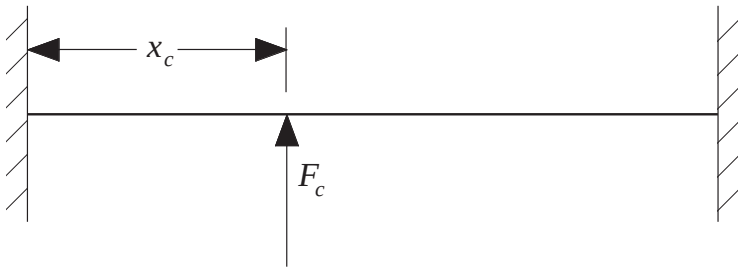

Figure 2.25: Concentrated force acting on beam

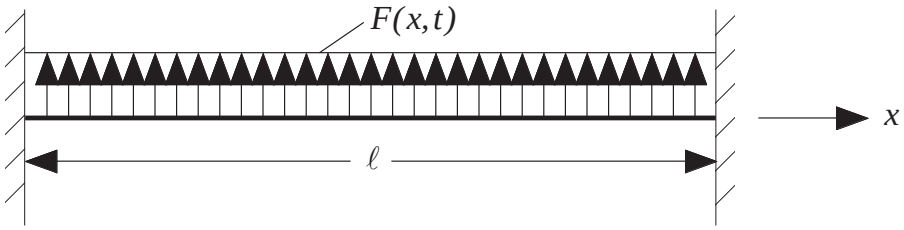

Figure 2.26: Distributed force $F(x,t)$ acting on beam

Thus, it may be defined by its integral property; for example, for $a < x_0 < b$

$$\begin{aligned} \int_a^b \delta(x - x_0)dx &= 1 \\ \int_a^b f(x)\delta(x - x_0)dx &= f(x_0) \end{aligned} \tag{2.145}$$

As a consequence the above integral expression for the generalized force can be applied to the concentrated load so that

$$\begin{aligned} \Xi_i(t) =& \int_0^\ell F_c(t)\delta(x - x_c)\phi_i(x)dx \\ =& F_c(t)\phi_i(x_c) \end{aligned} \tag{2.146}$$

2.6.2 Example calculation of generalized force

An example of a dynamically loaded beam will be considered to illustrate the generalized force computation. The specific example will be a uniformly distributed load of simple harmonic amplitude (in time) shown in Fig. 2.26 with

$$F(x,t) = \overline{F}\sin(\omega t) \tag{2.147}$$

Computation of the generalized force is simply

$$\Xi_i = \int_0^\ell \overline{F}\sin(\omega t)\phi_i(x)dx = \overline{F}\sin(\omega t)\int_0^\ell \phi_i(x)dx \tag{2.148}$$

With the above, the generalized equations of motion derive from Lagrange's equation and become

$$M_i(\ddot{\xi}_i + \omega_i^2\xi_i) = \overline{F}\sin(\omega t)\int_0^\ell \phi_i(x)dx \tag{2.149}$$

2.7 Ritz's Method

It also provides a set of approximate equations given the approximate discretization of a continuous system in terms of assumed modes based on the Ritz method. Building on the earlier treatment, we start with Lagrange's equations, given by

$$\frac{d}{dt}\left(\frac{\partial L}{\partial \dot{\xi}_i}\right) - \frac{\partial L}{\partial \xi_i} = \Xi_i \qquad\qquad i = 1, 2, \ldots, n \tag{2.150}$$

where the Lagrangean, $L = K - P$, the total kinetic energy is K, the total potential energy is P, n is the number of generalized coordinates retained, the generalized coordinates are ξ_i, and Ξ_i is the generalized force. Although it can be helpful, as we shall see below, it is not necessary to make use of potential energy, which can only account for conservative forces. The generalized force, however, can be used to include the effects of *any* loads. So as not to count the same physical effects more than once, the generalized force should only include those forces that are not accounted for in the potential energy. The generalized forces stem from virtual work, which can be written as

$$\overline{\delta W} = \sum_{i=1}^{n} \Xi_i \delta\xi_i \tag{2.151}$$

where $\delta\xi_i$ is an arbitrary increment in the i^{th} generalized coordinate.

Let us consider a beam in bending as an example. The total kinetic energy must include that of the beam as well as of any attached particles or rigid bodies. The contribution of the beam is

$$K_{\text{beam}} = \frac{1}{2}\int_0^\ell m\left(\frac{\partial v}{\partial t}\right)^2 dx \tag{2.152}$$

where m is the mass per unit length of the beam. The total potential energy $P = U + V$ comprises the internal strain energy of the beam, denoted by U, plus any additional potential energy, V, attributed to gravity, springs attached to the beam, or applied static loads. All other loads, such as aerodynamic loads, damping, follower forces, etc., must be accounted for in Ξ_i.

The strain energy for a beam in bending is given by

$$U = \frac{1}{2}\int_0^\ell EI\left(\frac{\partial^2 v}{\partial x^2}\right)^2 dx \tag{2.153}$$

The expression for V varies depending on the problem being addressed, as does the virtual work of all forces other than those accounted for in V. The virtual work can be written as

$$\overline{\delta W} = \int_0^\ell f(x,t)\delta v(x,t)dx \tag{2.154}$$

where δv is an increment of v in which time is held fixed and $f(x,t)$ is the distributed force per unit length and is positive in the direction of positive v.

To apply the Ritz method, one needs to express P, K, and $\overline{\delta W}$ in terms of a series of functions with one or more terms. For a beam in bending, this means that

$$v(x,t) = \sum_{i=1}^{n} \xi_i(t)\phi_i(x) \tag{2.155}$$

There are several characteristics that these "basis functions" ϕ_i must possess:

1. Each function at least must satisfy all boundary conditions on displacement and rotation (often called the "geometric" boundary conditions). It is not necessary that they satisfy the force and moment boundary conditions, but satisfaction of them may improve accuracy. However, it is not easy in general to find functions that satisfy all boundary conditions.

2. Each function must be continuous and p times differentiable, where p is the order of the highest spatial derivative in the Lagrangean. The p^{th} derivative of at least one function must be nonzero. Here, from Eq. (2.153), $p = 2$.

3. If more than one function is used, they must be chosen from a set of functions that is complete. This means that any function on the interval $0 \le x \le \ell$ and having the same boundary conditions as the problem under consideration can be expressed to any degree of accuracy whatsoever as a linear combination of the functions in the set. Examples of complete sets of functions on the interval $0 \le x \le \ell$ include

   $$1, x, x^2, \ldots$$
   $$\sin\left(\frac{\pi x}{\ell}\right), \sin\left(\frac{2\pi x}{\ell}\right), \sin\left(\frac{3\pi x}{\ell}\right), \ldots$$
   a set of mode shapes for *any* problem

   Completeness also implies that there can be no missing terms between the lowest and highest ones used in any series.

4. The set of functions must be linearly independent. This means that

$$\sum_{i=0}^{n} a_i \phi_i(x) = 0 \quad \Rightarrow \quad a_i = 0 \text{ for all } i \tag{2.156}$$

A set of functions that satisfies all these criteria is said to be "admissible."

By use of the series approximation, we have reduced a problem with an infinite number of degrees of freedom to one with n degrees of freedom. Instead of being governed by a partial differential equation, the behavior of this system is now defined by n second-order, ordinary differential equations in time. This reduction from a continuous system modeled by a partial differential equation with an infinite number of degrees of freedom to one described by a finite number of ordinary differential equations in time is sometimes called spatial discretization. The number n is usually increased until convergence is obtained. (It should be noted that if inertial forces are not considered, so that the kinetic energy is identically zero, then a system described by an ordinary differential equation in a single spatial variable is reduced by the Ritz method to one described by n algebraic equations.)

Now, let us illustrate how the approximating functions are actually used. Let ϕ_i, i=1, 2, ..., ∞, be a complete set of p-times differentiable, linearly independent functions that satisfy the displacement and rotation boundary conditions. Thus, U can be written as

$$U = \frac{1}{2} \sum_{i=1}^{n} \sum_{j=1}^{n} \xi_i \xi_j \int_0^\ell EI \phi_i'' \phi_j'' dx \tag{2.157}$$

The contributions of any springs that restrain the structure, as well as conservative loads, must be added to obtain the full potential energy P.

The kinetic energy of the beam is

$$K_{\text{beam}} = \frac{1}{2} \sum_{i=1}^{n} \sum_{j=1}^{n} \dot{\xi}_i \dot{\xi}_j \int_0^\ell m \phi_i \phi_j dx \tag{2.158}$$

Contributions of any additional particles and rigid bodies must be added to obtain the complete kinetic energy K.

The virtual work term must account for distributed and concentrated forces resulting from all other sources, such as damping, aerodynamics, etc. This can be written as

$$\overline{\delta W} = \sum_{i=1}^{n} \delta \xi_i \left[\int_0^\ell f(x,t) \phi_i dx + F_c(x_0,t) \phi_i(x_0) \right] \tag{2.159}$$

where x_0 is a value of x at which a concentrated force is located. Here the first term accounts for a distributed force $f(x,t)$ on the interior of the beam, and the second term accounts for a concentrated force on the interior. In aeroelasticity, the loads $f(x,t)$ and $F_c(x_0,t)$ may depend on the displacement in some complicated manner.

The integrands in the above quantities all involve the basis functions and their derivatives over the length of the beam. It should be noted that these integrals involve only known quantities and often can be evaluated analytically. Sometimes they are too complicated to undertake analytically, however, and they must be evaluated numerically. Numerical evaluation is often facilitated by nondimensionalization. Symbolic computation tools such as Mathematica™and Maple™may be quite helpful in both situations.

With all such things considered, the equations of motion can be written in a form that is quite common, that is,

$$[M]\left\{\ddot{\xi}\right\} + [C]\left\{\dot{\xi}\right\} + [K]\{\xi\} = \{F\} \tag{2.160}$$

where $\{\xi\}$ is a column matrix of the generalized coordinates, $\{F\}$ is a column matrix of the generalized force terms that do not depend on ξ_i, $(\dot{})$ is the time derivative of $(\ )$, $[M]$ is the mass matrix, $[C]$ is the gyroscopic/damping matrix, and $[K]$ is the stiffness matrix. The most important contribution to $[M]$ is from the kinetic energy, and this contribution is symmetric. The most important contribution to $[K]$ is from the strain energy of the structure and potential energy of any springs that restrain the motion of the structure. There can be contributions to all terms in the equations of motion from kinetic energy and virtual work. For example, there are contributions from kinetic energy to $[C]$ and $[K]$ when there is a rotating coordinate system. Damping makes contributions to $[C]$ through the virtual work. Finally, because aerodynamic loads in general depend on the displacement and its time derivatives, aeroelastic analyses may contain terms in $[M]$, $[C]$ and $[K]$ that stem from aerodynamic loads.

An interesting special case of this method occurs when the system is conservatively loaded. The resulting method is usually referred to as the Rayleigh-Ritz method, and there are many theorems that can be proved about the convergence of approximations to the natural frequency. Indeed, one of the most powerful of such theorems states that the approximate natural frequencies are always upper bounds, and another states that adding more terms to a given series always lowers the approximate natural frequencies (i.e., making them closer to the exact values).

A further specialized case is the simplest approximation, in which only one term is used. Then, an approximate expression for the lowest natural frequency can be written as a ratio called the Rayleigh quotient. This simplest special case is of more than merely academic interest. It is not at all uncommon that a rough estimate of the lowest natural frequency is needed early in the design of flexible structures.

2.7.1 Example: The Ritz Method Using Clamped-Free Modes

In the first example we consider a uniform, clamped-free beam that we modify by adding a tip mass of mass $\mu m\ell$. The exact solution can be easily obtained for this modified problem using the methodology spelled out earlier. However, it is desired here to illustrate the Ritz method, and we already have calculated the modes for a clamped-free beam (i.e., without a tip mass)

in Section 2.2.4. These mode shapes are solutions of an eigenvalue problem; and so, provided we do not skip any modes between the lowest and highest mode number that we use, this set is automatically complete. The set is also orthogonal and therefore linearly independent. Of course, these modes automatically satisfy the boundary conditions on displacement and rotation for our modified problem (since they are the same as for the clamped-free beam), and they are infinitely differentiable. Hence, they are admissible functions for the modified problem. Moreover, they satisfy the zero moment boundary condition at the free end, which is a boundary condition for our modified problem. However, because of the presence of the tip mass in the modified problem, the shear force, which the reader will recall is proportional to the third derivative of the displacement, does not vanish as it does for the clamped-free mode shapes.

The strain energy becomes

$$U = \frac{1}{2}\sum_{i=1}^{n}\sum_{j=1}^{n}\xi_i\xi_j\int_0^\ell EI\phi_i''\phi_j''dx \tag{2.161}$$

Substituting the mode shapes of Eq. (2.93) into Eq. (2.161) and taking advantage of orthogonality, one can simplify it to

$$U = \frac{\ell EI}{2}\sum_{i=1}^{n}\xi_i^2\alpha_i^4 \tag{2.162}$$

where α_i is the set of constants in Table 2.1. Similarly, accounting for the tip mass, the kinetic energy of which is

$$\begin{aligned} K_{\text{tip mass}} &= \frac{1}{2}\mu m\ell\left[\frac{\partial v}{\partial t}(\ell,t)\right]^2 \\ &= \frac{1}{2}\mu m\ell\sum_{i=1}^{n}\sum_{j=1}^{n}\dot{\xi}_i\dot{\xi}_j\phi_i(\ell)\phi_j(\ell) \end{aligned} \tag{2.163}$$

one obtains the total kinetic energy as

$$K = \frac{1}{2}\sum_{i=1}^{n}\sum_{j=1}^{n}\dot{\xi}_i\dot{\xi}_j\left[\int_0^\ell m\phi_i\phi_j dx + \mu m\ell\phi_i(\ell)\phi_j(\ell)\right] \tag{2.164}$$

With the use of the mode shapes of Eq. (2.93), one finds that $\phi_i(\ell) = 2(-1)^{i+1}$ and so the kinetic energy simplifies to

$$K = \frac{m\ell}{2}\sum_{i=1}^{n}\sum_{j=1}^{n}\dot{\xi}_i\dot{\xi}_j\left[\delta_{ij} + 4\mu(-1)^{i+j}\right] \tag{2.165}$$

where the Kronecker symbol $\delta_{ij} = 1$ for $i = j$ and $\delta_{ij} = 0$ for $i \neq j$. For free vibration, there are no additional forces. Thus, Lagrange's equations can be now written in matrix form as

$$[M]\left\{\ddot{\xi}\right\} + [\,\grave{}\,K\,\backprime\,]\{\xi\} = 0 \tag{2.166}$$

n	$\mu = 1$	$\mu = 10$	$\mu = 100$
1	1.57241	0.549109	0.175581
2	1.55964	0.542566	0.173398
3	1.55803	0.541748	0.173126
4	1.55761	0.541536	0.173055
5	1.55746	0.541458	0.173029
Exact	1.55730	0.541375	0.173001

Table 2.2: Approximate values of $\omega_1\sqrt{\frac{m\ell^4}{EI}}$ for clamped-free beam with tip mass of $\mu m\ell$ using n clamped-free modes of Section 2.2.4, Eq. (2.93)

where $[\grave{} K \acute{}]$ is a diagonal matrix with the diagonal elements given by

$$K_{ii} = EI\ell\alpha_i^4 \qquad\qquad i = 1, 2, \ldots, n \tag{2.167}$$

and $[M]$ is a symmetric matrix with elements given by

$$M_{ij} = m\ell\left[\delta_{ij} + 4\mu(-1)^{i+j}\right] \qquad\qquad i, j = 1, 2, \ldots, n \tag{2.168}$$

Assuming $\xi = \overline{\xi}\exp(i\omega t)$, one can write Eq. (2.166) as an eigenvalue problem of the form

$$\left[[\grave{} K \acute{}] - \omega^2[M]\right]\left\{\overline{\xi}\right\} = 0 \tag{2.169}$$

Results for the first modal frequency are shown in Table 2.2 and compared therein with the exact solution. As one can see, the approximate solution agrees with the exact solution to within engineering accuracy with only two terms. By way of contrast, results for the second modal frequency are shown in Table 2.3. These results are not nearly as accurate. Results for the higher modes, not shown, are less accurate still. This is one of the problems with modal approximation methods; fortunately, however, aeroelasticians and structural dynamicists are frequently interested only in the lower-frequency modes. Note that the one-term approximation (i.e., the Rayleigh quotient) is within 1.1% for all values of μ displayed.

2.7.2 Example: The Ritz Method Using a Simple Power Series

As an alternative to using the mode shapes of a closely related problem, let us repeat the solution of the above using a simple power series to construct a series of functions ϕ_i. Since the moment vanishes at the free end where $x = \ell$, one can make the second derivative of all terms proportional to $\ell - x$. To get a complete series, one can multiply this term by a complete power series $1, x, x^2$, etc. Thus, one may then write the second derivative of the i^{th} function as

$$\phi_i'' = \frac{1}{\ell^2}\left(1 - \frac{x}{\ell}\right)\left(\frac{x}{\ell}\right)^{i-1} \tag{2.170}$$

n	$\mu = 1$	$\mu = 10$	$\mu = 100$
2	16.5580	15.8657	15.7867
3	16.3437	15.6191	15.5367
4	16.2902	15.5576	15.4744
5	16.2708	15.5353	15.4518
Exact	16.2501	15.5115	15.4277

Table 2.3: Approximate values of $\omega_2\sqrt{\frac{m\ell^4}{EI}}$ for clamped-free beam with tip mass of $\mu m\ell$ using n clamped-free modes of Section 2.2.4, Eq. (2.93)

With the boundary conditions on displacement and rotation being $\phi_i(0) = \phi_i'(0) = 0$, one can then integrate to find an expression for the i^{th} function as

$$\phi_i = \frac{\left(\frac{x}{\ell}\right)^{i+1}\left[2 + i - i\left(\frac{x}{\ell}\right)\right]}{i\,(1+i)\,(2+i)} \tag{2.171}$$

Since the chosen admissible functions have non-zero third derivatives at the tip, they offer the possibility of satisfying the non-zero shear condition in combination with each other. Such admissible functions are sometimes called *quasi-comparison* functions.

In this case, the stiffness matrix becomes

$$K_{ij} = \frac{2EI}{\ell^3\,(i+j-1)\,(i+j)\,(1+i+j)} \qquad i,j = 1,2,\ldots,n \tag{2.172}$$

and the mass matrix

$$\begin{aligned} M_{ij} =& \frac{2m\ell\,[3(i^2+j^2)+7ij+23(i+j)+40]}{ij\,(i+1)\,(i+2)\,(j+1)\,(j+2)\,(i+j+3)\,(i+j+4)\,(i+j+5)} \\ &+ \frac{4\,\mu m\ell}{ij\,(i+1)\,(i+2)\,(j+1)\,(j+2)} \qquad i,j = 1,2,\ldots,n \end{aligned} \tag{2.173}$$

Results from this calculation are given in Tables 2.4 and 2.5 for the first two modes. It is clear that these results are *much* better than those obtained with the clamped-free beam modes. It is not unusual for polynomial functions to provide better results than those obtained with beam mode shapes. However, here it is worth noting that the beam mode shapes are at a disadvantage for this problem. Unlike the problem being solved (and the polynomials chosen), the beam mode shapes are constrained to have zero shear force at the free end and are thus not quasi-comparison functions for the problem with a tip mass. This one-term polynomial approximation (i.e., the Rayleigh quotient) is within 0.05%, which is exceptionally good given its simplicity.

It is sometimes suggested that the mode shapes of a closely related problem are, at least in some sense, superior to other approximate sets of functions. For example, in the first

n	$\mu = 1$	$\mu = 10$	$\mu = 100$
1	1.55812	0.541379	0.173001
2	1.55733	0.541375	0.173001
3	1.55730	0.541375	0.173001
4	1.55730	0.541375	0.173001
5	1.55730	0.541375	0.173001
Exact	1.55730	0.541375	0.173001

Table 2.4: Approximate values of $\omega_1\sqrt{\frac{m\ell^4}{EI}}$ for clamped-free beam with tip mass of $\mu m\ell$ using n polynomial functions

n	$\mu = 1$	$\mu = 10$	$\mu = 100$
2	16.2853	15.5443	15.4605
3	16.2841	15.5371	15.4524
4	16.2505	15.5119	15.4280
5	16.2501	15.5116	15.4277
Exact	16.2501	15.5115	15.4277

Table 2.5: Approximate values of $\omega_2\sqrt{\frac{m\ell^4}{EI}}$ for clamped-free beam with tip mass of $\mu m\ell$ using n polynomial functions

example we did see that the orthogonality of the modes used resulted in a diagonal stiffness matrix. That does provide a slight advantage in the ease of computing the eigenvalues. However, for the low-order problems of the sort we are discussing, that advantage is hardly noticeable. Indeed, symbolic computation tools such as Mathematica™and Maple™are capable of calculating the eigenvalues for problems of the size of this example in but a few seconds. Moreover, in some cases the simplicity of carrying out the integrals that result in approximate formulations is a more important factor in deciding what set of functions to use in a standard implementation of the Ritz method. Indeed, polynomial functions are generally much easier to deal with analytically than free-vibration modes such as those illustrated in Section 2.7.1, which frequently involve transcendental functions.

Alternatives to the standard Ritz method include the methods of Galerkin, finite elements, component mode synthesis and influence coefficients. We shall touch on Galerkin's method in the next section. Detailed descriptions of the other approaches may be found in more advanced texts on structural dynamics and aeroelasticity. The finite element method is by far the most popular way of solving realistic structural dynamics and aeroelasticity problems in industry. The finite element method can be developed as a special case of the Ritz method, and it typically makes use of polynomial shape functions over each of the finite elements into which the original structure is broken. Finite element equations have the same structure as Eq. (2.160) but are typically of large order, with n being of the order of thousands to millions. What keeps the computational effort from being overly burdensome is that the matrices have a narrow-banded structure, which allows specialized software to be used in solving the equations of motion that takes advantage of this structure, reducing both memory and floating point operations and resulting in very significant computational advantages.

2.8 Galerkin's Method

Rather than making use of energy and Lagrange's equation as with the Ritz method, Galerkin's method starts with the partial differential equation of motion. Let us denote this equation by

$$\mathcal{L}[v(x,t)] = 0 \tag{2.174}$$

where $\mathcal{L}$ is an operator on the unknown function $v(x,t)$ with maximum spatial partial derivatives of the order q. For the structural dynamics problems we have addressed so far, the operator $\mathcal{L}$ is linear and $q = 2p$, where p is the maximum order of spatial partial derivative in the Lagrangean. It is important to note, however, that it is not true in general that $q = 2p$; indeed, one does not need to consider the Lagrangean at all with this method.

To apply Galerkin's method, one needs to express $v(x,t)$, and hence the operator $\mathcal{L}$ in terms of a series of functions with one or more terms. For a beam in bending, for example,

this means as before that

$$v(x,t) = \sum_{j=1}^{n} \xi_j(t)\phi_j(x) \tag{2.175}$$

Relative to the basis functions used in the Ritz method, the characteristics that these functions ϕ_i must possess for use in Galerkin's method are more stringent:

1. Each function must satisfy all boundary conditions. Note that it is not easy in general to find functions that satisfy all boundary conditions.

2. Each function must be at least q times differentiable. The q^{th} derivative of at least one function must be nonzero.

3. If more than one function is used, they must be chosen from a set of functions that is complete.

4. The set of functions must be linearly independent.

Functions that satisfy all these criteria are said to be "comparison functions." The original partial differential equation is then multiplied by ϕ_i and integrated over the domain of the independent variable (say, $0 \leq x \leq \ell$). Thus, a set of n ordinary differential equations is obtained from the original partial differential equation. (It should be noted that if the original equation is an ordinary differential equation in x, then Galerkin's method yields n algebraic equations.)

Let us consider a beam in bending as an example. The equation of motion can be written as in Eq. (2.61), with a slight change in notation, as

$$\frac{\partial^2}{\partial x^2}\left(EI\frac{\partial^2 v}{\partial x^2}\right) + m\frac{\partial^2 v}{\partial t^2} - f(x,t) = 0 \tag{2.176}$$

where EI is the flexural rigidity, m is the mass per unit length, and the boundary conditions and loading term $f(x,t)$ must reflect any attached particles or rigid bodies. In aeroelasticity, the loads $f(x,t)$ may depend on the displacement in some complicated manner.

With all the ingredients as described above considered, the discretized equations of motion can be written in the same form as with the Ritz method, that is,

$$[M]\left\{\ddot{\xi}\right\} + [C]\left\{\dot{\xi}\right\} + [K]\{\xi\} = \{F\} \tag{2.177}$$

where $\{\xi\}$ is a column matrix of the generalized coordinates, $\{F\}$ is a column matrix of the generalized force terms that do not depend on ξ_i, $(\dot{})$ is the time derivative of $(\ )$, $[M]$ is the mass matrix, $[C]$ is the gyroscopic/damping matrix, and $[K]$ is the stiffness matrix. As before, inertial forces contribute to $[M]$, and there are contributions from the inertial forces to $[C]$ and $[K]$ when there is a rotating coordinate system; and damping also contributes to $[C]$. Finally, because aeroelastic loads in general depend on the displacement and its time derivatives, aerodynamics can contribute terms to $[M]$, $[C]$ and $[K]$.

2.8.1 Example: Galerkin's Method for a Beam in Bending

Now, let us illustrate how the approximating functions are actually used. Let ϕ_i, i=1, 2, ..., ∞, be a complete set of q-times differentiable, linearly independent functions that satisfy all the boundary conditions. Substituting Eq. (2.175) into Eq. (2.176), multiplying by $\phi_i(x)$, and integrating over x from 0 to ℓ, one obtains

$$\int_0^\ell \phi_i \left[\sum_{j=1}^n \xi_j (EI\phi_j'')'' + \sum_{j=1}^n \ddot{\xi}_j m\phi_j - f(x,t) \right] dx = 0 \qquad i = 1, 2, \ldots, n \tag{2.178}$$

After reversing the order of integration and summation and integrating the first term by parts, taking into account the boundary conditions, this equation becomes

$$\sum_{j=1}^n \left(\xi_j \int_0^\ell EI\phi_i''\phi_j'' dx + \ddot{\xi}_j \int_0^\ell m\phi_i\phi_j dx \right) - \int_0^\ell f\phi_i dx = 0 \qquad i = 1, 2, \ldots, n \tag{2.179}$$

When one compares the first two terms with the earlier derivation by the Ritz method, one sees the close relationship between these approaches. Indeed, if the starting partial differential equation is derivable from energy, which implies that $q = 2p$, and the same modal functions ϕ_i are used in both cases, the resulting discretized equations are the same.

Considering the clamped-free case, for example, one can develop a set of comparison functions by starting with

$$\phi_i'' = \frac{1}{\ell^2} \left(1 - \frac{x}{\ell}\right)^2 \left(\frac{x}{\ell}\right)^{i-1} \tag{2.180}$$

With the boundary conditions on displacement and rotation being $\phi_i(0) = \phi_i'(0) = 0$, one can then integrate to find an expression for the i^{th} function as

$$\phi_i = \frac{\left(\frac{x}{\ell}\right)^{1+i} \left\{ 6 + i^2 \left(1 - \frac{x}{\ell}\right)^2 + i \left[5 - \frac{6x}{\ell} + \left(\frac{x}{\ell}\right)^2 \right] \right\}}{i(1+i)(2+i)(3+i)} \tag{2.181}$$

Elements of the stiffness matrix can be found as

$$\begin{aligned} K_{ij} &= \int_0^\ell EI\phi_i''\phi_j'' dx \\ &= \frac{24EI}{\ell^3 (i+j-1)(i+j)(1+i+j)(2+i+j)(3+i+j)} \end{aligned} \tag{2.182}$$

Similarly, the elements of the mass matrix can be found as

$$\begin{aligned} M_{ij} &= \int_0^\ell m\phi_i\phi_j dx \\ &= \frac{m\ell p_1}{p_2} \end{aligned} \tag{2.183}$$

n	mode 1	mode 2	mode 3
1	3.53009	-	-
2	3.51604	22.7125	-
3	3.51602	22.0354	66.2562
4	3.51602	22.0354	61.7675
5	3.51602	22.0345	61.7395
exact	3.51602	22.0345	61.6972

Table 2.6: Approximate values of $\omega_i\sqrt{\frac{m\ell^4}{EI}}$ for i=1, 2, and 3, for a clamped-free beam using n polynomial functions

where

$$\begin{aligned} p_1 =& 30240 + 28512(i+j) + 9672(i^2+j^2) + 1392(i^3+j^3) + 72(i^4+j^4) \\ &+ 20040ij + 4520(i^2j+ij^2) + 320(i^3j+ij^3) + 520i^2j^2 \\ p_2 =& i(1+i)(2+i)(3+i)j(1+j)(2+j)(3+j)(3+ \\ & i+j)(4+i+j)(5+i+j)(6+i+j)(7+i+j) \end{aligned} \tag{2.184}$$

The fact that the governing equation is derivable from energy is reflected in the symmetry of $[M]$ and $[K]$. Results for free vibration (i.e., with $f = 0$) are given in Table 2.6. As with the Ritz method, one sees monotonic convergence from above and accuracy comparable to that achieved via the Ritz method. However, unlike the Ritz method, one does not always obtain results for free-vibration problems that converge from above.

2.8.2 Example: Galerkin's Method for a Beam in Bending Using an Alternative Form of the Equation of Motion

Consider again a clamped-free beam. To obtain an alternative equation of motion we integrate the equation of motion twice and use the zero shear and bending moment boundary conditions to obtain an integro-partial differential equation

$$EI\frac{\partial^2 v}{\partial x^2} + \int_x^\ell (x-\zeta)\left[f(\zeta,t) - m\frac{\partial^2 v(\zeta,t)}{\partial t^2}\right]d\zeta = 0 \tag{2.185}$$

where ζ is a dummy variable. Although this equation of motion is somewhat more complicated, it is only a second-order equation. Thus, it has only two boundary conditions, which are zero displacement and slope at $x = 0$. Thus, a much simpler set of comparison functions can be used, such as a simple power series x^2, x^3, ..., that is,

$$\phi_i = x^{i+1} \qquad i = 1, 2, \ldots, n \tag{2.186}$$

n	mode 1	mode 2	mode 3
1	7.48331	-	-
2	3.84000	57.2822	-
3	3.44050	24.1786	188.677
4	3.52131	20.3280	69.3819
5	3.51698	22.0793	53.2558
6	3.51607	22.1525	61.0295
exact	3.51602	22.0345	61.6972

Table 2.7: Approximate values of $\omega_i\sqrt{\frac{m\ell^4}{EI}}$ for i=1, 2, and 3, for a clamped-free beam using n terms of a power series with a reduced-order equation of motion

We should not expect greater accuracy from this simple set of functions, but the analytical effort is considerably less. Indeed, the elements of the stiffness matrix are

$$\begin{aligned} K_{ij} &= \int_0^\ell EI\phi_i\phi_j''dx \\ &= \frac{EIj(j+1)}{\ell(i+j+1)} \end{aligned} \tag{2.187}$$

and the elements of the mass matrix are

$$\begin{aligned} M_{ij} &= \int_0^\ell \phi_i \int_x^\ell (\zeta - x)m\phi_j(\zeta)d\zeta\, dx \\ &= \frac{m\ell^3}{(2+i)(3+i)(5+i+j)} \end{aligned} \tag{2.188}$$

Note that these matrices are not symmetric. Moreover, the results that are presented in Table 2.7 are not as accurate as those obtained before in Table 2.6, and the convergence is not monotonic from above.

The partial differential equations that govern the free vibration of beams in torsion and bending can be derived from energy-based approaches, such as Hamilton's principle. In those cases, the Ritz and Galerkin's methods give the same results when used with the same assumed mode functions. As we see here, however, Galerkin's method provides a viable alternative to the Ritz method in cases where the equations of motion are not of the form presented earlier in this chapter.

Chapter 3

OPERATOR NOTATION

Referring back to Fig. 1.1, one sees that there are three disciplines involved with aeroelasticity. One way to formally show the interaction of these three fields is through operator notation, which also provides a vehicle for solving problems of aeroelasticity in a high-level language of sorts. There are three types of operators: considering a set of generalized coordinates ξ, let us denote the inertial forces as $\Xi_I = \mathcal{I}(\xi)$, the aerodynamic forces as $\Xi_A = \mathcal{A}(\xi)$, the structural forces as $\Xi_S = \mathcal{S}(\xi)$ and external disturbances as Ξ_0. Although it is not required for the operators to be linear, most of the applications of operator notation in the literature are for the linear case. Here we will consider only the linear case.

3.1 Structural operators

Structural operators operate on the elastic deflections to yield the internal forces. They may be used to describe the behavior of an elastic flight vehicle under a system of applied loads from some other source. This operator notation is a convenient means to write down the

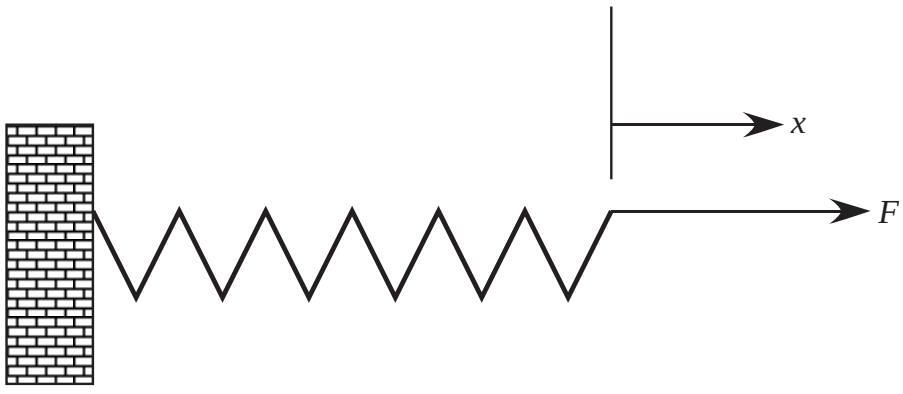

Figure 3.1: Schematic of a spring element undergoing a force F through a displacement x

governing equations for a system, because it encompasses algebraic, differential, integral, or matrix-based.

Consider a simple spring as shown in Fig. 3.1. The force across the spring element (i.e., the "internal force" of the spring) is F and is equal to the product of the spring constant k and the deflection across the spring x, so that $F = kx$ where the operator $\mathcal{S} = k$, $\xi = x$, and $\Xi_S = \mathcal{S}(\xi) = kx$. Here the structural operator is simply algebraic.

A more complex and meaningful illustration is a uniform beam undergoing applied distributed loading, so that the displacement v is governed by

$$EI\frac{d^4v}{dx^4} = F \tag{3.1}$$

as depicted in Fig. 2.26. Here the structural operator $\mathcal{S}$ is EId^4/dx^4, a differential operator.

When the operators are in matrix form as they frequently are with "real-life" problems, this lends itself easily to solution by numerical means. One way to obtain the operator in matrix form is to convert the governing equations to the form of an integral equation. For example, consider a nonuniform beam undergoing torsional deflection due to an applied distributed torque, the equation of equilibrium for which is

$$\frac{dT}{dx} = -t \tag{3.2}$$

where here t is the applied, distributed moment per unit span and T is the internal torque equal to the moment of all transverse shearing stresses on the cross-sectional plane at x. As before

$$T \equiv GJ\frac{d\theta}{dx} \tag{3.3}$$

where θ is the rotational angle due to torsion at x. From the point of view of continuum mechanics, the structural operator is the differential operator

$$\frac{d}{dx}\left(GJ\frac{d}{dx}\right) \tag{3.4}$$

The integral form of the structural operator can be useful. For this problem we postulate a structural influence function, $C^{\theta\theta}(x,\eta)$, which relates applied torque $t(\eta)$ per unit span to the resulting twist θ. Now,

$$d\theta(x) = C^{\theta\theta}(x,\eta)t(\eta)d\eta \tag{3.5}$$

Integrating with respect to η over the entire beam length we obtain

$$\theta(x) = \int_0^\ell C^{\theta\theta}(x,\eta)t(\eta)d\eta \tag{3.6}$$

$C^{\theta\theta}(x,\eta)$ is the value of θ at x due to a unit concentrated torque at η. The internal torque for this condition is easily found by noting that

$$\frac{dT}{dx} = -\delta(x-\eta) \tag{3.7}$$

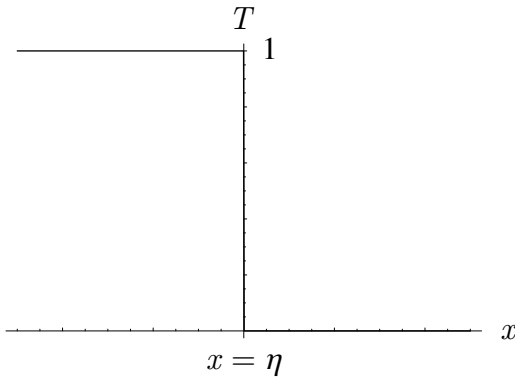

Figure 3.2: Schematic of internal twisting moment at x for unit applied twisting moment at η

For a beam with the $x = 0$ end fixed and the $x = \ell$ end free, we then stipulate that $T(\ell) = 0$ so that

$$T = \int_x^\ell \delta(x - \eta)dx = \begin{cases} 1 & x \leq \eta \\ 0 & x \geq \eta \end{cases} \tag{3.8}$$

This relationship is depicted in Fig. 3.2. Therefore, with Eq. (3.3) one finds that

$$C^{\theta\theta}(x, \eta) = \begin{cases} \int_0^x \frac{d\lambda}{GJ(\lambda)} & x \leq \eta \\ \int_0^\eta \frac{d\lambda}{GJ(\lambda)} & x \geq \eta \end{cases} \tag{3.9}$$

When this equation cannot be integrated analytically, one must resort to a numerical approach.

Once we have the influence function, it can used in equations such as Eq. (3.6) to obtain θ (or whatever the displacement variable under consideration is). The integral in such cases can be represented numerically in terms of weighting numbers. Let us introduce weights W_i for i=1, 2, ..., n such that

$$I = \int_a^b f(x)dx \approx \sum_{i=1}^n f_i W_i \tag{3.10}$$

where the coordinate axis x is subdivided into intervals and an appropriate integration routine is applied, such as the trapezoidal rule, Simpson's rule, Gaussian quadrature, etc. The number n could represent the number of intervals, the number of grid points, or the number of Gaussian quadrature points. In the above example matrix notation can be used as

$$I = \lfloor 1 \quad 1 \quad \dots \quad 1 \rfloor [\grave{} W \acute{}] \{f\} \tag{3.11}$$

where $[\grave{} W \acute{}]$ is a diagonal matrix with the weights W_i on the diagonal. For example, this procedure can be applied to our beam (here representing an elastic lifting surface) to yield

$$\{\theta\} = \left[C^{\theta\theta}\right] [\grave{} W \acute{}] \{t\} \tag{3.12}$$

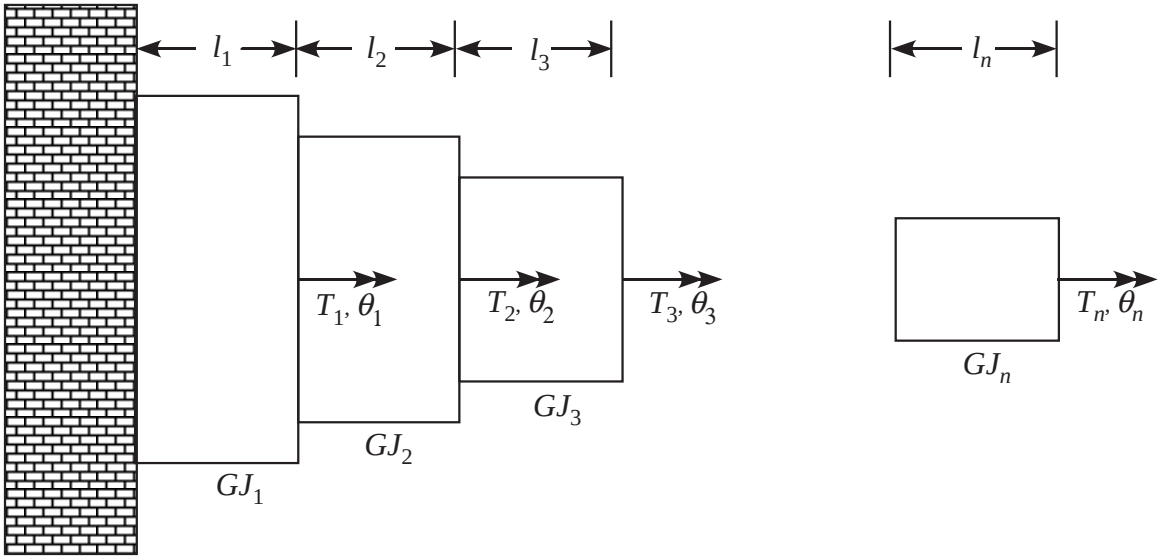

Figure 3.3: Schematic of a tapered beam with internal torques discretized

A complementary concept to the structural influence function is the matrix of structural influence coefficients. To examine this possibility, it is of interest to construct the structural operator from a different point of view, namely letting the beam be broken up into segments of length l_i for i=1, 2, ..., n as in Fig. 3.3. Letting

$$\{\theta\} = \begin{Bmatrix} \theta_1 \\ \theta_2 \\ \vdots \\ \theta_n \end{Bmatrix} \qquad \{T\} = \begin{Bmatrix} T_1 \\ T_2 \\ \vdots \\ T_n \end{Bmatrix} \tag{3.13}$$

where T_i is the internal torque at $x = x_i = l_1 + l_2 + \ldots + l_i$ and θ_i is the rotation at that point. The matrix operator takes the form

$$\{\theta\} = \left[C^{\theta\theta}\right] \{T\} \tag{3.14}$$

where $\left[C^{\theta\theta}\right]$ is a matrix of influence coefficients and is a way of representing the response of the structure. In particular, C_{ij} is the response θ_i at $x = x_i$ to a unit internal torque at $x = x_j$. We should note that $\{T\}$ can be regarded as an approximation of $[\grave{W}\acute{}]\{t\}$ for a particular quadrature rule that takes t as piecewise constant so that $T_i = t_i \Delta x_i$.

To construct the matrix $[C^{\theta\theta}]$ we consider the first element, governed by

$$\frac{d\theta}{dx} = \frac{T_1}{GJ_1} \tag{3.15}$$

and the boundary condition on $\theta(0) = 0$ so that

$$\theta = \frac{T_1}{GJ_1}x \tag{3.16}$$

where the constant of integration is zero owing to the boundary condition. Thus,

$$\theta_1 = \frac{T_1 l_1}{GJ_1} \tag{3.17}$$

The torques at values of $x > x_1$ are simply passed through the outboard elements so that

$$\theta_1 = \frac{T_2 l_1}{GJ_1} \qquad \theta_1 = \frac{T_3 l_1}{GJ_1} \quad \ldots \quad \theta_1 = \frac{T_n l_1}{GJ_1} \tag{3.18}$$

so that for all i

$$C_{1i} = \frac{l_1}{GJ_1} \qquad i = 1, 2, \ldots, n \tag{3.19}$$

If there are no other loads, all values of θ_i outboard of where the unit torque is applied are the same, so that

$$\theta_1 = \frac{T_1 l_1}{GJ_1} \qquad \theta_2 = \frac{T_1 l_1}{GJ_1} \quad \ldots \quad \theta_n = \frac{T_1 l_1}{GJ_1} \tag{3.20}$$

or

$$C_{i1} = \frac{l_1}{GJ_1} \qquad i = 1, 2, \ldots, n \tag{3.21}$$

Moving to the second element, for a torque T_2 at $x = x_2$

$$\theta_2 = \theta_1 + \frac{T_2 l_2}{GJ_2} = \frac{T_2 l_1}{GJ_1} + \frac{T_2 l_2}{GJ_2} \tag{3.22}$$

By the same logic as above, the response θ_2 for torques acting outboard of $x = x_2$ is

$$\theta_2 = \frac{T_3 l_1}{GJ_1} + \frac{T_3 l_2}{GJ_2} \qquad \theta_2 = \frac{T_4 l_1}{GJ_1} + \frac{T_4 l_2}{GJ_2} \quad \ldots \quad \theta_2 = \frac{T_n l_1}{GJ_1} + \frac{T_n l_2}{GJ_2} \tag{3.23}$$

and the response at values of $x > x_2$ to a torque T_2 at $x = x_2$ is

$$\theta_3 = \frac{T_2 l_1}{GJ_1} + \frac{T_2 l_2}{GJ_2} \qquad \theta_4 = \frac{T_2 l_1}{GJ_1} + \frac{T_2 l_2}{GJ_2} \quad \ldots \quad \theta_n = \frac{T_2 l_1}{GJ_1} + \frac{T_2 l_2}{GJ_2} \tag{3.24}$$

Thus,

$$C_{22} = \frac{l_1}{GJ_1} + \frac{l_2}{GJ_2} \tag{3.25}$$

and

$$C_{2i} = C_{i2} = \frac{l_1}{GJ_1} + \frac{l_2}{GJ_2} \qquad i = 2, 3, \ldots, n \tag{3.26}$$

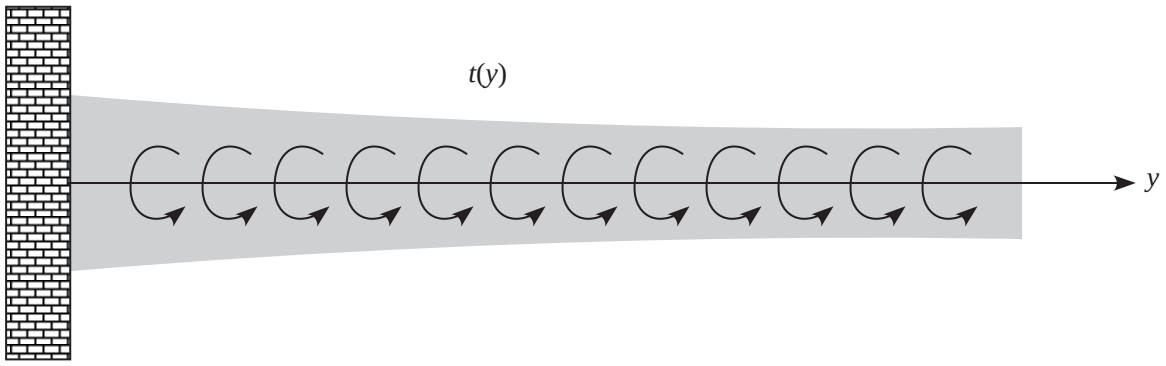

Figure 3.4: Schematic of a tapered beam with distributed external torque

By induction it can be shown that

$$\left[C^{\theta\theta}\right] = \begin{bmatrix} \frac{l_1}{GJ_1} & \frac{l_1}{GJ_1} & \cdots & \frac{l_1}{GJ_1} \\ \frac{l_1}{GJ_1} & \frac{l_1}{GJ_1} + \frac{l_2}{GJ_2} & \cdots & \frac{l_1}{GJ_1} + \frac{l_2}{GJ_2} \\ \vdots & \vdots & \frac{l_1}{GJ_1} + \frac{l_2}{GJ_2} + \frac{l_3}{GJ_3} & \cdots \\ \vdots & \vdots & \vdots & \frac{l_1}{GJ_1} + \ldots + \frac{l_n}{GJ_n} \end{bmatrix} \tag{3.27}$$

which is none other than the flexibility matrix of the tapered beam in torsion. One can make this as simple or as complex as the problem demands.

Now it is clear that

$$\{\theta\} = \left[C^{\theta\theta}\right]\{T\} \tag{3.28}$$

so that

$$\{T\} = \left[C^{\theta\theta}\right]^{-1}\{\theta\} \tag{3.29}$$

and the structural operator is the inverse of $\left[C^{\theta\theta}\right]$. While the influence coefficient matrix relates to the flexibility of the structure (i.e., the response at station i due to a load at station j), the inverse relates to the structural stiffness matrix as the force at i to maintain a unit displacement (or rotation) at j holding all other coordinates fixed. Thus, the structural operator shows up here as the structural stiffness matrix. So here, $\mathcal{S}(\xi) = \left[C^{\theta\theta}\right]^{-1}\{\theta\}$ in accordance with the convention on the operator notation.

It is seen from the above that either the structural influence functions or coefficients can be used to represent the static equilibrium of a structure as a matrix equation. These concepts are not just complementary – they are equivalent to within the degree of approximation in the discretization method. The structural operator can also be found by other methods, including, for example, the finite element method. Indeed, when dealing with complex systems it is often convenient to model the structure through a discrete approach such as the finite element method.

For example, consider a cantilevered wing subjected to a distributed torque $t(y)$ as depicted in Fig. 3.4. Note that the coordinate along the wing is taken to be y in accordance with the standard convention of aeroelasticity. The total potential energy of the system can be written as

$$U + V = \frac{1}{2}\int_0^\ell GJ(y)\left(\frac{d\theta}{dy}\right)^2 dy - \int_0^\ell t(y)\theta dy \tag{3.30}$$

where $GJ(y)$ is the torsional stiffness of the wing and $\theta(y)$ the elastic twist. In the finite element approach, the wing is divided into a number of elements as shown in Fig. 3.3. Although there is no requirement to make the elements of constant stiffness, we will do so anyway for convenience. Element i is connected to two end nodes i and $i+1$ with coordinates y_i and y_{i+1}, respectively. Within element i, the torsional stiffness is assumed to be a constant GJ_i. The discrete values of the twist and applied torque per unit span at the node i are denoted θ_i and t_i, respectively. Both twist and applied moment are linearly interpolated between the nodal values so that

$$\begin{aligned}\theta(y) =& \theta_i + \frac{y - y_i}{\ell_i}\left(\theta_{i+1} - \theta_i\right)\\ t(y) =& t_i + \frac{y - y_i}{\ell_i}\left(t_{i+1} - t_i\right)\end{aligned} \tag{3.31}$$

where $\ell_i = y_{i+1} - y_i$. Introducing this approximation into the total potential energy expression, Eq. (3.30), and integrating over the wing span yields

$$U + V = \frac{1}{2}\{\theta\}^T[K]\{\theta\} - \{\theta\}^T[D]\{t\} \tag{3.32}$$

where the array $\{\theta\}$ stores the values of the twist at the nodes

$$\{\theta\}^T = \lfloor \theta_1\, \theta_2\, \cdots\, \theta_n \rfloor \tag{3.33}$$

and the array $\{t\}$ the values of the applied torques per unit span at the nodes

$$\{t\}^T = \lfloor t_1, t_2, \cdots t_n \rfloor \tag{3.34}$$

The stiffness matrix $[K]$ is found as

$$[K] = \begin{bmatrix} \frac{GJ_1}{\ell_1} & -\frac{GJ_1}{\ell_1} & 0 & 0 & 0 & 0 & \cdots \\ -\frac{GJ_1}{\ell_1} & \frac{GJ_1}{\ell_1} + \frac{GJ_2}{\ell_2} & -\frac{GJ_2}{\ell_2} & 0 & 0 & 0 & \cdots \\ 0 & -\frac{GJ_2}{\ell_2} & \frac{GJ_2}{\ell_2} + \frac{GJ_3}{\ell_3} & -\frac{GJ_3}{\ell_3} & 0 & 0 & \cdots \\ 0 & 0 & -\frac{GJ_3}{\ell_3} & \frac{GJ_3}{\ell_3} + \frac{GJ_4}{\ell_4} & -\frac{GJ_4}{\ell_4} & 0 & \cdots \\ 0 & 0 & 0 & \cdots & \cdots & \cdots & \cdots \end{bmatrix} \tag{3.35}$$

and the loading matrix $[D]$ is

$$[D] = \begin{bmatrix} \frac{\ell_1}{3} & \frac{\ell_1}{6} & 0 & 0 & 0 & 0 & \cdots \\ \frac{\ell_1}{6} & \frac{\ell_1}{3} + \frac{\ell_2}{3} & \frac{\ell_2}{6} & 0 & 0 & 0 & \cdots \\ 0 & \frac{\ell_2}{6} & \frac{\ell_2}{3} + \frac{\ell_3}{3} & \frac{\ell_3}{6} & 0 & 0 & \cdots \\ 0 & 0 & \frac{\ell_3}{6} & \frac{\ell_3}{3} + \frac{\ell_4}{3} & \frac{\ell_4}{6} & 0 & \cdots \\ 0 & 0 & 0 & \cdots & \cdots & \cdots & \cdots \end{bmatrix} \tag{3.36}$$

The Principle of Minimum Total Potential Energy states that *among all kinematically admissible displacement fields, the displacement field that corresponds to the equilibrium configuration of the system makes the total potential energy $U + V$ an absolute minimum.* Admissibility is defined and discussed in Chapter 2. Given the approximation of the twist field in Eq. (3.31), the only unknowns of the problem are the nodal twists θ_i (except for the boundary condition $\theta_1 = 0$), and the principle implies

$$\frac{\partial(U+V)}{\partial\{\theta\}} = [K]\{\theta\} - [D]\{t\} = \{0\} \tag{3.37}$$

Hence, the discretized governing equations for the system are

$$[K]\{\theta\} = [D]\{t\} \tag{3.38}$$

Comparing Eqs. (3.38) and the operator form $\Xi_S = \mathcal{S}(\xi)$, it is clear that $\Xi = \{t\}$ is the nodal torque per unit span applied to the system, the displacement $\{\xi\} = \{\theta\}$ the column matrix of resulting nodal twists, and $\mathcal{S} = [D]^{-1}[K]$, *i.e.* the structural operator is again a matrix stiffness operator.

Very complex wing structures, or entire aircraft structures can be modeled with the finite element method. The resulting discretized equations will be similar to Eq. (3.38) where $\{\theta\}$ is an array of nodal displacements and/or rotations, $\{t\}$ an array of nodal forces and/or torques, and $[K]$ a stiffness matrix characterizing the elastic behavior of the entire structure. As the complexity of the model increases, the size of the various arrays increases. It is not uncommon to have tens of thousands or even hundreds of thousands of degrees of freedom to model a complete wing structure. It should be noted that although the size of the stiffness matrix $[K]$ can be very large, this matrix posesses important properties. First, it is banded, i.e. the non-vanishing entries are concentrated around the diagonal of the matrix. Second, it is at least positive semi-definite and, in the absence of rigid-body modes, it is positive-definite since it results from the computation of the strain energy of the structure, itself a positive-definite quantity when rigid-body motion is excluded.

3.2 Aerodynamic operators

For the aerodynamic operator, we want an operation on something related to deflection (such as angle of attack or pitch angle) to yield the applied force or moment caused by aerodynamics. We want to describe the relation between lift distribution and the angle of attack as it varies along the wing. Unfortunately, to use operator notation for the aerodynamics requires that many assumptions be made.

A simple aerodynamic operator can be derived by invoking the assumption of "strip theory" – that each sectional "strip" of the wing acts independently of all the others. Given a wing section at angle of attack α we have the sectional lift (i.e., the lift per unit span) as

$$L' = qcc_\ell \tag{3.39}$$

where c is the airfoil chord, c_ℓ is the sectional lift coefficient, and q is the dynamic pressure given by

$$q = \frac{1}{2}\rho_\infty U^2 \tag{3.40}$$

where U is the freestream velocity and ρ_∞ is the freestream air density. In the linear range $c_\ell = a_0\alpha$, where a_0 is the slope of the lift curve and is a constant, independent of the angle of attack. The value of a_0 is 2π for the case of incompressible flow over a flat plate; this value is used only if there are neither experimental data nor CFD results available.

The lift acting on the airfoil then becomes

$$L' = qca_0\ \alpha \tag{3.41}$$

which can be written symbolically as $\Xi_A = \mathcal{A}(\xi)$, where Ξ_A represents L', the sectional lift applied on the airfoil, ξ is the angular displacement, and $\mathcal{A}$ the aerodynamic operator. Comparing Eqs. (3.41) with $\Xi_A = \mathcal{S}(\xi)$, it is clear that $\xi = \alpha$, the angle of attack, $\Xi_A = L'$ the resulting aerodynamic force applied on the airfoil, and $\mathcal{A} = qca_0$, the aerodynamic operator, which in this case is simply an algebraic entity.

In the above, even for a spanwise uniform wing, both c_ℓ and α are functions of the spanwise coordinate y because of the nonuniformity of the wing twist and hence the angle of attack. Let us now broaden this description to treat spanwise nonuniform wings in a manner consistent with the operator notation. Owing to the way certain aerodynamic theories make use of Eq. (3.39) and the quantity cc_ℓ, we rewrite the relation as

$$\alpha = \frac{c_\ell}{a_0} = \frac{cc_\ell}{a_0 c} \tag{3.42}$$

Introducing

$$\{\alpha\} = \begin{Bmatrix} \alpha_1 \\ \alpha_2 \\ \vdots \\ \alpha_n \end{Bmatrix} \qquad \{cc_\ell\} = \begin{Bmatrix} (cc_\ell)_1 \\ (cc_\ell)_2 \\ \vdots \\ (cc_\ell)_n \end{Bmatrix} \tag{3.43}$$

one can then write

$$\begin{Bmatrix} \alpha_1 \\ \alpha_2 \\ \vdots \\ \alpha_n \end{Bmatrix} = \begin{bmatrix} \frac{1}{(a_0c)_1} & 0 & \cdots & 0 \\ 0 & \frac{1}{(a_0c)_2} & 0 & \vdots \\ \vdots & 0 & \ddots & 0 \\ 0 & \cdots & 0 & \frac{1}{(a_0c)_n} \end{bmatrix} \begin{Bmatrix} (cc_\ell)_1 \\ (cc_\ell)_2 \\ \vdots \\ (cc_\ell)_n \end{Bmatrix} \tag{3.44}$$

or

$$\{\alpha\} = [\mathcal{A}]^{-1}\{cc_\ell\} \tag{3.45}$$

where the aerodynamic operator here assumes the form of a matrix of influence coefficients $\mathcal{A}_{ij}$ as the cc_ℓ at station i dues to an angle of attack at station j.

Prandtl's 3-D lifting line theory is a generalization of strip theory that takes into account the interaction of the strips with each other. It only applies to the full span of an unswept wing; see Section 4.5.1. For steady, incompressible flow one may write

$$\alpha(y) = \underbrace{\frac{cc_\ell}{a_0 c}}_{\text{strip theory}} + \underbrace{\frac{1}{8\pi}\int_{-\frac{\ell}{2}}^{\frac{\ell}{2}} \frac{d}{d\eta}(cc_\ell)\frac{d\eta}{y-\eta}}_{\text{correction for finite span}} \tag{3.46}$$

It should be noted that the correction term tends to zero as the wingspan ℓ tends to infinity. The lifting line theory is easily put into the matrix form of Eq. (3.45) where the aerodynamic operator assumes the form of a matrix of influence coefficients

$$[\mathcal{A}^{-1}] = \begin{bmatrix} \frac{1}{(a_0 c)_1} & 0 & \cdots & 0 \\ 0 & \frac{1}{(a_0 c)_2} & 0 & \vdots \\ \vdots & 0 & \ddots & 0 \\ 0 & \cdots & 0 & \frac{1}{(a_0 c)_n} \end{bmatrix} + \frac{1}{8\ell}\begin{bmatrix} b_{11} & b_{12} & \cdots & b_{1n} \\ b_{21} & b_{22} & \cdots & b_{2n} \\ \vdots & \vdots & \ddots & \vdots \\ b_{n1} & b_{n2} & \cdots & b_{nn} \end{bmatrix} \tag{3.47}$$

where b_{ij} can be calculated from the integral in Eq. (3.46).

This lifting line theory can be used for unswept wings for which $\mathcal{AR} \geq 4$. Otherwise another method must be used, such as Humbold's theory. There are analytical corrections for compressibility, aspect ratio, and small sweep angles. For example, the correction for compressibility can be undertaken by using a corrected lift curve slope

$$a = \frac{a_0}{\sqrt{1 - M_\infty^2}} \tag{3.48}$$

for 2-D or

$$a = \frac{a_0}{a_0\left(\frac{1+\tau}{\pi \mathcal{AR}}\right) + \sqrt{1 - M_\infty^2}} \tag{3.49}$$

for 3-D, where $0.1 \leq \tau \leq 0.3$ is a correction factor. To account for small to moderate sweep angles in the presence of incompressibility, one may let

$$a = \frac{a_0 \cos\Lambda}{\sqrt{1 - M_\infty^2 \cos^2\Lambda}} \tag{3.50}$$

for 2-D or

$$a = \frac{a_0 \cos\Lambda}{a_0\left(\frac{1+\tau}{\pi \mathcal{AR}}\right) + \sqrt{1 - M_\infty^2 \cos^2\Lambda}} \tag{3.51}$$

for 3-D.

3.3 Inertial operators

The inertial operator acts on the deflections to yield the inertia forces. For a particle of mass m in rectilinear motion along x, the inertia force is

$$F_I = -m\frac{d^2x}{dt^2} = \mathcal{I}(\xi) \tag{3.52}$$

so that in the operator notation we can write

$$\mathcal{I} = -m\frac{d^2}{dt^2} \tag{3.53}$$

with $\xi = x$. In the case of simple harmonic motion, the inertial operator takes the form of $\mathcal{I} = m\omega^2$ where ω is the frequency of the sinusoidal motion.

3.4 Summary

Now, in terms of the operator notation, the governing equation(s) for any aeroelastic problem can be put into the form

$$\mathcal{S}(\xi) = \mathcal{A}(\xi) + \mathcal{I}(\xi) + \Xi_0 \tag{3.54}$$

where the external disturbance Ξ_0 is not dependent on any configuration or motion variable. It would be used, for example, to represent the effects of a gust. Now, if $\mathcal{A} = 0$, we have a structural dynamics problem. Instead, if $\mathcal{I} = 0$, we have a static aeroelasticity problem. A flutter problem would be posed with $\Xi_0 = 0$, and a dynamic response problem would have all terms present.

Problems

1. Consider the planar bending of a cantilevered beam with bending stiffness

$$EI = EI_0 \left(1 - \frac{x}{\ell}\right) + \frac{EI_0}{2}\frac{x}{\ell}$$

   (a) Defining the influence function $C^{ww}(x, \eta)$ as the deflection at x due to a unit force at η, find $C^{ww}(x, \eta)$ analytically.

   (b) Using segments with piecewise constant stiffness, determine the matrix of structural influence coefficients.

   (c) Using the trapezoidal rule, determine the matrix of structural influence coefficients.

   (d) Varying the number of segments, compare the results of parts 1b and 1c with the exact solution for a uniformly distributed load. You may assume that a solution using either a numerical ODE solver or numerical quadrature from MATLAB™ is for all intents and purposes exact.

Chapter 4

STATIC AEROELASTICITY

The field of static aeroelasticity is the study of flight vehicle phenomena associated with the interaction of aerodynamic loading induced by steady flow and the resulting elastic deformation of the lifting surface structure. These phenomena do not involve time as a variable and are characterized as being insensitive to the rates and accelerations of the structural deflections. There are two classes of design problems that are encountered in this area. The first and most common to all flight vehicles is the effect of elastic deformation on the airloads associated with normal operating conditions. These effects can have a profound influence on the performance, handling qualities, flight stability, structural load distribution, and control effectiveness/reversal phenomena. The second class of problems involves the potential for static instability of the structure that will result in a catastrophic failure. This instability is often termed "divergence" and can impose a limit on the flight envelope.

The material presented in this chapter provides an introduction to some of these static aeroelastic phenomena. To illustrate the physical mechanics of these problems and maintain a low level of mathematical complexity, relatively simple configurations are considered. The first items treated are rigid aerodynamic models that are elastically mounted in the test section of a wind tunnel. Such elastic mounting is characteristic of most load measurement systems. The second aeroelastic configuration to be treated is a uniform elastic lifting surface of finite span. Its static aeroelastic properties are quite similar to most lifting surfaces on conventional flight vehicles. Finally, the analysis of nonuniform lifting surfaces will be illustrated.

4.1 Rigid Wind-Tunnel Models on Flexible Supports

In this section we consider three types of mounting for wind-tunnel models: wall-mounted, sting-mounted, and strut-mounted. Expressions for the aeroelastic pitch deflections are developed for these simple models that, in turn, lead us to a cursory understanding of the divergence instability. Finally, we will return to the wall-mounted model briefly in this section to consider the qualitatively different phenomenon of aileron reversal.

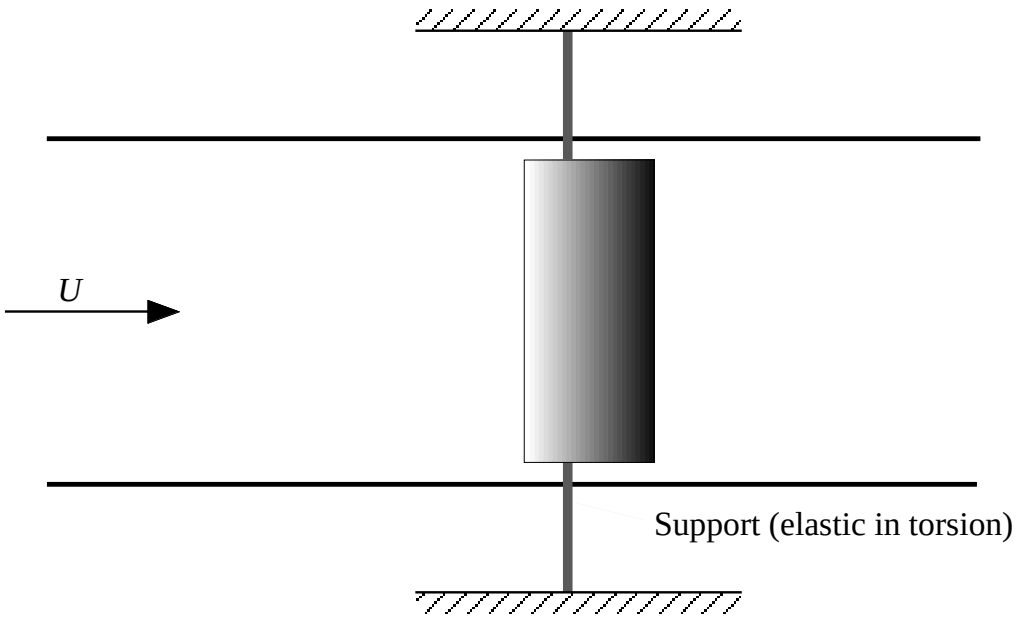

Figure 4.1: Planform view of a rigid wind-tunnel model on a torsionally elastic support

4.1.1 Wall-Mounted Model

Consider a rigid, spanwise-uniform model of a wing that is mounted to the side walls of a wind tunnel in such a way as to allow the wing to pitch about the support axis, as illustrated in Fig. 4.1. The support is flexible in torsion, which means that it restricts the pitch rotation of the wing in the same way as a rotational spring would. We denote the rotational stiffness of the support by k; see Fig. 4.2. If we assume the body to be pivoted about its support O, located at a distance x_O from the leading edge, moment equilibrium requires that the sum of all moments about O must equal zero. In anticipation of using linear aerodynamics, we assume the angle of attack, α, to be a small angle, such that $\sin(\alpha) = \alpha$ and $\cos(\alpha) = 1$. Thus,

$$M_{\text{ac}} + L\left(x_O - x_{\text{ac}}\right) - W\left(x_O - x_{\text{cg}}\right) - k\theta = 0 \tag{4.1}$$

If the support were rigid, the angle of attack would be α_{r}, positive nose-up. The elastic part of the pitch angle is denoted by θ, which is also positive nose-up. The wing angle of attack is then $\alpha \equiv \alpha_{\text{r}} + \theta$. For linear aerodynamics, the lift for a rigid support is simply

$$L_{\text{rigid}} = qSC_{L_\alpha}\alpha_{\text{r}} \tag{4.2}$$

whereas the lift for an elastic support is

$$L = qSC_{L_\alpha}\left(\alpha_{\text{r}} + \theta\right) \tag{4.3}$$

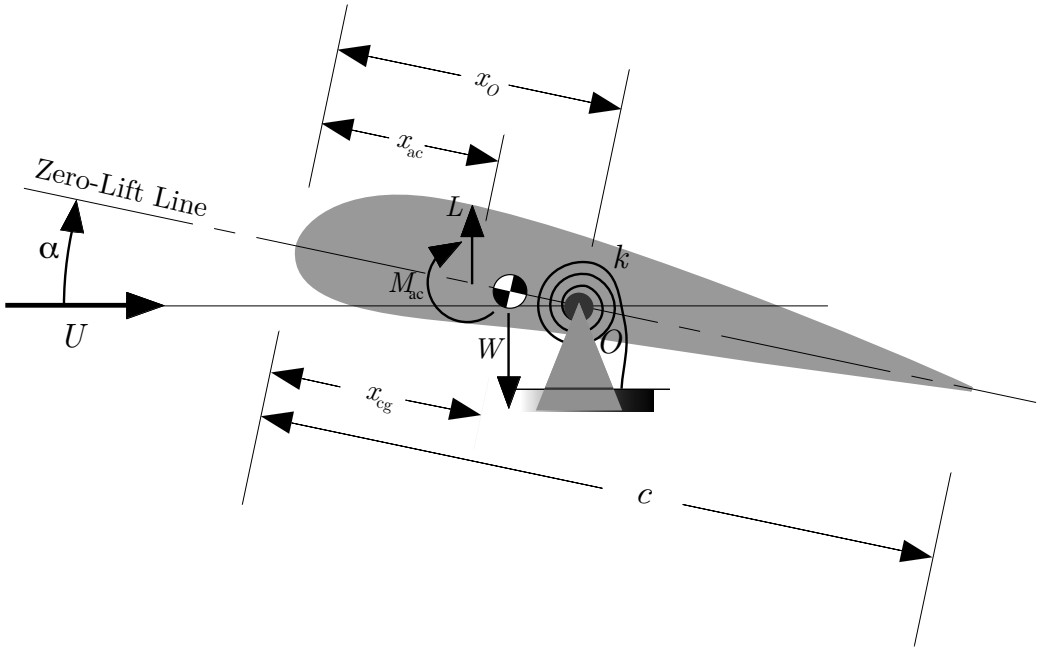

Figure 4.2: Airfoil for wind-tunnel model

where $q = \frac{1}{2}\rho_\infty U^2$ is the freestream dynamic pressure (i.e., in the far field – often denoted by q_∞), U is the freestream air speed, ρ_∞ is the freestream air density, S is the planform area, and C_{L_α} is the wing lift-curve slope. Note that $L \neq L_{\text{rigid}}$; and, for positive θ, $L > L_{\text{rigid}}$. We can express the moment of aerodynamic forces about the aerodynamic center as

$$M_{\text{ac}} = qScC_{M\text{ac}} \tag{4.4}$$

If the angle of attack is small, $C_{M\text{ac}}$ can be regarded as a constant. It should be noted here that linear aerodynamics implies that the lift-curve slope C_{L_α} is a constant. A further simplification may be that $C_{L_\alpha} = 2\pi$ in accordance with two-dimensional thin-airfoil theory. If experimental data or results from computational fluid dynamics provide an alternative value, then it should be used.

Using Eqs. (4.3) and (4.4), the equilibrium equation, Eq. (4.1), can be expanded as

$$qScC_{M\text{ac}} + qSC_{L_\alpha}\left(\alpha_{\text{r}} + \theta\right)\left(x_O - x_{\text{ac}}\right) - W\left(x_O - x_{\text{cg}}\right) = k\theta \tag{4.5}$$

Solving Eq. (4.5) for the elastic deflection, one obtains

$$\theta = \frac{qScC_{M\text{ac}} + qSC_{L_\alpha}\alpha_{\text{r}}\left(x_O - x_{\text{ac}}\right) - W\left(x_O - x_{\text{cg}}\right)}{k - qSC_{L_\alpha}\left(x_O - x_{\text{ac}}\right)} \tag{4.6}$$

When α_{r} and q are specified the total lift can be determined.

When the support point O is aft of the aerodynamic center, so that $x_O > x_{\text{ac}}$, the denominator can vanish, which implies that θ blows up. This behavior is a static aeroelastic instability called "divergence." The dynamic pressure at which divergence occurs for this case is

$$q_D = \frac{k}{SC_{L_\alpha}\left(x_O - x_{\text{ac}}\right)} \tag{4.7}$$

From Eq. (4.7) one can also see that the divergence condition depends on the altitude (through the air density) and the speed. The air speed at which divergence occurs can be found as

$$U_D = \sqrt{\frac{2k}{\rho_\infty SC_{L_\alpha}\left(x_O - x_{\text{ac}}\right)}} \tag{4.8}$$

It is evident that when the aerodynamic center is coincident with the pivot, so that $x_O = x_{\text{ac}}$, the divergence dynamic pressure becomes infinite. Also, when the aerodynamic center is aft of the pivot, so that $x_O < x_{\text{ac}}$, the divergence dynamic pressure becomes negative. In either case divergence is impossible.

To pursue the character of this instability a bit further, consider the case of a symmetric airfoil ($C_{M\text{ac}} = 0$). Furthermore, let $x_O = x_{\text{cg}}$ so that the weight term drops out of the equation for θ. From Eq. (4.7) we can let $k = q_D SC_{L_\alpha}\left(x_O - x_{\text{ac}}\right)$, and so θ can be written simply as

$$\theta = \frac{\alpha_{\text{r}}}{\frac{q_D}{q} - 1} \tag{4.9}$$

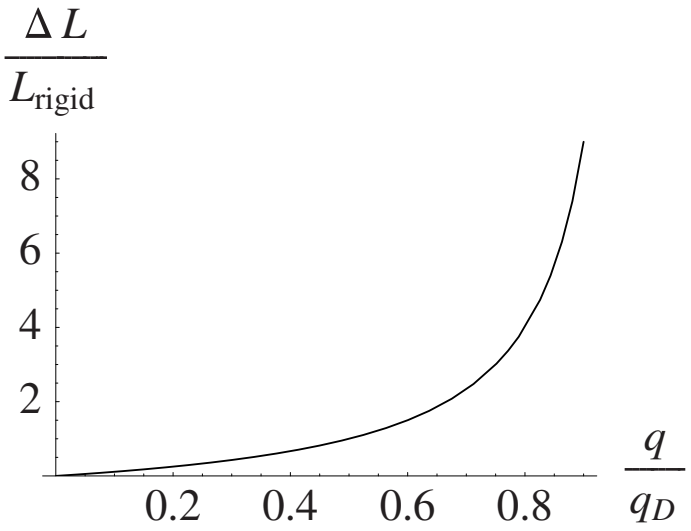

Figure 4.3: Relative change in lift due to aeroelastic effect

The lift is proportional to $\alpha_r + \theta$. Thus, the change in lift divided by the rigid lift is given by

$$\frac{\Delta L}{L_{\text{rigid}}} = \frac{\theta}{\alpha_r} = \frac{\frac{q}{q_D}}{1 - \frac{q}{q_D}} \tag{4.10}$$

Both θ and $\Delta L/L_{\text{rigid}}$ clearly approach infinity as $q \to q_D$. Indeed, a plot of the latter is given in Fig. 4.3 and shows the large change in lift caused by the aeroelastic effect. The lift evidently starts from its "rigid" value, that is, the value it would have were the support rigid, and increases to infinity as $q \to q_D$. However, keep in mind that there are limitations on the validity of both expressions. Namely, the lift will not continue to increase as stall is encountered. Moreover, the structure will not tolerate infinite deformation, and failure will take place at some finite value of θ.

When the system parameters are within the bounds of validity for linear theory, another fascinating feature of this problem emerges. One can invert the expression for θ to obtain

$$\frac{1}{\theta} = \frac{q_D}{\alpha_r}\left(\frac{1}{q} - \frac{1}{q_D}\right) \tag{4.11}$$

making it evident that $1/\theta$ is proportional to $1/q$ (see Fig. 4.4). Therefore, for a model of this type only two data points are needed to extrapolate the line down and to the left until it intercepts the $1/q$ axis at a distance $1/q_D$ from the origin. As can be seen from the figure, the slope of this line can also be used to estimate q_D. The form of this plot is of great practical value because estimates of q_D can be extrapolated from data taken at speeds far below the divergence speed. This means that q_D can be estimated even when the values of the model parameters are not precisely known, thus circumventing the need to risk destruction of the model by testing all the way up to the divergence boundary.

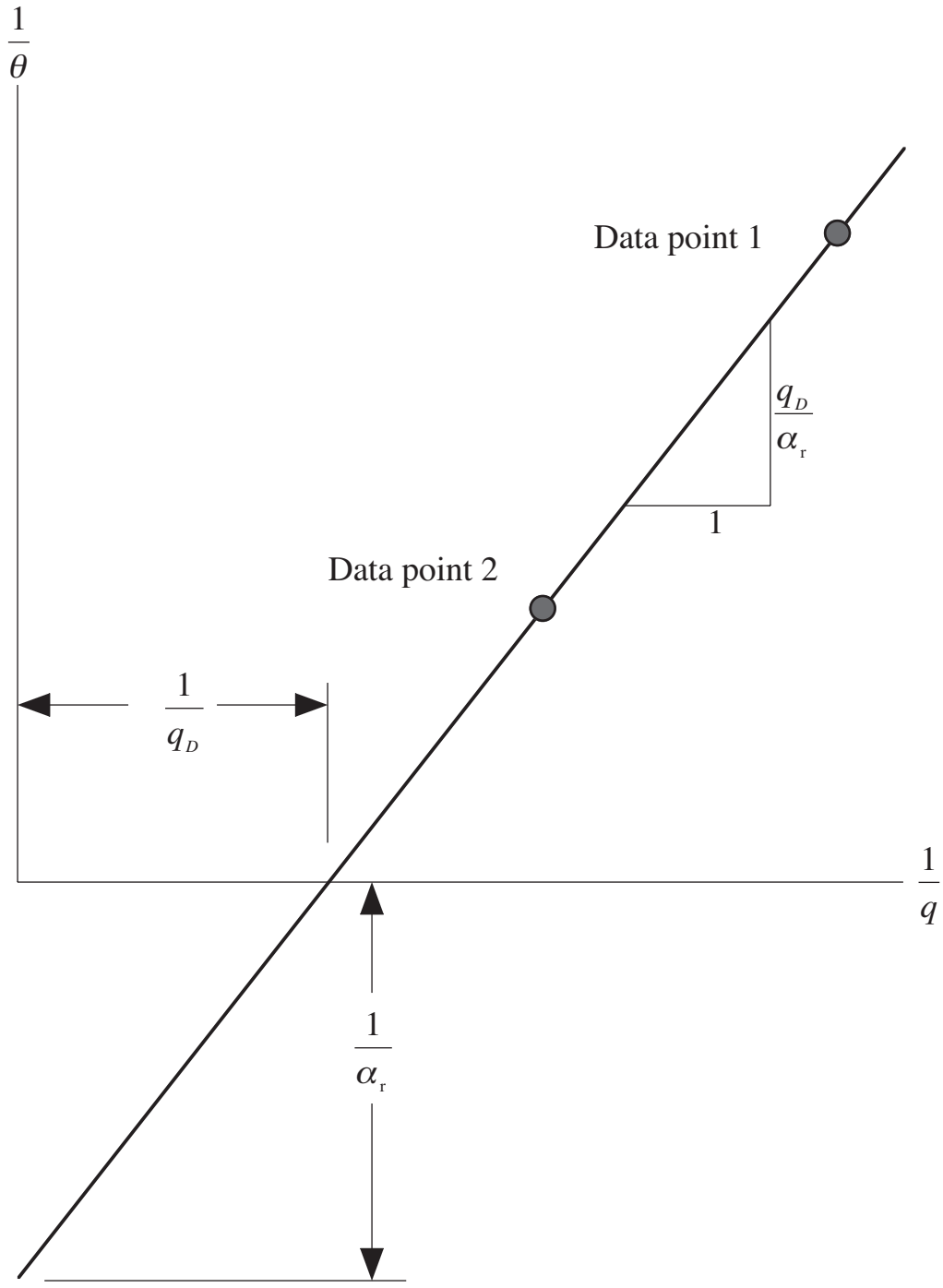

Figure 4.4: Plot of $1/\theta$ versus $1/q$

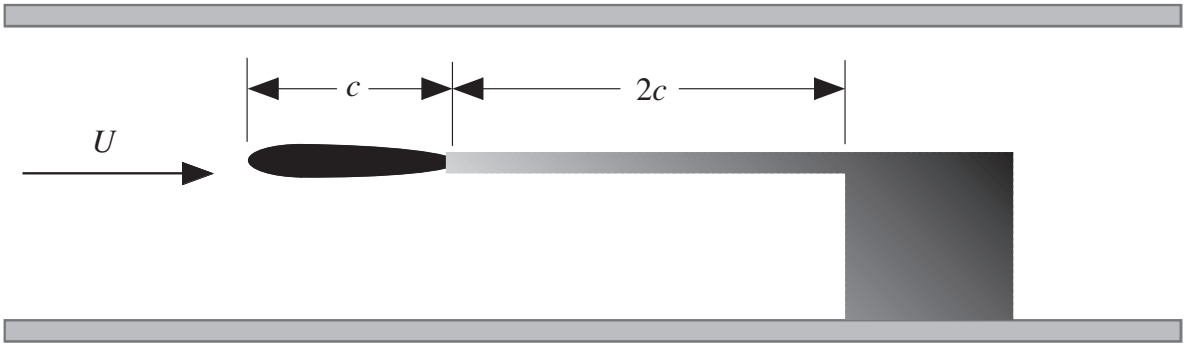

Figure 4.5: Schematic of a sting-mounted wind-tunnel model

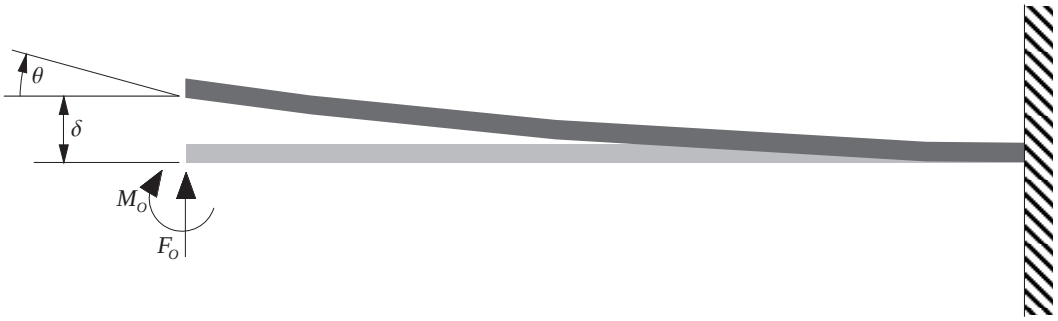

Figure 4.6: Detailed view of the cantilevered beam

4.1.2 Sting-Mounted Model

A second configuration of potential interest is a rigid model mounted on an elastic sting. A simplified version of this kind of model is shown in Figs. 4.5 – 4.7 where the sting is modeled as a uniform, elastic, cantilevered beam with bending stiffness EI and length $2c$. The model is mounted in such a way as to have angle of attack of α_r when the beam is undeformed. Thus, as before $\alpha = \alpha_r + \theta$ where θ is the nose up rotation of the wing resulting from bending of the sting, as shown in Fig. 4.6. Also in Fig. 4.6 we denote the tip deflection of the cantilever beam as δ, although we do not need it for this analysis. One should note the equal and opposite directions on the force F_0 and moment M_0 at the trailing edge of the wing in Fig. 4.7 versus at the tip of the sting in Fig. 4.6.

From superposition one can deduce the total bending slope at the tip of the sting as the sum of contributions from the tip force F_0 and tip moment M_0, denoted by θ_F and θ_M, respectively, so that

$$\theta = \theta_F + \theta_M \tag{4.12}$$

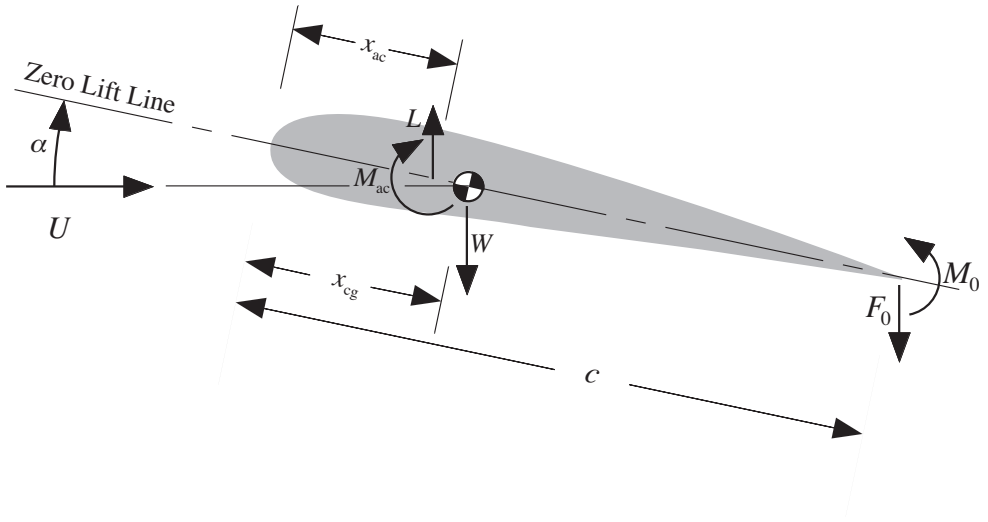

Figure 4.7: Detailed view of the sting-mounted wing

From elementary beam theory these constituent parts can be written as

$$\begin{aligned} \theta_F &= \frac{F_0(2c)^2}{2EI} \\ \theta_M &= \frac{M_0(2c)}{EI} \end{aligned} \tag{4.13}$$

so that

$$\begin{aligned} F_0 &= \frac{2EI\,\theta_F}{(2c)^2} \\ M_0 &= \frac{EI\,\theta_M}{2c} \end{aligned} \tag{4.14}$$

Two static aeroelastic equilibrium equations can now be written for the determination of θ_F and θ_M. Using Eqs. (4.3) and (4.4) for the lift and pitching moment, the force equilibrium equation can be written as

$$qSC_{L_\alpha}\left(\alpha_{\mathrm{r}} + \theta_F + \theta_M\right) - W - F_0 = 0 \tag{4.15}$$

and the sum of moments about the trailing edge yields

$$qScC_{M_{\mathrm{ac}}} + qSC_{L_\alpha}\left(\alpha_{\mathrm{r}} + \theta_F + \theta_M\right)\left(c - x_{\mathrm{ac}}\right) - W\left(c - x_{\mathrm{cg}}\right) - M_0 = 0 \tag{4.16}$$

Substitution of Eqs. (4.14) into Eqs. (4.15) and (4.16), simultaneous solution for θ_F and θ_M, and use of Eq. (4.12) yields

$$\theta = \frac{\alpha_{\mathrm{r}}\left(2 - \frac{x_{\mathrm{ac}}}{c}\right) + \frac{C_{M\mathrm{ac}}}{C_{L_\alpha}} - \frac{W}{qSC_{L_\alpha}}\left(2 - \frac{x_{\mathrm{cg}}}{c}\right)}{\frac{EI}{2qSc^2C_{L_\alpha}} - \left(2 - \frac{x_{\mathrm{ac}}}{c}\right)} \tag{4.17}$$

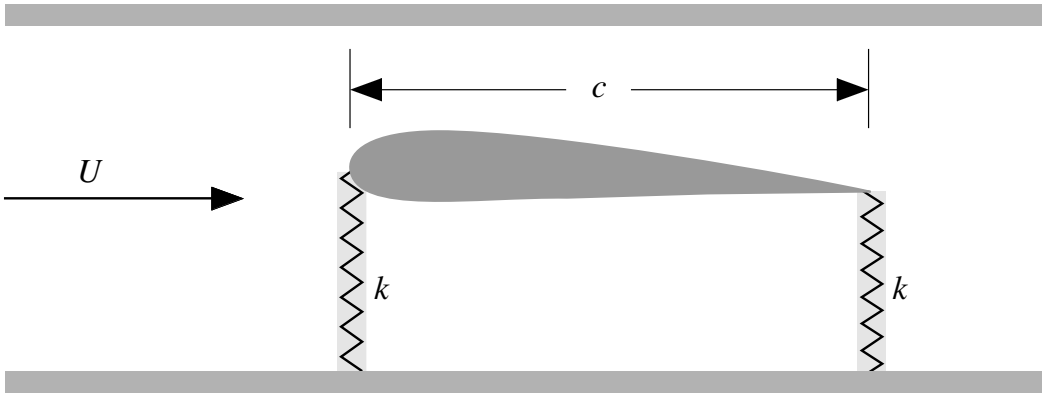

Figure 4.8: Schematic of strut-supported wind-tunnel model

Here again the condition for divergence can be obtained by setting the denominator to zero, so that

$$q_D = \frac{EI}{2\left(2 - \frac{x_{\text{ac}}}{c}\right) Sc^2 C_{L_\alpha}} \tag{4.18}$$

However, unlike the previous example, one cannot make the divergence dynamic pressure infinite or negative (thereby making divergence mathematically impossible) by choice of configuration parameters because $x_{\text{ac}}/c \leq 1$. For a given wing configuration, one is left only with the possibility of increasing the sting bending stiffness to make the divergence dynamic pressure larger.

4.1.3 Strut-Mounted Model

A third configuration of a wind-tunnel mount is a strut system as idealized in Figs. 4.8 and 4.9. The two linearly elastic struts have the same extensional stiffness, k, and are mounted at the leading and trailing edges of the wing. The model is mounted in such a way as to have angle of attack of α_{r} when the springs are both undeformed. Thus, as before, the angle of attack is $\alpha = \alpha_{\text{r}} + \theta$. As illustrated in Fig. 4.9, the elastic pitch angle, θ, can be related to the extension of the two struts as

$$\theta = \frac{\delta_1 - \delta_2}{c} \tag{4.19}$$

The sum of the forces in the vertical direction shows that

$$L - W - k(\delta_1 + \delta_2) = 0 \tag{4.20}$$

The sum of the moments about the trailing edge yields

$$M_{\text{ac}} + L(c - x_{\text{ac}}) - W(c - x_{cg}) - kc\delta_1 = 0 \tag{4.21}$$

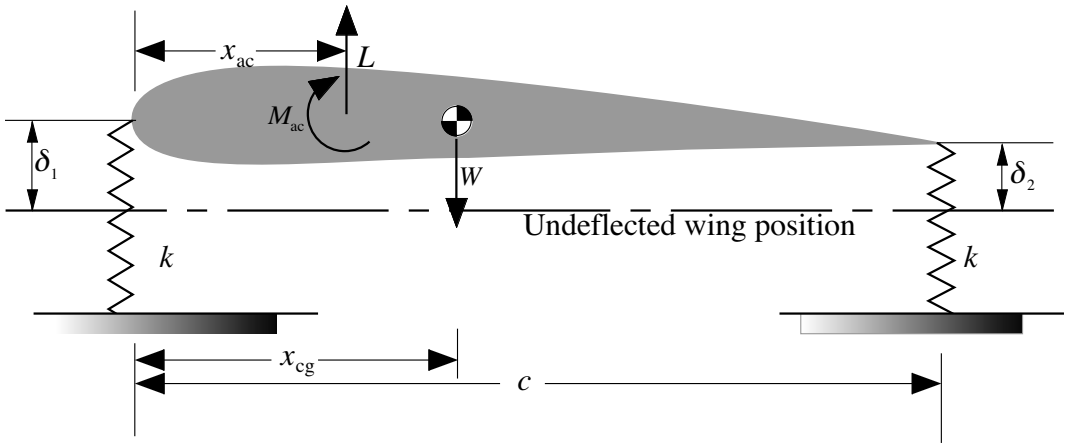

Figure 4.9: Cross section of strut-supported wind-tunnel model

Again, using Eqs. (4.3) and (4.4) for the lift and pitching moment, the simultaneous solution of the force and moment equations yields

$$\theta = \frac{\alpha_r \left(1 - 2\frac{x_{ac}}{c}\right) + 2\frac{C_{Mac}}{C_{L_\alpha}} - \frac{W}{qSC_{L_\alpha}}\left(1 - 2\frac{x_{cg}}{c}\right)}{\frac{kc}{qSC_{L_\alpha}} - \left(1 - 2\frac{x_{ac}}{c}\right)} \tag{4.22}$$

As usual, the divergence condition is indicated by the vanishing of the denominator, so that

$$q_D = \frac{kc}{SC_{L_\alpha}\left(1 - 2\frac{x_{ac}}{c}\right)} \tag{4.23}$$

It is evident for this problem as specified that when the aerodynamic center is in front of the mid-chord (as it is in subsonic flow), the divergence condition cannot be eliminated. However, divergence can be eliminated if the leading-edge spring stiffness is increased relative to that of the trailing-edge spring. This is left as an exercise for the reader; see Problem 5.

4.1.4 Wall-Mounted Model for Application to Aileron Reversal

Before putting aside the wind-tunnel type models dealt with so far in this chapter, we here consider the problem of aileron reversal. It is known that wing torsional flexibility causes certain primary flight control devices, such as ailerons, to function in a manner that is completely at odds with their intended purpose. The primary danger posed by the loss of control effectiveness is that the pilot cannot control the aircraft in the usual way. There are additional concerns for aircraft, the missions of which depend on their being highly maneuverable. For example, when control effectiveness is lost, the pilot may not be able

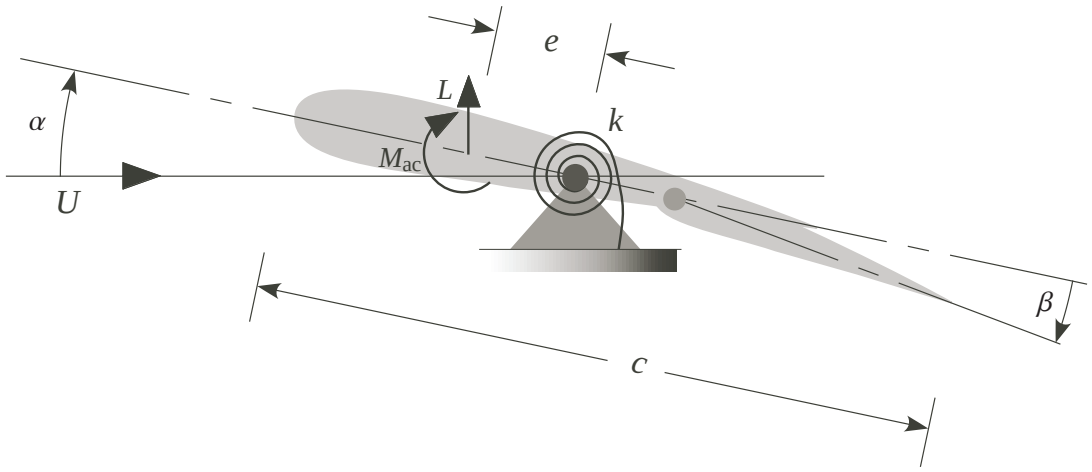

Figure 4.10: Schematic of the airfoil section of a flapped two-dimensional wing in a wind tunnel

to count on the aircraft's ability to execute evasive maneuvers. It is this loss in control effectiveness and eventual reversal that is the focus of this section.

To this end, consider the airfoil section of a flapped two-dimensional wing, shown in Fig. 4.10. Similar to the model discussed in Section 4.1.1, the wing is pivoted and restrained by a rotational spring with spring constant k. The main differences are that (1) a trailing-edge flap is added such that the flap angle β can be arbitrarily set by the flight control system; and (2) we need not consider gravity to illustrate this phenomenon, so the weight is not shown in the figure. Moment equilibrium for this system about the pivot requires that

$$M_{\text{ac}} + eL = k\theta \tag{4.24}$$

The lift and pitching moment for a two-dimensional wing can be written as before, namely

$$\begin{aligned} L =& qSC_L \\ M_{\text{ac}} =& qcSC_{M\text{ac}} \end{aligned} \tag{4.25}$$

When $\beta \neq 0$, the effective camber of the airfoil changes, inducing changes in both lift and pitching moment. For a linear theory, both α and β should be small angles, so that

$$\begin{aligned} C_L =& C_{L_\alpha}\alpha + C_{L_\beta}\beta \\ C_{M\text{ac}} =& C_{M_0} + C_{M_\beta}\beta \end{aligned} \tag{4.26}$$

Note that $C_{M_\beta} < 0$. For convenience, we assume a symmetric airfoil ($C_{M_0} = 0$).

We now substitute Eqs. (4.25) into the moment equilibrium equation, Eq. (4.24), making use of Eqs. (4.26), and determine θ to be

$$\theta = \frac{qS\left[eC_{L_\alpha}\alpha_{\text{r}} + \left(eC_{L_\beta} + cC_{M_\beta}\right)\beta\right]}{k - eqSC_{L_\alpha}} \tag{4.27}$$

We see that because of the torsional flexibility (represented here by the rotational spring), θ is a function of β. Substituting Eq. (4.27) back into Eqs. (4.25a) and (4.26a), one obtains an expression for the aeroelastic lift

$$L = \frac{qS\left[C_{L_\alpha}\alpha_{\mathrm{r}} + C_{L_\beta}\left(1 + \frac{cqSC_{L_\alpha}C_{M_\beta}}{kC_{L_\beta}}\right)\beta\right]}{1 - \frac{eqSC_{L_\alpha}}{k}} \tag{4.28}$$

It is evident from the two terms in the coefficient of β in this expression that lift is a function of β in two counteracting ways. Ignoring the effect of the denominator for the time being, one sees that the first term in the numerator that multiplies β is purely aerodynamic and leads to an *increase* in lift with β, because of a change in the effective camber. The second term is aeroelastic. Recalling that $C_{M_\beta} < 0$, one sees that as β is increased, the effective change in the camber also induces a nose-down pitching moment that, because the wing is torsionally flexible, tends to decrease θ and in turn *decrease* lift. At low speed, the purely aerodynamic increase in lift overpowers the aeroelastic tendency to decrease the lift, so that the lift indeed increases with β (and the aileron works as advertised). However, as dynamic pressure increases, the aeroelastic effect becomes stronger; and there is a point at which the net rate of change of lift with respect to β vanishes so that

$$\frac{\partial L}{\partial \beta} = 0 = \frac{qSC_{L_\beta}\left(1 + \frac{cqSC_{L_\alpha}C_{M_\beta}}{kC_{L_\beta}}\right)}{1 - \frac{eqSC_{L_\alpha}}{k}} \tag{4.29}$$

Thus, one finds that the dynamic pressure at which the reversal occurs is

$$q_R = -\frac{kC_{L_\beta}}{cSC_{L_\alpha}C_{M_\beta}} \tag{4.30}$$

Notice that since $C_{M_\beta} < 0$, $q_R > 0$. Obviously, a stiffer k gives a higher reversal speed, and a torsionally rigid wing will not undergo reversal. For dynamic pressures above q_R (but still below the divergence dynamic pressure), a positive β will actually decrease the lift.

Now let us consider the effect of both numerator and denominator. As before, the denominator in L (and θ) can vanish, resulting in divergence. The dynamic pressure at which divergence occurs can be found by setting the denominator of Eq. (4.28) equal to zero, which yields

$$q_D = \frac{k}{eSC_{L_\alpha}} \tag{4.31}$$

Equations (4.30) and (4.31) can be used to simplify the expression for the lift in Eq. (4.28) to obtain

$$L = \frac{qS\left[C_{L_\alpha}\alpha_{\mathrm{r}} + C_{L_\beta}\left(1 - \frac{q}{q_R}\right)\beta\right]}{1 - \frac{q}{q_D}} \tag{4.32}$$

It is clear from this expression that the coefficient of β can be positive, negative or zero. Thus, a positive β could increase the lift, decrease the lift, or not change the lift at all. The aileron's lift efficiency, η, can be thought of as the aeroelastic (i.e., actual) change in lift per unit change in β divided by the change in lift per unit change in β that would result were the wing not flexible in torsion; that is,

$$\eta = \frac{\text{change in lift per unit change in } \beta \text{ for elastic wing}}{\text{change in lift per unit change in } \beta \text{ for rigid wing}}$$

Using the above, one can easily find that

$$\eta = \frac{1 - \dfrac{q}{q_R}}{1 - \dfrac{q}{q_D}} \tag{4.33}$$

which implies that the wing will remain divergence-free and control efficiency will not be lost as long as $q < q_D \leq q_R$. Obviously, if the wing were rigid, both q_D and q_R become infinite and $\eta = 1$.

Thinking unconventionally for the moment, let us allow the possibility of $q_R << q_D$. This will result in aileron reversal at a low speed, of course. Although the aileron will now work the opposite of the usual way at most of the operational speeds of the aircraft, this type of design should not be ruled out on these grounds alone. Active flight-control systems can certainly compensate for this. Moreover, one can get considerably more (negative) lift for positive β in this unusual regime than positive lift for positive β in the more conventional setting. This may have important implications for development of highly maneuverable aircraft. Exactly what other potential advantages and disadvantages exist from following this strategy, particularly in this era of composite materials, smart structures, and active controls, is not presently known and is the subject of current research. However, there are helicopter rotor blades built by Kaman Aerospace with servo-flaps that work in the post-reversal regime – and are hence much more efficient than a conventional flap would be. Helicopter rotor blades do not have to have flap authority at low rotor angular speed, and thus a cleaner design is possible. Fixed-wing aircraft would have to have flight control at a much wider range of speeds. Research between 1995 and 2005 on the Active Aeroelastic Wing by the Air Force and NASA has reported difficulties achieving reversal for the configuration under consideration. Flow separation brought on by high effective camber is evidently a factor.

4.2 Uniform Lifting Surface

Up to now, our aeroelastic analyses have focused on rigid wings with a flexible support. These idealized configurations do give some insight into the aeroelastic stability and response, but

practical analyses must take flexibility of the lifting surface into account. That being the case, in this section we address flexible wings, albeit with simplified structural representation.

Consider an unswept uniform elastic lifting surface as illustrated in Figs. 4.11 and 4.12. The lifting surface is modeled as a beam and is presumed to be built in at its root ($y = 0$, to represent attachment to a wind-tunnel wall or a fuselage) and free at its tip ($y = \ell$). The y-axis corresponds to the elastic axis, which may be defined as the line of effective shear centers, assumed here to be straight. For isotropic beams, a transverse force applied at any point along this axis will result in bending with no elastic torsional rotation about the axis. This axis is also the axis of twist in response to a pure twisting moment applied to the wing. Because the primary concern here is the determination of the airload distributions, the only elastic deformation that will influence these loads is rotation due to twist about the elastic axis.

4.2.1 Equilibrium Equation

The total applied moment (per unit span) about this axis will be denoted as $M'(y)$, which is positive leading-edge up and given by

$$M' = M'_{\text{ac}} + eL' - Nmgd \tag{4.34}$$

where L' and M'_{ac} are the distributed spanwise lift and pitching moment (i.e., the lift and pitching moment per unit length), mg is the spanwise weight distribution (i.e., the weight per unit length) and N is the "normal load factor" for the case in which the wing is level (i.e., the z-axis is directed vertically upward). Thus, N can be written as

$$N = \frac{L}{W} = 1 + \frac{A_z}{g} \tag{4.35}$$

where A_z is the z-component of the wing's inertial acceleration, W is the total weight of the aircraft, and L is the total lift. The distributed aerodynamic loads can be written in coefficient form as

$$\begin{aligned} L' &= qcc_\ell \\ M'_{\text{ac}} &= qc^2 c_{m\text{ac}} \end{aligned} \tag{4.36}$$

where the freestream dynamic pressure, q, is

$$q = \frac{1}{2}\rho_\infty U^2 \tag{4.37}$$

Now, a static equilibrium equation for the elastic torsional rotation, θ, about the elastic axis can be obtained from the fundamental torsional relation

$$T = GJ\frac{d\theta}{dy} \tag{4.38}$$

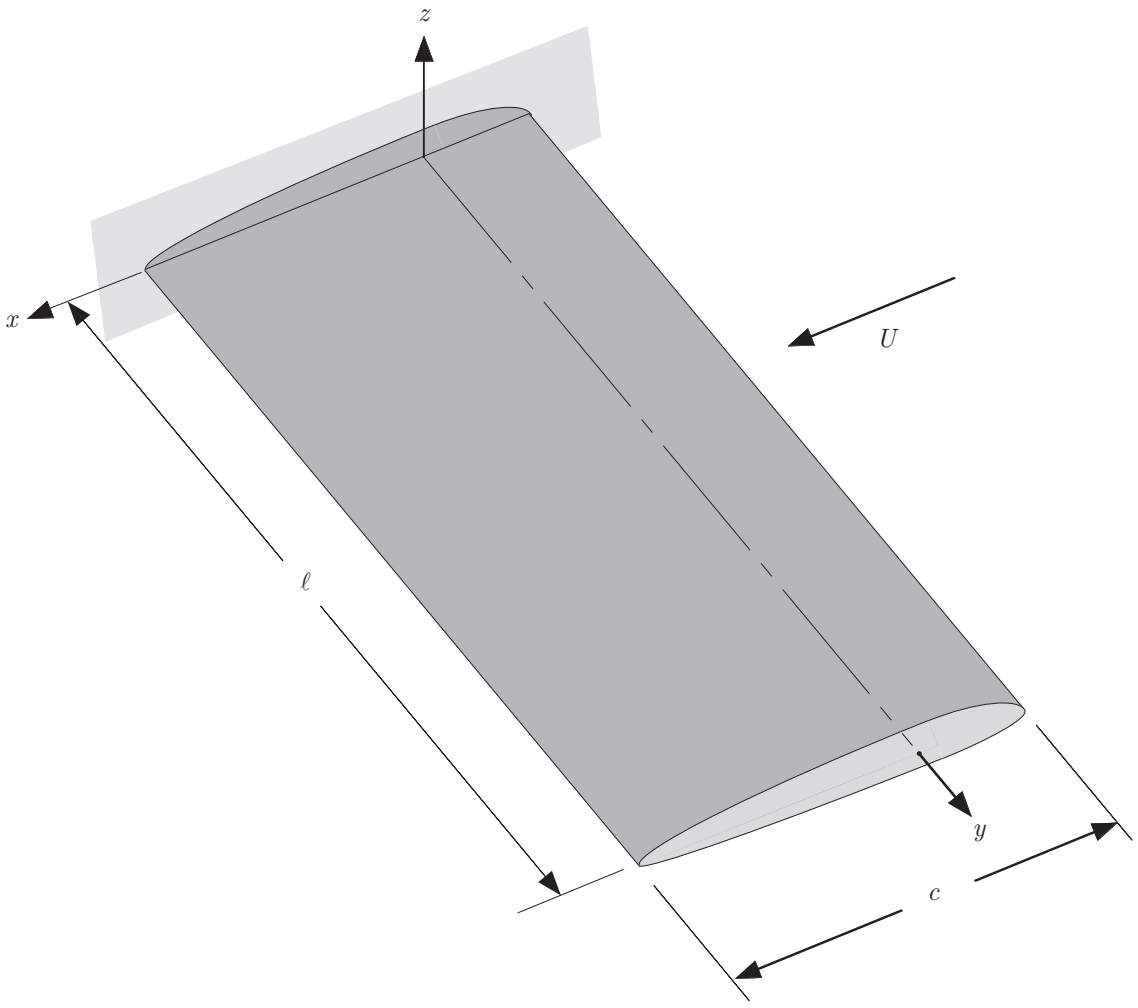

Figure 4.11: Uniform unswept cantilevered lifting surface

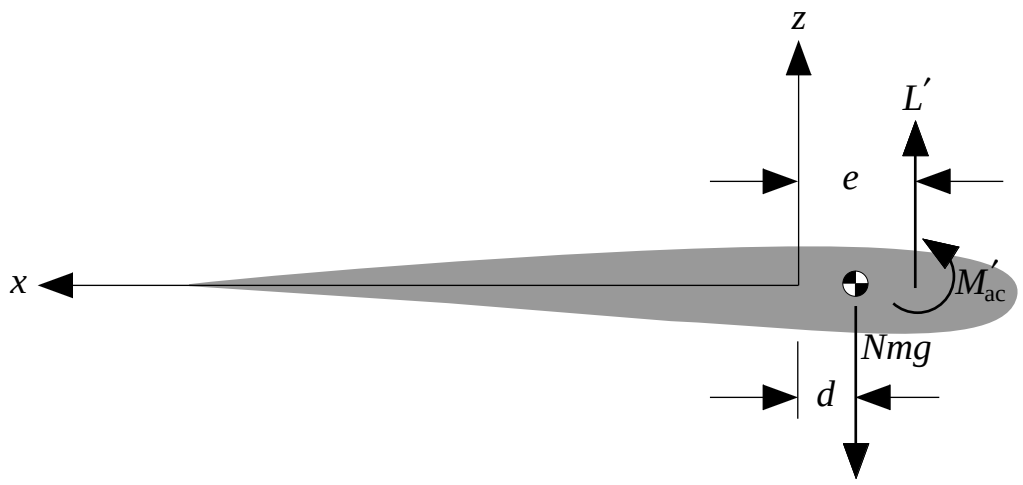

Figure 4.12: Cross section of spanwise uniform lifting surface

where GJ is the effective torsional stiffness and T is the twisting moment about the elastic axis. One can obtain an equilibrium equation by equating the rate of change of twisting moment to the negative of the applied torque distribution so that

$$\frac{dT}{dy} = \frac{d}{dy}\left(GJ\frac{d\theta}{dy}\right) = -M' \tag{4.39}$$

Recognizing that uniformity implies GJ is constant over the length, substituting Eqs. (4.36) into Eq. (4.34) to obtain the applied torque, and finally substituting the applied torque and Eq. (4.38) for the internal torque into the equilibrium equation, Eq. (4.39), one obtains

$$GJ\frac{d^2\theta}{dy^2} = -qc^2c_{m_{\text{ac}}} - eqcc_\ell + Nmgd \tag{4.40}$$

The sectional lift coefficient can be related to the angle of attack by an appropriate aerodynamic theory as some function $c_\ell(\alpha)$ where the functional relation generally involves integration over the planform. To simplify the calculation, the wing can be broken up into spanwise segments of infinitesimal length, where the local lift can be estimated from two-dimensional theory. This theory, commonly known as strip theory, frequently makes use of table look-up for efficient calculation. Here we will use an even simpler, linear form in which the lift-curve slope is assumed to be a constant along the span. Thus,

$$c_\ell(\alpha) = \frac{dc_\ell}{d\alpha}\alpha(y) = a\alpha(y) \tag{4.41}$$

where the constant sectional lift-curve slope is denoted by a_0.

The angle of attack will be represented by two components. The first is a rigid contribution, α_{r}, from a "rigid" rotation of the surface (plus any built-in twist although none is assumed to exist here). The second component is the elastic torsional rotation θ. Hence,

$$\alpha(y) = \alpha_{\text{r}} + \theta(y) \tag{4.42}$$

Associated with each angle of attack contribution is a component of sectional lift coefficient given by strip theory as

$$c_\ell(y) = a_0[\alpha_{\text{r}} + \theta(y)] \tag{4.43}$$

This aerodynamic representation can be substituted into the equilibrium equation to yield its final form as

$$\frac{d^2\theta}{dy^2} + \frac{qca_0e}{GJ}\theta = -\frac{1}{GJ}\left(qc^2c_{m_{\text{ac}}} + qca_0e\alpha_{\text{r}} - Nmgd\right) \tag{4.44}$$

Finally, a complete description of this equilibrium condition requires specification of the boundary conditions. Since the surface is built in at the root and free at the tip, these conditions can be written as

$$\begin{aligned} y = 0\text{:} \quad & \theta = 0 \quad && \text{(zero deflection)} \\ y = \ell\text{:} \quad & \frac{d\theta}{dy} = 0 \quad && \text{(zero twisting moment)} \end{aligned} \tag{4.45}$$

Obviously, these boundary conditions are only valid for the clamped-free condition. The boundary conditions for other end conditions for beams in torsion are given in Chapter 2, Section 2.1.2.

4.2.2 Torsional Divergence

If it is presumed that the configuration parameters of the above uniform wing are known, then it should be possible to solve Eq. (4.44) to determine the resulting twist distribution and associated airload. To simplify the notation let

$$\begin{aligned} \lambda^2 \equiv & \frac{qca_0e}{GJ} \\ \lambda^2\overline{\alpha}_{\text{r}} \equiv & \frac{1}{GJ}\left(qc^2c_{m_{\text{ac}}} - Nmgd\right) \end{aligned} \tag{4.46}$$

so that

$$\overline{\alpha}_{\text{r}} = \frac{cc_{m_{\text{ac}}}}{a_0e} - \frac{Nmgd}{qca_0e} \tag{4.47}$$

Note that λ^2 and $\overline{\alpha}_{\text{r}}$ are independent of y since the wing is assumed to be uniform. The static aeroelastic equilibrium equation can now be written as

$$\frac{d^2\theta}{dy^2} + \lambda^2\theta = -\lambda^2\left(\alpha_{\text{r}} + \overline{\alpha}_{\text{r}}\right) \tag{4.48}$$

The general solution to this linear ordinary differential equation is

$$\theta = A_1 \sin(\lambda y) + A_2 \cos(\lambda y) - (\alpha_{\mathrm{r}} + \overline{\alpha}_{\mathrm{r}}) \tag{4.49}$$

Applying the boundary conditions, one finds that

$$\begin{aligned} \theta(0) = 0: \qquad & A_2 = \alpha_{\mathrm{r}} + \overline{\alpha}_{\mathrm{r}} \\ \theta'(\ell) = 0: \qquad & A_1 = A_2 \tan(\lambda \ell) \end{aligned} \tag{4.50}$$

where $(\,)' = d(\,)/dy$. Thus, the elastic twist distribution becomes

$$\theta = (\alpha_{\mathrm{r}} + \overline{\alpha}_{\mathrm{r}}) \left[\tan(\lambda \ell) \sin(\lambda y) + \cos(\lambda y) - 1\right] \tag{4.51}$$

Since θ is now known, the spanwise lift distribution can be found using the relation

$$L' = q c a_0 (\alpha_{\mathrm{r}} + \theta) \tag{4.52}$$

It is important to note from the above expression for elastic twist that θ becomes infinite as $\lambda \ell$ approaches $\pi/2$. This phenomenon is called "torsional divergence" and depends on the numerical value of

$$\lambda = \sqrt{\frac{q c a_0 e}{GJ}} \tag{4.53}$$

Thus, it is apparent that there exists a value of the dynamic pressure $q = q_D$, at which $\lambda \ell$ equals $\pi/2$, where the elastic twist theoretically becomes infinite. In practice, this static aeroelastic instability causes catastrophic failure of the wing structure. The value q_D is called the "divergence dynamic pressure" and is given by

$$q_D = \frac{GJ}{e c a_0} \left(\frac{\pi}{2\ell}\right)^2 \tag{4.54}$$

Noting now that one can write

$$\lambda \ell = \frac{\pi}{2} \sqrt{\overline{q}} \tag{4.55}$$

with

$$\overline{q} = \frac{q}{q_D} \tag{4.56}$$

the twist angle of the wing at the tip can be written as

$$\begin{aligned} \theta(\ell) &= (\alpha_{\mathrm{r}} + \overline{\alpha}_{\mathrm{r}}) \left[\sec(\lambda \ell) - 1\right] \\ &= (\alpha_{\mathrm{r}} + \overline{\alpha}_{\mathrm{r}}) \left[\sec\left(\frac{\pi}{2} \sqrt{\overline{q}}\right) - 1\right] \end{aligned} \tag{4.57}$$

where Eq. (4.47) can now be written as

$$\overline{\alpha}_{\mathrm{r}} = \frac{c c_{m_{\mathrm{ac}}}}{a_0 e} - \frac{4 \ell^2 N m g d}{GJ \pi^2 \overline{q}} \tag{4.58}$$

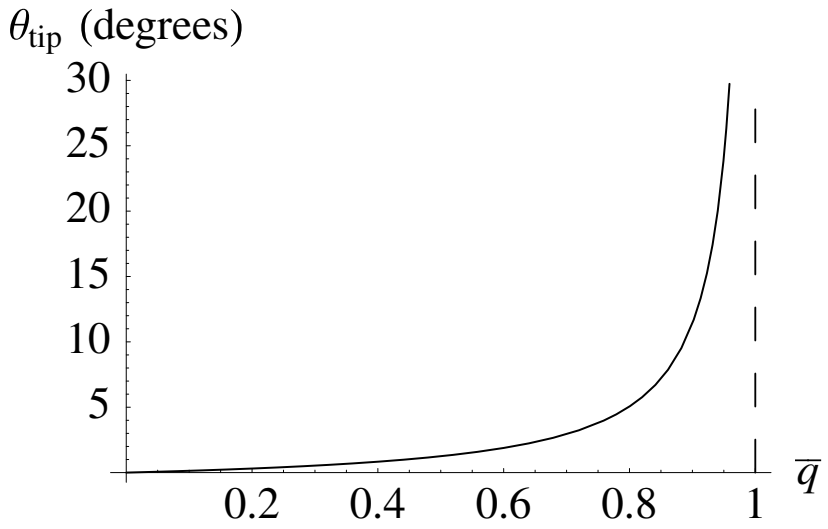

Figure 4.13: Plot of tip twist angle for wing versus $\overline{q}$ for $\alpha_{\rm r} + \overline{\alpha}_{\rm r} = 1^\circ$

Letting d be zero, so that $\overline{\alpha}_{\rm r}$ becomes independent of $\overline{q}$, one can examine the behavior of $\theta(\ell)$ versus $\overline{q}$. Such a function is plotted in Fig. 4.13 where one sees that the tip twist angle goes to infinity as $\overline{q}$ approaches unity. Note that the character of the plot in Fig. 4.13 is quite similar to the pre-buckling behavior of columns that have imperfections. It is of practical interest to note that the tip twist angle becomes sufficiently large to warrant concern about the structural integrity for dynamic pressures well below q_D.

Because this instability occurs at a dynamic pressure that is independent of the right-hand side of Eq. (4.48), as long as the right-hand side is nonzero, it seems possible that the divergence condition could be obtained from the homogeneous equilibrium equation

$$\frac{d^2\theta}{dy^2} + \lambda^2\theta = 0 \tag{4.59}$$

The general solution to this eigenvalue problem of the Sturm-Liouville type is

$$\theta = A_1 \sin(\lambda y) + A_2 \cos(\lambda y) \tag{4.60}$$

Applying the boundary conditions, one obtains

$$\begin{aligned} \theta(0) = 0: &\qquad A_2 = 0 \\ \theta'(\ell) = 0: &\qquad A_1 \lambda \cos(\lambda \ell) = 0 \end{aligned} \tag{4.61}$$

If $A_1 = 0$ in the last condition, there is no deflection; this is a so-called trivial solution. However, if $\lambda = 0$ the given general solution is not valid. Thus, the desired result is obtained when $\cos(\lambda\ell) = 0$. This is the "characteristic equation" with solutions given by

$$\lambda_n \ell = (2n-1)\frac{\pi}{2} \qquad (n = 1, 2, \ldots) \tag{4.62}$$

These values are called "eigenvalues." Note that this set of λs corresponds to a set of dynamic pressures

$$q_n = (2n-1)^2 \left(\frac{\pi}{2\ell}\right)^2 \frac{GJ}{eca_0} \qquad (n = 1, 2, \ldots) \tag{4.63}$$

The lowest of these values, q_1, is equal to the divergence dynamic pressure, q_D, previously obtained from the nonhomogeneous equilibrium equation. This result implies that there exist nontrivial solutions of the homogeneous equation for the elastic twist. In other words, even for cases in which the right-hand side of Eq. (4.48) is zero (when $\alpha_{\mathrm{r}} + \overline{\alpha}_{\mathrm{r}} = 0$), there is a nontrivial solution

$$\theta_n = B_n \sin(\lambda_n y) \tag{4.64}$$

for each of these discrete values of dynamic pressure. Since B_n is undetermined, the amplitude of θ_n is arbitrary, which means that the effective torsional stiffness is zero whenever the dynamic pressure $q = q_n$. The mode shape θ_1 is the divergence mode shape, which must not be confused with the twist distribution obtained from the nonhomogeneous equation.

It may be noted that if the elastic axis is upstream of the aerodynamic center then $e < 0$ and λ is imaginary in the preceding analysis. The characteristic equation for the divergence condition becomes $\cosh(|\lambda|\ell) = 0$. Because there is no real value of λ that satisfies this equation, the divergence phenomenon will not occur in this case.

4.2.3 Airload Distribution

It has been observed that the spanwise lift distribution can be determined as

$$L' = qca_0(\alpha_{\mathrm{r}} + \theta) \tag{4.65}$$

where we recall from Eq. (4.51) that

$$\theta = (\alpha_{\mathrm{r}} + \overline{\alpha}_{\mathrm{r}}) \left[\tan(\lambda\ell)\sin(\lambda y) + \cos(\lambda y) - 1\right] \tag{4.66}$$

and where $\overline{\alpha}_{\mathrm{r}}$ is given in Eq. (4.47). If the lifting surface is a wind-tunnel model of a wing and is fastened to the wind-tunnel wall, then the load factor, N, is equal to unity and α_{r} can be specified. The resulting computation of L' is straightforward.

If, however, the lifting surface represents half the wing surface of a flying vehicle, the computation of L' is not as direct. It may be noted that the constant $\overline{\alpha}_{\mathrm{r}}$ is a function of N. Thus, for given value of α_{r} there will be a corresponding distribution of elastic twist and a particular airload distribution. This airload can be integrated over the vehicle to obtain the total lift, L. Recall that $N = L/W$, where W is the vehicle weight. It is thus apparent that the load factor, N, is related to the rigid angle of attack, α_{r}, through the elastic twist angle, θ. For this reason either of the two variables α_{r} and N can be specified; the other can then be obtained from the total lift L. Assuming a two-winged vehicle with all the lift being generated from the wings, one finds

$$L = 2\int_0^\ell L'\, dy \tag{4.67}$$

Substituting for L' and α_r as given above yields

$$\begin{aligned} L =& 2qca_0 \int_0^\ell \left\{ \alpha_r + (\alpha_r + \overline{\alpha}_r) \left[\tan(\lambda\ell)\sin(\lambda y) + \cos(\lambda y) - 1 \right] \right\} dy \\ =& 2qca_0\ell \left\{ (\alpha_r + \overline{\alpha}_r) \left[\frac{\tan(\lambda\ell)}{\lambda\ell} \right] - \overline{\alpha}_r \right\} \end{aligned} \tag{4.68}$$

Since $N = L/W$, the above expression can be divided by the vehicle weight to yield a relation for N in terms of α_r and $\overline{\alpha}_r$. This relation can then be solved simultaneously with the preceding expression for $\overline{\alpha}_r$, Eq. (4.47), in terms of α_r and N. In this manner $\overline{\alpha}_r$ can be eliminated, providing either a relation that expresses N in terms of α_r, given by

$$N = \frac{2GJ(\lambda\ell)^2 \left\{ a_0 e\alpha_r + cc_{m_{ac}} \left[1 - \dfrac{\lambda\ell}{\tan(\lambda\ell)} \right] \right\}}{a_0 e\ell \left\{ \dfrac{We\lambda\ell}{\tan(\lambda\ell)} + 2mg\ell d \left[1 - \dfrac{\lambda\ell}{\tan(\lambda\ell)} \right] \right\}} \tag{4.69}$$

or a relation that expresses α_r in terms of N,

$$\alpha_r = \frac{NW\ell e}{2GJ\lambda\ell\tan(\lambda\ell)} + \left[1 - \frac{\lambda\ell}{\tan(\lambda\ell)} \right] \left[\frac{Nmg\ell^2 d}{GJ(\lambda\ell)^2} - \frac{cc_{m_{ac}}}{a_0 e} \right] \tag{4.70}$$

These relations permit one to specify a constant α_r and find $N(q)$ or, alternatively, to specify a constant N and find $\alpha_r(q)$. One finds that $N(q)$ starts out at zero for $q = 0$. On the other hand, $\alpha_r(q)$ starts out at infinity for $q = 0$. The limiting values as $q \to q_D$ depend on the other parameters. These equations can be used to find the torsional deformation and the resulting airload distribution for a specified flight condition.

The calculation of the spanwise aeroelastic airload distribution is immensely practical and is used in industry in two separate ways. One way is to satisfy a requirement of the aerodynamicist or performance engineer who needs to know the total forces and moments on the flight vehicle as a function of its altitude and flight condition. In this instance the dynamic pressure q (and altitude or Mach number) and α_r are specified, and the load factor N or total lift L is computed using Eq. (4.69). A second requirement is that of the structural engineer, who must ensure the structural integrity of the lifting surface for a specified load factor N and flight condition. Such a specification is normally described by what is called a V-N diagram. For the conditions of given load factor and flight condition it is necessary for the structural engineer to know the airload distribution to conduct a subsequent loads and stress analysis. When q (and altitude or Mach number) and N are specified, α_r is then determined from Eq. (4.70). Knowing q, α_r, and N, one then uses Eq. (4.47) to find $\overline{\alpha}_r$. The torsional deformation, θ, then follows from Eq. (4.66) and the spanwise airload distribution follows from Eq. (4.65). From this, the torsional and bending moment distributions along the wing can be found, leading directly to the maximum stress in the wing, generally somewhere in the root cross section.

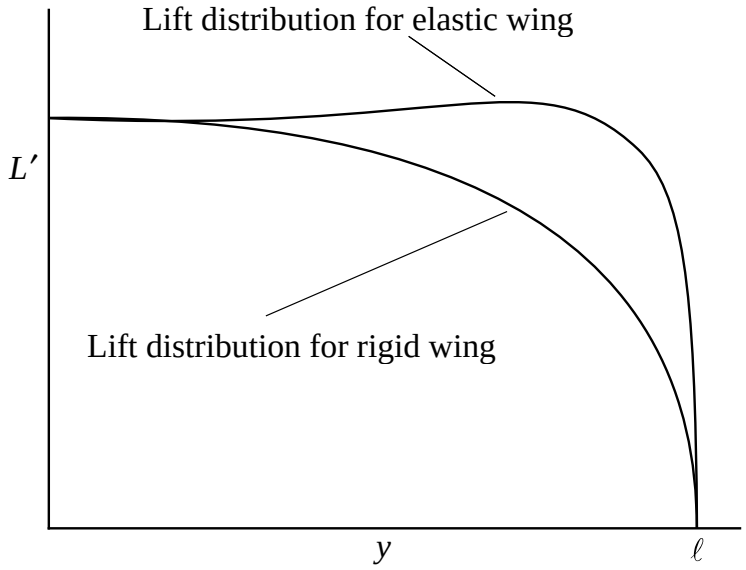

Figure 4.14: Rigid and elastic wing lift distributions holding α_{r} constant

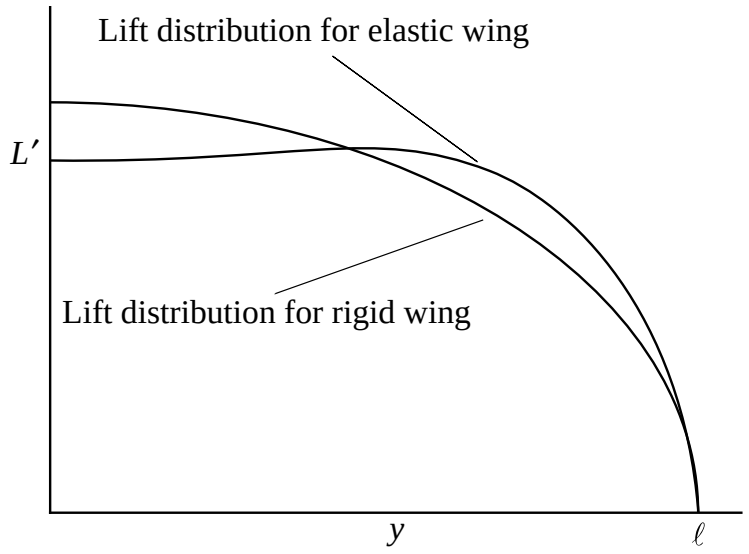

Figure 4.15: Rigid and elastic wing lift distributions holding total lift constant

It may be observed that the overall effect of torsional flexibility on the unswept lifting surface is to significantly change the spanwise airload distribution. This effect can be seen as the presence of the elastic part of the lift coefficient, which is of course proportional to $\theta(y)$. Since this elastic torsional rotation will generally increase as the distance from the root (i.e., out along the span), so also will the resultant airload distribution. The net effect will depend on whether α_{r} or N is specified. If α_{r} is specified as in the case of a wall-mounted elastic wind-tunnel model ($N = 1$) or as in performance computations, then the total lift will increase with the additional load appearing in the outboard region as shown in Fig. 4.14.

In the other case, when N is specified by the structural engineer, the total lift (area under L' versus y) is unchanged, as shown in Fig. 4.15. The addition of lift in the outboard region must be balanced by a decrease inboard. This is accomplished by decreasing α_{r} as the surface is made more flexible.

All the preceding equations for torsional divergence and airload distribution have been based on a strip-theory aerodynamic representation. It may be noted that a slight numerical improvement in their predictive capability can be obtained if the two-dimensional lift-curve slope, a_0, is replaced everywhere by the total (three-dimensional) lift-curve slope. Although there is little theoretical justification for this modification, it does alter the numerical results in the direction of the exact answer. Also, it is important to note that the lift distributions depicted in Figs. 4.14 and 4.15 cannot be generated with strip-theory aerodynamics, because strip theory fails to pick up the dropoff of the airload to zero at the wing tip caused by three-dimensional effects. A theory at least as sophisticated as lifting-line theory would have to be used to capture that effect.

4.2.4 Sweep Effects

To observe the effect of sweeping a wing aft or forward on the aeroelastic characteristics, it will be presumed that the swept geometry is obtained by rotating the surface about the root of the elastic axis as illustrated in Fig. 4.16. The aerodynamic reactions will depend on the angle of attack as measured in the streamwise direction as

$$\alpha = \alpha_{\mathrm{r}} + \theta \tag{4.71}$$

where θ is the change in the streamwise angle of attack caused by elastic deformation. To develop a kinematical relation for θ, we introduce the unit vectors $\hat{\mathbf{a}}_1$ and $\hat{\mathbf{a}}_2$, aligned with the y-axis and the freestream, respectively. Another set of unit vectors, $\hat{\mathbf{b}}_1$ and $\hat{\mathbf{b}}_2$, are obtained by rotating $\hat{\mathbf{a}}_1$ and $\hat{\mathbf{a}}_2$ by the sweep angle Λ as shown in Fig. 4.16, so that $\hat{\mathbf{b}}_1$ is aligned with the elastic axis (i.e., the $\overline{y}$-axis). From Fig. 4.16 one sees that

$$\begin{aligned} \hat{\mathbf{b}}_1 &= \cos(\Lambda)\hat{\mathbf{a}}_1 + \sin(\Lambda)\hat{\mathbf{a}}_2 \\ \hat{\mathbf{b}}_2 &= -\sin(\Lambda)\hat{\mathbf{a}}_1 + \cos(\Lambda)\hat{\mathbf{a}}_2 \end{aligned} \tag{4.72}$$

It should be observed that the total rotation of the local wing cross-sectional frame caused by elastic deformation can be written as the combination of rotations caused by wing torsion,

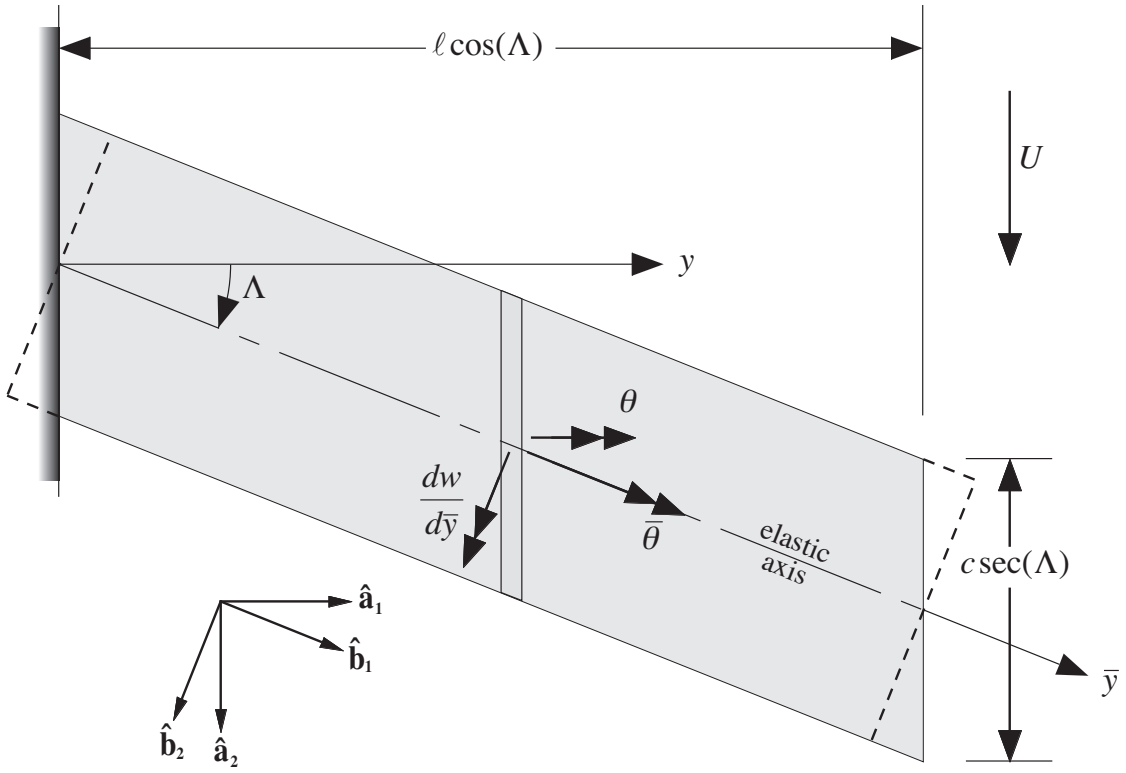

Figure 4.16: Schematic of swept wing (positive Λ)

$\overline{\theta}$ about $\hat{\mathbf{b}}_1$, and wing bending, $dw/d\overline{y}$ about $\hat{\mathbf{b}}_2$, where w is the wing bending deflection (positive up). Now, θ is the component of this total rotation about $\hat{\mathbf{a}}_1$, that is,

$$\begin{aligned}\theta &= \left(\overline{\theta}\hat{\mathbf{b}}_1 + \frac{dw}{d\overline{y}}\hat{\mathbf{b}}_2\right)\cdot\hat{\mathbf{a}}_1 \\ &= \overline{\theta}\cos(\Lambda) - \frac{dw}{d\overline{y}}\sin(\Lambda)\end{aligned} \tag{4.73}$$

From this relation, it can be noted that, as the result of sweep, the effective angle of attack is altered by bending. This coupling between bending and torsion will affect both the static aeroelastic response of the wing in flight as well as the conditions under which divergence occurs. Also it can be observed that, for combined bending and torsion of a swept elastic wing, the section in the direction of the streamwise airflow exhibits a change in camber, a higher-order effect that is here neglected.

To facilitate direct comparison with the previous unswept results, to the extent possible the same structural and aerodynamic notation will be retained as was used for the unswept planform. To determine the total elastic deflection two equilibrium equations are required, one for torsional moment equilibrium as in the unswept case and one for transverse force equilibrium (associated with bending). These equations can be written as

$$\begin{aligned}\frac{d}{d\overline{y}}\left(GJ\frac{d\overline{\theta}}{d\overline{y}}\right) &= -qec\overline{a}_0\alpha - qc^2c_{m_{\rm ac}} + Nmgd \\ \frac{d^2}{d\overline{y}^2}\left(EI\frac{d^2w}{d\overline{y}^2}\right) &= qc\overline{a}_0\alpha - Nmg\end{aligned} \tag{4.74}$$

In these equilibrium equations $\overline{a}_0$ is used to denote the two-dimensional lift-curve slope of the swept surface. This aerodynamic derivative is related to the unswept derivative by

$$\overline{a}_0 = a_0\cos(\Lambda) \tag{4.75}$$

for moderate- to high-aspect-ratio surfaces. Substituting for $\overline{a}_0$, $\alpha = \alpha_{\rm r} + \theta$ and in turn the dependence of θ on $\overline{\theta}$ and w from Eq. (4.73), specializing for spanwise uniformity so that GJ and EI are constants, and letting $(\,)'$ denote $d(\,)/d\overline{y}$, one obtains two coupled, ordinary differential equations for torsion and bending given by

$$\begin{aligned}\overline{\theta}'' + \frac{qeca_0}{GJ}\overline{\theta}\cos^2(\Lambda) - \frac{qeca_0}{GJ}w'\sin(\Lambda)\cos(\Lambda) &= -\frac{1}{GJ}\left[qeca_0\alpha_{\rm r}\cos(\Lambda) + qc^2c_{m_{\rm ac}} - Nmgd\right] \\ w'''' + \frac{qca_0}{EI}w'\sin(\Lambda)\cos(\Lambda) - \frac{qca_0}{EI}\overline{\theta}\cos^2(\Lambda) &= \frac{1}{EI}\left[qca_0\alpha_{\rm r}\cos(\Lambda) - Nmg\right]\end{aligned} \tag{4.76}$$

Since the surface is built-in at the root and free at the tip the following boundary conditions

must be imposed on the solution:

$$\begin{array}{lllll} \overline{y}=0: & \overline{\theta} & = & 0 & \text{(zero torsional rotation)} \\ & w & = & 0 & \text{(zero deflection)} \\ & w' & = & 0 & \text{(zero bending slope)} \\ \overline{y}=\ell: & \overline{\theta}' & = & 0 & \text{(zero twisting moment)} \\ & w'' & = & 0 & \text{(zero bending moment)} \\ & w''' & = & 0 & \text{(zero shear force)} \end{array} \tag{4.77}$$

Bending-torsion coupling is exhibited in Eqs. (4.76) through the term involving w in the torsion equation and through the term involving $\overline{\theta}$ in the bending equation.

There are two special cases of interest in which the coupling either vanishes or is very much simplified, so that one can solve the equations analytically. The first is for the case of vanishing sweep in which the uncoupled torsion equation (the first of Eqs. 4.76) is the same as previously discussed and clearly leads to solutions for either the torsional divergence condition or the torsional deformation and airload distribution, as discussed in sections 4.2.2 and 4.2.3, respectively. In the latter case, once the torsional deformation is obtained, the solution for $\theta = \overline{\theta}$ can be substituted into the bending equation (the second of Eqs. 4.76). Simple integration of the resulting ordinary differential equation leads to the shear force, bending moment, bending slope, and bending deflection.

A second special case occurs when $e = 0$. In this case, torsional divergence does not take place, and a polynomial solution for $\overline{\theta}$ can be found from the $\overline{\theta}$ equation and substituted into the bending equation. This leads to a fourth-order ordinary differential equation for w with a polynomial forcing function; note that the $\overline{\theta}$ terms are now part of that forcing function. This equation can be solved for the bending deflection, but the solution is not straightforward. Alternatively, to solve this equation for a divergence condition, one needs only the homogeneous part, which can be written as a third-order equation in $\zeta = w'$, namely,

$$\zeta''' + \frac{qca_0}{EI}\zeta \sin(\Lambda)\cos(\Lambda) = 0 \tag{4.78}$$

For the clamped-free boundary conditions $\zeta(0) = \zeta'(\ell) = \zeta''(\ell) = 0$, this equation has a known analytical solution that yields a divergence dynamic pressure of

$$q_D = -6.32970\frac{EI}{a_0 c\ell^3 \sin(\Lambda)\cos(\Lambda)} \tag{4.79}$$

The minus sign implies that this bending divergence instability only takes place for forward-swept wings, that is, where $\Lambda < 0$.

Examination of Eqs. (4.76) illustrates that there are two ways in which the sweep influences the aeroelastic behavior. One is the loss of aerodynamic effectiveness as exhibited by the change in the second term of the torsion equations from

$$\frac{qeca_0}{GJ}\overline{\theta} \qquad \text{to} \qquad \frac{qeca_0}{GJ}\overline{\theta}\cos^2(\Lambda) \tag{4.80}$$

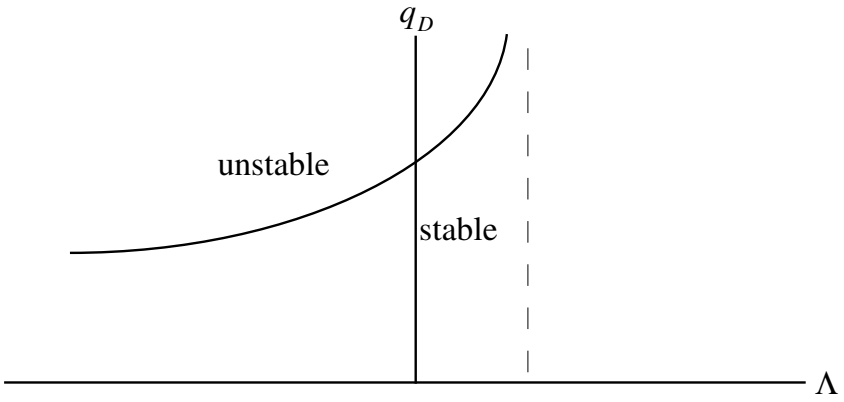

Figure 4.17: Divergence dynamic pressure versus Λ

Note that this effect is independent of the direction of sweep. The second effect is the influence of bending slope on the effective angle of attack (see Eq. 4.73), which leads to bending-torsion coupling. This coupling has a strong influence on both divergence and load distribution. The total effect of sweep depends strongly on whether the surface is swept back or forward. This can be illustrated by its influence on the divergence dynamic pressure, q_D, as shown in Fig. 4.17. It is apparent that forward sweep causes the surface to be more susceptible to divergence whereas backward sweep increases the divergence dynamic pressure. Indeed, a small amount of backward sweep (for the idealized case under consideration, depending on e/ℓ and GJ/EI, only 5° or 10°) can cause the divergence dynamic pressure to become infinite, thus eliminating the instability altogether. Some specific cases are discussed later in this section in conjunction with an approximate solution of the governing equations.

The overall effect of sweep on the aeroelastic load distribution also strongly depends on whether the surface is swept forward or aft. This is illustrated in Fig. 4.18, which shows spanwise load distributions for an elastic surface for which the total lift (or N) is held constant by adjusting α_{r}. From a structural loads standpoint it is apparent that the root bending moment is significantly greater for forward sweep than for backward sweep at a given value of total lift.

The primary motivation for sweeping a lifting surface is to improve the vehicle performance through drag reduction, although some loss in lifting capability may be experienced. However, the above aeroelastic considerations can have a significant impact on design decisions. From an aeroelastic standpoint forward sweep exacerbates divergence instability and increases structural loads whereas backward sweep can alleviate these concerns. The advent of composite lifting surfaces has enabled the use of bending-twist elastic coupling to passively stabilize forward sweep, making it possible to use forward-swept wings. Indeed, the X-29 could not have been flown without some means to stabilize the wings against divergence. We will discuss this further below under aeroelastic tailoring.

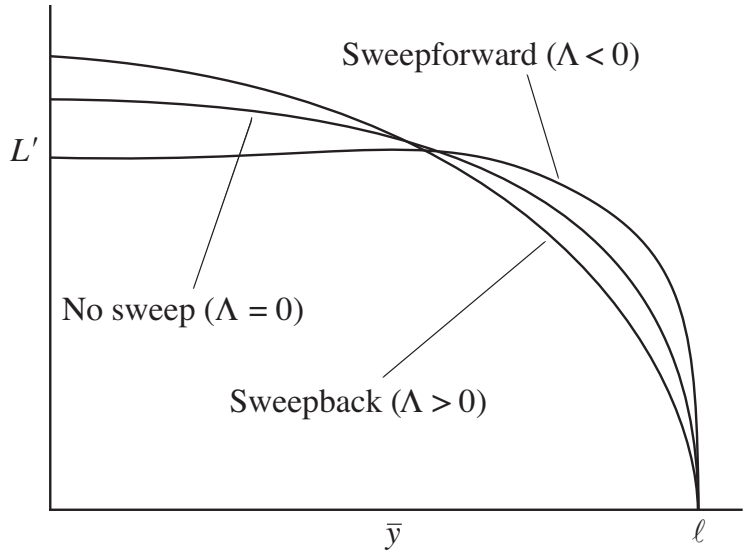

Figure 4.18: Lift distribution for positive, zero, and negative Λ

Exact Solution for Bending-Torsion Divergence

Extraction of the analytical solution of the above set of coupled ordinary differential equations, Eqs. (4.76), is very complicated. The exact analytical solution is most easily obtained by first converting the coupled set of equations into a single equation governing the elastic component of the angle of attack. For calculation of only the divergence dynamic pressure, one can consider just the homogeneous parts of Eqs. (4.76):

$$\begin{aligned} \overline{\theta}'' + \frac{qeca_0}{GJ}\overline{\theta}\cos^2(\Lambda) - \frac{qeca_0}{GJ}w'\sin(\Lambda)\cos(\Lambda) &= 0 \\ w'''' + \frac{qca_0}{EI}w'\sin(\Lambda)\cos(\Lambda) - \frac{qca_0}{EI}\overline{\theta}\cos^2(\Lambda) &= 0 \end{aligned} \tag{4.81}$$

To get a single equation one differentiates the first equation with respect to $\overline{y}$ and multiplies it by $\cos(\Lambda)$. From this modified first equation, one subtracts $\sin(\Lambda)$ times the second equation, replacing $\overline{\theta}\cos(\Lambda) - w'\sin(\Lambda)$ with θ, to obtain

$$\theta''' + \frac{qeca_0}{GJ}\cos^2(\Lambda)\theta' + \frac{qca_0}{EI}\sin(\Lambda)\cos(\Lambda)\theta = 0 \tag{4.82}$$

Introducing a dimensionless axial coordinate $\eta = \overline{y}/\ell$, the above equation can be written as

$$\theta''' + \frac{qeca_0\ell^2}{GJ}\cos^2(\Lambda)\theta' + \frac{qca_0\ell^3}{EI}\sin(\Lambda)\cos(\Lambda)\theta = 0 \tag{4.83}$$

where $(\,)'$ now denotes $d(\,)/d\eta$. The boundary conditions can be derived from Eqs. (4.77) as

$$\theta(0) = \theta'(1) = \theta''(1) + \frac{qeca_0\ell^2}{GJ}\cos^2(\Lambda)\theta(1) = 0 \tag{4.84}$$

Here the first of Eqs. (4.81) and the final boundary condition from Eqs. (4.77) are used to derive the third boundary condition.

The exact solution for Eqs. (4.83) and (4.84) has been obtained by Diederich and Budiansky (1948). First, one defines

$$\begin{aligned} \tau &= \frac{qeca_0\ell^2}{GJ}\cos^2(\Lambda) \\ \beta &= \frac{qca_0\ell^3}{EI}\sin(\Lambda)\cos(\Lambda) \end{aligned} \tag{4.85}$$

so that the differential equation and boundary conditions can be written simply as

$$\theta''' + \tau\theta' + \beta\theta = 0 \tag{4.86}$$

and

$$\theta(0) = \theta'(1) = \theta''(1) + \tau\theta(1) = 0 \tag{4.87}$$

Next, one sets $\theta = \hat{\theta}\exp(\lambda\eta)$ where λ and $\hat{\theta}$ are unknown constants. Then, the general solution has the form

$$\theta = A_1 \exp(\lambda_1\eta) + A_2 \exp(\lambda_2\eta) + A_3 \exp(\lambda_3\eta) \tag{4.88}$$

where λ_i for i =1, 2, and 3, are the three roots of

$$\lambda^3 + \tau\lambda + \beta = 0 \tag{4.89}$$

which we do not list here because they are quite lengthy functions of β and τ. However, they can be easily obtained in closed form by use of Mathematica™. Substituting Eq. (4.88) into the three boundary conditions found in Eqs. (4.84) yields three linear, homogeneous, algebraic equations in the unknowns A_1, A_2, A_3, given by

$$\begin{aligned} &A_1 + A_2 + A_3 = 0 \\ &A_1\lambda_1 \exp(\lambda_1) + A_2\lambda_2 \exp(\lambda_2) + A_3\lambda_3 \exp(\lambda_3) = 0 \\ &A_1 \exp(\lambda_1)(\lambda_1^2 + \tau) + A_2 \exp(\lambda_2)(\lambda_2^2 + \tau) + A_3 \exp(\lambda_3)(\lambda_3^2 + \tau) = 0 \end{aligned} \tag{4.90}$$

where β and τ appear as additional unknowns. A non-trivial solution only exists when β and τ satisfy the characteristic equation, which is found by setting the determinant of the 3×3 coefficient matrix equal to zero, so that

$$\begin{vmatrix} 1 & 1 & 1 \\ \lambda_1 \exp(\lambda_1) & \lambda_2 \exp(\lambda_2) & \lambda_3 \exp(\lambda_3) \\ (\lambda_1^2 + \tau)\exp(\lambda_1) & (\lambda_2^2 + \tau)\exp(\lambda_2) & (\lambda_3^2 + \tau)\exp(\lambda_3) \end{vmatrix} = 0 \tag{4.91}$$

The non-trivial solutions are those that lie on a divergence boundary. Therefore, one can solve the characteristic equation numerically for β_D in terms of τ_D, or vice versa, where the subscript D is added because these values lie on the divergence boundary. The behavior of this solution is quite complex, having multiple branches, and it is not easily used in a design context. However, a simple approximation of the most important branch from a physical point of view is presented next and compared with plots of the exact solution.

Approximate Solution for Bending-Torsion Divergence

In view of the complexity of the exact solution, it is fortunate that there are various approximate methods for treating such equations, one of which is the application of the method of Ritz to the virtual work principle (see Section 2.7). In this special case, the kinetic energy is zero, and the resulting algebraic equations are a special case of the generalized equations of motion or Lagrange's equations, termed here the generalized equations of equilibrium. Determination of such an approximate solution is left as an exercise for the reader; see Problems 11 – 15. The divergence dynamic pressure is found from solution of an eigenvalue problem based on a set of homogeneous, linear, algebraic equations. The response for a

given dynamic pressure is found in terms of the solution of a set of nonhomogeneous, linear, algebraic equations.

An alternative approach is to obtain an approximate solution of Eq. (4.83) with boundary conditions as in Eq. (4.84) by Galerkin's method. Note that Eqs. (4.83) and (4.84) can be reduced to a second-order integro-differential equation

$$\theta'' + \tau\theta - r\tau \int_{\eta}^{1} \theta(\xi) d\xi = 0 \tag{4.92}$$

with boundary conditions $\theta(0) = \theta'(1) = 0$. Because the order is reduced, the number of boundary conditions is thus reduced as well. Moreover, the form of the boundary conditions is greatly simplified, so that application of Galerkin's method is facilitated. The outworking of this approximate solution is left as an exercise for the reader in Problem 18; Galerkin's method is discussed in Section 2.8.

Here we consider instead an approximation of one branch of the analytical solution for the bending-torsion divergence problem. Fortunately, the most important branch from a physical point of view behaves quite simply. Indeed, as shown by Diederich and Budiansky (1948), the divergence boundary can be approximately represented within a certain range in terms of a straight line

$$\tau_D = \frac{\pi^2}{4} + \frac{3\pi^2}{76}\beta_D \tag{4.93}$$

with τ_D and β_D as defined in Eqs. (4.85). Such a straight line approximation follows naturally from a one-term Galerkin approximation; see Problem 18. However, we have adjusted the two constants so that, for a wing rigid in bending we have $\beta_D = 0$; thus, $\tau_D = \frac{\pi^2}{4}$, the exact solution for pure torsional divergence. Also, for a torsionally rigid wing we want $\tau_D = 0$; thus, $\beta_D = -6.3297$, the exact solution for bending divergence. Diederich and Budiansky (1948) used instead $\beta_D = -19/3$, which is very close to $\beta_D = -6.3297$. For the cases in between the error is quite small.

It is very important to note that the sign of τ is driven by the sign of e, whereas the sign of β is driven by the sign of Λ. The approximate solution in Eq. (4.93) is plotted along with some of the exact solution branches in Fig. 4.19. Note the excellent agreement between the straight line approximation and the exact solution near the origin. Also note that the intersections of the solution with the τ_D axis (where $\beta_D = 0$) coincide with the squares of the roots previously obtained in Section 4.2.2, Eq. (4.62), as $(2n-1)^2\pi^2/4$ for n=1, 2, ..., ∞ (i.e., $\pi^2/4$, $9\pi^2/4$, ...).

A somewhat more convenient way of depicting the behavior of the divergence dynamic pressure is to plot τ_D versus a parameter that depends only on the configuration. This can be accomplished by introducing the dimensionless parameter r, given by

$$r \equiv \frac{\beta}{\tau} = \frac{\ell}{e}\frac{GJ}{EI}\tan(\Lambda) \tag{4.94}$$

which can be positive, negative, or zero. Equation (4.93) can then be written as

$$\tau_D = \frac{\pi^2}{4} + \frac{3\pi^2 r}{76}\tau_D \tag{4.95}$$

Thus, one can solve for τ_D, such that

$$\tau_D = \frac{\pi^2}{4\left(1 - \frac{3\pi^2 r}{76}\right)} \tag{4.96}$$

or alternatively for q_D, equal to

$$q_D = \frac{GJ\pi^2}{4eca_0\ell^2\cos^2(\Lambda)\left[1 - \frac{3\pi^2}{76}\frac{\ell}{e}\frac{GJ}{EI}\tan(\Lambda)\right]} \tag{4.97}$$

Behavior of the Exact and Approximate Solutions

Several branches of the exact solution of Eqs. (4.83) and (4.84) for the smallest absolute values of τ_D versus r are plotted as solid lines in Fig. 4.20. It is noted that there is at least one branch in all quadrants but the third, and there is only one branch in the fourth quadrant. The approximate solutions for τ_D versus r from Eq. (4.96) are plotted as dashed hyperbolae in the first, second, and fourth quadrants. Moreover, as r becomes large the solution in the fourth quadrant asymptotically approaches the parabola $\tau_D = -27r^2/4$, also shown as a dashed curve. We note that, as with Fig. 4.19, the intersections of the roots with the τ_D axis are $\pi^2/4$, $9\pi^2/4$, $25\pi^2/4$, etc. The configuration of any wing fixes the value of r. For positive e one considers only positive values of τ_D. Thus, one starts from zero and proceeds in the positive τ_D direction on this plot (i.e., at constant r) to find the first intersection with a solid line. This is the dynamic pressure parameter τ_D at which divergence occurs. In Fig. 4.21 a blowup of these results in a more practical range is shown. It is easily seen that the dashed lines in the first and second quadrants are very close to the solid ones when $r < 1.5$. We note that when $e < 0$ a negative value of τ_D leads to a positive value of q_D. In this case, one should proceed along a line of constant r in the negative τ_D direction.

It is interesting to note that the approximate solution, despite its close proximity to the exact solution, exhibits a qualitatively different behavior mathematically. The approximate solution exhibits an asymptotic behavior, with τ_D tending to plus infinity from the left and to minus infinity from the right at the value of r that causes the denominator to vanish, namely, when $r = 76/(3\pi^2) = 2.56680$. If the approximate solution were exact, mathematically it would mean that divergence is not possible at that value of r. Moreover, physically it would mean that divergence is not possible for $e > 0$ and $r \geq 76/(3\pi^2)$ [or for $e < 0$ and $r \leq 76/(3\pi^2)$]. Actually, however, the exact solution is of the "limit point" variety. For $e > 0$ this means that divergence occurs for small and positive values of r. Moreover, as r is increased in the first quadrant, τ_D also increases until a certain point is reached at which two things happen: (1) Above this value of τ_D, the curve turns back to the left instead

of reaching an asymptote; and (2) any slight increase in r beyond this point will cause the solution to jump to a higher branch. This point is called a limit point. On the main branch of the curve in the first quadrant, for example, the limit point is at $r = 1.59768$ and $\tau_D = 10.7090$. It can be seen from the plot in Fig. 4.20 that any slight increase in r will cause the solution to jump from the lower branch, where its value is 10.7090, to a higher branch where its value is 66.8133, at which point τ_D is rapidly increasing with r. So, although there is no value of r that will result in an infinite exact value of the divergence dynamic pressure, practically speaking, divergence in the vicinity of the limit point value of r is all but eliminated. Thus, it is sufficient for practical purposes to say that divergence is not possible near those points where the approximate solution blows up, and one may regard the approximate solution as being sufficiently close to the exact solution for design purposes. The limit point in the fourth quadrant is appropriate for the situation in which $e < 0$, namely when the aerodynamic center is behind the elastic axis. There the exact limit point is at $r = 3.56595$ and $\tau_D = -14.8345$. Note that the negative values of e and τ_D yield a positive q_D. It is left to the reader as an exercise to explore this possibility further; see Problem 17.

Although there are qualitative differences as noted between the exact and approximate solutions, within the practical range of interest, the above linear approximation of the divergence boundary in terms of τ_D and β_D is numerically quite accurate and leads to a very simple expression for the divergence dynamic pressure in terms of the structural stiffnesses, e/ℓ, and the sweep angle, that is, Eq. (4.97). This approximate formula can be used in design to explore the behavior of the divergence dynamic pressure as a function of the various configuration parameters therein. For the purpose of displaying results for the divergence dynamic pressure when $e > 0$, it is convenient to normalize q_D with its value at zero sweep angle, namely

$$q_{D_0} = \frac{\pi^2 GJ}{4eca_0\ell^2} \tag{4.98}$$

so that

$$\frac{q_D}{q_{D_0}} = \frac{1 + \tan^2(\Lambda)}{1 - \frac{3\pi^2}{76}\frac{\ell}{e}\frac{GJ}{EI}\tan(\Lambda)} \tag{4.99}$$

Thus, for a wing structural design with given values of $e > 0$, GJ, EI, and ℓ, there are multiple values of sweep angle Λ for which the divergence dynamic pressure goes to infinity, implying that divergence is not possible at those values of Λ. There are evidently some values of Λ that make the numerator term $\tan(\Lambda)$ infinite, whereas there are other values that make the denominator vanish. Therefore, within the principal range of Λ, we can surmise that divergence will only take place for cases in which $|\Lambda| \neq 90^\circ$ and that $3\pi^2 r \neq 76$; that is, divergence is not possible for $e > 0$ unless $-90^\circ < \Lambda < \Lambda_\infty$ where

$$\tan(\Lambda_\infty) = \frac{76EIe}{3\pi^2 GJ\ell} \tag{4.100}$$

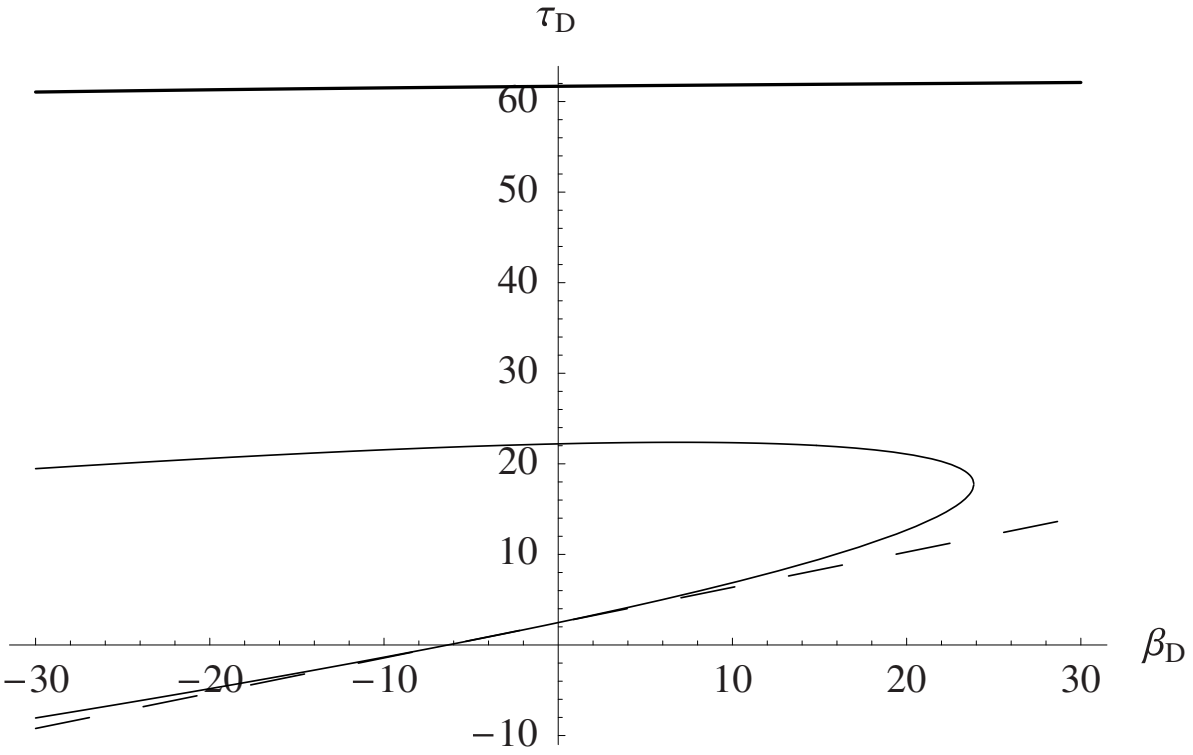

Figure 4.19: τ_D versus β_D for coupled bending-torsion divergence; solid lines (exact solution) and dashed line (Eq. 4.93)

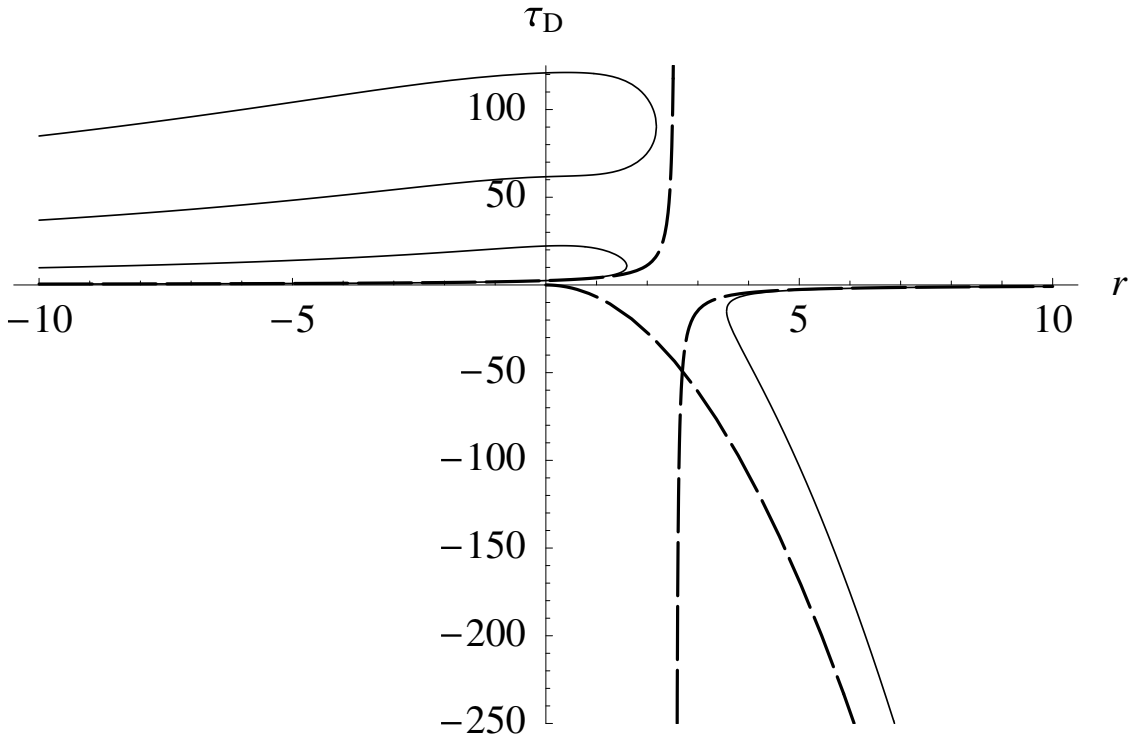

Figure 4.20: τ_D versus r for coupled bending-torsion divergence; solid lines (exact solution) and dashed lines (Eq. 4.96 and $\tau_D = -27r^2/4$ in fourth quadrant)

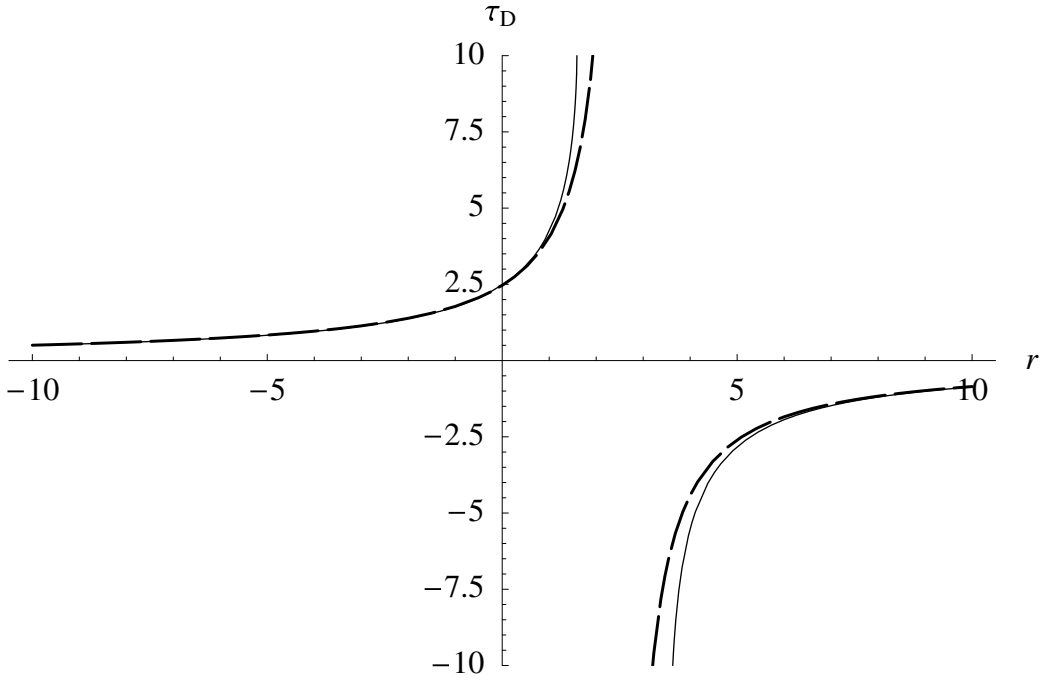

Figure 4.21: τ_D versus r for coupled bending-torsion divergence; solid lines (exact solution) and dashed lines (Eq. 4.96)

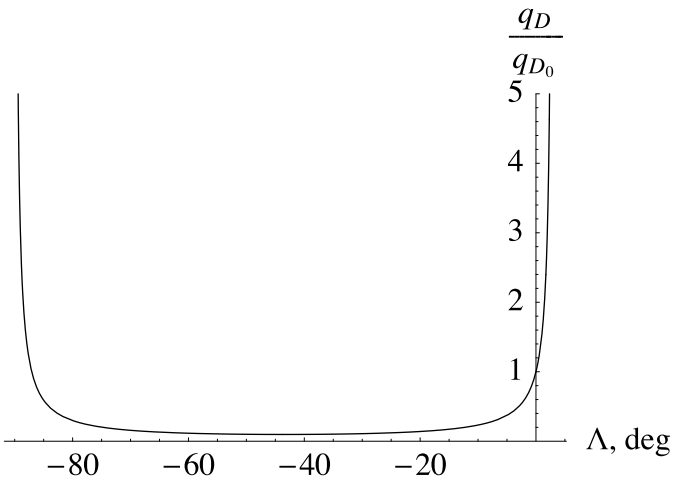

Figure 4.22: Normalized divergence dynamic pressure for an elastically uncoupled, swept wing with $GJ/EI = 1.0$ and $e/\ell = 0.02$

Thus, Eq. (4.99) can be written as

$$\frac{q_D}{q_{D_0}} = \frac{1 + \tan^2(\Lambda)}{1 - \frac{\tan(\Lambda)}{\tan(\Lambda_\infty)}} \tag{4.101}$$

In other words, one avoids divergence by choosing $\Lambda \geq \Lambda_\infty$, and the divergence dynamic pressure drops drastically as Λ is decreased below Λ_∞. Because Λ_∞ is likely to be small, this frequently means that backswept wings are free of divergence, and that divergence dynamic pressure drops drastically for forward-swept wings. Because Λ_∞ is the asymptotic value of Λ from the approximate solution, which is greater than the limit point value of Λ from the exact solution, we may surmise that the approximate solution provides a conservative design. Figure 4.22 shows the behavior of divergence dynamic pressure for an elastically uncoupled wing with $GJ/EI = 1.0$ and $e/\ell = 0.02$. The plot, as expected, passes through unity when the sweep angle is zero. Since Λ_∞ is very small for this case, the divergence dynamic pressure goes to infinity for a very small positive value of sweep angle. Thus, even a small backward sweep angle can make divergence impossible. Figure 4.23 shows the result of decreasing GJ/EI to 0.2 and holding e/ℓ constant. Because Λ_∞ increases, the wing must be swept back further than in the previous case to avoid divergence. Finally, the accuracy of the approximate solution may be better appreciated by looking at the normalized divergence dynamic pressure versus Λ, as shown in Fig. 4.24. A case is shown with a larger than usual value of e/ℓ to elucidate the possible difference, conservative from a design point of view, between the limit point of the exact solution at $\Lambda = 21.7728°$ and $q_D = 5.08109 q_{D_0}$ versus the asymptote of the approximate solution at $\Lambda = \Lambda_\infty = 32.6734°$.

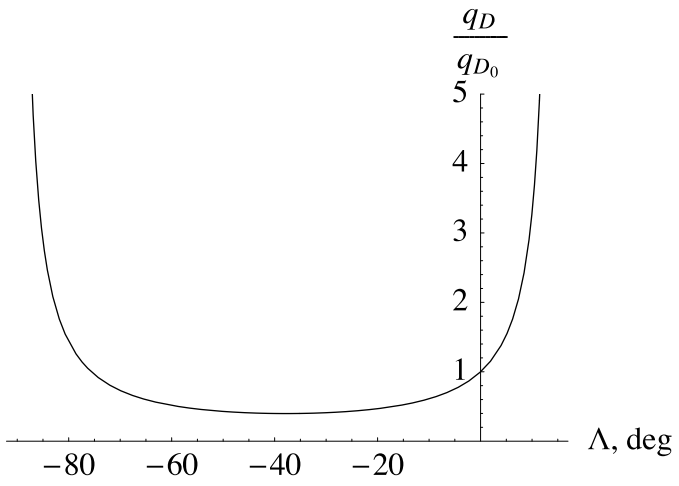

Figure 4.23: Normalized divergence dynamic pressure for an elastically uncoupled, swept wing with $GJ/EI = 0.2$ and $e/\ell = 0.02$

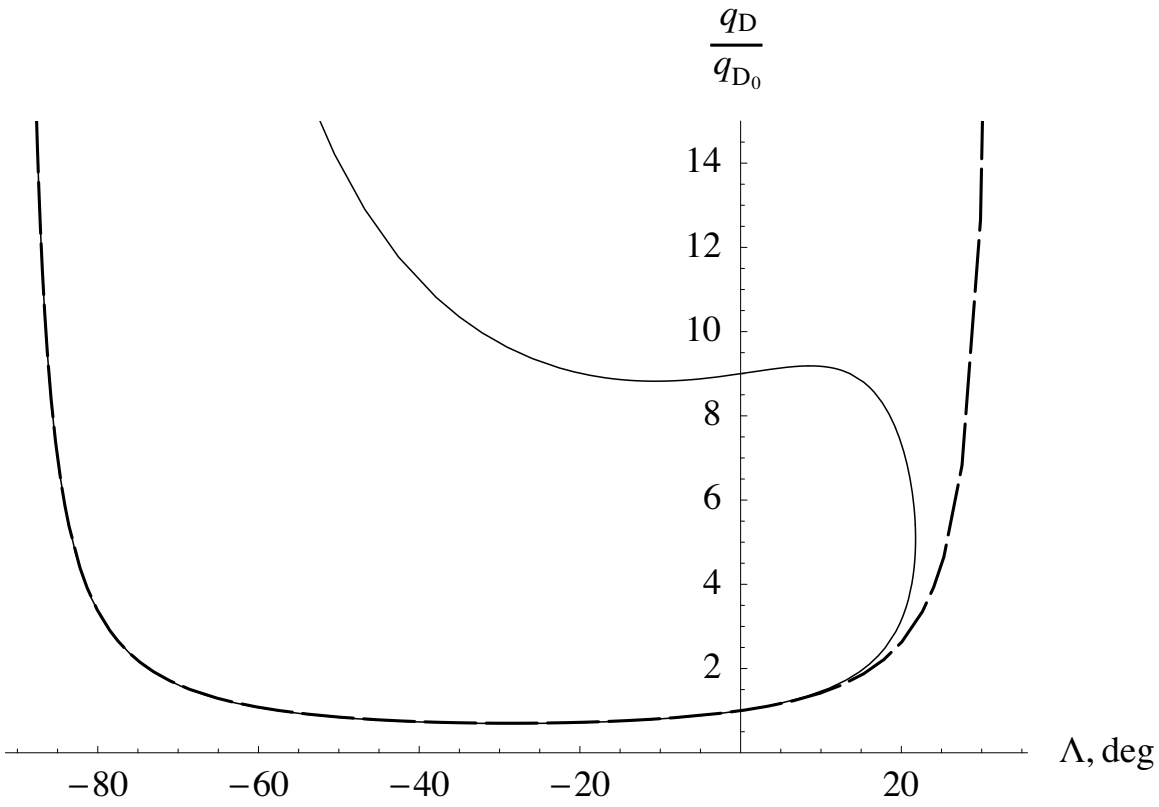

Figure 4.24: Normalized divergence dynamic pressure for an elastically uncoupled, swept wing with $e = 0.05\,\ell$ and $GJ/EI = 0.2$: exact solution (solid line) and closed-form approximate solution (dashed line)

Aeroelastic Tailoring

Aeroelastic tailoring is the design of wings using the directional properties of composite materials to optimize aeroelastic performance. The concept of aeroelastic tailoring is relatively new and came into the forefront during the design of forward-swept wings in the 1980s. Equation (4.101) shows that q_D drops dramatically for forward-swept, untailored wings. The low divergence speed was a major hurdle in the design of wings with forward sweep. As will be seen in this section, use of composite materials can help remove the disadvantages of forward sweep. Presently, aeroelastic tailoring is an integral part of composite wing designs and can be used to provide optimum performance.

Composite materials are anisotropic, which implies different material characteristics (such as stiffness) in different directions. A simple beam model is quite helpful in developing an understanding of the behavior of composite wings. Such models may exhibit bending-torsion elastic coupling. Analysis of beams with elastic coupling is a bit more involved, but it leads to results that are quite helpful.

Let us introduce such coupling in our beam equations. For anisotropic beams with bending-torsion coupling, the "constitutive law" (i.e., the relation between cross-sectional stress resultants and the generalized strains) changes from

$$\begin{Bmatrix} T \\ M \end{Bmatrix} = \begin{bmatrix} GJ & 0 \\ 0 & EI \end{bmatrix} \begin{Bmatrix} \overline{\theta}' \\ w'' \end{Bmatrix} \tag{4.102}$$

to

$$\begin{Bmatrix} T \\ M \end{Bmatrix} = \begin{bmatrix} GJ & -K \\ -K & EI \end{bmatrix} \begin{Bmatrix} \overline{\theta}' \\ w'' \end{Bmatrix} \tag{4.103}$$

where K is the bending-torsion coupling stiffness (having the same dimensions as EI and GJ) and $(\ )'$ indicates the derivative with respect to $\overline{y}$. A positive value of K means that a positive bending deflection will be accompanied by a nose-up twist of the wing, which is normally destabilizing for cases with the elastic axis behind the aerodynamic center.

Using the coupled constitutive law, the equations of equilibrium become

$$\begin{aligned} \left(GJ\overline{\theta}' - Kw''\right)' &= -qec\overline{a}_0\alpha - qc^2c_{m_{ac}} + Nmgd \\ \left(EIw'' - K\overline{\theta}'\right)'' &= qc\overline{a}_0\alpha - Nmg \end{aligned} \tag{4.104}$$

Let us again consider a wing that is clamped at the root and free at the tip, so that the boundary conditions that must be imposed on the solution are

$$\begin{array}{lrl} \overline{y} = 0\text{:} & \overline{\theta} = 0 & \text{(zero torsional rotation)} \\ & w = 0 & \text{(zero deflection)} \\ & w' = 0 & \text{(zero bending slope)} \\ \overline{y} = \ell\text{:} & T = 0 & \text{(zero twisting moment)} \\ & M = 0 & \text{(zero bending moment)} \\ & M' = 0 & \text{(zero shear force)} \end{array} \tag{4.105}$$

For composite beams the offsets d and e may be defined in a manner similar to the way they were defined for isotropic beams: d is the distance from the $\overline{y}$-axis to the cross-sectional mass centroid, positive when the mass centroid is toward the leading edge from the $\overline{y}$-axis; and e is the distance from the $\overline{y}$-axis to the aerodynamic center, positive when the aerodynamic center is toward the leading edge from the $\overline{y}$-axis. However, for composite beams the $\overline{y}$-axis must have different properties from those it possesses for isotropic beams, and the term "elastic axis" has a different meaning. Recall that for a spanwise uniform isotropic beam, the elastic axis is along the $\overline{y}$-axis and is the locus of cross-sectional shear centers; transverse forces acting through this axis do not twist the beam. For spanwise uniform composite beams with bending-twist coupling no axis can be defined as the locus of a cross-sectional property through which transverse shear forces can act without twisting the beam. For such beams we must place the $\overline{y}$-axis along the locus of generalized shear centers, a point in the cross-section at which transverse shear forces are structurally decoupled from the twisting moment. Although transverse shear forces acting at the $\overline{y}$-axis do not *directly* induce twist, the bending moment induced by the shear force will still induce twist when $K \neq 0$.

We can now write the homogeneous part of the equations of equilibrium as

$$\begin{aligned} \overline{\theta}'' - \frac{K}{GJ} w''' + \frac{qeca_0}{GJ} \theta \cos(\Lambda) &= 0 \\ w'''' - \frac{K}{EI} \overline{\theta}''' - \frac{qca_0}{EI} \theta \cos(\Lambda) &= 0 \end{aligned} \tag{4.106}$$

Differentiating the first equation with respect to $\overline{y}$ and transforming the set of equations so that they are uncoupled in the highest derivative terms $\overline{\theta}'''$ and w'''', we obtain

$$\begin{aligned} \overline{\theta}''' + \frac{EI\ GJ}{EI\ GJ - K^2} \frac{qeca_0}{GJ} \theta' \cos(\Lambda) - \frac{K\ EI}{EI\ GJ - K^2} \frac{qca_0}{EI} \theta \cos(\Lambda) &= 0 \\ w'''' + \frac{K\ GJ}{EI\ GJ - K^2} \frac{qeca_0}{GJ} \theta' \cos(\Lambda) - \frac{EI\ GJ}{EI\ GJ - K^2} \frac{qca_0}{EI} \theta \cos(\Lambda) &= 0 \end{aligned} \tag{4.107}$$

Multiplying the first equation by $\cos(\Lambda)$ and the second equation by $\sin(\Lambda)$ and subtracting the second equation from the first, we obtain a single equation in terms of $\theta = \overline{\theta} \cos(\Lambda) - w' \sin(\Lambda)$ as

$$\begin{aligned} \theta''' + \frac{EI\ GJ}{EI\ GJ - K^2} \frac{qeca_0 \ell^2}{GJ} \cos^2(\Lambda) \left[1 - \frac{K}{EI} \tan(\Lambda) \right] \theta' \\ + \frac{EI\ GJ}{EI\ GJ - K^2} \frac{qca_0 \ell^3}{EI} \sin(\Lambda) \cos(\Lambda) \left[1 - \frac{K}{GJ} \frac{1}{\tan(\Lambda)} \right] \theta = 0 \end{aligned} \tag{4.108}$$

where $(\ )'$ now denotes $d(\ )/d\eta$ as in the parallel development for the elastically uncoupled wing above.

The boundary conditions can be derived from Eqs. (4.105) as

$$\theta(0) = \theta'(1) = \theta''(1) + \frac{EI\ GJ}{EI\ GJ - K^2} \frac{qeca_0 \ell^2}{GJ} \cos^2(\Lambda) \left[1 - \frac{K}{EI} \tan(\Lambda) \right] \theta(1) = 0 \tag{4.109}$$

Note that the aeroelastic divergence problem with structural coupling has the same mathematical form as the problem without coupling, an approximate solution of which is given in the previous section. One can see that the parameters τ and β can be redefined as

$$\begin{aligned}\tau =& \frac{EI\ GJ}{EI\ GJ - K^2}\frac{qeca_0\ell^2}{GJ}\cos^2(\Lambda)\left[1 - \frac{K}{EI}\tan(\Lambda)\right] \\ \beta =& \frac{EI\ GJ}{EI\ GJ - K^2}\frac{qca_0\ell^3}{EI}\sin(\Lambda)\cos(\Lambda)\left[1 - \frac{K}{GJ}\frac{1}{\tan(\Lambda)}\right]\end{aligned} \tag{4.110}$$

and, again, the divergence boundary can be expressed approximately in terms of the line

$$\tau_D = \frac{\pi^2}{4} + \frac{3\pi^2}{76}\beta_D \tag{4.111}$$

Using the expressions for the parameters in the equation of the divergence boundary, we have

$$q_D = \frac{\pi^2}{4}\frac{EI\ GJ - K^2}{EI\ GJ}\frac{GJ}{eca_0\ell^2\cos^2(\Lambda)}\frac{1}{\left\{1 - \frac{K}{EI}\tan(\Lambda) - \frac{3\pi^2}{76}\frac{\ell}{e}\frac{GJ}{EI}\left[\tan(\Lambda) - \frac{K}{GJ}\right]\right\}} \tag{4.112}$$

One can simplify the above by introducing the dimensionless parameter

$$\kappa = \frac{K}{\sqrt{EI\ GJ}} \tag{4.113}$$

so that

$$q_D = \frac{\pi^2 GJ(1-\kappa^2)}{4eca_0\ell^2\cos^2(\Lambda)\left\{1 - \kappa\sqrt{\frac{GJ}{EI}}\tan(\Lambda) - \frac{3\pi^2}{76}\frac{\ell}{e}\frac{GJ}{EI}\left[\tan(\Lambda) - \kappa\sqrt{\frac{EI}{GJ}}\right]\right\}} \tag{4.114}$$

With Eq. (4.114) one may determine the divergence dynamic pressure with sufficient accuracy to ascertain its trends versus sweep angle Λ and elastic coupling parameter κ. The formula shows that there is a strong relationship between these two quantities.

To illustrate the utility of the above analysis, let us first normalize q_D with the value it would have at zero sweep angle and zero coupling, namely, q_{D_0}, so that

$$\frac{q_D}{q_{D_0}} = \frac{(1-\kappa^2)\left[1 + \tan^2(\Lambda)\right]}{1 - \kappa\sqrt{\frac{GJ}{EI}}\tan(\Lambda) - \frac{3\pi^2}{76}\frac{\ell}{e}\frac{GJ}{EI}\left[\tan(\Lambda) - \kappa\sqrt{\frac{EI}{GJ}}\right]} \tag{4.115}$$

The denominator's vanishing corresponds to infinite divergence dynamic pressure, and crossing this "boundary" means crossing from a regime in which divergence exists to one in which it does not. Setting the denominator to zero and solving for the tangent of the sweep angle, one obtains

$$\tan(\Lambda_\infty) = \frac{1 + \frac{3\pi^2}{76}\sqrt{\frac{GJ}{EI}}\frac{\ell}{e}\kappa}{\frac{3\pi^2}{76}\frac{GJ}{EI}\frac{\ell}{e} + \sqrt{\frac{GJ}{EI}}\kappa} \tag{4.116}$$

where Λ_∞ is the sweep angle at which the divergence dynamic pressure goes to infinity. With this definition, one can rewrite Eq. (4.115) as

$$\frac{q_D}{q_{D_0}} = \frac{(1-\kappa^2)\left[1+\tan^2(\Lambda)\right]}{\left(1+\frac{3\pi^2}{76}\sqrt{\frac{GJ}{EI}}\frac{\ell}{e}\kappa\right)\left[1-\frac{\tan(\Lambda)}{\tan(\Lambda_\infty)}\right]} \tag{4.117}$$

Again, for positive e divergence is possible only if $-90^\circ < \Lambda < \Lambda_\infty$. Thus, because of the presence of κ as an additional design parameter, the designer can at least partially compensate for the destabilizing effect of forward sweep by appropriately choosing $\kappa < 0$, which for an increment of upward bending of the wing provides an increment of nose-down twisting. There is a limit to how much coupling can be achieved, however, as typically, $|\kappa| < 0.5$.

There are two main differences in isotropic wing design versus design with composite wings. First, it is possible to achieve a much wider range of values for GJ/EI. Second, and significantly more powerful, is the fact that composite wings can be designed with nonzero values of κ. From Eq. (4.116), the value of Λ_∞ is decreased as κ is decreased, which means that the range of Λ over which divergence occurs is decreased. To confirm this and our earlier statement about positive κ being destabilizing, Fig. 4.25 shows results for $\kappa = -0.4$, 0, and 0.4. It is clear that one can sweep a composite wing forward and still avoid divergence with a proper choice (i.e., a sufficiently large and negative value) of κ. Since forward sweep has advantages for the design of highly maneuverable aircraft, this is a result of practical importance. The sweep angles at which divergence becomes impossible, Λ_∞, are also somewhat sensitive to GJ/EI and e/ℓ as shown in Figs. 4.26 and 4.27. Evidently, one may design divergence-free, forward-swept wings with larger sweep angles by decreasing torsional stiffness relative to bending stiffness and by decreasing e/ℓ.

4.2.5 Effect of Drag on Divergence of Slender Wings

In the above we have assumed that nonlinear effects are unimportant and that bending is in the softer direction, i.e. about the airfoil chordline, which is shown as the x axis in Fig. 4.12 and as the unit vector $\hat{\mathbf{b}}_2$ in Fig. 4.16. This bending gives rise to deflections that are approximately in the direction of lift. However, the drag force also induces a bending moment, nominally about the z axis, that tends to bend the wing in the plane of greatest flexural rigidity and gives rise to bending deflections approximately parallel to the drag force. When $EI_z >> EI_x = EI$, the drag force results in negligible bending *deflection*, but the resulting bending *moment* can affect divergence. Indeed, if this moment is sufficiently large it can lead to lateral-torsional buckling, even without consideration of any aeroelastic effects. This type of buckling can be a factor in design of wind turbine blades, helicopter blades, and sail plane wings.

Consider an unswept, cantilevered wing with its elastic axis along y, and with cross-sectional coordinates x and z as shown in Fig. 4.12. The beam has torsional stiffness GJ

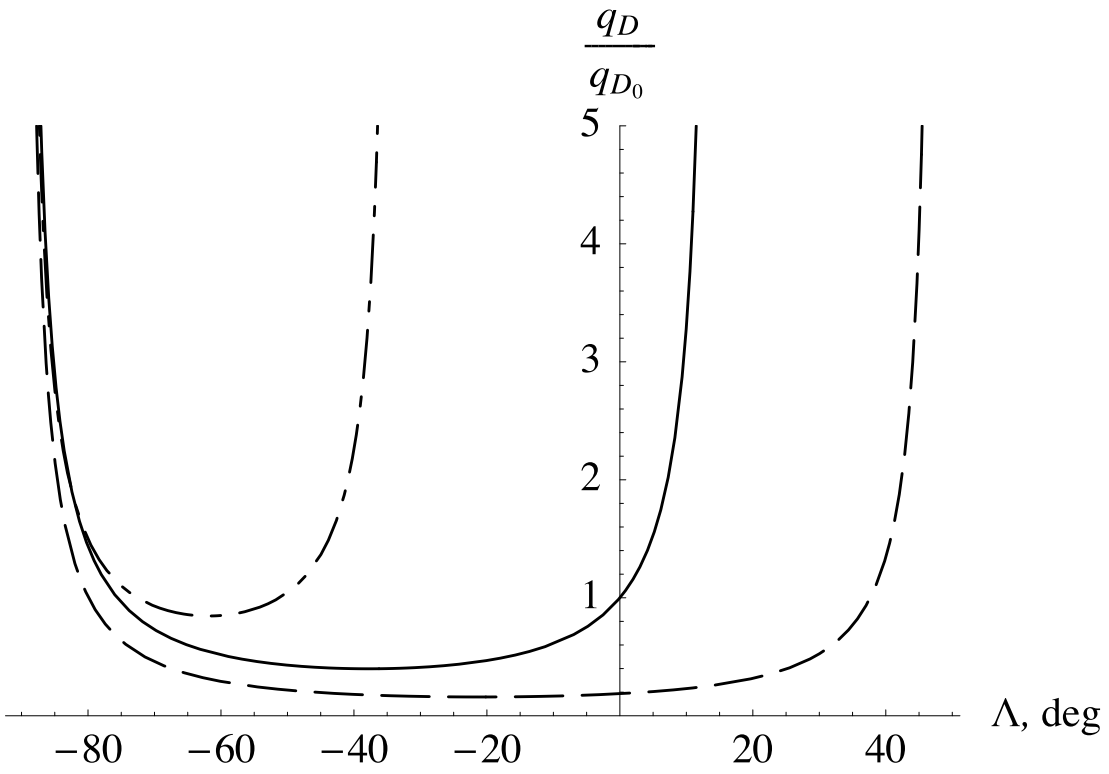

Figure 4.25: Normalized divergence dynamic pressure for an elastically coupled, swept wing with $GJ/EI = 0.2$ and $e/\ell = 0.02$; $\kappa = -0.4$ (dots and dashes), $\kappa = 0$ (solid lines), $\kappa = 0.4$ (dashed lines)

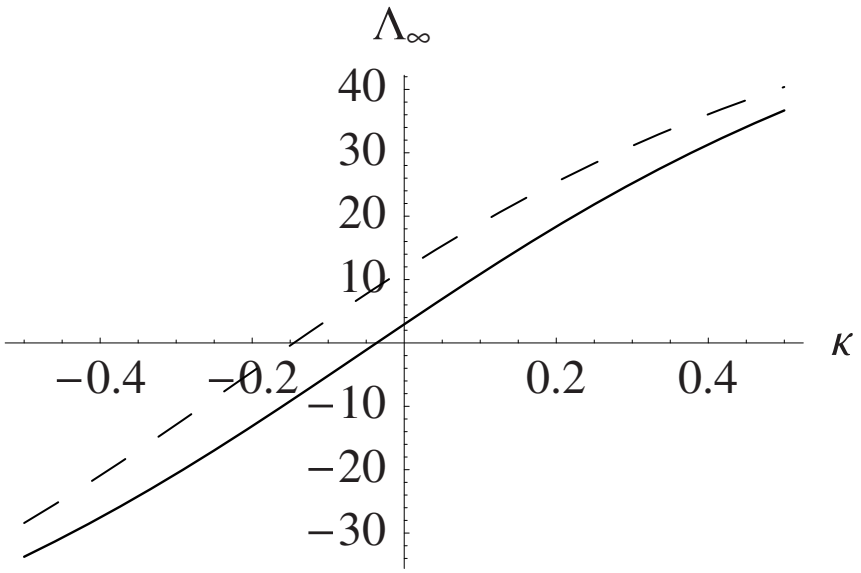

Figure 4.26: Sweep angle for which divergence dynamic pressure is infinite for a wing with $GJ/EI = 0.5$; solid line is for $e/\ell = 0.01$; dashed line is for $e/\ell = 0.04$

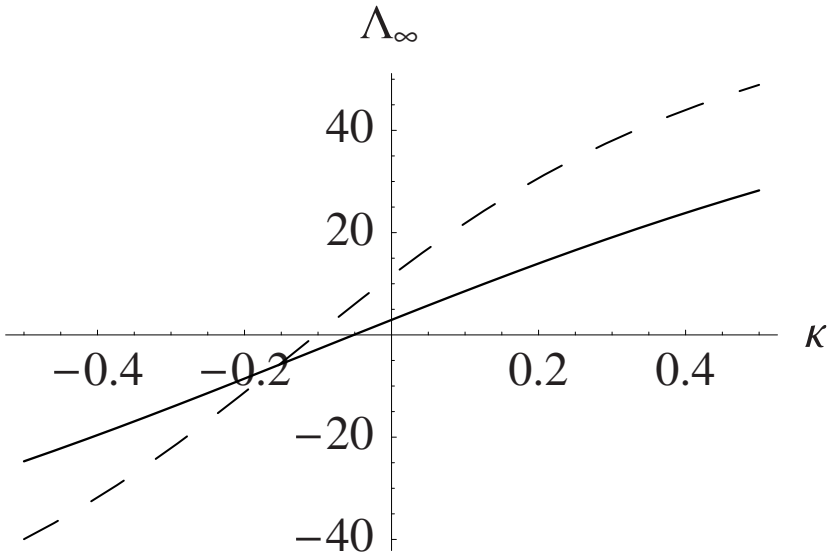

Figure 4.27: Sweep angle for which divergence dynamic pressure is infinite for a wing with $e/\ell = 0.02$; solid line is for $GJ/EI = 1.0$; dashed line is for $GJ/EI = 0.25$

and bending stiffnesses EI and EI_z with $EI_z >> EI$ and $EI_z >> GJ$. We wish to consider the equilibrium state as loaded by drag only, so that the bending deflection w along the z axis and the section rotation angle θ caused by torsion about the y axis are both zero. Thus, the equilibrium deflections are only in the plane of greatest flexural rigidity. Perturbations about that state are w and θ. Let us write the strain energy in the most basic form, as

$$U = \frac{1}{2}\int_0^\ell \left(EI\kappa_x^2 + GJ\kappa_y^2 + EI_z\kappa_z^2\right) dy \tag{4.118}$$

where the κ_x, κ_y, and κ_z are the so-called moment strains of nonlinear beam theory. Moment strains have the properties that (a) differentiation of the strain energy per unit length with respect to one of them gives the corresponding section moment and (b) they are approximately the components of the curvature vector $\boldsymbol{\kappa}$ in the deformed beam cross-sectional basis. So, we need to find them.

Let us consider the wing at zero angle of attack, loaded only by drag, as the equilibrium state about which we wish to linearize. For such a linearized analysis about the equilibrium deformed state, we may drop all terms of third and higher degree in the perturbation variables. The dominant parts of the first two terms in the strain energy stem from $\kappa_x \approx w''$ and $\kappa_y \approx \theta'$, and no further development is necessary for those terms. However, the geometric stiffness from the third term is needed. For this κ_z may be written as $\kappa_z = \overline{\kappa}_z + \hat{\kappa}_z$. Thus, the geometric stiffness associated with the equilibrium state is found by recognizing that the strain energy density associated with κ_z can be written as

$$\frac{1}{2}EI_z(\overline{\kappa}_z + \hat{\kappa}_z)^2 + \ldots = \frac{1}{2}EI_z\overline{\kappa}_z^2 + EI_z\overline{\kappa}_z\hat{\kappa}_z + \ldots \tag{4.119}$$

Assuming the equilibrium state is known, and since the equilibrium state bending moment about z is $M_z = EI_z\overline{\kappa}_z$, U can then be written as

$$U = \int_0^\ell \left(\frac{EI}{2}\kappa_x^2 + \frac{GJ}{2}\kappa_y^2 + M_z\hat{\kappa}_z\right) dy \tag{4.120}$$

Since M_z can now be treated as a known quantity induced by the drag and independent of the perturbation variables, it will be necessary to derive the perturbation terms $\hat{\kappa}_z$ up through second degree. This is conceptually easy but somewhat tedious. To simplify the notation, we drop the hat in what follows.

The curvature vector is most easily derived by taking advantage of the well known Kirchhoff kinetic analog as discussed by Love (1944). The analogy draws a parallel between angular velocity and the curvature vector. So, we introduce a finite rotation of the undeformed beam cross-sectional plane to its final orientation in the deformed beam in terms of three orientation angles: θ_z about the z axis of the undeformed beam, θ_x about the rotated x axis, and finally $\theta_y = \theta$ about the rotated y axis (which is the same as the y axis of the deformed beam). Denoting unit vectors along the undeformed beam x, y, and z axes as $\hat{\mathbf{I}}$,

$\hat{\mathbf{J}}$, and $\hat{\mathbf{K}}$, respectively, and unit vectors along the deformed beam x, y, and z axes as $\hat{\mathbf{i}}$, $\hat{\mathbf{j}}$, and $\hat{\mathbf{k}}$, one can represent the change in orientation in terms of intermediate triads $\hat{\mathbf{I}}'$, $\hat{\mathbf{J}}'$, and $\hat{\mathbf{K}}'$ and $\hat{\mathbf{I}}''$, $\hat{\mathbf{J}}''$, and $\hat{\mathbf{K}}''$ such that

$$\begin{aligned}
\begin{Bmatrix} \hat{\mathbf{I}}' \\ \hat{\mathbf{J}}' \\ \hat{\mathbf{K}}' \end{Bmatrix} &= \begin{bmatrix} \cos\theta_z & \sin\theta_z & 0 \\ -\sin\theta_z & \cos\theta_z & 0 \\ 0 & 0 & 1 \end{bmatrix} \begin{Bmatrix} \hat{\mathbf{I}} \\ \hat{\mathbf{J}} \\ \hat{\mathbf{K}} \end{Bmatrix} \\
\begin{Bmatrix} \hat{\mathbf{I}}'' \\ \hat{\mathbf{J}}'' \\ \hat{\mathbf{K}}'' \end{Bmatrix} &= \begin{bmatrix} 1 & 0 & 0 \\ 0 & \cos\theta_x & \sin\theta_x \\ 0 & -\sin\theta_x & \cos\theta_x \end{bmatrix} \begin{Bmatrix} \hat{\mathbf{I}}' \\ \hat{\mathbf{J}}' \\ \hat{\mathbf{K}}' \end{Bmatrix} \\
\begin{Bmatrix} \hat{\mathbf{i}} \\ \hat{\mathbf{j}} \\ \hat{\mathbf{k}} \end{Bmatrix} &= \begin{bmatrix} \cos\theta_y & 0 & -\sin\theta_y \\ 0 & 1 & 0 \\ \sin\theta_y & 0 & \cos\theta_y \end{bmatrix} \begin{Bmatrix} \hat{\mathbf{I}}'' \\ \hat{\mathbf{J}}'' \\ \hat{\mathbf{K}}'' \end{Bmatrix}
\end{aligned} \tag{4.121}$$

From these relationships, all needed direction cosines associated with the finite rotation are available. The curvature vector can be written as

$$\boldsymbol{\kappa} = \theta_z' \hat{\mathbf{K}} + \theta_x' \hat{\mathbf{I}}' + \theta_y' \hat{\mathbf{j}} \tag{4.122}$$

from which it can be shown that $\kappa_y = \theta_y' + \ldots$. The omitted terms are not needed to capture all terms in Eq. (4.120) up through second degree in the unknowns. To determine κ_x and κ_z, however, one needs to relate the displacement variables to the rotation variables.

The position of an arbitrary point on the deformed beam reference line is

$$\mathbf{R} = u\hat{\mathbf{I}} + (y+v)\hat{\mathbf{J}} + w\hat{\mathbf{K}} \tag{4.123}$$

so that the unit tangent to the beam axis can be expressed as

$$\hat{\mathbf{j}} = \frac{u'\hat{\mathbf{I}} + (1+v')\hat{\mathbf{J}} + w'\hat{\mathbf{K}}}{s'} \tag{4.124}$$

where s is the arc-length along the deformed beam. Because $\hat{\mathbf{j}}$ is a unit vector, it is easily shown that

$$s' = \sqrt{u'^2 + (1+v')^2 + w'^2} = 1 + \epsilon_y \approx 1 \tag{4.125}$$

The approximation that $1 + \epsilon_y \approx 1$ stems from the observation that the stretching strain is small compared to unity. Thus,

$$\begin{aligned}
u' &= s'\hat{\mathbf{I}} \cdot \hat{\mathbf{j}} = -s' \cos\theta_x \sin\theta_z \approx -\theta_z \\
w' &= s'\hat{\mathbf{K}} \cdot \hat{\mathbf{j}} = s' \sin\theta_x \approx \theta_x
\end{aligned} \tag{4.126}$$

This result in conjunction with the direction cosines yields

$$\begin{aligned}
\kappa_x &= w'' + \ldots \\
\kappa_y &= \theta_y' + \ldots \\
\kappa_z &= -u'' + \theta_y w'' + \ldots
\end{aligned} \tag{4.127}$$

Thus, recalling that $\theta_y = \theta$ one may now write the strain energy as

$$U = \int_0^\ell \left[\frac{GJ}{2}\theta'^2 + \frac{EI}{2}w''^2 + M_z\left(-u'' + \theta w''\right) \right] dy \tag{4.128}$$

The virtual work done by the aerodynamic forces and pitching moment may be written as

$$\overline{\delta W} = \int_0^\ell \left(q\, c\, c_{d_0}\, \delta u + q\, c\, a_0 \theta \delta w + q\, e\, c\, a_0 \theta \delta\theta \right) dy \tag{4.129}$$

For the equilibrium deformation of the beam, one may consider only the terms that involve δu in $\delta U - \overline{\delta W}$, such that

$$\int_0^\ell \left(M_z \delta u'' + q\, c\, c_{d_0} \delta u \right) dy = 0 \tag{4.130}$$

Knowing that $M_z(\ell) = M_z'(\ell) = 0$, one finds that

$$M_z = -q\, c\, c_{d_0} \frac{(\ell - y)^2}{2} \tag{4.131}$$

To obtain equations that govern perturbations about the static equilibrium, one may set all other terms in $\delta U - \overline{\delta W}$ equal to zero, so that

$$\int_0^\ell \left[EI w'' \delta w'' + GJ\theta' \delta\theta' - q\, c\, c_{d_0} \frac{(\ell - y)^2}{2} \left(\theta \delta w'' + w'' \delta\theta \right) - q\, c\, a_0 \theta \delta w - q\, e\, c\, a_0 \theta \delta\theta \right] dy = 0 \tag{4.132}$$

where all external disturbances other than drag are ignored, such as α_{r}, $c_{m_{\mathrm{ac}}}$, and weight.

Introducing $\eta = y/\ell$ and letting $(\,)'$ represent $d(\,)/d\eta$, the governing equations can be nondimensionalized and collapsed into one integro-differential equation given by

$$\theta'' - A\left(\frac{c_{d_0}}{a_0}\right) \frac{(1-\eta)^2}{2} \lambda^4 \int_\eta^1 (\eta - \xi)\theta(\xi) d\xi + \lambda^2 \left[1 + A\left(\frac{c_{d_0}}{a_0}\right)^2 \frac{(1-\eta)^4}{4} \lambda^2 \right] \theta = 0 \tag{4.133}$$

with boundary conditions $\theta(0) = \theta'(1) = 0$ where

$$\begin{aligned} A &= \frac{GJ}{EI}\left(\frac{\ell}{e}\right)^2 \\ \lambda^2 &= \frac{qcea_0\ell^2}{GJ} \end{aligned} \tag{4.134}$$

Clearly, the lowest value of λ for which there is a nontrivial solution gives the divergence condition. Details of this derivation are left as an exercise for the reader, along with a one-term Galerkin approximation for the solution (see Problem 19). Although small, the drag effect is slightly destabilizing.

4.3 Nonuniform Lifting Surfaces

Heretofore we have analyzed wings with all properties being spanwise uniform. However, wings are not in general uniform spanwise, and the effects of spanwise nonuniformities and 3-D aerodynamics must be taken into account. In this Section, to facilitate the analysis of nonuniform lifting surfaces, we will make use of the operator notation introduced in Chapter 3.

4.3.1 Unswept Wings Attached to a Frame

Here we analyze an idealized cantilevered beam attached to a frame. We are interested in predicting the loads and divergence condition. For simplicity we assume the existence of a straight elastic axis and introduce $w(y)$, the displacement of the elastic axis caused by bending in the soft direction. The load is considered to act as a distributed force applied at the elastic axis and a distributed moment about the elastic axis. The aerodynamic lift and pitching moment act through the line of aerodynamic centers.

The local angle of attack is

$$\alpha(y) = \alpha_{\mathrm{r}}(y) + \theta(y) \tag{4.135}$$

where

$$\alpha_{\mathrm{r}}(y) = \alpha_F + \alpha_g(y) \tag{4.136}$$

with α_F being the angle of attack at the wing root (where it joins, say, a wind-tunnel wall or a fuselage with prescribed motion) and $\alpha_g(y)$ is the built-in twist angle of the wing (the pitch angle of the wing section at y).

Figs. 4.28 and 4.29 show the wing planform and the cross section. The i^{th} strip contributes to the lift and moment. Replacing the system of forces with a force applied at the elastic axis and the moment about the elastic axis, one finds that the force and moment at the i^{th} station are

$$\begin{aligned} F_i = L_i' W_i =& q c_i a_0 \alpha_i W_i \\ M_{\mathrm{ea}_i} = \left(M_{\mathrm{ac}_i}' + e_i L_i'\right) W_i =& q c_i e_i a_0 \alpha_i W_i + q c_i^2 c_{m\mathrm{ac}_i} W_i \end{aligned} \tag{4.137}$$

where $e = x_{\mathrm{ea}} - x_{\mathrm{ac}}$ and W_i can be written as Δy_i for the simplest quadrature rule.

Using the notation of Chapter 3 one can write

$$\begin{aligned} F_i =& q W_i \left[(c c_\ell^{\mathrm{r}})_i + (c c_\ell^{\mathrm{e}})_i\right] \\ M_i =& q W_i e_i \left[(c c_\ell^{\mathrm{r}})_i + (c c_\ell^{\mathrm{e}})_i\right] + q W_i c_i^2 c_{m\mathrm{ac}_i} \end{aligned} \tag{4.138}$$

where $c_\ell^{\mathrm{r}} = a_0 \alpha_{\mathrm{r}}$ and $c_\ell^{\mathrm{e}} = a_0 \theta$. For the entire wing we must consider all i=1, 2, ..., n, so matrix notation is natural:

$$\begin{aligned} \{F\} =& q[\grave{} W \acute{}] \{c c_\ell^{\mathrm{r}} + c c_\ell^{\mathrm{e}}\} \\ \{M_{\mathrm{ea}}\} =& q[\grave{} eW \acute{}] \{c c_\ell^{\mathrm{r}} + c c_\ell^{\mathrm{e}}\} + q[\grave{} c^2 W \acute{}] \{c_{m\mathrm{ac}}\} \end{aligned} \tag{4.139}$$

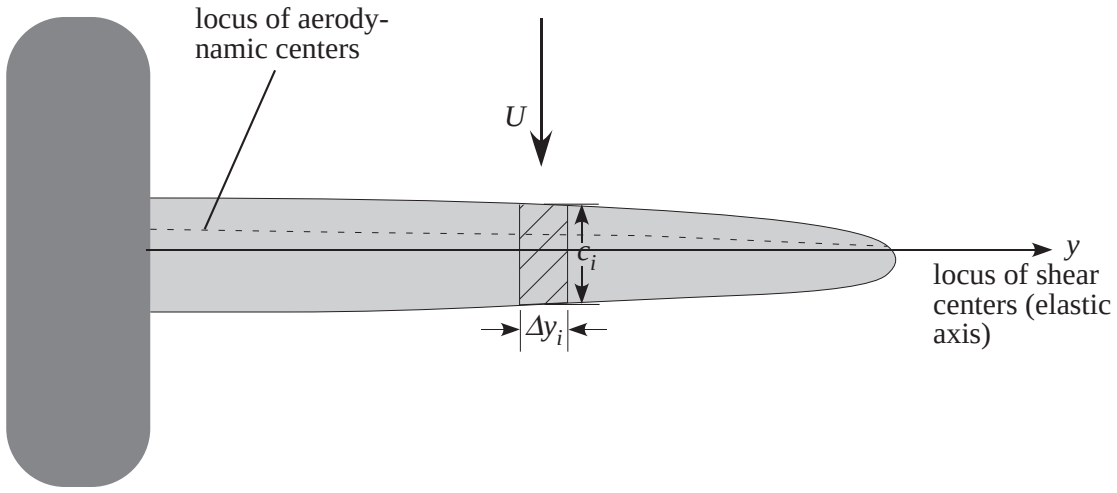

Figure 4.28: Schematic of nonuniform wing attached to fuselage

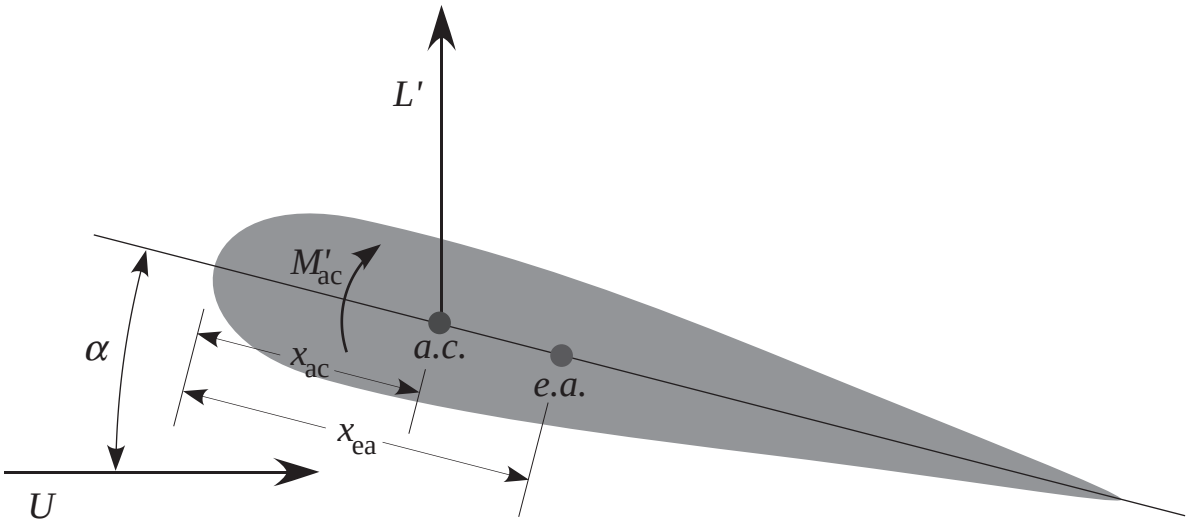

Figure 4.29: Cross section of nonuniform wing at station i

Note that the diagonal matrices containing W can be replaced by similar matrices with Δy_i, if desired.

Now, assuming there is no structural coupling and using the operator notation, we can write equations for the equilibrium of the wing

$$\{w\} = [C^{ww}]\{F\} \qquad \{\theta\} = \left[C^{\theta\theta}\right]\{M_{\text{ea}}\} \tag{4.140}$$

and the aerodynamic formulation can be written as

$$\{\alpha\} = [\mathcal{A}]^{-1}\{cc_\ell\} \tag{4.141}$$

or, in particular

$$\{\theta\} = [\mathcal{A}]^{-1}\{cc_\ell^{\text{e}}\} \qquad \{\alpha_{\text{r}}\} = [\mathcal{A}]^{-1}\{cc_\ell^{\text{r}}\} \tag{4.142}$$

Eqs. (4.139), (4.140), and (4.142) now offer a complete description of the problem. The solution proceeds as follows. Multiply the second of Eqs. (4.139) by $\left[C^{\theta\theta}\right]$, replacing the left-hand side with $\{\theta\}$. Next, rewrite $\{\theta\}$ using the first of Eqs. (4.142). This eliminates $\{M_{\text{ea}}\}$ and $\{\theta\}$, so that

$$\begin{aligned}&[\mathcal{A}]^{-1}\{cc_\ell^{\text{e}}\} - q\left[C^{\theta\theta}\right]\left[\grave{}\, eW \acute{}\right]\{cc_\ell^{\text{e}}\}\\ &= q\left[C^{\theta\theta}\right]\left[\grave{}\, eW \acute{}\right]\{cc_\ell^{\text{r}}\} + q\left[C^{\theta\theta}\right]\left[\grave{}\, c^2W \acute{}\right]\{c_{m_{\text{ac}}}\}\end{aligned} \tag{4.143}$$

To avoid this rather cumbersome equation, we introduce

$$\begin{aligned}[E] &= \left[C^{\theta\theta}\right]\left[\grave{}\, eW \acute{}\right]\\ [F] &= \left[C^{\theta\theta}\right]\left[\grave{}\, c^2W \acute{}\right]\end{aligned} \tag{4.144}$$

so that Eq. (4.143) becomes

$$\left[[\mathcal{A}]^{-1} - q[E]\right]\{cc_\ell^{\text{e}}\} = q[E]\{cc_\ell^{\text{r}}\} + q[F]\{c_{m_{\text{ac}}}\} \tag{4.145}$$

The formulation is made still more explicit and clear by recognizing that the second of Eqs. (4.142) can be written as

$$\begin{aligned}\{cc_\ell^{\text{r}}\} &= [\mathcal{A}]\{\alpha_{\text{r}}\}\\ &= [\mathcal{A}]\{\alpha_F\} + [\mathcal{A}]\{\alpha_g\}\\ &= \alpha_F[\mathcal{A}]\{1\} + [\mathcal{A}]\{\alpha_g\}\end{aligned} \tag{4.146}$$

where $\{1\}$ is a column matrix with unity in every element. Therefore, introducing $\{\tau\}$ as the column matrix of loads independent of the deformation, viz.,

$$\{\tau\} = q\alpha_F[E][\mathcal{A}]\{1\} + q[E][\mathcal{A}]\{\alpha_g\} + q[F]\{c_{m_{\text{ac}}}\} \tag{4.147}$$

one can then simplify the governing equations to

$$\left[[\mathcal{A}]^{-1} - q[E]\right]\{cc_\ell^{\text{e}}\} = \{\tau\} \tag{4.148}$$

The divergence of the wing is governed by the homogeneous governing equations, namely the eigenvalue problem

$$[\mathcal{A}]^{-1}\{cc_\ell^{\mathrm{e}}\} = q\,[E]\,\{cc_\ell^{\mathrm{e}}\} \tag{4.149}$$

where q is the unknown eigenvalue. The divergence dynamic pressure q_D is the smallest real eigenvalue.

For solution of the static response, the only unknowns in Eq. (4.148) are the quantities cc_ℓ^{e} at each strip. We can solve this set of equations and find the lift distribution from Eq. (4.139a), the twisting moment distribution from Eq. (4.139b), the bending displacement from Eq. (4.140a), and the elastic twist from Eq. (4.140b). The lift distribution should be determined using an aerodynamic theory that is more accurate than strip theory, such as Prandtl's lifting line theory. Results obtained will be of the form of Figs. 4.14 and 4.15.

4.3.2 Effect of Weight and Load Factor

The above equilibrium equation can be generalized by consideration of the weight per unit span, magnified by the load factor. It is somewhat more convenient to formulate the problem in terms of $\{cc_\ell\}$ instead of $\{cc_\ell^{\mathrm{e}}\}$ and $\{cc_\ell^{\mathrm{r}}\}$, so that Eq. (4.145) becomes

$$\left[[\mathcal{A}]^{-1} - q\,[E]\right]\{cc_\ell\} = \alpha_F\,\{1\} + \{\alpha_g\} + q\,[F]\,\{c_{m_{\mathrm{ac}}}\} - Ng\,[G]\,\{m\} \tag{4.150}$$

where m is the mass per unit length, N is the load factor, g is the gravitational acceleration, and

$$[G] = \left[C^{\theta\theta}\right]\left[\grave{}\,W\,\acute{}\right]\left[\grave{}\,d\,\acute{}\right] \tag{4.151}$$

It is noted that since α_F and N are related through the unknown elastic twist, then one of these two variables must specified to determine $\{cc_\ell\}$.

The aerodynamicist or performance engineer usually specifies α_F in order to determine the total lift or the lift distribution. Assuming that the total lift is equal to NW and is caused only by the wings, it may be computed as

$$NW = 2q\int_0^\ell cc_\ell dy = 2q\,\lfloor 1\rfloor\left[\grave{}\,W\,\acute{}\right]\{cc_\ell\} \tag{4.152}$$

where $\lfloor 1\rfloor = \{1\}^T$. The scalar W should not be confused with the quadrature weights W_i or their matrix representation as $\left[\grave{}\,W\,\acute{}\right]$. Rewriting the equilibrium equation, Eq. (4.150), as

$$\left[[\mathcal{A}]^{-1} - q\,[E]\right]\{cc_\ell\} + Ng\,[G]\,\{m\} = \alpha_F\,\{1\} + \{\alpha_g\} + q\,[F]\,\{c_{m_{\mathrm{ac}}}\} \tag{4.153}$$

and the lift relation as

$$\frac{2q}{W}\,\lfloor 1\rfloor\left[\grave{}\,W\,\acute{}\right]\{cc_\ell\} - N = 0 \tag{4.154}$$

one can write this pair of equations as a single, partitioned matrix equilibrium equation as

$$\begin{bmatrix} [\mathcal{A}]^{-1} - q\,[E] & g\,[G]\,\{m\} \\ \frac{2q}{W}\,\lfloor 1\rfloor\left[\grave{}\,W\,\acute{}\right] & -1 \end{bmatrix}\begin{Bmatrix} \{cc_\ell\} \\ N \end{Bmatrix} = \begin{Bmatrix} \alpha_F\,\{1\} + \{\alpha_g\} + q\,[F]\,\{c_{m_{\mathrm{ac}}}\} \\ 0 \end{Bmatrix} \tag{4.155}$$

An alternative problem is posed by specification of N which is usually made by the structures engineer who ultimately needs to know the maximum stress in the wing, which can be determined in terms of the lift distribution. In this event Eq. (4.150) is rewritten as

$$\left[[\mathcal{A}]^{-1} - q\,[E]\right]\{cc_\ell\} - \alpha_F\,\{1\} = \{\alpha_g\} + q\,[F]\,\{c_{m_{ac}}\} - Ng\,[G]\,\{m\} \tag{4.156}$$

which, taken together with the lift equation may again be written as a single, partitioned matrix equilibrium equation

$$\begin{bmatrix} [\mathcal{A}]^{-1} - q\,[E] & -\{1\} \\ \frac{2q}{W}\,\lfloor 1\rfloor\,[\,\grave{}\,W\,\acute{}\,] & 0 \end{bmatrix} \begin{Bmatrix} \{cc_\ell\} \\ \alpha_F \end{Bmatrix} = \begin{Bmatrix} \{\alpha_g\} + q\,[F]\,\{c_{m_{ac}}\} - Ng\,[G]\,\{m\} \\ N \end{Bmatrix} \tag{4.157}$$

which, as before, may be readily solved for $\{cc_\ell\}$ and α_F.

4.4 Complete Aircraft

To consider a complete aircraft, one needs to add suitable models for the fuselage and tail. Moreover, treatment of a complete aircraft in flight requires that the vehicle is "trimmed" for the desired flight condition. Finding the trimmed state requires that control settings are found that put the aircraft in a steady-state flight condition (such as steady and level flight, steady climb, steady turning, etc.). Other parameters for a trimmed flight condition include dynamic pressure and altitude (or any other two associated parameters such as airspeed and Mach number).

4.4.1 Aircraft with Unswept Wings

Let us first consider an aircraft with unswept wings (sometimes referred to as straight wings). For the case of longitudinal flight being trimmed for an equilibrium condition implies that the pitching moment about the vehicle's center of mass is zero for a desired, specified load factor. To achieve this trim condition it is necessary to have a longitudinal control surface, such as an elevator mounted at the tail on a horizontal stabilizer as shown in Figs. 4.30 and 4.31.

Considering the tail and fuselage as rigid for now, we must represent the lift on the tail as a function of the control surface deflections. Letting the root angle of attack for the tail $\alpha_{\mathrm{r}}(0)$ be replaced by α_F, the tail lift can be described by

$$L^T = qS_T\left(\frac{\partial C_L^T}{\partial \alpha}\alpha_F + \frac{\partial C_L^T}{\partial \delta}\delta\right) \tag{4.158}$$

where C_L^T is the lift coefficient of the tail, S_T is the tail area, δ is the elevator deflection, x_T is the distance between the wing elastic axis to the tail center of pressure, and x_c is the distance from the wing elastic axis to the vehicle center of mass.

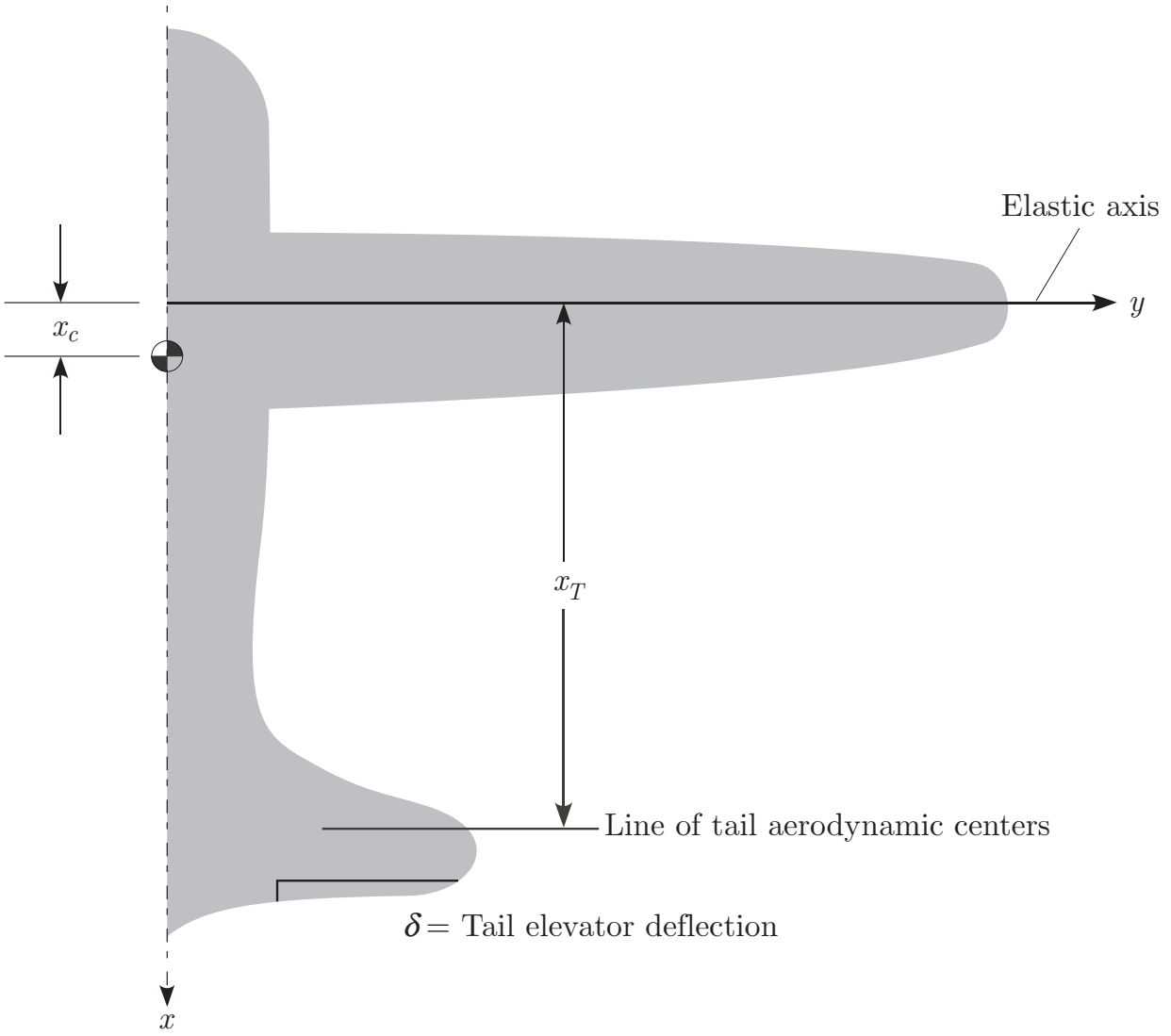

Figure 4.30: Schematic of complete aircraft

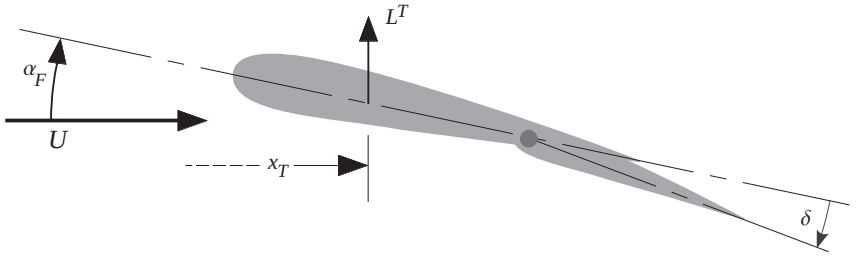

Figure 4.31: Schematic of aircraft tail airfoil section

The equations for the elastic deformation of the wings remain the same as before in Eq. (4.150), viz.,

$$[\mathcal{A}]^{-1}\{cc_\ell\} = \alpha_F\{1\} + \{\alpha_g\} + q[E]\{cc_\ell\} + q[F]\{c_{mac}\} - Ng[G]\{m\} \tag{4.159}$$

The total lift is equal to NW so that

$$2\int_0^\ell qcc_\ell dy + qS_T\left(\frac{\partial C_L^T}{\partial\alpha}\alpha_F + \frac{\partial C_L^T}{\partial\delta}\delta\right) = NW \tag{4.160}$$

or, in matrix form,

$$2q\lfloor 1\rfloor\lceil W\rceil\{cc_\ell\} + qS_T\left(\frac{\partial C_L^T}{\partial\alpha}\alpha_F + \frac{\partial C_L^T}{\partial\delta}\delta\right) = NW \tag{4.161}$$

The total pitching moment about the center of mass is zero for trim. Thus,

$$2\int_0^\ell q\left[(e+x_c)cc_\ell + c^2c_{mac}\right]dy - (x_T - x_c)qS_T\left(\frac{\partial C_L^T}{\partial\alpha}\alpha_F + \frac{\partial C_L^T}{\partial\delta}\delta\right) = 0 \tag{4.162}$$

Note that the coefficient of x_c in this relation is equal to NW. This allows us to write

$$2\int_0^\ell q\left(ecc_\ell + c^2c_{mac}\right)dy - x_TqS_T\left(\frac{\partial C_L^T}{\partial\alpha}\alpha_F + \frac{\partial C_L^T}{\partial\delta}\delta\right) + x_cNW = 0 \tag{4.163}$$

or, in matrix form,

$$\begin{aligned} &2q\lfloor e\rfloor\lceil W\rceil\{cc_\ell\} + 2q\lfloor c^2\rfloor\lceil W\rceil\{c_{mac}\} \\ &\quad - x_TqS_T\left(\frac{\partial C_L^T}{\partial\alpha}\alpha_F + \frac{\partial C_L^T}{\partial\delta}\delta\right) + x_cNW = 0 \end{aligned} \tag{4.164}$$

Eqs. (4.159), (4.161), and (4.164) can now be solved simultaneously for either α_F or N depending on which is specified.

Defining

$$b_\alpha = S_T\frac{\partial C_L^T}{\partial\alpha} \qquad b_\delta = S_T\frac{\partial C_L^T}{\partial\delta} \tag{4.165}$$

one can now write the governing equations for the case of prescribed normal load factor N as

$$\begin{bmatrix} [\mathcal{A}]^{-1} - q[E] & -\{1\} & \{0\} \\ 2q\lfloor 1\rfloor\lceil W\rceil & qb_\alpha & qb_\delta \\ 2q\lfloor e\rfloor\lceil W\rceil & -x_Tqb_\alpha & -x_Tqb_\delta \end{bmatrix}\begin{Bmatrix}\{cc_\ell\}\\ \alpha_F\\ \delta\end{Bmatrix} = \begin{Bmatrix}\{\alpha_g\} + q[F]\{c_{mac}\} - Ng[G]\{m\}\\ NW\\ -2q\lfloor c^2\rfloor\lceil W\rceil\{c_{mac}\} - x_cNW\end{Bmatrix} \tag{4.166}$$

from which the unknown column matrix $\{cc_\ell\}$ and the scalars α_F and δ can be found by premultiplying by the inverse of the coefficient matrix. Once the unknowns are found, the

load distribution and control settings (i.e., α_F and δ) are easily found, and the stress state of the wing is completely determined.

For the case of a rigid aircraft it should be noted that the structural influence function is zero, so that $[E] = [F] = [G] = [0]$. The lower right 2×2 submatrix of the coefficient matrix of Eq. (4.166) is unaffected by flexibility and can thus be determined from a rigid model of the aircraft or from a wind-tunnel test of the complete aircraft.

The above set of equations is not well suited for determining the condition of divergence. The elements of $\{cc_\ell\}$ are not in general zero even when the wing is undeformed. To rectify this situation we must make a change of variable. Recall that

$$\{cc_\ell\} = \{cc_\ell^{\mathrm{r}}\} + \{cc_\ell^{\mathrm{e}}\} \tag{4.167}$$

and that

$$\{cc_\ell^{\mathrm{r}}\} = \alpha_F [\mathcal{A}] \{1\} + [\mathcal{A}] \{\alpha_g\} \tag{4.168}$$

Therefore, Eq. (4.166) can be rewritten with $\{cc_\ell^{\mathrm{e}}\}$ as the unknown instead of $\{cc_\ell\}$. This way, the divergence condition can be identified by asking if $\{cc_\ell^{\mathrm{e}}\}$ can be finite for zero disturbances. The case of zero disturbances can be found by setting the following quantities to zero:

$$\{\alpha_g\}; \quad \{c_{m_{\mathrm{AC}}}\}; \quad N \tag{4.169}$$

so that the governing equation for divergence becomes

$$\begin{bmatrix} [\mathcal{A}]^{-1} - q[E] & -q[E][\mathcal{A}]\{1\} & \{0\} \\ 2q\lfloor 1 \rfloor [\grave{W}] & qb_\alpha + 2q\lfloor 1 \rfloor [\grave{W}][\mathcal{A}]\{1\} & qb_\delta \\ 2q\lfloor e \rfloor [\grave{W}] & -x_T qb_\alpha + 2q\lfloor e \rfloor [\grave{W}][\mathcal{A}]\{1\} & -x_T qb_\delta \end{bmatrix} \begin{Bmatrix} \{cc_\ell^{\mathrm{e}}\} \\ \alpha_F \\ \delta \end{Bmatrix} = 0 \tag{4.170}$$

This is a generalized eigenvalue problem in q which can be solved by commercially available packages (such as Mathematica™ or Maple™) for the lowest value of q as the divergence dynamic pressure.

It is also easy to set the problem in a different way, by specifying α_F and have the load factor N as the unknown. This is left as an exercise for the reader. As before, the lift distribution should be determined using an aerodynamic theory that is more accurate than strip theory, such as Prandtl's lifting line theory. Results obtained will be of the form of Figs. 4.14 and 4.15.

4.4.2 Aircraft with Swept Wings

The analysis of a swept-wing aircraft differs from the unswept case by two factors. First, the aerodynamic loading for a given angle of attack distribution depends on the sweep angle of the surface. This effect can be handled by noting that the aerodynamic influence coefficient matrix is altered by sweep. The second factor is associated with the effect of elastic deflection on the streamwise angle of attack. This was discussed earlier in Section 4.2.4. According to

Fig. 4.16 one can relate the elastic twist and bending slope, $\overline{\theta}$ and $\zeta = dw/d\overline{y}$, to the elastic part of the angle of attack through Eq. (4.73), the latter part of which is rewritten here as

$$\theta = \overline{\theta}\cos(\Lambda) - \zeta\sin(\Lambda) \tag{4.171}$$

or, in operator notation

$$\{\theta\} = \cos(\Lambda)\left\{\overline{\theta}\right\} - \sin(\Lambda)\{\zeta\} \tag{4.172}$$

Note that to use strip theory or lifting line theory for the aerodynamics, Λ must be small. Otherwise, a more sophisticated aerodynamic theory must be used.

The structural analysis may be written in terms of influence coefficient matrices involving the deflection w, the bending slope ζ, and the torsion angle $\overline{\theta}$. We consider the case in which there is no structural coupling between bending and torsion. Generalization to include coupling is left as an exercise for the reader; see Problem 22. The influence coefficients now related the loads and deflections as follows:

$$\begin{aligned}
\{w\} =& [C^{ww}]\{F\} - [C^{w\zeta}]\{M_{\text{ea}}\}\sin(\Lambda) \\
\{\zeta\} =& [C^{\zeta w}]\{F\} - [C^{\zeta\zeta}]\{M_{\text{ea}}\}\sin(\Lambda) \\
\left\{\overline{\theta}\right\} =& [C^{\overline{\theta\theta}}]\{M_{\text{ea}}\}\cos(\Lambda)
\end{aligned} \tag{4.173}$$

where here $\{F\}$ and $\{M_{\text{ea}}\}$ are the applied force at the elastic axis and moment component about the elastic axis and along $\hat{\mathbf{a}}_1$; see Fig. 4.16.

Now let us place these definitions into the expression for $\{\theta\}$, so that

$$\{\theta\} = \cos^2(\Lambda)[C^{\overline{\theta\theta}}]\{M_{\text{ea}}\} - \sin(\Lambda)[C^{\zeta w}]\{F\} + \sin^2(\Lambda)[C^{\zeta\zeta}]\{M_{\text{ea}}\} \tag{4.174}$$

or

$$\{\theta\} = -\sin(\Lambda)[C^{\zeta w}]\{F\} + \left[\cos^2(\Lambda)[C^{\overline{\theta\theta}}] + \sin^2(\Lambda)[C^{\zeta\zeta}]\right]\{M_{\text{ea}}\} \tag{4.175}$$

From this we may identify

$$\begin{aligned}
[C^{w\theta}] =& -\sin(\Lambda)[C^{w\zeta}] \\
[C^{\theta\theta}] =& \cos^2(\Lambda)[C^{\overline{\theta\theta}}] + \sin^2(\Lambda)[C^{\zeta\zeta}]
\end{aligned} \tag{4.176}$$

and thereby write

$$\begin{aligned}
\{w\} =& [C^{ww}]\{F\} + [C^{w\theta}]\{M_{\text{ea}}\} \\
\{\theta\} =& [C^{\theta w}]\{F\} + [C^{\theta\theta}]\{M_{\text{ea}}\}
\end{aligned} \tag{4.177}$$

With Eqs. (4.177) replacing Eqs. (4.140), the previous development regarding unswept wings remains valid. As a result, we need only change the definitions of these matrices:

$$\begin{aligned}
[E] &= [C^{\theta\theta}][\grave{}\, W \,\acute{}][\grave{}\, e \,\acute{}] + [C^{\theta w}][\grave{}\, W \,\acute{}] \\
[G] &= [C^{\theta\theta}][\grave{}\, W \,\acute{}][\grave{}\, d \,\acute{}] + [C^{\theta w}][\grave{}\, W \,\acute{}]
\end{aligned} \tag{4.178}$$

while $[F]$ remains unchanged, so that

$$\{\theta\} = q\,[E]\,\{cc_\ell\} + q\,[F]\,\{c_{m_{\rm ac}}\} - Ng\,[G]\,\{m\} \tag{4.179}$$

The determination of the airload distribution and divergence condition can now proceed as in the unswept case. Typical results for the load distribution are found in Fig. 4.18 while the divergence effects are shown in Fig. 4.17. Backward sweep reduces the angle of attack at the tip of the wing, which makes it stabilizing. It also results in a decrease in the root bending moment. The opposite is true for forward sweep.

4.4.3 Aileron Reversal

The problem of aileron reversal, addressed earlier in Section 4.1.4 in terms of a rigid wing on a flexible support, can also be posed for flexible wings as well as for complete aircraft. In this section we will consider a complete aircraft, first with unswept wings and then with swept wings. It should be noted that a similar problem can be posed in the framework of dynamic aeroelasticity, where the objective is to predict the angular acceleration caused by deflection of a control surface or the time to roll from, say, zero roll angle to 90°. Depending on the aircraft and the maneuver, it may be necessary to take nonlinearities into account. Only a static, linear treatment is included here.

Unswept Wings

Consider a rolling aircraft with unswept wings, as shown in Fig. 4.32 with the roll rate denoted by p. As shown in Fig. 4.33, the wing airfoil section has an incidence angle with respect to the freestream velocity of $\alpha_{\rm r}(y) + \theta(y)$. However, because the aircraft is rolling, the airfoil also "sees" an additional component of wind velocity equal to py perpendicular to the freestream velocity. From the figure, because $py << U$, the angle of attack is the incidence angle reduced by py/U.

The entire aircraft must be modeled since one wing is moving upward while the other is moving downward. There are some contributions to the lift and pitching moment that are the same on both sides of the aircraft. These are referred to as symmetric components. Separate problems can be posed in terms of symmetric and antisymmetric parts, which are uncoupled from each other. In particular, we can treat the antisymmetric problem separately because all symmetric components cancel out in pure roll. Hence, we can set them to zero a priori. For example, in the relation

$$\alpha = \cancelto{0}{\alpha_{\rm r}(y)} + \theta(y) - \frac{py}{U} \tag{4.180}$$

the first term, $\alpha_{\rm r} = \alpha_F + \alpha_g(y)$, drops out because of symmetry. Both $\theta(y)$ and the roll rate term are antisymmetric because θ and β will have the opposite sense across the mid-plane of the aircraft. The last term represents the increment in the angle of attack from the roll rate p based on the assumption of a small angle of attack.

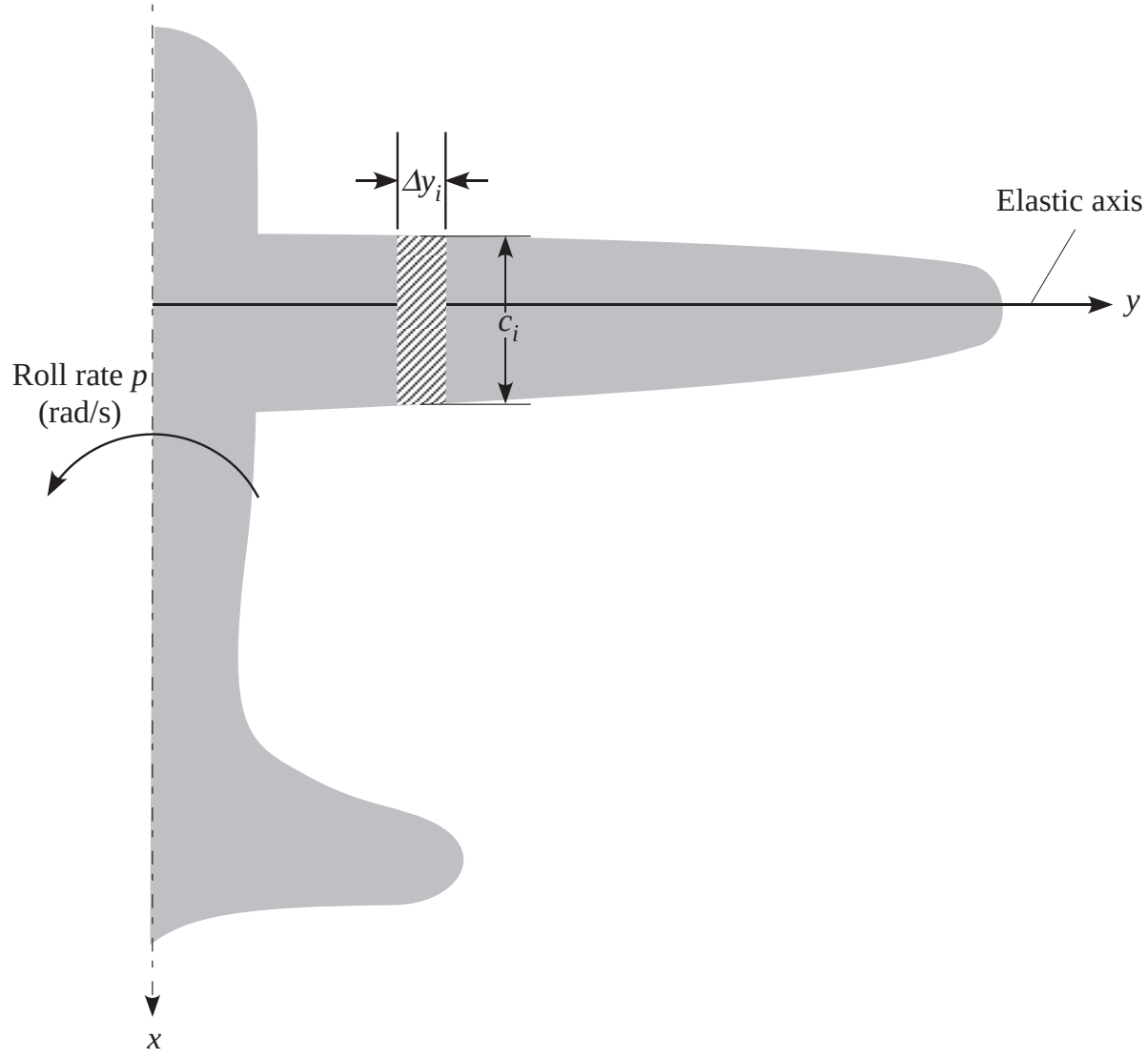

Figure 4.32: Schematic of a rolling aircraft

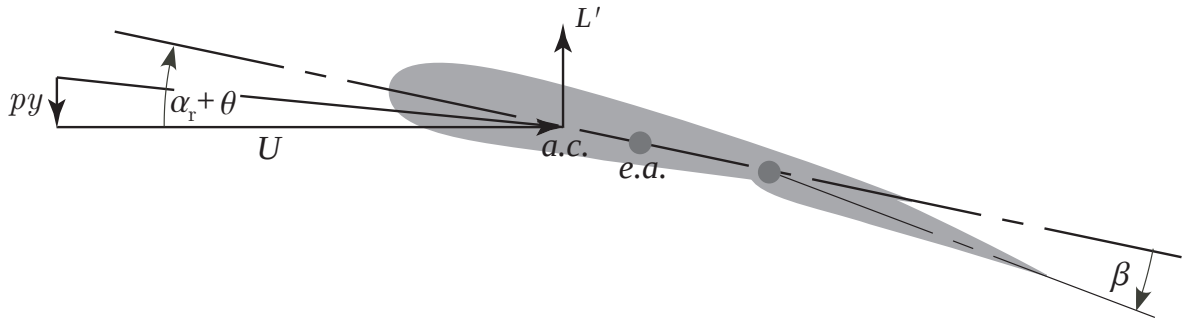

Figure 4.33: Wing section with aileron

We use the same expressions for force and moment as found in Section 4.1.4, modified for the present matrix and operator notation. Therefore, in light of the above, the force on the i^{th} strip of the wing can be written as

$$F_i = qW_i \left[(cc_\ell^{\text{e}})_i + (cc_\ell^{\text{p}})_i + \left(cc_\ell^{\beta} \right)_i \right] \tag{4.181}$$

where the superscripts refer to twist (e), roll (p), and aileron deflection (β), and the moment as

$$M_{\text{ea}_i} = qW_i e_i \left[(cc_\ell^{\text{e}})_i + (cc_\ell^{\text{p}})_i + \left(cc_\ell^{\beta} \right)_i \right] + qW_i c_i^2 c_{m_{\beta_i}} \beta \tag{4.182}$$

The coefficient c_{m_β} is set equal to zero at any station where there is no flap. These equations are easily cast in the matrix form as

$$\begin{aligned} \{F\} =& q[\grave{} W \acute{}] \left\{ \{cc_\ell^{\text{e}}\} + \{cc_\ell^{\text{p}}\} + \left\{ cc_\ell^{\beta} \right\} \right\} \\ \{M_{\text{ea}}\} =& q[\grave{} eW \acute{}] \left\{ \{cc_\ell^{\text{e}}\} + \{cc_\ell^{\text{p}}\} + \left\{ cc_\ell^{\beta} \right\} \right\} + q[\grave{} c^2 W \acute{}] \left\{ c_{m_\beta} \right\} \beta \end{aligned} \tag{4.183}$$

In addition to these equations we must also consider three other classes of equations. First, we must consider the global equilibrium of the aircraft, viz.,

$$\lfloor y \rfloor \{F\} = 0 \tag{4.184}$$

Second, the governing equations for the elastic deformation of the wing are

$$\begin{aligned} \{w\} &= [C^{ww}] \{F\} \\ \{\theta\} &= \left[C^{\theta\theta} \right] \{M_{\text{ea}}\} \end{aligned} \tag{4.185}$$

Finally, the aerodynamic modeling equations are

$$\{\alpha\} = \left[\mathcal{A}_a^{-1} \right] \{cc_\ell\} \tag{4.186}$$

where $[\mathcal{A}_a]$ is the aerodynamic operator for antisymmetric loads on the wings. An example of such an operator would include the lifting line theory

$$[\mathcal{A}_a^{-1}] = [\,\grave{}\,\frac{1}{a_0 c}\,\acute{}\,] + \frac{1}{8\ell}[\,\grave{}\,\frac{1}{\sin\phi}\,\acute{}\,]\,[r\sin(r\phi)]\,[\sin(r\phi)]^{-1} \tag{4.187}$$

the details of which are described in Bisplinghoff, Ashley, and Halfman, art. 5-5. If we consider basic strip theory, there is no essential difference between an antisymmetric and a symmetric aerodynamic operator. So, for now we will just mark the matrices with a subscript a and return to this aspect of the problem later.

In the equation for the aerodynamic operator we note that

$$\{cc_\ell\} = \{cc_\ell^{\mathrm{e}}\} + \{cc_\ell^{\mathrm{p}}\} + \left\{cc_\ell^{\beta}\right\} \tag{4.188}$$

Thus, the aerodynamic twist angle due to the change in wing orientation is

$$\{\theta\} = \left[\mathcal{A}_a^{-1}\right]\{cc_\ell^{\mathrm{e}}\} \tag{4.189}$$

while the steady roll effect is governed by

$$-\left\{\frac{py}{U}\right\} = \left[\mathcal{A}_a^{-1}\right]\{cc_\ell^{\mathrm{p}}\} \tag{4.190}$$

which with the introduction of the nondimensional parameter $p\ell/U$ can be inverted to yield

$$\{cc_\ell^{\mathrm{p}}\} = -\left(\frac{p\ell}{U}\right)[\mathcal{A}_a]\left\{\frac{y}{\ell}\right\} = \left(\frac{p\ell}{U}\right)\{\mathcal{A}_a^{\mathrm{p}}\} \tag{4.191}$$

Finally, because the aileron may not extend the full length of the wing (see Fig. 4.34), we may write something like

$$\left\{cc_\ell^{\beta}\right\} = [\,\grave{}\,cc_\ell^{\beta}\,\acute{}\,]\begin{Bmatrix}0\\ \vdots\\ 0\\ 1\\ \vdots\\ 1\\ 0\\ \vdots\\ 0\end{Bmatrix}\beta = \left\{\mathcal{A}_a^{\beta}\right\}\beta \tag{4.192}$$

We now have equations necessary to solve the problem at hand. Let's begin as we have in previous cases by rewriting our twist equation as

$$\{\theta\} = q\left[C^{\theta\theta}\right]\left\{[\,\grave{}\,eW\,\acute{}\,]\left\{\{cc_\ell^{\mathrm{e}}\} + \{cc_\ell^{\mathrm{p}}\} + \left\{cc_\ell^{\beta}\right\}\right\} + [\,\grave{}\,c^2W\,\acute{}\,]\left\{c_{m_\beta}\right\}\beta\right\} \tag{4.193}$$

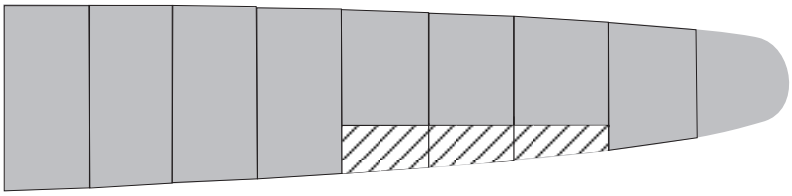

Figure 4.34: Wing section with aileron as a part of length

As before we can define a set of shorthand matrices to reduce the size of the expression:

$$\begin{aligned}[E] &= \left[C^{\theta\theta}\right]\left[\,\grave{}\, eW \,\acute{}\,\right] \\ [F] &= \left[C^{\theta\theta}\right]\left[\,\grave{}\, c^2W \,\acute{}\,\right]\end{aligned} \tag{4.194}$$

Note that these definitions are the same as we've used before. Thus, our $\{\theta\}$ expression becomes

$$\left[\left[\mathcal{A}_a^{-1}\right] - q\,[E]\right]\{cc_\ell^{\mathrm{e}}\} - q\left(\frac{p\ell}{U}\right)[E]\,\{\mathcal{A}_a^{\mathrm{p}}\} = q\,[E]\left\{\mathcal{A}_a^{\beta}\right\}\beta + q\,[F]\left\{c_{m_\beta}\right\}\beta \equiv \{f\}\,\beta \tag{4.195}$$

This equation plus Eq. (4.184) are $n{+}1$ equations in $n{+}1$ unknowns, which are the n elements of $\{cc_\ell^{\mathrm{e}}\}$ and $p\ell/U$. In particular, by introducing

$$\lfloor y \rfloor \left[\,\grave{}\, W \,\acute{}\,\right] = \lfloor yW \rfloor \tag{4.196}$$

Eq. (4.184) can be rewritten as

$$\lfloor yW \rfloor \left\{\{cc_\ell^{\mathrm{e}}\} + \{\mathcal{A}_a^{\mathrm{p}}\}\left(\frac{p\ell}{U}\right) + \left\{\mathcal{A}_a^{\beta}\right\}\beta\right\} = 0 \tag{4.197}$$

which defines the response of the vehicle to a known deflection β of the ailerons:

$$\lfloor yW \rfloor \left\{\{cc_\ell^{\mathrm{e}}\} + \{\mathcal{A}_a^{\mathrm{p}}\}\left(\frac{p\ell}{U}\right)\right\} = -\lfloor yW \rfloor \left\{\mathcal{A}_a^{\beta}\right\}\beta \equiv B_3\beta \tag{4.198}$$

Note that B_3 is a scalar, and this is a scalar equation because of the nature of the matrix multiplications. It can be combined with Eq. (4.195) and put in matrix form as

$$\begin{bmatrix} \left[\mathcal{A}_a^{-1}\right] - q\,[E] & -q\,[E]\,\{\mathcal{A}_a^{\mathrm{p}}\} \\ \lfloor yW \rfloor & \lfloor yW \rfloor \{\mathcal{A}_a^{\mathrm{p}}\} \end{bmatrix} \begin{Bmatrix} cc_\ell^{\mathrm{e}} \\ \frac{p\ell}{U} \end{Bmatrix} = \begin{Bmatrix} \{f\} \\ B_3 \end{Bmatrix}\beta \tag{4.199}$$

We can solve this system of equations symbolically as follows. Solve the first equation for $\{cc_\ell^{\mathrm{e}}\}$ to obtain

$$\{cc_\ell^{\mathrm{e}}\} = \left[\left[\mathcal{A}_a^{-1}\right] - q\,[E]\right]^{-1}\left\{\{f\}\,\beta + q\,[E]\,\{\mathcal{A}_a^{\mathrm{p}}\}\left(\frac{p\ell}{U}\right)\right\} \tag{4.200}$$

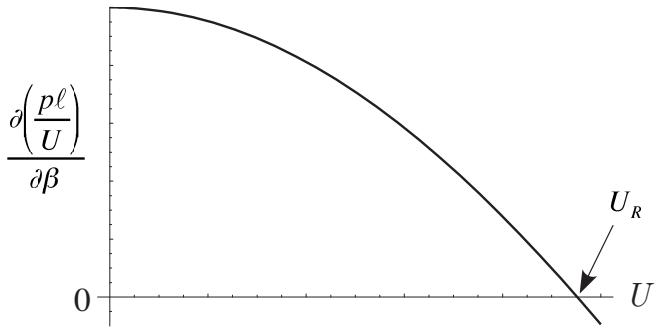

Figure 4.35: Typical variation of nondimensional roll rate versus aircraft speed U

Now the second equation can be written as

$$\begin{aligned} \lfloor yW \rfloor \left[q \left[\left[\mathcal{A}_a^{-1} \right] - q \left[E \right] \right]^{-1} \left[E \right] + \left[\grave{} 1 \acute{} \right] \right] \left\{ \mathcal{A}_a^{\mathrm{p}} \right\} \left(\frac{p\ell}{U} \right) \\ = - \lfloor yW \rfloor \left\{ \left\{ \mathcal{A}_a^{\beta} \right\} + \left[\left[\mathcal{A}_a^{-1} \right] - q \left[E \right] \right]^{-1} \left\{ f \right\} \right\} \beta \end{aligned} \tag{4.201}$$

where $\left[\grave{} 1 \acute{} \right]$ is the identity matrix. Thus,

$$\frac{\partial \left(\frac{p\ell}{U} \right)}{\partial \beta} = - \frac{\lfloor yW \rfloor \left\{ \left\{ \mathcal{A}_a^{\beta} \right\} + q \left[\left[\mathcal{A}_a^{-1} \right] - q \left[E \right] \right]^{-1} \left\{ \left[E \right] \left\{ \mathcal{A}_a^{\beta} \right\} + \left[F \right] \left\{ c_{m_\beta} \right\} \right\} \right\}}{\lfloor yW \rfloor \left[q \left[\left[\mathcal{A}_a^{-1} \right] - q \left[E \right] \right]^{-1} \left[E \right] + \left[\grave{} 1 \acute{} \right] \right] \left\{ \mathcal{A}_a^{\mathrm{p}} \right\}} \tag{4.202}$$

For a unit deflection of β this equation will tell us how much of a roll rate p we will obtain. The quantity on the left-hand side of Eq. (4.202) is known as the aileron effectiveness of the aircraft. A typical result is depicted in Fig. 4.35. As U (or q) increases, the elastic terms begin to take over and dominate the rigid term, thus resulting in a loss of control effectiveness for the aircraft and eventual control reversal at $U = U_R$.

The various components of the rolling moment, which must all sum to zero, can be defined by the equilibrium equation, given by

$$2 \lfloor y \rfloor \left\{ F \right\} = 2q \lfloor yW \rfloor \left\{ \left\{ cc_\ell^{\mathrm{e}} \right\} + \left\{ \mathcal{A}_a^{\mathrm{p}} \right\} \left(\frac{p\ell}{U} \right) + \left\{ \mathcal{A}_a^{\beta} \right\} \beta \right\} \tag{4.203}$$

where the "2" is present because of having to take into account both wings of the aircraft. The first term we can denote by R^{e}, the component of the rolling moment caused by elastic twist. The second term we can denote by R^{p}, the component of the rolling moment caused by the roll rate p. The third term we can denote by R^{β}, the component of the rolling moment caused by the aileron deflection. These all must sum to zero at any flight speed U, and in particular at the point of control reversal, where $U = U_R$, R^{p} must be zero (recall there is no roll) so that $R^{\mathrm{e}} = -R^{\beta}$. Typical behavior is depicted in Fig. 4.36.

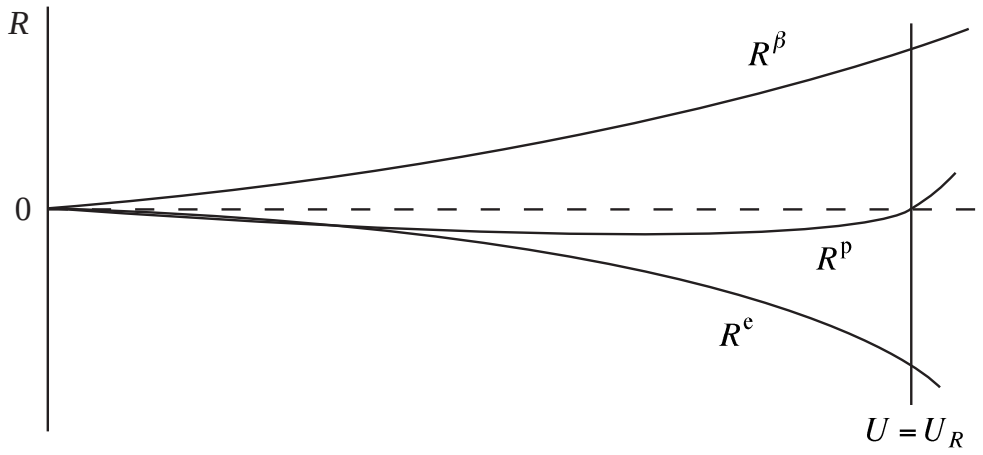

Figure 4.36: Typical variation of the components of the rolling moment versus aircraft speed U

Divergence of this antisymmetric configuration is found by setting the determinant of the coefficient matrix in Eq. (4.199) equal to zero. Usually, however, $q_{D_a} > q_{D_s}$, so it is not usually a critical design parameter. Also, in general $q_R < q_D$.

As in the divergence discussion for complete aircraft with unswept wings, rigid models in a wind tunnel can be used to guide and/or estimate the aeroelastic behavior. Thus,

$$\begin{aligned} R =& 2q \lfloor yW \rfloor \left\{ \cancelto{0}{\{cc_\ell^{\mathrm{e}}\}} + \{\mathcal{A}_a^{\mathrm{p}}\} \left(\frac{p\ell}{U}\right) + \left\{\mathcal{A}_a^\beta\right\} \beta \right\} \\ =& 2qS\ell \left(C_{L_p}^{\mathrm{p}}\right)_{\text{rigid}} \left(\frac{p\ell}{U}\right) + 2qS\ell \left(C_{L_\beta}^{\beta}\right)_{\text{rigid}} \beta \end{aligned} \tag{4.204}$$

In the rigid model, one may put β to zero and measure the torque needed to create a given $p\ell/U$. This will give $\left(C_{L_p}^{\mathrm{p}}\right)_{\text{rigid}}$. Also, one may set $p\ell/U$ to zero and measure the torque for a unit β, which gives $\left(C_{L_\beta}^{\beta}\right)_{\text{rigid}}$. One can also write

$$\frac{\partial\left(\frac{p\ell}{U}\right)}{\partial\beta} = -\frac{\left(C_{L_\beta}^{\beta}\right)_{\text{rigid}} + \frac{q}{S\ell} \lfloor yW \rfloor \left\{ \left[\left[\mathcal{A}_a^{-1}\right] - q\left[E\right]\right]^{-1} \left\{ \left[E\right] \left\{\mathcal{A}_a^\beta\right\} + \left[F\right] \left\{c_{m_\beta}\right\} \right\} \right\}}{\left(C_{L_p}^{\mathrm{p}}\right)_{\text{rigid}} + \frac{q}{S\ell} \lfloor yW \rfloor \left[\left[\mathcal{A}_a^{-1}\right] - q\left[E\right]\right]^{-1} \left[E\right] \left\{\mathcal{A}_a^{\mathrm{p}}\right\}} \tag{4.205}$$

Backswept Wings

Just as our development of swept wing aircraft utilized the equations for aircraft with unswept wings with minor modifications, the same is true in the case of aileron reversal. Typically, q_R decreases with backsweep. The reason this happens is that upward bending of the wing decreases the angle of attack, especially near the tip. A decrease in α will lead to

a decrease in lift and hence a decrease in the aileron effect. Some experimental aircraft, in an attempt to increase maneuverability, use spoilers that are scheduled to deflect similar to ailerons, deploying them on the side to dump lift while still creating a large rolling moment.

4.5 Treatment of Low-Aspect-Ratio Wings

The treatment of low-aspect-ratio wings is important because some fighters and other supersonic designs are configured as delta wings. What do we mean by "low aspect ratio"? Recall that for rectangular wings the aspect ratio is

$$\mathcal{AR} = \frac{\text{span}^2}{\text{area}} = \frac{\text{span}^2}{\text{span}\cdot\text{chord}} = \frac{\text{span}}{\text{chord}} \tag{4.206}$$

The larger the value of $\mathcal{AR}$, the more accurate 2-D (i.e. strip theory) becomes; so, for very large $\mathcal{AR}$ strip theory and beam theory will do quite well. When $\mathcal{AR}$ is not large compared to unity, other theories must be used.

4.5.1 Aerodynamic Operator

Consider wings with aspect ratios $\mathcal{AR} \geq 4$ but finite enough so that we wish to use a method more accurate than strip theory. For wings with $\mathcal{AR} \geq 4$, lifting line and 2-D corrected strip theory will give reasonably accurate results within the range of Mach number for which their physics are appropriate (i.e. not transonic or hypersonic).

Note, however, that as the span decreases, the 3-D effects become more and more prominent and even these theories become inaccurate. Recalling the elliptical distribution of lift on a uniform wing, one sees that the region near the tips becomes a more and more significant chunk of the wings. This has motivated the treatment of the tips in more detail.

For unswept wings of moderate to high aspect ratio Prandtl's lifting line theory is often used. The fundamental concept of this theory relies on the effective angle of attack, defined as

$$\alpha_{\text{eff}} = \alpha_{\text{r}} + \theta - \alpha_{\text{ind}} \tag{4.207}$$

where the last term is the induced angle of attack. Using the definitions of downwash and bound circulation Γ, one can write

$$\Gamma(y) = \frac{a_0(y)c(y)U}{2}\left[\alpha_{\text{r}}(y) + \theta(y) - \frac{1}{4\pi U}\int_{-\frac{\ell}{2}}^{\frac{\ell}{2}} \frac{d\Gamma}{d\eta}\frac{d\eta}{y-\eta}\right] \tag{4.208}$$

where the integral term is the induced angle of attack. This can be rearranged somewhat to obtain an expression in terms of the geometric angle of attack, viz.,

$$\alpha_{\text{r}}(y) + \theta(y) = \frac{\Gamma(y)}{\frac{1}{2}a_0(y)c(y)U} + \frac{1}{4\pi U}\int_{-\frac{\ell}{2}}^{\frac{\ell}{2}} \frac{d\Gamma}{d\eta}\frac{d\eta}{y-\eta} \tag{4.209}$$

The most popular manner in which to solve this expression is to use a Glauert series expansion, where

$$y = \frac{\ell \cos\psi}{2} \qquad 0 \le \psi \le \pi \qquad \eta = \frac{\ell \cos\phi}{2} \qquad 0 \le \phi \le \pi \tag{4.210}$$

so that the two wing tips are at $\psi = \phi = 0$ and $\psi = \phi = \pi$. For a general case we can now replace $\Gamma(y)$ with

$$\Gamma(\psi) = 2\ell U \sum_{n=1}^{N} A_n \sin(n\psi) \tag{4.211}$$

where the constants A_n are the unknowns. We now replace $d\Gamma(\eta)/d\eta$ under the integral in Eq. (4.209) with

$$\frac{d\Gamma}{d\eta} = \frac{d\Gamma}{d\phi}\frac{d\phi}{d\eta} = 2\ell U \sum_{n=1}^{N} nA_n \cos(n\phi)\frac{d\phi}{d\eta} \tag{4.212}$$

Substituting into Eq. (4.209), one obtains

$$\begin{aligned} \alpha_{\mathrm{r}}(\psi) + \theta(\psi) =& \frac{4\ell}{c(\psi)a_0(\psi)} \sum_{n=1}^{N} A_n \sin(n\psi) + \frac{1}{\pi} \sum_{n=1}^{N} \int_0^{\pi} \frac{nA_n \cos(n\phi)}{\cos\phi - \cos\psi} d\phi \\ =& \frac{4\ell}{c(\psi)a_0(\psi)} \sum_{n=1}^{N} A_n \sin(n\psi) + \sum_{n=1}^{N} nA_n \frac{\sin(n\psi)}{\sin\psi} \end{aligned} \tag{4.213}$$

Recalling that

$$\rho_\infty U\Gamma = \frac{1}{2}\rho_\infty U^2 c c_\ell \tag{4.214}$$

it follows that

$$c(y)c_\ell(y) = 4\ell \sum_{n=1}^{N} A_n \sin(n\psi) \tag{4.215}$$

which can be easily expressed in matrix form as

$$\{cc_\ell\} = 4\ell \left[\sin(n\psi)\right] \{A\} \tag{4.216}$$

where, for the rectangular matrix $[\sin(n\psi)]$, there is a value of ψ for each station along the wing, the station number of which serves as the row index; and n serves as the column index. Thus,

$$\{A\} = \frac{1}{4\ell} \left[\sin(n\psi)\right]^{-1} \{cc_\ell\} \tag{4.217}$$

It follows from Eq. (4.213) that

$$\frac{1}{4\ell}\left[\begin{matrix} a_0 c \end{matrix}\right] \{\alpha_{\mathrm{r}} + \theta\} = \left[\sin(n\psi)\right] \{A\} + \frac{1}{4\ell}\left[\begin{matrix} a_0 c \end{matrix}\right]\left[\begin{matrix} \frac{1}{\sin\psi} \end{matrix}\right] \left[n \sin(n\psi)\right] \{A\} \tag{4.218}$$

which can be simplified as

$$\{\alpha_{\mathrm{r}} + \theta\} = [\mathcal{A}]^{-1} \{cc_\ell\} \tag{4.219}$$

with

$$[\mathcal{A}]^{-1} = [\, \frac{1}{a_0 c} \,] + \frac{1}{4\ell} [\, \frac{1}{\sin\psi} \,] \, [n \sin(n\psi)] \, [\sin(n\psi)]^{-1} \tag{4.220}$$

For the symmetric case we take only the odd values of n, whereas for the antisymmetric case we take the even values of n and set the values of all midspan quantities equal to zero.

Below $\mathcal{AR} = 4$, the 3-D tip effects cannot be ignored. The simplest method in most Mach regimes is a panel method. For subsonic flow one may use kernel function methods, vortex lattice, or doublet lattice methods. For transonic flow, because of the complexity of this regime, solvers based on full potential or Euler/Navier-Stokes equations must be used. For low supersonic flow, the Mach box method is sufficient. When the flow is hypersonic, depending on the purpose of the calculation, piston theory may sometimes yield satisfactory results; but Euler/Navier-Stokes is needed in many cases, especially when the details of the flow mechanics are needed.

4.5.2 Structural Operator

As the wing becomes less and less beam-like, a beam model becomes less and less accurate. Plate models become an option for treating low-aspect-ratio wings, but in some cases a full 3-D finite element model is more appropriate. In any case, chordwise flexibility must be brought into the model.

Consider the aircraft shown in Fig. 4.37. The wings deform as plate models, so that at any value of x and y, the local plate deflection is $w(x, y)$. The local angle of attack is changed by

$$\theta(x, y) = -\frac{\partial w}{\partial x} \tag{4.221}$$

as illustrated in Fig. 4.38, so that

$$\alpha(x, y) = \alpha_{\mathrm{r}}(x, y) + \theta(x, y) \tag{4.222}$$

where $\alpha_{\mathrm{r}}(x, y) = \alpha_F + \beta(x, y)$, so that $\beta(x, y)$ gives the contribution of the unloaded shape of the lifting surface to the angle of attack.

Because of the small angle assumption, we may write the load on the i^{th} element with differential area ΔA_i as

$$F_i = \Delta A_i \left(\Delta p_i^{\mathrm{r}} + \Delta p_i^{\mathrm{e}} + \Delta p_i^{\delta} - Nmg \right) \tag{4.223}$$

where the superscript δ here refers to the elevator deflection. In matrix form this is equivalent to

$$\{F\} = [\, \Delta A \,] \left\{ \{\Delta p^{\mathrm{r}}\} + \{\Delta p^{\mathrm{e}}\} + \left\{\Delta p^{\delta}\right\} - Ng \{m\} \right\} \tag{4.224}$$

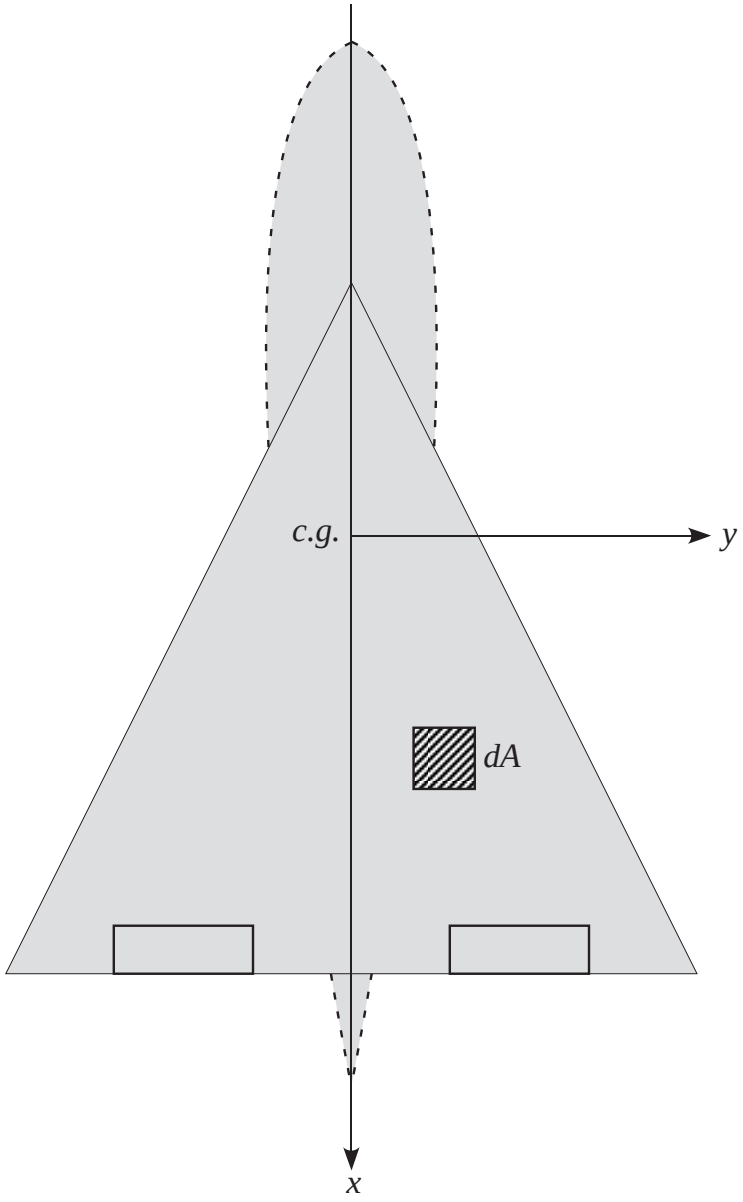

Figure 4.37: Schematic of delta-winged aircraft showing differential area of lifting surface

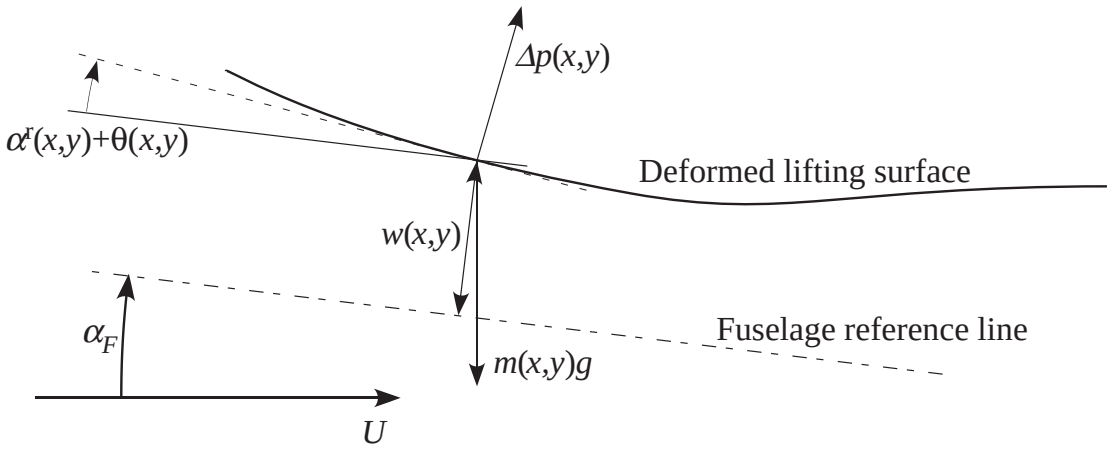

Figure 4.38: Schematic of local deformation and the angle of attack

The equilibrium equation for the wing may be expressed as

$$\{w\} = [C^{ww}]\{F\} \qquad \{\theta\} = \left[C^{\theta w}\right]\{F\} \tag{4.225}$$

where for lifting surfaces of low to moderate , the deflection w predicted from plate theory will typically be larger than that predicted by beam theory. We note here in passing that

$$C^{\theta w} = -\frac{\partial C^{ww}}{\partial x} \tag{4.226}$$

The equilibrium of the complete aircraft can be written as

$$\lfloor 1 \rfloor \{F\} = 0 \qquad \lfloor x \rfloor \{F\} = 0 \tag{4.227}$$

We can now combine these equations as before. First we substitute Eq. (4.224) into Eqs. (4.225) to obtain

$$\begin{aligned} \{w\} - [C^{ww}]\left[\grave{}\,\Delta A\,\acute{}\right]\left\{\{\Delta p^{\mathrm{r}}\} + \{\Delta p^{\mathrm{e}}\} + \left\{\Delta p^{\delta}\right\}\right\} &= -Ng\,[C^{ww}]\left[\grave{}\,\Delta A\,\acute{}\right]\{m\} \\ \{\theta\} - \left[C^{\theta w}\right]\left[\grave{}\,\Delta A\,\acute{}\right]\left\{\{\Delta p^{\mathrm{r}}\} + \{\Delta p^{\mathrm{e}}\} + \left\{\Delta p^{\delta}\right\}\right\} &= -Ng\left[C^{\theta w}\right]\left[\grave{}\,\Delta A\,\acute{}\right]\{m\} \end{aligned} \tag{4.228}$$

the second of which can be written as

$$\{\theta\} - [E]\left\{\{\Delta p^{\mathrm{r}}\} + \{\Delta p^{\mathrm{e}}\} + \left\{\Delta p^{\delta}\right\}\right\} = -Ng\left[C^{\theta w}\right]\left[\grave{}\,\Delta A\,\acute{}\right]\{m\} \tag{4.229}$$

where

$$[E] = \left[C^{\theta w}\right]\left[\grave{}\,\Delta A\,\acute{}\right] \tag{4.230}$$

Similarly, use of Eq. (4.224) in Eqs. (4.227) yields

$$\begin{aligned} \lfloor 1 \rfloor \left[\grave{}\,\Delta A\,\acute{}\right]\left\{\{\Delta p^{\mathrm{e}}\} + \{\Delta p^{\mathrm{r}}\} + \left\{\Delta p^{\delta}\right\}\right\} &= Ng\,\lfloor 1 \rfloor \{m\} = \frac{NW_{\mathrm{total}}}{2} \\ \lfloor x \rfloor \left[\grave{}\,\Delta A\,\acute{}\right]\left\{\{\Delta p^{\mathrm{e}}\} + \{\Delta p^{\mathrm{r}}\} + \left\{\Delta p^{\delta}\right\}\right\} &= 0 \end{aligned} \tag{4.231}$$

The right-hand side of the first of these equations has the 2 in the denominator because of symmetry. The right-hand side of the second of these equations is zero because the static moment about the x-axis (which passes through the center of mass) must be zero. The final form of the governing equations is obtained by use of a suitable aerodynamic operator.

Let us assume hypersonic flow and use piston theory, among the simplest of all aerodynamic operators:

$$\alpha = \left[\mathcal{A}^{-1}\right] \left\{ \frac{\Delta p}{q} \right\} \tag{4.232}$$

so that

$$\begin{aligned} \{\theta\} &= \left[\mathcal{A}^{-1}\right] \left\{ \frac{\Delta p^{\mathrm{e}}}{q} \right\} \\ \left\{ \frac{\Delta p^{\mathrm{r}}}{q} \right\} &= [\mathcal{A}] \left\{ \{1\} \alpha_F + \{\beta\} \right\} \\ \left\{ \frac{\Delta p^{\delta}}{q} \right\} &= [\mathcal{A}] \{\psi\} \delta \end{aligned} \tag{4.233}$$

where ψ is a weighting matrix of 0's and 1's with 1's at values of (x, y) that coincide with the elevator and 0's at points unaffected by the elevator.

Eqs. (4.231) and (4.229) can be combined and written as a matrix equation of the form

$$\begin{bmatrix} [\mathcal{A}^{-1}] - q\,[E] & -q\,[E]\,[\mathcal{A}]\,\{1\} & -q\,[E]\,[\mathcal{A}]\,\{\psi\} \\ \lfloor 1 \rfloor \left[\grave{} \, \Delta A \, \acute{} \right] & \frac{S}{2} \left(C_{L_\alpha}\right)_{\text{rigid}} & \frac{S}{2} \left(C_{L_\delta}\right)_{\text{rigid}} \\ \lfloor x \rfloor \left[\grave{} \, \Delta A \, \acute{} \right] & \frac{S\ell}{2} \left(C_{M_\alpha}\right)_{\text{rigid}} & \frac{S\ell}{2} \left(C_{M_\delta}\right)_{\text{rigid}} \end{bmatrix} \begin{Bmatrix} \left\{ \frac{\Delta p^{\mathrm{e}}}{q} \right\} \\ \alpha_F \\ \delta \end{Bmatrix} = \begin{Bmatrix} \{f\} \\ B_2 \\ B_3 \end{Bmatrix} \tag{4.234}$$

where

$$\begin{aligned} \frac{S}{2} \left(C_{L_\alpha}\right)_{\text{rigid}} &= \lfloor 1 \rfloor \left[\grave{} \, \Delta A \, \acute{} \right] [\mathcal{A}]\,\{1\} \\ \frac{S}{2} \left(C_{L_\delta}\right)_{\text{rigid}} &= \lfloor 1 \rfloor \left[\grave{} \, \Delta A \, \acute{} \right] [\mathcal{A}]\,\{\psi\} \\ \frac{S\ell}{2} \left(C_{L_\alpha}\right)_{\text{rigid}} &= \lfloor x \rfloor \left[\grave{} \, \Delta A \, \acute{} \right] [\mathcal{A}]\,\{1\} \\ \frac{S\ell}{2} \left(C_{L_\delta}\right)_{\text{rigid}} &= \lfloor x \rfloor \left[\grave{} \, \Delta A \, \acute{} \right] [\mathcal{A}]\,\{\psi\} \end{aligned} \tag{4.235}$$

and

$$\begin{aligned} \{f\} &= q\,[E]\,[\mathcal{A}]\,\{\beta\} - Ng\,[E]\,\{m\} \\ B_2 &= \frac{NW_{\text{total}}}{2q} - \lfloor 1 \rfloor \left[\grave{} \, \Delta A \, \acute{} \right] [\mathcal{A}]\,\{\beta\} \\ B_3 &= -\lfloor x \rfloor \left[\grave{} \, \Delta A \, \acute{} \right] [\mathcal{A}]\,\{\beta\} \end{aligned} \tag{4.236}$$

Eq. (4.234) is of the same form as similar equations developed previously. However, it should be noted that here the size is much larger because of the increase in dimensionality from 1 to 2. For a given N one can solve for $\{\Delta p^{\mathrm{e}}/q\}$, α_F, and δ. Then the airload distribution

can be found in terms of $\{\Delta p/q\}$. Finally, the divergence dynamic pressure can be found by taking the determinant of the coefficient matrix in Eq. (4.234). Generally, in trimming the flexible aircraft, one will find that δ becomes large, well before the point of instability and thus before the determinant actually vanishes, contradictory to the assumption of linear aerodynamics.

4.6 Epilogue

In this chapter we have considered divergence and aileron reversal of simple wind-tunnel models, torsional divergence and load redistribution in flexible beam representations of lifting surfaces, the effects of sweep on coupled bending-torsion divergence, the role of aeroelastic tailoring, nonuniform lifting surfaces, and complete aircraft, with and without the influence of sweep. In all these cases, the inertial loads are inconsequential and have thus been neglected. In Chapter 5, inertial loads are introduced into the aeroelastic analysis of flight vehicles, and the flutter problem is explored.

Problems

1. Consider a rigid, wind-tunnel model of a uniform wing, which is pivoted in pitch about the mid-chord and elastically restrained in pitch by a linear spring with spring constant of 225 lb/in mounted at the trailing edge. The model has a symmetric airfoil, a span of 3 ft, and a chord of 6 in. The total lift-curve slope is 6 per rad. The aerodynamic center is located at the quarter-chord, and the mass centroid is at the mid-chord.

   (a) Calculate the divergence dynamic pressure at sea level.

   (b) Calculate the divergence airspeed at sea level.

   ans.: $q_D = 150$ lb/ft^2; $U_D = 355$ ft/sec

2. For the model of Problem 1, for a dynamic pressure of 30 lb/ft^2, compute the percentage change in lift caused by the aeroelastic effect.

   ans.: 25%

3. For the model of Problem 1, propose design changes in the support system that would double the divergence dynamic pressure by

   (a) changing the stiffness of the restraining spring.

   (b) relocating the pivot point.

   ans.: (a) $k = 450$ lb/in; (b) $x_O = 2.513$ in

4. For the model of Problem 1 as altered by the design changes of Problem 3, calculate the percentage change in lift caused by the aeroelastic effect for a dynamic pressure of 30 lb/ft^2, a weight of 3 lb, $\alpha_r = 0.5°$, and for

   (a) the design change of Problem 3a

   (b) the design change of Problem 3b

   ans.: 11.11%; 17.91%

5. Consider a strut-mounted wing similar to the one discussed in Section 4.1.3, except that the two springs may have different stiffnesses. Denoting the leading-edge spring constant by k_1 and the trailing-edge spring constant by k_2 and assuming that the aerodynamic center is at the quarter chord, show that divergence can be eliminated if $k_1/k_2 \geq 3$.

6. Using Excel or a similar tool, plot a family of curves that depict the relationship of the aileron elastic efficiency, η, versus normalized dynamic pressure, $\overline{q} = q/q_D$ for various values of $R = q_R/q_D$ and $0 < \overline{q} < 1$. You should make two plots on the following scales to reduce confusion:

   (a) Plot $R < 1$ using axes $-3 < \eta < 3$.

   (b) Plot $R > 1$ using axes $-3 < \eta < 3$.

Hint: Do not compute values for the cases where $1 < R < 1.1$; Excel does not handle these well and you may get confused. For some cases you may want to plot symbols only and nicely sketch the lines that form the curves.

Answer the following questions: Where does aileron reversal occur? If you had to design a wing, what R would you try to match (or approach) and why? What happens when $q_R = q_D$? How does the efficiency change as q approaches q_R? Why do you think this happens? What other pertinent features can you extract from these plots? Explain how you came to these conclusions.

7. Consider a torsionally elastic ($GJ = 8000$ lb in^2) wind-tunnel model of a uniform wing, the ends of which are rigidly fastened to the wind-tunnel walls. The model has a symmetric airfoil, a span of 3 ft, and a chord of 6 in. The sectional lift-curve slope is 6 per rad. The aerodynamic center is located at the quarter-chord, and both the mass centroid and the elastic axis are at the mid-chord.

   (a) Calculate the divergence dynamic pressure at sea level.

   (b) Calculate the divergence airspeed at sea level.

   ans.: (a) $q_D = 162.46$ lb/ft^2; (b) $U_D = 369.65$ ft/sec

8. For the model of Problem 7, propose design changes in the model that would double the divergence dynamic pressure by

   (a) changing the torsional stiffness of the wing.

   (b) relocating the elastic axis.

   ans.: $GJ = 16000$ lb in^2; $x_{\text{ea}} = 2.25$ in

9. For the model of Problem 7, for a dynamic pressure of 30 lb/ft^2, compute the percentage increase in the sectional lift at mid-span caused by the aeroelastic effect.

   ans.: 28.094%

10. For the model of Problem 7, for a dynamic pressure of 30 lb/ft^2, compute the percentage increase in the total lift caused by the aeroelastic effect.

    ans.: 18.59%

11. Consider a swept clamped-free wing, as described in Section 4.2.4. The governing partial differential equations are given in Eqs. (4.76) and the boundary conditions in Eqs. (4.77). An approximate solution is sought for a wing with a symmetric airfoil, using a truncated set of assumed modes and the generalized equations of equilibrium – a specialized version of the generalized equations of motion for which all time-dependent terms are zero. Note that what is being asked for here is equivalent to the application of the method of Ritz to the principle of virtual work; see Section 2.7. With the wing weight ignored, only structural

and aerodynamic terms are involved. The structural terms of the generalized equations of equilibrium are based on the potential energy (here the strain energy) given by

$$P = \frac{1}{2}\int_0^\ell \left(EIw''^2 + GJ\overline{\theta}'^2\right) d\overline{y}$$

and the bending and torsion deformation is represented in terms of a truncated series, such that

$$w = \sum_{i=1}^{N_w} \eta_i \Psi_i(\overline{y})$$

$$\overline{\theta} = \sum_{i=1}^{N_\theta} \phi_i \Theta_i(\overline{y})$$

where N_w and N_θ are the numbers of assumed modes used to represent bending and torsion, respectively; η_i and ϕ_i are the generalized coordinates associated with bending and torsion, respectively; and Ψ_i and Θ_i are the assumed mode shapes for bending and torsion, respectively. Determine the potential energy in terms of the generalized coordinates using as assumed modes the uncoupled, clamped-free, free-vibration modes of torsion and bending. For torsion

$$\Theta_i = \sqrt{2}\sin\left[\frac{\pi\left(i-\frac{1}{2}\right)\overline{y}}{\ell}\right]$$

For bending, according to Eq. (2.93), Ψ_i is given as

$$\Psi_i = \cosh(\alpha_i\overline{y}) - \cos(\alpha_i\overline{y}) - \beta_i[\sinh(\alpha_i\overline{y}) - \sin(\alpha_i\overline{y})]$$

with α_i and β_i as given in Table 2.1.

12. Work Problem 11, but for assumed modes, instead of using the expressions given therein, use

$$\Theta_i = \left(\frac{\overline{y}}{\ell}\right)^i$$

$$\Psi_i = \left(\frac{\overline{y}}{\ell}\right)^{i+1}$$

keeping in mind that these functions are not orthogonal.

13. Referring back to either Problem 11 or 12, starting with the virtual work of the aerodynamic forces as

$$\overline{\delta W} = \int_0^\ell \left(L'\delta w + M'\delta\overline{\theta}\right) d\overline{y}$$

where L' and M' are the sectional lift and pitching moment expressions used to develop Eqs. (4.76), and using the given deformation modes, find the generalized forces Ξ_i, $i = 1, 2, \ldots, N = N_w + N_\theta$. As discussed in the text, generalized forces are the coefficients of the variations of the generalized coordinates in the virtual work expression. (Hint: neglecting the weight terms on the right-hand sides of Eqs. 4.74, one finds L' is the right-hand side of the second of those equations, whereas M' is the negative of the right-hand side of the first and equal to eL'.)

14. Referring back to Problems 13 and either 11 or 12, determine the generalized equations of equilibrium in the form

$$[K]\{\xi\} = \overline{q}\,\{[A]\{\xi\} + \{\Xi_0\}\}$$

where $\overline{q}$ is the dimensionless dynamic pressure given by q/q_{D_0}, q_{D_0} is the torsional divergence dynamic pressure of the unswept clamped-free wing, given by Eq. (4.54), $\{\xi\}$ is the column matrix of all unknowns $\overline{\eta}_i = \eta_i/\ell$, $i = 1, 2, \ldots, N_w$, and ϕ_i, $i = 1, 2, \ldots, N_\theta$, and $\{\Xi_0\}$ is a column matrix containing the parts of the aerodynamic generalized forces that do not depend on any unknowns. The $N \times N$ matrices $[K]$ and $[A]$ are the stiffness and aerodynamic matrices, respectively. If Problem 11 is the basis for solution, then the stiffness matrix $[K]$ is diagonal since the normal modes used to represent the wing structural behavior are orthogonal with respect to the stiffness properties of the wing.

15. Referring back to Problem 14, perform the following numerical studies:

    a. *Divergence*: To determine the divergence dynamic pressure, write the *homogeneous* generalized equations of equilibrium in the form

$$\frac{1}{\overline{q}}\{\xi\} = [K]^{-1}[A]\{\xi\}$$

    which is obviously an eigenvalue problem with $1/\overline{q}$ as the eigenvalue. After you solve the eigenvalue problem, the largest $1/\overline{q}$ provides the lowest dimensionless critical divergence dynamic pressure $\overline{q}_D = q_D/q_{D_0}$ at the sweep angle under consideration. By numerical experimentation, determine how many modes are needed for each of w and $\overline{\theta}$ to obtain the divergence dynamic pressure to within plotting accuracy. Plot the divergence dynamic pressure versus sweep angle for a range of values for the sweep angle $-45^\circ \leq \Lambda \leq 45^\circ$ and values of the dimensionless parameters e/ℓ (0.05 and 0.1) and EI/GJ (1 and 5). Compare your results with those obtained from Eq. (4.99). Comment on the accuracy of the approximate solution in the text versus your modal solution. Which one should be more accurate? Discuss the trends of divergence dynamic pressure that you see regarding the sweep angle, stiffness ratio, and location of the aerodynamic center.

    b. *Response*: For the response you will need to consider the nonhomogeneous equations, which should be put into the form

$$[[K] - \overline{q}[A]]\{\xi\} = \overline{q}\{\Xi_0\}$$

    Letting $\alpha_r = 1^\circ$, obtain the response by solving the linear system of equations represented in this matrix equation. Plot the response of the wing tip (i.e., w and $\overline{\theta}$ at $\overline{y} = \ell$) for varying dynamic pressures up to $q = 0.95q_D$ for the above values of e/ℓ and EI/GJ with $\Lambda = -25^\circ$ and 0°. Plot the lift, twist, and bending moment distributions for the case with the largest tip twist angle. Comment on this result and on the trends of static aeroelastic response that you see regarding the sweep angle, stiffness ratio, and location of the aerodynamic center.

16. Consider the divergence of an unswept composite wing with $\kappa = 0$, $GJ/EI = 0.2$ and $e/\ell = .025$. Using Eq. (4.114), determine the value of κ, as defined by Eq. (4.113), needed to keep the divergence dynamic pressure unchanged for forward-swept wings with various values of $\Lambda < 0$. Plot these values of κ versus Λ.

17. Using the approximate formula found in Eq. (4.114), determine the divergence dynamic pressure for swept, composite wings when $e < 0$. Discuss the situations in which one might encounter a negative value of e. What sign of κ would you expect to be stabilizing in this case? Plot the divergence dynamic pressure for a swept composite wing with $GJ/EI = 0.2$ and $e/\ell = -.025$ versus $\kappa = 0$ and ± 0.4 for varying Λ.

18. Consider the divergence of a swept composite wing. Show that the governing equation and boundary conditions found in Eqs. (4.108) and (4.109) can be written as a second-order, integro-differential equation of the form

$$\theta'' + \tau\theta - r\tau \int_{\eta}^{1} \theta(\xi) d\xi = 0$$

with boundary conditions $\theta(0) = \theta'(1) = 0$ and with $r = \beta/\tau$. Determine the two simplest polynomial comparison functions for this reduced-order equation and boundary conditions. Use Galerkin's method to obtain one- and two-term approximations to the divergence dynamic pressure τ_D versus r. Plot your approximate solutions for the case in which $GJ/EI = 0.2$, $e/\ell = 0.02$, and $\kappa = -0.4$, depicted in Fig. 4.25, and compare these with the approximate solution given in the text. For the two-term approximation, determine the limit point for positive e, noting that the exact values are $r = 1.59768$ and $\tau_D = 10.7090$.

ans.: The one-term approximation is

$$\tau_D = \frac{30}{12 - 5r}$$

The two-term approximation is

$$\tau_D = \frac{1260}{282 - 105r \pm \sqrt{3}\sqrt{15r(197r - 1036) + 17408}}$$

The approximate limit point in the first quadrant is at $r = 1.61804$ and $\tau_D = 11.2394$. Within plotting accuracy, the two-term approximation is virtually indistinguishable from the exact solution when $-10 \leq \tau_D \leq 10$.

19. Show that Eq. (4.132) leads to the integro-differential equation in the text, Eq. (4.133), with boundary conditions $\theta(0) = \theta'(1) = 0$. Assuming that $c_{d_0} << a_0$, construct a one-term Galerkin approximation of the solution for q_D and show that drag is destabilizing.

ans.: Taking into account the fact that $c_{d_0} << a_0$, the one-term approximation is

$$q_D \approx \frac{12\,GJ}{eca_0\ell^2} \frac{\left[\sqrt{144 + 35\frac{GJ}{EI}\left(\frac{\ell}{e}\right)^2 \frac{c_{d_0}}{a_0}} - 12\right]}{7\frac{GJ}{EI}\left(\frac{\ell}{e}\right)^2 \frac{c_{d_0}}{a_0}}$$

$$\approx \frac{5\,GJ}{2\,eca_0\ell^2} \left[1 - \frac{35}{576}\frac{GJ}{EI}\left(\frac{\ell}{e}\right)^2 \frac{c_{d_0}}{a_0}\right]$$

where the second expression further assumes that the quantity $\frac{GJ}{EI}\left(\frac{\ell}{e}\right)^2\frac{c_{d_0}}{a_0}$ is small compared to unity. Thus, in addition to the fact that drag can lead to its own instability (lateral-torsional buckling), it is destabilizing when taken into account along with aeroelastic effects.

20. Consider the straight (i.e. unswept) wing aircraft shown in Fig. 4.30. The wing is uniform, has zero built-in twist, and has an airfoil that is symmetric so that $c_{m_{\rm ac}} = 0$. The aircraft is assumed to be in steady, level flight. Use two-dimensional aerodynamic strip theory. The loading on a typical wing section is detailed in fig. 4.29. The tail airfoil is shown in Fig. 4.31. For the aircraft properties, denote W as the total weight of the aircraft and x_c as the distance the center of mass of aft the wing elastic axis. For the wing properties, denote c as the chord length, $e = x_{\rm ac} - x_{\rm ea}$ as the distance the elastic axis is aft the aerodynamic center, $d = x_{\rm cg} - x_{\rm ea}$ as the distance the elastic axis is aft the center of mass of the wing section, GJ as the torsional stiffness, m as the mass per unit span, a_0 as the slope of the lift curve, and $S = Lc$ as the wing area. For the tail properties, denote S_T as the tail area, x_T as the distance the aerodynamic center of the tail is aft the elastic axis of the wing, $\partial C_L/\partial\alpha$ as the slope of the lift curve for the tail, and $\partial C_L/\partial\delta$ as the increment of the lift due to unit elevator deflection. Find:

    (a) The elastic twist distribution, $\theta(y)$.

    (b) The lift distribution, $L'(y)$.

    (c) The total lift on the wing.

    (d) The twisting moment on the wing $T(y)$.

    (e) The attitude of the aircraft, α_F and δ.

    (f) The attitude of the aircraft if the wing were rigid, $\alpha_{\rm r}^F$ and $\delta_{\rm r}$.

21. Consider the straight (i.e. unswept) wing aircraft shown in Fig. **??**. The wing is spanwise nonuniform, has built-in twist and a symmetric airfoil so that $c_{m_{\rm ac}} = 0$. The aircraft is assumed to be flying with incidence angle α_F. Consider the case of arbitrary aerodynamic theory. The loading on a typical wing section is detailed in Fig. 4.29. The tail airfoil is shown in Fig. 4.31. For the aircraft properties, denote W as the total weight of the aircraft and x_c as the distance the center of mass of aft the wing elastic axis. For the wing properties, denote c as the chord length, $e(y) = x_{\rm ea} - x_{\rm ac}$ as the distance the elastic axis is aft the aerodynamic center, $d(y) = x_{\rm ea} - x_{\rm cg}$ as the distance the elastic axis is aft the center of mass of the wing section, $GJ(y)$ as the torsional stiffness, m as the mass per unit span, a_0 as the slope of the lift curve, and

$$S = \int_0^\ell c(y)dy$$

as the wing area. For the tail properties, denote S_T as the tail area, x_T as the distance the aerodynamic center of the tail is aft the elastic axis of the wing, $\partial C_L/\partial\alpha$ as the slope of the lift curve for the tail, and $\partial C_L/\partial\delta$ as the increment of the lift due to unit elevator deflection. Find:

(a) The elastic twist distribution

(b) The twisting moment distribution along each wing

(c) The lift distribution along each wing

(d) The total lift on the wings

(e) The load factor

(f) The elevator angle δ

(g) The bending moment distribution along each wing

(h) The load factor of the aircraft if the wing were rigid, N and δ_{r}.

Comment on the similarities and differences of the form of this solution and one for 20.

22. Consider a complete aircraft with high-aspect-ratio, swept wings made of composite materials so that there is bending-twist coupling. Using operator notation, set up the airload distribution and divergence problems, generalizing the development in Section 4.4.2 to include the structural coupling.

23. A rectangular, high aspect ratio, cantilevered wing of length L is placed in a wind tunnel, with a cross section as depicted in Fig. 4.29. The airfoil is such that $c_{m_{\mathrm{ac}}} = 0$, and there is no built-in twist. Use a simple finite element formulation to model the torsional deformation of the wing.

(a) Use two-dimensional strip theory for the aerodynamic loads. Determine the matrix form of the aerodynamic operator. Determine the lift distribution and elastic twist based on the resulting matrix formulation.

(b) Compare your results with the exact solution of the problem obtained in class. Plot the exact and approximate elastic twist on the same graph. Plot the exact and approximate lift distribution on the same graph. Study the convergence of the process as you increase the number of elements.

(c) Use Prandtl lifting-line theory for the aerodynamic loads. Determine the matrix form of the aerodynamic operator. Determine the lift distribution and elastic twist based on the resulting matrix formulation.

(d) Compare the results obtained with the strip theory and the lifting line theory. On the same graph, plot the lift distribution for the two aerodynamic theories. On the same graph, plot the elastic twist for the two aerodynamic theories. Study the convergence of the process as you increase the number of terms in the Glauert expansion.

(e) Determine the divergence speed of the wing based on the matrix formulation of both aerodynamic theories. Give a physical explanation for the difference in divergence speed.

Show that the problem depends on the single non-dimensional parameter $\lambda^2 = qea_0cL^2/GJ$. For Prandtl lifting-line theory let the wing $\mathcal{AR}$=5.

Chapter 5

DYNAMIC AEROELASTICITY

Structural dynamics is the study of phenomena associated with the interaction of inertial and elastic forces in mechanical systems. In particular, the mechanical systems typically considered are one- and two-dimensional continuous configurations that exhibit the general structural dynamic behavior of flight vehicles. If in the analysis of these structural dynamic systems aerodynamic loading is included, then the resulting dynamic phenomena may be classified as aeroelastic. As has been observed in Chapter 4, aeroelastic phenomena can have a significant influence on the design of flight vehicles. Indeed, these effects can greatly alter the design requirements that are specified for the disciplines of performance, structural loads, flight stability and control, and even propulsion. In addition, aeroelastic phenomena can introduce catastrophic instabilities of the structure that are unique to aeroelastic interactions and can limit the flight envelope.

Recalling the diagram in Fig. 1.1, one can classify aeroelastic phenomena as either static or dynamic. Whereas Chapter 4 dealt only with static aeroelasticity, in the present chapter we examine dynamic aeroelasticity. Although there are many other dynamic aeroelastic phenomena that could be treated, we focus in this chapter entirely on only two aspects. First there is the instability called flutter, which generally leads to a catastrophic structural failure of the flight vehicle. A formal definition of aeroelastic flutter may be given as: *A dynamic instability of a flight vehicle associated with the interaction of aerodynamic, elastic and inertial forces.* Second, we look at dynamic response and transient stresses in the aircraft and its components. It is apparent that any investigation of flutter stability or dynamic aeroelastic response requires an adequate knowledge of the system's structural dynamic and aerodynamic properties.

Of the various phenomena that are categorized as aeroelastic flutter, lifting surface flutter is the one that is most often encountered and most likely to result in a catastrophic structural failure. As a result, it is required that all flight vehicle lifting surfaces be analyzed and tested to assure that this dynamic instability will not occur for any condition within the vehicle's flight envelope. If the airflow about the surface becomes separated during any portion of the elastic oscillation, the instability is called stall flutter and the governing equations

become nonlinear. This type of instability most commonly occurs on turbojet compressor and helicopter rotor blades. Other phenomena that result in nonlinear behavior include large deflections, mechanical slop, and nonlinear control systems. Nonlinear phenomena will not be considered in the present treatment.

Even with this obvious paring down of the problem, one still finds that linear flutter analysis of clean lifting surfaces is complicated. We can only offer a simplified discussion of the theory of flutter. The reader is urged to consult the bibliography for additional reading on the subject.

This chapter begins with consideration of flutter problems from the field of dynamic stability. Then, the modal representation is used to set up a lifting surface flutter analysis as a linear set of ordinary differential equations. These are transformed into an eigenvalue problem, and the stability characteristics are then discussed in terms of the eigenvalues. Then, as an example of this methodology, a two-degree-of-freedom "typical section" analysis is formulated using the simple steady-flow aerodynamic model used in Chapter 4. The main shortcoming of this simple analysis is the neglect of unsteady effects in the aerodynamic model. Motivated by the need to consider unsteady aerodynamics in a meaningful but simple way, we then introduce classical flutter analysis. Engineering solutions that partially overcome the shortcomings of classical flutter analysis are then presented. To complete the set of analytical tools needed for flutter analysis, two very different unsteady aerodynamic theories are outlined, one suitable for use with classical flutter analysis and its derivatives, and the other suitable for eigenvalue-based flutter analysis. After illustrating how to approach the flutter analysis of a flexible wing using the assumed modes method, the flutter section concludes with a discussion of flutter boundary characteristics. The subjects of transient response and transient stresses are then addressed.

5.1 Dynamic Stability

The study of the stability of structures under follower force systems apparently started with work by Nikolai in the late 1920's. At this time there are many papers and some books (see Bolotin's books) devoted to this subject. Much of the analytical research to date has focused on the stability of beams subjected to various types of follower forces and examination of the effects of various physical phenomena, such as damping and transverse shear deformation. The relationship of follower force systems to aeroelasticity is centered on the notion that the aerodynamic forces developed in the previous chapter are all nonconservative. That is, there exists no potential energy which, when varied, will give the virtual work of the forces. To put it another way, the virtual work of the forces cannot be "integrated" to provide a potential energy. Analytical examples of solved follower force problems help to clarify the nature of these systems and their analysis. For example, it is now commonly understood that static analysis of elastic systems subjected to follower forces may erroneously show that the system is free of instability. The example of Beck's problem below will illustrate that. In order to ascertain whether a system subjected to follower forces is stable requires a kinetic

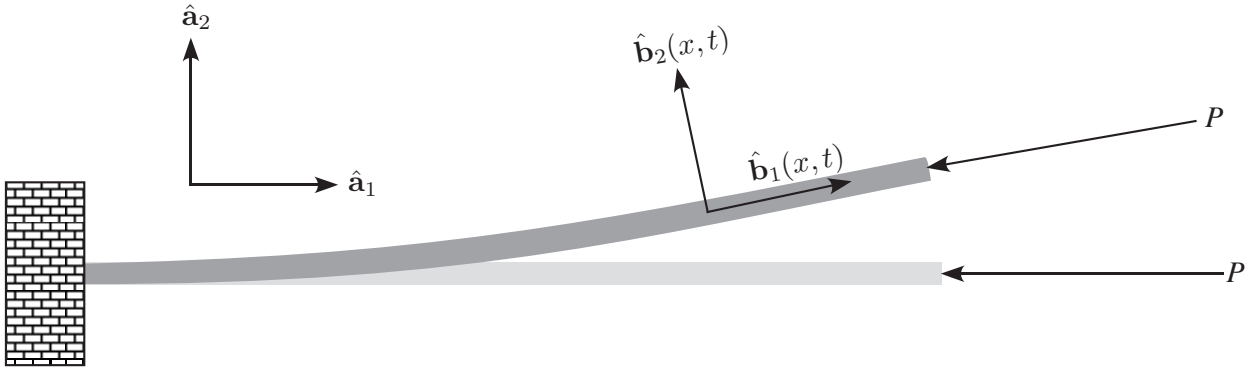

Figure 5.1: Schematic of beam undergoing compressive axial follower force

analysis. In addition to possible buckling instabilities, one may also find flutter instabilities. By this we mean that small perturbations about the static equilibrium state oscillate with increasing amplitude.

Consider a cantilevered beam of length ℓ undergoing planar deformation and having bending stiffness EI and mass per unit length m that are constant along the beam. The beam is subjected to a force of constant magnitude F, the line of action of which passes through the elastic axis of the beam at the end cross section and remains tangent to the beam in its deformed state.

The beam is depicted in Fig. 5.1 and the transverse displacement along the beam is $v(x,t)$ and the longitudinal displacement is $u(x,t)$. Thus, the position vector to any point along the beam is

$$\mathbf{r} = (x+u)\hat{\mathbf{a}}_1 + v\hat{\mathbf{a}}_2 \tag{5.1}$$

where the unit vectors $\hat{\mathbf{a}}_1$ and $\hat{\mathbf{a}}_2$ are along the undeformed beam and perpendicular to it in the plane of deformation. Considering the beam as inextensible, one finds the unit vector tangent to the beam to be

$$\hat{\mathbf{b}}_1 = \frac{\partial \mathbf{r}}{\partial x} = \left(1 + \frac{\partial u}{\partial x}\right)\hat{\mathbf{a}}_1 + \frac{\partial v}{\partial x}\hat{\mathbf{a}}_2 \tag{5.2}$$

Since this is a unit vector, the length of the vector must be equal to unity, so that

$$\left(1 + \frac{\partial u}{\partial x}\right)^2 + \left(\frac{\partial v}{\partial x}\right)^2 = 1 \tag{5.3}$$

which leads to a constraint on u of the form

$$\frac{\partial u}{\partial x} = \sqrt{1 - \left(\frac{\partial v}{\partial x}\right)^2} - 1 \tag{5.4}$$

For small deflections, this means that

$$\frac{\partial u}{\partial x} \approx -\frac{1}{2}\left(\frac{\partial v}{\partial x}\right)^2 \tag{5.5}$$

or

$$u(x,t) = -\frac{1}{2}\int_0^x \left[\frac{\partial v(\xi,t)}{\partial \xi}\right]^2 d\xi \tag{5.6}$$

Now the relationship between the unit tangent vector $\hat{\mathbf{b}}_1$ and the unit vectors of the inertial frame $\hat{\mathbf{a}}_i$ may be written as

$$\hat{\mathbf{b}}_1 = \frac{\partial \mathbf{r}}{\partial x} \approx \left[1 - \frac{1}{2}\left(\frac{\partial v}{\partial x}\right)^2\right]\hat{\mathbf{a}}_1 + \frac{\partial v}{\partial x}\hat{\mathbf{a}}_2 \tag{5.7}$$

The strain energy of such a beam is

$$U = \frac{1}{2}\int_0^\ell EI\left(\frac{\partial^2 v}{\partial x^2}\right)^2 dx \tag{5.8}$$

and we find the kinetic energy, ignoring longitudinal motion, to be

$$K = \frac{1}{2}\int_0^\ell m\left(\frac{\partial v}{\partial t}\right)^2 dx \tag{5.9}$$

Ignoring higher-order terms in the section rotation $\partial v/\partial x$, the virtual work of the applied force is

$$\begin{aligned}\overline{\delta W} =& -F\hat{\mathbf{b}}_1(\ell,t)\cdot[\delta u(\ell,t)\hat{\mathbf{a}}_1 + \delta v(\ell,t)\hat{\mathbf{a}}_2]\\ =& -F\hat{\mathbf{b}}_1(\ell,t)\cdot\left[-\hat{\mathbf{a}}_1\int_0^\ell \frac{\partial v}{\partial x}\frac{\partial \delta v}{\partial x}dx + \delta v(\ell,t)\hat{\mathbf{a}}_2\right]\\ =& F\left[\int_0^\ell \frac{\partial v}{\partial x}\frac{\partial \delta v}{\partial x}dx - \frac{\partial v}{\partial x}(\ell,t)\delta v(\ell,t)\right]\end{aligned} \tag{5.10}$$

Clearly, the first term of the last line can be expressed as the variation of a potential energy functional and is the standard term one finds in energy treatments of strings and beams undergoing axial forces. However, the second term cannot be derived from a potential. Using integration by parts and the root boundary conditions, one may write the virtual work in the simplest form as

$$\overline{\delta W} = -F\int_0^\ell \frac{\partial^2 v}{\partial x^2}\delta v dx \tag{5.11}$$

Applying Hamilton's principle to obtain the equation of motion and boundary conditions, one first obtains

$$\int_{t_1}^{t_2}\left(\delta U - \delta K - \overline{\delta W}\right)dt = 0 \tag{5.12}$$

or

$$\int_{t_1}^{t_2}\left[\int_0^\ell\left(EI\frac{\partial^2 v}{\partial x^2}\frac{\partial^2\delta v}{\partial x^2}-m\frac{\partial v}{\partial t}\frac{\partial\delta v}{\partial t}+F\frac{\partial^2 v}{\partial^2 x}\delta v\right)dx\right]dt=0 \tag{5.13}$$

Integrating by parts in time and setting virtual displacement $\delta v(x,t)$ equal to zero at $t=t_1$ and t_2, one finds that the time integral is no longer necessary. The result is a weak form of the equation of motion

$$\int_0^\ell\left[EI\frac{\partial^2 v}{\partial x^2}\frac{\partial^2\delta v}{\partial x^2}+\left(m\frac{\partial^2 v}{\partial t^2}+F\frac{\partial^2 v}{\partial x^2}\right)\delta v\right]dx=0 \tag{5.14}$$

Integrating by parts in x one now finds

$$\int_0^\ell\left[\frac{\partial^2}{\partial x^2}\left(EI\frac{\partial^2 v}{\partial x^2}\right)+m\frac{\partial^2 v}{\partial t^2}+F\frac{\partial^2 v}{\partial x^2}\right]\delta v dx+\left[EI\frac{\partial^2 v}{\partial x^2}\frac{\partial\delta v}{\partial x}-\frac{\partial}{\partial x}\left(EI\frac{\partial^2 v}{\partial x^2}\right)\delta v\right]\Bigg|_0^\ell=0 \tag{5.15}$$

The virtual displacement and rotation are arbitrary everywhere except at the beam root where they both vanish. In order for this expression to vanish, the integrand must vanish. The result is the Euler-Lagrange partial differential equation of motion

$$\frac{\partial^2}{\partial x^2}\left(EI\frac{\partial^2 v}{\partial x^2}\right)+m\frac{\partial^2 v}{\partial t^2}+F\frac{\partial^2 v}{\partial x^2}=0 \tag{5.16}$$

and the boundary conditions are

$$v(0,t)=\frac{\partial v}{\partial x}(0,t)=EI(\ell)\frac{\partial^2 v}{\partial x^2}(\ell,t)=\frac{\partial}{\partial x}\left(EI\frac{\partial^2 v}{\partial x^2}\right)(\ell,t)=0 \tag{5.17}$$

For constant EI one may simplify these to

$$EI\frac{\partial^4 v}{\partial x^4}+m\frac{\partial^2 v}{\partial t^2}+F\frac{\partial^2 v}{\partial x^2}=0 \tag{5.18}$$

with

$$v(0,t)=\frac{\partial v}{\partial x}(0,t)=\frac{\partial^2 v}{\partial x^2}(\ell,t)=\frac{\partial^3 v}{\partial x^3}(\ell,t)=0 \tag{5.19}$$

It can be shown that the static problem (i.e. without the inertial term) has only the trivial solution. The dynamic problem, however, has a nontrivial solution that can be found exactly. Introducing $\eta=x/\ell$, $f=F\ell^2/EI$, and nondimensional time $\tau=t\sqrt{EI/(m\ell^4)}$, and substituting $v(x,t)=\hat{v}(x)\exp(s\tau)$ into the equation of motion, Eq. (5.18), one finds the governing equation reduces to

$$\hat{v}''''+f\hat{v}''+s^2\hat{v}=0 \tag{5.20}$$

where $(\,)'=d(\,)/d\eta$. The general solution is

$$\hat{v}=A_1\sin(\alpha\eta)+A_2\cos(\alpha\eta)+A_3\sinh(\beta\eta)+A_4\cosh(\beta\eta) \tag{5.21}$$

where A_i are arbitrary constants and

$$\begin{aligned}\alpha =& \frac{\sqrt{\sqrt{f^2 - 4\,s^2} + f}}{\sqrt{2}} \\ \beta =& \frac{\sqrt{\sqrt{f^2 - 4\,s^2} - f}}{\sqrt{2}}\end{aligned} \tag{5.22}$$

Using the boundary conditions as above, one finds that

$$\begin{Bmatrix} \hat{v}(0) \\ \hat{v}'(0) \\ \hat{v}''(\ell) \\ \hat{v}'''(\ell) \end{Bmatrix} = \begin{bmatrix} 0 & 1 & 0 & 1 \\ \alpha & 0 & \beta & 0 \\ -\alpha^2 \sin\alpha & -\alpha^2 \cos\alpha & \beta^2 \sinh\beta & \beta^2 \cosh\beta \\ -\alpha^3 \cos\alpha & \alpha^3 \sin\alpha & \beta^3 \cosh\beta & \beta^3 \sinh\beta \end{bmatrix} \begin{Bmatrix} A_1 \\ A_2 \\ A_3 \\ A_4 \end{Bmatrix} = \begin{Bmatrix} 0 \\ 0 \\ 0 \\ 0 \end{Bmatrix} \tag{5.23}$$

which, according to Cramer's rule, leads to

$$\begin{vmatrix} 0 & 1 & 0 & 1 \\ 1 & 0 & 1 & 0 \\ -\alpha \sin\alpha & -\alpha^2 \cos\alpha & \beta \sinh\beta & \beta^2 \cosh\beta \\ -\alpha^2 \cos\alpha & \alpha^3 \sin\alpha & \beta^2 \cosh\beta & \beta^3 \sinh\beta \end{vmatrix} = 0 \tag{5.24}$$

which reduces to

$$\alpha^4 + \beta^4 + \alpha\,\beta\left[2\,\alpha\,\beta\cos\alpha\,\cosh\beta + (\alpha^2 - \beta^2)\sin\alpha\,\sinh\beta\right] = 0 \tag{5.25}$$

This can be simplified by noting that

$$\begin{aligned}\alpha^4 + \beta^4 =& f^2 - 2s^2 \\ \alpha^2 - \beta^2 =& f \\ \alpha^2\beta^2 =& -s^2\end{aligned} \tag{5.26}$$

so that

$$f^2 - 2s^2(1 + \cos\alpha\cosh\beta) \pm i f s \sin\alpha\sinh\beta = 0 \tag{5.27}$$

Since the solution is represented in the form of $\exp(s\tau)$, the characteristic equation must be independent of the sign of the imaginary part of s. Thus, we can further simplify the last term yielding

$$f^2 - 2s^2(1 + \cos\alpha\cosh\beta) - i\,f\,s\,\mathrm{sgn}[\Im(s)]\,\sin\alpha\sinh\beta = 0 \tag{5.28}$$

The roots of Eq. (5.28) must be found by numerical methods. When $f = 0$, the roots are all pure imaginary and are equal to the nondimensional natural frequencies of the unloaded beam: $s = \pm i1.87510^2$, $\pm i4.69409^2$, ... The curves in Figs. 5.2 and 5.3 show the variation

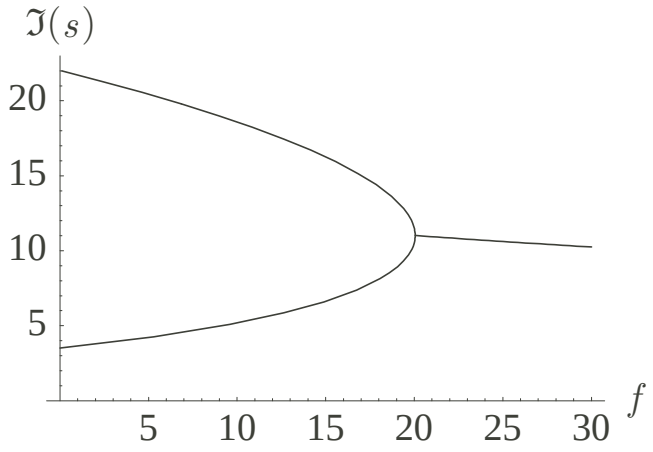

Figure 5.2: Exact solution for imaginary part of nondimensional eigenvalue s versus nondimensional force f for Beck's column

of the lowest two roots with f. As f tends toward $f = f_F = 20.0510$, the imaginary parts of the first two roots coalesce near $\Im(s) = 11.0156$ and the real parts remain zero. When f exceeds f_F, the real parts of the two roots being tracked suddenly become nonzero, while the imaginary parts lock onto one another, exhibiting only one curve. Thus, as long as $f \leq f_F$ the beam vibrates with frequencies equal to $\Im(s)\sqrt{EI/(m\ell^4)}$. When $f > f_F$ one root will always have a positive real part, which means that we have vibrations with growing amplitude. This is, then, is termed a flutter instability even though aerodynamics is not involved. As is the case with aerodynamic forces, the work done by the follower force is path-dependent, making it nonconservative.

We can also gain insight from application of the Ritz method, which is frequently more convenient than an exact solution. Let

$$v(x,t) = \sum_{i=1}^{N} \xi_i(t)\phi_i(x) \tag{5.29}$$

where ϕ_i are the uniform cantilever beam mode shapes of Section 2.2.4. For application of the Ritz method, we substitute this series into the weak form, yielding

$$\sum_{i=1}^{N} \delta\xi_i \left[\sum_{j=1}^{N} \xi_j \int_0^\ell \left(EI\phi_i''\phi_j'' + F\phi_i\phi_j'' \right) dx + \sum_{j=1}^{N} \ddot{\xi}_j \int_0^\ell m\phi_i\phi_j dx \right] = 0 \tag{5.30}$$

which, for arbitrary $\delta\xi_i$ yields a system of linear, second-order, ordinary differential equations of the form

$$\sum_{j=1}^{N} \left(M_{ij}\ddot{\xi}_j + K_{ij}\xi_j \right) = 0 \qquad i = 1, 2, \ldots, N \tag{5.31}$$

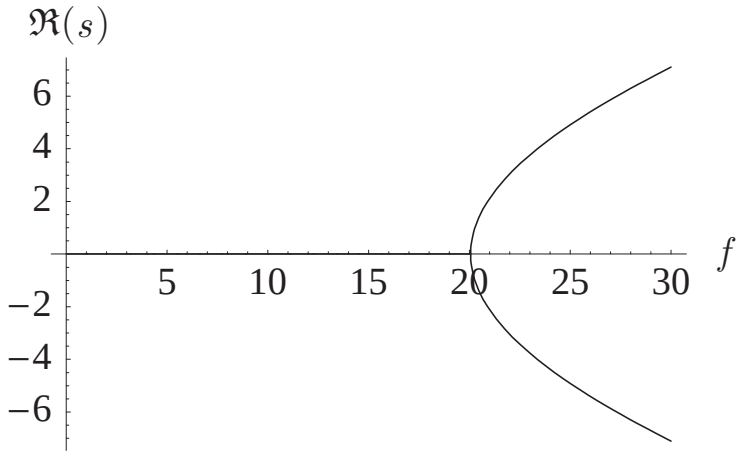

Figure 5.3: Exact solution for real part of nondimensional eigenvalue s versus nondimensional force f for Beck's column

or

$$[M]\left\{\ddot{\xi}\right\} + [K]\{\xi\} = 0 \tag{5.32}$$

where

$$\begin{aligned} K_{ij} &= \int_0^\ell \left(EI\phi_i''\phi_j'' + F\phi_i\phi_j''\right) dx \\ M_{ij} &= \int_0^\ell m\phi_i\phi_j dx \end{aligned} \tag{5.33}$$

We note that $[K]$ is not symmetric, thus allowing for the possibility of complex eigenvalues. The matrix $[K]$ carries the elastic forces, proportional to EI and the applied forces, proportional to F. The matrix $[M]$ carries the inertial forces, proportional to m. The system is linear with constant coefficients.

Letting $\{\xi\} = \left\{\hat{\xi}\right\}\exp(\nu t)$, $s^2 = m\ell^4\nu^2/EI$, $f = F\ell^2/EI$ and $\eta = x/\ell$, one finds that the equation can be expressed as

$$\left[s^2[\,1\,] + [\,(\alpha_i\ell)^4\,] + f\,[A]\right]\left\{\hat{\xi}\right\} = 0 \tag{5.34}$$

where

$$A_{ij} = \int_0^1 \phi_i(\eta)\phi_j''(\eta)d\eta \tag{5.35}$$

This system has only a trivial solution for arbitrary values of f and s. For $N = 2$, $A_{11} = 0.858244$, $A_{12} = -11.7432$, $A_{21} = 1.87385$, $A_{22} = -13.2943$. For $f = 0$ the roots for s are purely imaginary and equal to the values of $\pm i(\alpha_1\ell)^2 = \pm 1.87510^2 i$ and $\pm i(\alpha_2\ell)^2 = \pm 4.69409^2 i$. The magnitudes of these roots are the natural frequencies of the unforced system. As f increases the roots remain imaginary at first as they come together, and there

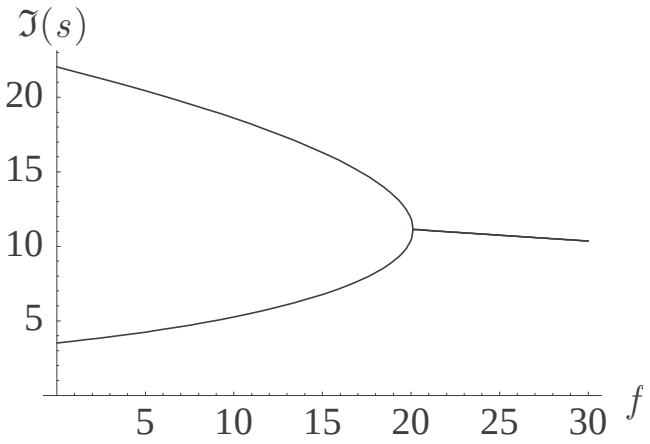

Figure 5.4: Approximate solution for imaginary part of nondimensional eigenvalue s versus nondimensional force f for Beck's column

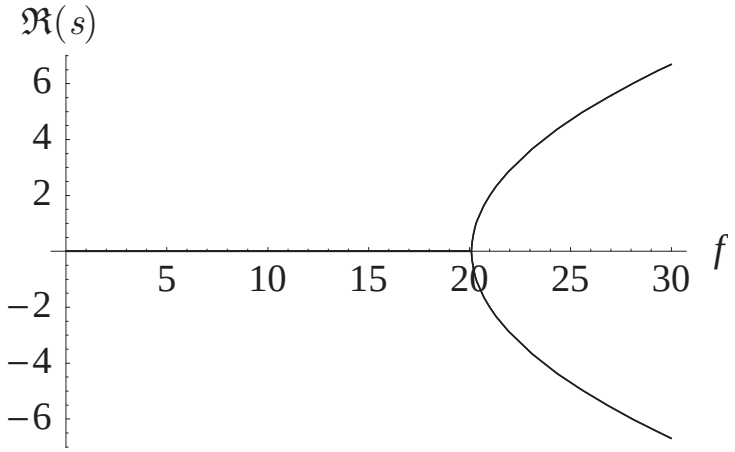

Figure 5.5: Approximate solution for real part of nondimensional eigenvalue s versus nondimensional force f for Beck's column

is a point at which the roots coalesce; see Figs. 5.4 and 5.5. At this value there is a pair of double roots, both of which are pure imaginary. Since the governing eigenvalue problem reduces to a bi-quadratic in s, i.e.

$$as^4 + bs^2 + c = 0 \tag{5.36}$$

with $a = 1$, $b = (\alpha_1\ell)^4 + (\alpha_2\ell)^4 + f(A_{11} + A_{22})$, and

$$c = f^2\left(A_{11}A_{22} - A_{12}A_{21}\right) + fA_{22}\left(\alpha_1\ell\right)^4 + fA_{11}\left(\alpha_2\ell\right)^4 + \left(\alpha_1\ell\right)^4\left(\alpha_2\ell\right)^4 \tag{5.37}$$

the point of the coalescence can be determined to be when the discriminant, b^2-4ac, vanishes. The value of f at this point is then the value at flutter, denoted by f_F and given by

$$f_F = \frac{\left(\alpha_2\ell\right)^4 - \left(\alpha_1\ell\right)^4}{A_{11} - A_{22} - 2\sqrt{-A_{12}}\sqrt{A_{21}}} = 20.1048 \tag{5.38}$$

at which point the nondimensional flutter frequency $\Im(s_F) = 11.1323$. These values are very close to the exact solution, where $f_F = 20.0510$ and $\Im(s_F) = 11.0156$. When $f > f_F$, the imaginary parts of the two roots remain equal to each other, while the real parts of the roots have the same magnitude but opposite signs. This means that when $f > f_F$ there is always a root with a positive real part, which means that the system will oscillate sinusoidally with an exponentially increasing amplitude.

Because aerodynamic models are nonconservative, we expect similar behavior for simple aeroelastic analyses. Because aerodynamic models possess additional complexity, however, the behavior is not exactly the same. Aerodynamic models typically have damping as well, which will mean that subcritical values of s will not be purely imaginary. In this case we would look for the value of f for which the real part of s crosses the zero axis and becomes positive.

5.2 Panel Flutter

Consider a rectangular panel with thickness h, length along the flow direction ℓ and width b where $h << b$. Furthermore, if $b << \ell$ the panel can be treated as a beam, the boundary conditions of which we assume to be pinned-pinned. Once again we choose the free-vibration modes of the beam as basis functions for application of the Ritz method. Thus,

$$w = \sum_{i=1}^{N} \xi_i(t)\phi_i(x) \tag{5.39}$$

where

$$\phi_i = \sqrt{2}\sin\left(\frac{i\pi x}{\ell}\right) \tag{5.40}$$

and the natural frequencies are

$$\omega_i = (i\pi)^2 \sqrt{\frac{EI}{m\ell^4}} \tag{5.41}$$

Thus, the potential energy is simply

$$\begin{aligned} P =& \frac{1}{2}\int_0^\ell EI \left[-\sqrt{2}\sum_{i=1}^{N} \xi_i \left(\frac{i\pi}{\ell}\right)^2 \sin\left(\frac{i\pi x}{\ell}\right)\right]^2 dx \\ =& \frac{1}{2}\frac{EI}{\ell^3}\sum_{i=1}^{N}(i\pi)^4 \xi_i^2 \end{aligned} \tag{5.42}$$

and the kinetic energy is

$$\begin{aligned} K =& \frac{1}{2}\int_0^\ell m \left[\sqrt{2}\sum_{i=1}^{N} \dot{\xi}_i \sin\left(\frac{i\pi x}{\ell}\right)\right]^2 dx \\ =& \frac{1}{2} m\ell \sum_{i=1}^{N} \dot{\xi}_i^2 \end{aligned} \tag{5.43}$$

Panel flutter is usually a supersonic phenomenon, though it can occur in the transonic regime. Here we introduce the local speed of sound in the air a_∞ and the Mach number $M_\infty = U/a_\infty$. Now, assuming $M_\infty > 1.7$ and that only the upper surface is loaded, the force per unit length on the panel can be written as

$$\begin{aligned} f =& -\frac{\rho_\infty U^2 b}{\sqrt{M_\infty^2 - 1}} \left(\frac{\partial w}{\partial x} + \frac{M_\infty^2 - 2}{M_\infty^2 - 1}\frac{1}{U}\frac{\partial w}{\partial t}\right) \\ =& -g_x \frac{\partial w}{\partial x} - g_t \frac{\partial w}{\partial t} \end{aligned} \tag{5.44}$$

The virtual work done by the applied load is then

$$\overline{\delta W} = -\int_0^\ell \left(g_x \frac{\partial w}{\partial x} + g_t \frac{\partial w}{\partial t}\right) \delta w \, dx \tag{5.45}$$

With the Ritz approximation, the virtual work of the applied forces becomes

$$\begin{aligned} \overline{\delta W} =& -\int_0^\ell \sqrt{2}\sum_{j=1}^{N} \left[g_x \xi_j \left(\frac{j\pi}{\ell}\right)\cos\left(\frac{j\pi x}{\ell}\right) + g_t \dot{\xi}_j \sin\left(\frac{j\pi x}{\ell}\right)\right] \sqrt{2}\sum_{i=1}^{N} \delta\xi_i \sin\left(\frac{i\pi x}{\ell}\right) dx \\ =& -2g_x \sum_{i=1}^{N}\sum_{\substack{j=1 \\ j\neq i}}^{N} \frac{ij\left[(-1)^{i+j} - 1\right]\delta\xi_i \xi_j}{j^2 - i^2} - g_t \ell \sum_{i=1}^{N} \delta\xi_i \dot{\xi}_i \end{aligned} \tag{5.46}$$

The generalized equations of motion then become

$$m\ell\ddot{\xi}_i + g_t\ell\dot{\xi}_i + \frac{EI(i\pi)^4}{\ell^3}\xi_i + g_x\sum_{j=1}^{N} A_{ij}\xi_j = 0 \tag{5.47}$$

where

$$A_{ij} = \begin{cases} 0 & \text{for } i = j \\ \frac{2ij\left[(-1)^{i+j}-1\right]}{j^2-i^2} & \text{for } i \neq j \end{cases} \tag{5.48}$$

Multiplying through the equations of motion by $\ell^3/(EI\pi^4)$, using the expression for the first natural frequency

$$\frac{\pi^4 EI}{m\ell^4} = \omega_1^2 \tag{5.49}$$

and introducing

$$\mu = \frac{\rho_\infty b^3}{m\ell} \qquad \overline{a} = \frac{a_\infty}{b\omega_1} \qquad \overline{b} = \frac{b}{\ell} \tag{5.50}$$

one can rewrite the generalized equations of motion as

$$\frac{1}{\omega_1^2}\ddot{\xi}_i + \frac{\mu\overline{a}M_\infty(M_\infty^2-2)}{\overline{b}\omega_1(M_\infty^2-1)^{\frac{3}{2}}}\dot{\xi}_i + i^4\xi_i + \frac{\mu\overline{a}^2M_\infty^2}{\sqrt{M_\infty^2-1}}\sum_{j=1}^{N} A_{ij}\xi_j = 0 \tag{5.51}$$

The quantity μ is related to a parameter sometimes called the mass ratio, and $\overline{a}$ can be called the reduced speed of sound.

Now we assume a solution of the form $\xi_i = \hat{\xi}_i \exp(\nu t)$ and introduce $s = \nu/\omega_1$. Consider the case $N = 2$, for which the equations of motion become

$$\begin{bmatrix} s^2 + sc_a + 1 & \lambda \\ -\lambda & s^2 + sc_a + 16 \end{bmatrix} \begin{Bmatrix} \hat{\xi}_1 \\ \hat{\xi}_2 \end{Bmatrix} = \begin{Bmatrix} 0 \\ 0 \end{Bmatrix} \tag{5.52}$$

where

$$\begin{aligned} c_a &= \frac{\mu\overline{a}M_\infty(M_\infty^2-2)}{\overline{b}(M_\infty^2-1)^{\frac{3}{2}}} \\ \lambda &= \frac{8\mu\overline{a}^2M_\infty^2}{3\sqrt{M_\infty^2-1}} \end{aligned} \tag{5.53}$$

For a non-trivial solution the determinant of the coefficient matrix must vanish, yielding a quartic polynomial

$$\left(s^2 + sc_a + 1\right)\left(s^2 + sc_a + 16\right) + \lambda^2 = 0 \tag{5.54}$$

A sample of the solution is plotted in Figs. 5.6 – 5.8, the imaginary part in Fig. 5.6 and the only distinct two real parts of the four roots in Fig. 5.7. Fig. 5.8 shows only the root that crosses the zero axis, and Fig. 5.9 shows this same root in the complex plane. For the

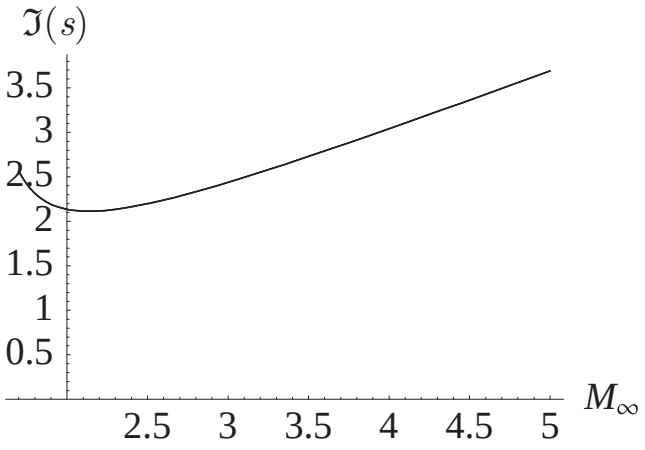

Figure 5.6: Imaginary part of nondimensional eigenvalue s versus M_∞ for $\overline{a} = 1$, $\overline{b} = 0.1$, and $\mu = 5$.

case shown there appears to be no coalescence point, but there is a critical flutter point at $M_\infty = 3.80035$ where the real part crosses the zero axis, and Mach numbers beyond that point result in flutter. Unlike the case of Beck's column, however, the real part is not zero at values of M_∞ below the onset of flutter. The imaginary part of s at this point is 2.91548, the nondimensional flutter frequency.

Much of the research on panel flutter in recent decades has been focused on the nonlinear problem, which is characterized by steady-state, amplitude dependent oscillations termed limit-cycle oscillations (LCO). The amplitude normally depends on the altitude and dynamic pressure (or altitude and Mach number) as well as on configuration parameters. When LCO develop with sufficiently large amplitudes, fatigue becomes of paramount importance. Nonlinear problems are beyond the scope of this text.

5.3 Aeroelastic Stability Characteristics

The lifting surface flutter of immediate concern can be described by a linear set of structural dynamic equations that include a linear representation of the unsteady airloads in terms of the elastic deformations. The surface could correspond to a wing or stabilizer either with or without control surfaces. Analytical simulation of the surface is sometimes made more difficult by the presence of external stores, engine nacelles, landing gear, or internal fuel tanks. Although such complexities complicate the analysis, they do not significantly alter the physical character of the flutter instability. For this reason the following discussion will be limited to a "clean" lifting surface.

When idealized for linear analysis, the nature of flutter is such that the flow over the lifting surface not only creates steady components of lift and pitching moment but also

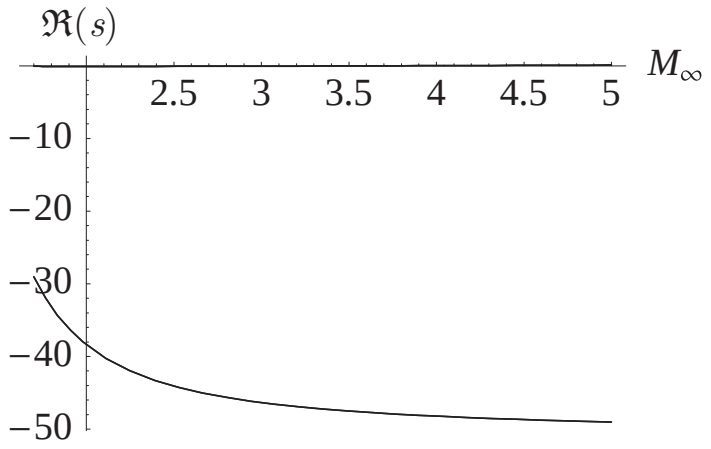

Figure 5.7: Real part of nondimensional eigenvalue s versus M_∞ for $\overline{a} = 1$, $\overline{b} = 0.1$, and $\mu = 5$ (note that there is a root very near the zero axis shown in more detail in Fig. 5.8)

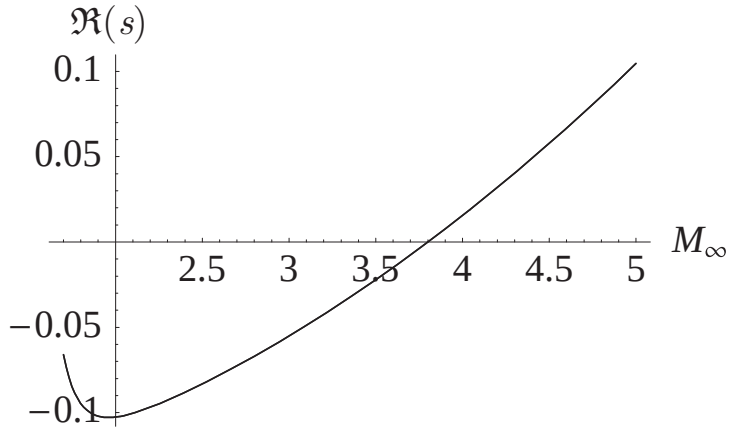

Figure 5.8: Closeup of the real part of the critical nondimensional eigenvalue s versus M_∞ for $\overline{a} = 1$, $\overline{b} = 0.1$, and $\mu = 5$.

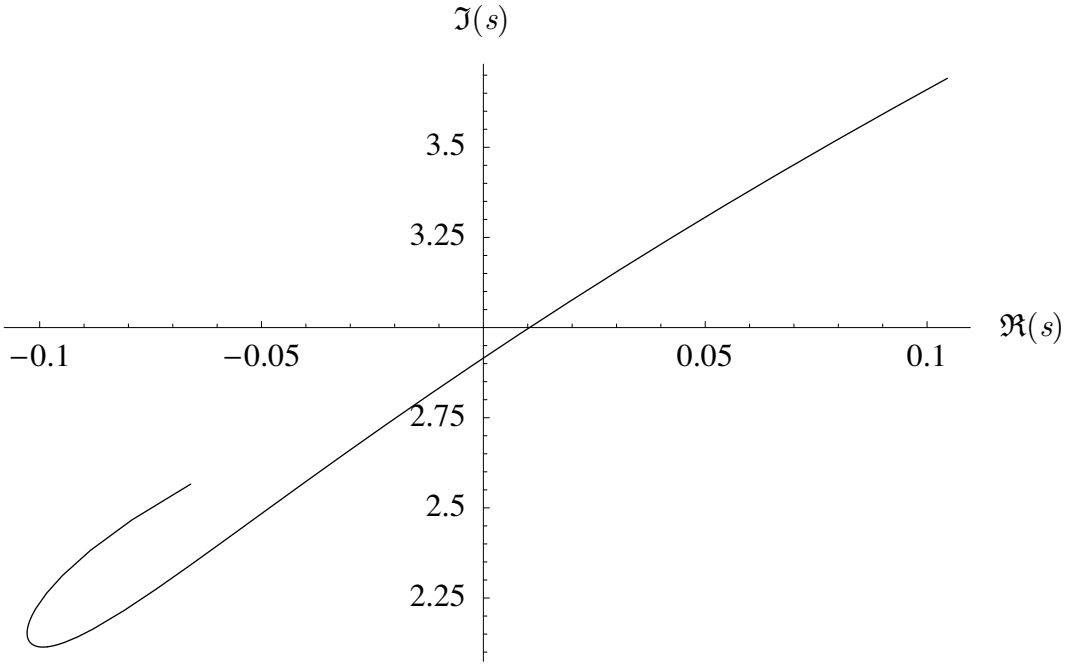

Figure 5.9: Closeup of the critical nondimensional eigenvalue s versus M_∞ for $\overline{a} = 1$, $\overline{b} = 0.1$, and $\mu = 5$; the left end of the curve is for $M_\infty = 1.7$ and the right end for $M_\infty = 5.0$.

creates dynamic forces in response to small perturbations of the lifting surface motion, pitch and plunge motions in particular. Recall that the pitching motion of an airfoil may arise from torsional deformation, and the plunging of the airfoil may arise from bending deformation. When a lifting surface that is statically stable below its flutter speed is disturbed, the oscillatory motions caused by those disturbances will die out in time with exponentially decreasing amplitudes. That is, one could say that the air is providing damping for all such motions. Above the flutter speed, however, rather than damping out the motions due to small perturbations in the configuration, the air can be said to be providing negative damping. Thus, these oscillatory motions grow with exponentially increasing amplitudes. This qualitative description of flutter can be observed in a general discussion of stability characteristics.

5.3.1 Overview of Typical Aeroelastic System Equations

Before attempting to conduct an analysis of flutter, it will be instructive to first examine the possible solutions to a structural dynamic representation in the presence of airloads. We will presume that the flight vehicle can be represented in terms of its normal modes of vibration. We illustrate this with the lifting surface modeled as a plate rather than a beam. This is somewhat more realistic for low-aspect-ratio wings, but in the present

framework this increased realism presents very little increase in complexity because of the modal representation. For displacements $w(x, y, t)$ in the z-direction normal to the plane of the planform (the x-y plane), the normal mode shapes can be represented by $\phi_i(x, y)$ and the associated natural frequencies by ω_i. A typical displacement of the structure can be written as

$$w(x, y, t) = \sum_{i=0}^{n} \xi_i(t)\phi_i(x, y) \tag{5.55}$$

where $\xi_i(t)$ is the generalized coordinate of the i^{th} mode. It should be noted that the summation includes the index value $i = 0$, which symbolically denotes that rigid-body degrees of freedom have been included. The set of generalized equations of motion for the flight vehicle can be written as

$$M_i(\ddot{\xi}_i + \omega_i^2 \xi_i) = \Xi_i \qquad (i = 0, 1, \ldots, n) \tag{5.56}$$

where M_i is the generalized mass associated with the mass distribution, $m(x, y)$, and can be determined as

$$M_i = \iint_{\text{planform}} m(x, y)\phi_i^2(x, y)dxdy \tag{5.57}$$

The generalized force, $\Xi_i(t)$, associated with the external loading, $F(x, y, t)$ can be evaluated as

$$\Xi_i(t) = \iint_{\text{planform}} F(x, y, t)\phi_i(x, y)dxdy \tag{5.58}$$

To examine the stability properties of the flight vehicle, the only external loading to be considered is from the aerodynamic forces, which can be represented as a linear function of $w(x, y, t)$ and its time derivatives. It will be presumed that all other external disturbances have been eliminated. Such external disturbances would normally include atmospheric gusts, store ejection reactions, etc. Recalling that the displacement can be represented as a summation of the modal contributions, the induced pressure distribution, $\Delta p(x, y, t)$ can be described as a linear function of all the generalized coordinates and their derivatives. Such a relationship can be written as

$$\Delta p(x, y, t) = \sum_{j=0}^{n} \left[a_j(x, y)\xi_j(t) + b_j(x, y)\dot{\xi}_j(t) + c_j(x, y)\ddot{\xi}_j(t) \right] \tag{5.59}$$

The corresponding generalized force of the i^{th} mode can now be determined from

$$\begin{aligned}\Xi_i(t) &= \iint\limits_{\text{planform}} \Delta p(x,y,t)\phi_i(x,y)dxdy \\ &= \sum_{j=0}^{n} \xi_j(t) \iint\limits_{\text{planform}} a_j(x,y)\phi_i(x,y)dxdy \\ &\quad + \sum_{j=0}^{n} \dot{\xi}_j(t) \iint\limits_{\text{planform}} b_j(x,y)\phi_i(x,y)dxdy \\ &\quad + \sum_{j=0}^{n} \ddot{\xi}_j(t) \iint\limits_{\text{planform}} c_j(x,y)\phi_i(x,y)dxdy \\ &= \rho_\infty \sum_{j=0}^{n} \left(a_{ij}\xi_j + \frac{b}{U} b_{ij}\dot{\xi}_j + \frac{b^2}{U^2} c_{ij}\ddot{\xi}_j \right)\end{aligned} \tag{5.60}$$

Following the convention in some published work, we have factored out the freestream air density ρ_∞ from the aerodynamic generalized force expression. Although not necessary, this step does enable the analyst to identify altitude effects more readily. It also shows explicitly that all aerodynamic effects vanish in a vacuum where ρ_∞ vanishes. Moreover, the normalization involving powers of b/U, where b is a reference semi-chord of the lifting surface, allows the matrices $[a]$, $[b]$, and $[c]$ to have the same units. Any nonhomogeneous terms in the generalized forces can be eliminated by redefinition of the generalized coordinates so that they are measured with respect to a different reference configuration. Thus, the generalized equations of motion can be written as a homogeneous set of differential equations when this form of the generalized force is included. They are

$$M_i\ddot{\xi}_i - \rho_\infty \frac{b^2}{U^2} \sum_{j=0}^{n} c_{ij}\ddot{\xi}_j - \rho_\infty \frac{b}{U} \sum_{j=0}^{n} b_{ij}\dot{\xi}_j + M_i\omega_i^2\xi_i - \rho_\infty \sum_{j=0}^{n} a_{ij}\xi_j = 0 \quad (i = 0, 1, \ldots, n) \tag{5.61}$$

The general solution to this set of second-order, linear, ordinary differential equations can be described as a simple exponential function of time, because they are homogeneous. The form of this solution will be taken as

$$\xi_i(t) = \overline{\xi}_i \exp(\nu t) \tag{5.62}$$

Substitution of this expression into Eqs. (5.61) yields $n+1$ simultaneous linear, homogeneous, algebraic equations for the $\overline{\xi}_i$s since each term will contain an $\exp(\nu t)$. Thus,

$$M_i\left(\nu^2 + \omega_i^2\right)\overline{\xi}_i - \rho_\infty \sum_{j=0}^{n} \left(\frac{b^2\nu^2}{U^2} c_{ij} + \frac{b\nu}{U} b_{ij} + a_{ij} \right) \overline{\xi}_j = 0 \quad (i = 0, 1, \ldots, n) \tag{5.63}$$

For a nontrivial solution of the generalized coordinate amplitudes, the determinant of the array formed by the coefficients of $\overline{\xi}_i$ must be zero. It is apparent that this determinant is a polynomial of degree $2(n+1)$ in ν. Subsequent solution of this polynomial equation for ν will typically yield $n+1$ complex conjugate pairs, represented as

$$\nu_k = \Gamma_k \pm i\Omega_k \qquad (k = 0, 1, \ldots, n) \tag{5.64}$$

For each ν_k there is a corresponding complex column matrix $\overline{\xi}_j^{(k)}$, $j = 0, 1, \ldots, n$. Alternatively, one may think of this as a square matrix, the k^{th} column of which is the k^{th} complex eigenvector. The solution of the generalized equations of motion with the aerodynamic coupling can then be written as

$$w(x, y, t) = \sum_{k=0}^{n} \{w_k(x, y) \exp[(\Gamma_k + i\Omega_k)t] + \overline{w}_k(x, y) \exp[(\Gamma_k - i\Omega_k)t]\} \tag{5.65}$$

where $\overline{w}_k$ is the complex conjugate of w_k. This expression for $w(x, y, t)$ turns out to be real, as expected. Each w_k represents a unique, complex, linear combination of the free-vibration mode shapes of the structure, viz.,

$$w_k(x, y) = \sum_{i=0}^{n} \overline{\xi}_i^{(k)} \phi_i(x, y) \qquad (k = 0, 1, \ldots, n) \tag{5.66}$$

and may be referred to as the waveform of the k^{th} complex mode. Note that only the relative values of $\overline{\xi}_i^{(k)}$ can be determined unless the initial displacement and rate of displacement are specified.

It is apparent from the general solution for $w(x, y, t)$, Eq. (5.65), that the k^{th} component of the summation represents a simple harmonic oscillation that is modified by an exponential function. The nature of this dynamic response to any specified initial condition is strongly dependent on the sign of each Γ_k. Typical response behavior is illustrated in Fig. 5.10 for positive, zero, and negative values of Γ_k when Ω_k is nonzero. We note that the negative of Γ_k is sometimes called the *modal damping* of the k^{th} mode, and Ω_k is called the *modal frequency*. It is also possible to classify these motions from the standpoint of stability. The convergent oscillations when $\Gamma_k < 0$ are termed dynamically stable and the divergent oscillations for $\Gamma_k > 0$ are dynamically unstable. The case of $\Gamma_k = 0$ represents the boundary between the two and is often called the "stability boundary." If these solutions are for an aeroelastic system, the dynamically unstable condition is called *flutter*; and the stability boundary corresponding to simple harmonic motion is called the *flutter boundary*.

Recall from Eq. (5.65) that the total displacement is a sum of all modal contributions. It is therefore necessary to consider all possible combinations of Γ_k and Ω_k, where Γ_k can be < 0, $= 0$, or > 0 and Ω_k can be $= 0$ or $\neq 0$. The corresponding type of motion and stability characteristics are indicated in Table 5.1 for various combinations of Γ_k and Ω_k. Although our primary concern here is with regard to the dynamic instability of flutter for

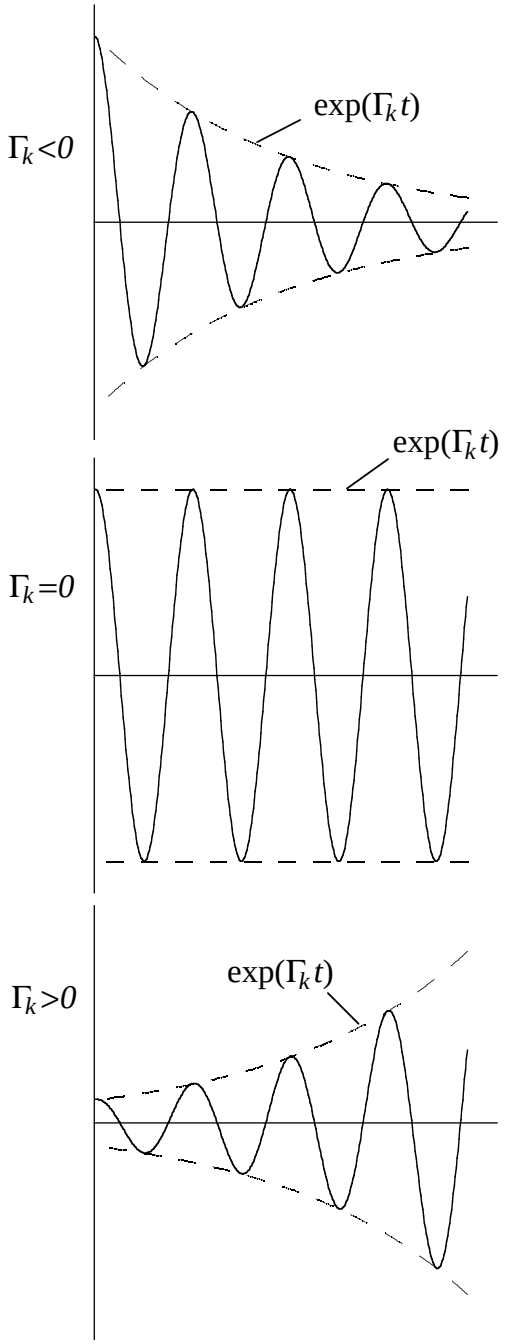

Figure 5.10: Behavior of typical mode amplitude when $\Omega_k \neq 0$

Γ_k	Ω_k	Type of Motion	Stability Characteristic
< 0	$\neq 0$	Convergent Oscillations	Stable
$= 0$	$\neq 0$	Simple Harmonic	Stability Boundary
> 0	$\neq 0$	Divergent Oscillations	Unstable
< 0	$= 0$	Continuous Convergence	Stable
$= 0$	$= 0$	Time Independent	Stability Boundary
> 0	$= 0$	Continuous Divergence	Unstable

Table 5.1: Types of motion and stability characteristics for various values of Γ_k and Ω_k

which $\Omega_k \neq 0$, Table 5.1 shows that the generalized equations of motion can also provide solutions to the static aeroelastic problem of divergence. This phenomenon is indicated by the unstable condition for $\Omega_k = 0$, and the divergence boundary occurs when $\Gamma_k = \Omega_k = 0$.

In many published works on flutter analysis, the method outlined in this section is known as the p method, named for the reduced complex eigenvalue $p = b\nu/U$, which appears in Eq. (5.63) and in terms of which the eigenvalue problem can be posed instead of in terms of ν as we have done. To provide accurate prediction of flutter characteristics the p method must use an aerodynamic theory that accurately represents the loads for transient motion of the lifting surface. In addition to the structural generalized coordinates, such theories may involve aerodynamic states and their time derivatives; see, for example, the theory outlined in Section 5.7.2. These additional states do not affect the meaning of the real and imaginary parts of the eigenvalues as discussed here.

5.3.2 Analytical and Numerical Solution Methods

The above equations of motion have the structure

$$\left[\left[\,\grave{}\,M\,\acute{}\,\right] - \rho_\infty \frac{b^2}{U^2}\,[c]\right]\left\{\ddot{\xi}\right\} - \rho_\infty \frac{b}{U}\,[b]\left\{\dot{\xi}\right\} + \left[\left[\,\grave{}\,M\omega^2\,\acute{}\,\right] - \rho_\infty\,[a]\right]\{\xi\} = 0 \tag{5.67}$$

In a more general case, such as when either nonorthogonal assumed modes or the finite element method is used, the diagonal matrices $[\,\grave{}\,M\,\acute{}\,]$ and $[\,\grave{}\,M\omega^2\,\acute{}\,]$ become fully populated matrices $[M]$ and $[K]$. Moreover, when structural damping models of various types are included, an additional matrix $[C]$ should be added to the equation. With these generalizations, the equations of motion become

$$\left[[M] - \rho_\infty \frac{b^2}{U^2}\,[c]\right]\left\{\ddot{\xi}\right\} + \left[[C] - \rho_\infty \frac{b}{U}\,[b]\right]\left\{\dot{\xi}\right\} + \left[[K] - \rho_\infty\,[a]\right]\{\xi\} = 0 \tag{5.68}$$

The matrix $[M]$ is called the mass matrix of the structure, and it is in general symmetric and positive definite. The matrix $[K]$ is called the stiffness matrix of the structure and is in general symmetric. The matrix $[C]$ accounts for structural damping and frequently is

symmetric and positive definite, but not always. The aerodynamic matrices $[a]$, $[b]$, and $[c]$ do not possess any particular structure to them. If we recast the problem in terms of new matrices

$$\begin{aligned}\left[\overline{M}\right] &= [M] - \rho_\infty \frac{b^2}{U^2}[c] \\ \left[\overline{C}\right] &= [C] - \rho_\infty \frac{b}{U}[b] \\ \left[\overline{K}\right] &= [K] - \rho_\infty [a]\end{aligned} \tag{5.69}$$

then the equations of motion reduce to

$$\left[\overline{M}\right]\left\{\ddot{\xi}\right\} + \left[\overline{C}\right]\left\{\dot{\xi}\right\} + \left[\overline{K}\right]\{\xi\} = 0 \tag{5.70}$$

Now none of these $n \times n$ matrices has any particular structure.

There are two ways to study the solutions of Eq. (5.70). They being linear, ordinary differential equations with constant coefficients, the most straightforward approach is to assume a solution of the form

$$\xi(t) = \hat{\xi} \exp(\nu t) \tag{5.71}$$

so that Eq. (5.70) becomes

$$\left[\nu^2\left[\overline{M}\right] + \nu\left[\overline{C}\right] + \left[\overline{K}\right]\right]\left\{\hat{\xi}\right\} = 0 \tag{5.72}$$

Non-trivial solutions only exist when the determinant of the coefficient matrix of Eq. (5.72) is equal to zero. As we've already seen, the system is unstable if any root ν has a positive real part. As we've seen, this procedure works fine as an analytical solution for low-order systems. Unfortunately, it becomes difficult to carry out and computationally demanding when n is large, and loss of accuracy becomes a problem.

A state-variable approach is more amenable to solution by numerical methods. For this we proceed by writing Eq. (5.70) and another equation

$$\left[\overline{M}\right]\left\{\dot{\xi}\right\} - \left[\overline{M}\right]\left\{\dot{\xi}\right\} = 0 \tag{5.73}$$

which is an identity. Combining these equations into one, we write

$$\begin{bmatrix}\left[\overline{M}\right] & [0] \\ [0] & \left[\overline{M}\right]\end{bmatrix}\begin{Bmatrix}\left\{\dot{\xi}\right\} \\ \left\{\ddot{\xi}\right\}\end{Bmatrix} + \begin{bmatrix}[0] & -\left[\overline{M}\right] \\ \left[\overline{K}\right] & \left[\overline{C}\right]\end{bmatrix}\begin{Bmatrix}\{\xi\} \\ \left\{\dot{\xi}\right\}\end{Bmatrix} = \begin{Bmatrix}\{0\} \\ \{0\}\end{Bmatrix} \tag{5.74}$$

Defining the state vector

$$\{x\} = \begin{Bmatrix}\{\xi\} \\ \left\{\dot{\xi}\right\}\end{Bmatrix} \tag{5.75}$$

which is of length $2n$, and solving Eq. (5.74) for $\{\dot{x}\}$, one obtains

$$\{\dot{x}\} = [S]\{x\} \tag{5.76}$$

with

$$[S] = \begin{bmatrix} [0] & [\,`1\,`] \\ -\left[\overline{M}\right]^{-1}\left[\overline{K}\right] & -\left[\overline{M}\right]^{-1}\left[\overline{C}\right] \end{bmatrix} \tag{5.77}$$

Assuming a solution of the form

$$\{x(t)\} = \{\hat{x}\}\exp(\nu t) \tag{5.78}$$

one finds that

$$\nu\{\hat{x}\} = [S]\{\hat{x}\} \tag{5.79}$$

which is a standard eigenvalue problem. There are many available numerical procedures, including those in MATLAB™. Again, if any eigenvalue has a positive real part, the system is unstable. These equations can be written in terms of the nondimensional complex eigenvalue $p = b\nu/U$, which puts them in the usual form for application of the so-called p method.

5.4 Aeroelastic Analysis of a Typical Section

In this section we will demonstrate the flutter analysis of a linear aeroelastic system, applying the p method to a simple configuration. To do this a simple model is needed. In the older literature of aeroelasticity flutter analyses were often performed using simple, spring-restrained, rigid-wing models such as the one shown in Fig. 5.11. These were called typical section models and are still very appealing because of their physical simplicity. This configuration could represent the case of a rigid, two-dimensional wind-tunnel model that is elastically mounted in a wind-tunnel test section, or it could correspond to a typical airfoil section along a finite wing. In the latter case the discrete springs would reflect the wing structural bending and torsional stiffnesses, and the reference point would represent the elastic axis.

Of interest in such models are points P, C, Q, and T, which refer, respectively, to the reference point (i.e., where the plunge displacement h is measured), the center of mass, the aerodynamic center (presumed to be the quarter-chord in thin-airfoil theory), and the three-quarter-chord (an important chordwise location in thin-airfoil theory). The dimensionless parameters e and a ($-1 \le e \le 1$ and $-1 \le a \le 1$) determine the locations of the points C and P; when these parameters are zero, the points lie on the mid-chord, and when they are positive (negative), the points lie toward the trailing (leading) edge. In the literature, the chordwise offset of the center of mass from the reference point, rather than e, often appears in the equations of motion. It is typically made dimensionless by the airfoil semi-chord b and denoted by $x_\theta = e - a$. This so-called static unbalance parameter is positive when the

center of mass is toward the trailing edge from the reference point. The rigid plunging and pitching of the model is restrained by light, linear springs with spring constants k_h and k_θ.

It is convenient to formulate the equations of motion from Lagrange's equations. To do this, one needs kinetic and potential energies as well as the generalized forces resulting from aerodynamic loading. One can immediately write the potential energy as

$$P = \frac{1}{2}k_h h^2 + \frac{1}{2}k_\theta \theta^2 \tag{5.80}$$

To deduce the kinetic energy, one needs the velocity of the mass center C, which can be found as

$$\mathbf{v}_C = \mathbf{v}_P + \dot{\theta}\hat{\mathbf{b}}_3 \times b\left[(1+a) - (1+e)\right]\hat{\mathbf{b}}_1 \tag{5.81}$$

where the inertial velocity of the reference point P is

$$\mathbf{v}_P = -\dot{h}\hat{\mathbf{i}}_2 \tag{5.82}$$

and thus

$$\mathbf{v}_C = -\dot{h}\hat{\mathbf{i}}_2 + b\dot{\theta}(a-e)\hat{\mathbf{b}}_2 \tag{5.83}$$

The kinetic energy is then given by

$$K = \frac{1}{2}m\mathbf{v}_C \cdot \mathbf{v}_C + \frac{1}{2}I_C\dot{\theta}^2 \tag{5.84}$$

where I_C is the moment of inertia about C. By virtue of the relationship between $\hat{\mathbf{b}}_2$ and the inertially fixed unit vectors $\hat{\mathbf{i}}_1$ and $\hat{\mathbf{i}}_2$, assuming θ to be small, one finds that

$$\begin{aligned} K &= \frac{1}{2}m\left(\dot{h}^2 + b^2x_\theta^2\dot{\theta}^2 + 2bx_\theta\dot{h}\dot{\theta}\right) + \frac{1}{2}I_C\dot{\theta}^2 \\ &= \frac{1}{2}m\left(\dot{h}^2 + 2bx_\theta\dot{h}\dot{\theta}\right) + \frac{1}{2}I_P\dot{\theta}^2 \end{aligned} \tag{5.85}$$

where $I_P = I_C + mb^2x_\theta^2$.

The generalized forces associated with the degrees of freedom h and θ are easily derived from the work done by the aerodynamic lift through a virtual displacement of the point Q and by the aerodynamic pitching moment about Q through a virtual rotation of the model. The velocity of Q is

$$\mathbf{v}_Q = -\dot{h}\,\hat{\mathbf{i}}_2 + b\,\dot{\theta}\left(\frac{1}{2} + a\right)\hat{\mathbf{b}}_2 \tag{5.86}$$

The virtual displacement of the point Q can be obtained simply by replacing the dot over each unknown in Eq. (5.86) with a δ in front of it, that is,

$$\delta\mathbf{p}_Q = -\delta h\,\hat{\mathbf{i}}_2 + b\,\delta\theta\left(\frac{1}{2} + a\right)\hat{\mathbf{b}}_2 \tag{5.87}$$

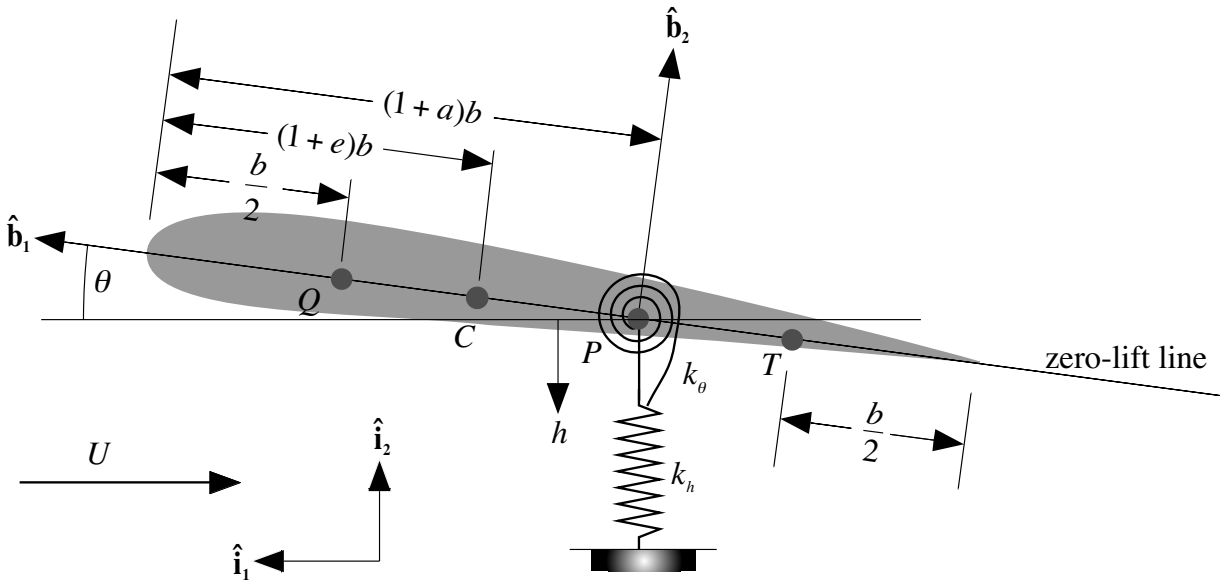

Figure 5.11: Schematic showing geometry of the wing section with pitch and plunge spring restraints

where $\delta\mathbf{p}_Q$ is the virtual displacement at Q. The angular velocity of the wing is $\dot{\theta}\hat{\mathbf{b}}_3$, so that the virtual rotation of the wing is simply $\delta\theta\hat{\mathbf{b}}_3$. Therefore, the virtual work of the aerodynamic forces is

$$\overline{\delta W} = L\left[-\delta h + b\left(\frac{1}{2}+a\right)\delta\theta\right] + M_{\frac{1}{4}}\delta\theta \tag{5.88}$$

and the generalized forces become

$$\begin{aligned} Q_h &= -L \\ Q_\theta &= M_{\frac{1}{4}} + b\left(\frac{1}{2}+a\right)L \end{aligned} \tag{5.89}$$

It is clear that the generalized force associated with h is the negative of the lift, whereas the one associated with θ is the pitching moment about the reference point P.

Lagrange's equations (as found in the Appendix, Eqs. A.35) are here specialized for the case in which the kinetic energy K depends only on $\dot{q}_1, \dot{q}_2, \ldots$, and so

$$\frac{d}{dt}\left(\frac{\partial K}{\partial \dot{q}_i}\right) + \frac{\partial P}{\partial q_i} = Q_i \qquad (i = 1, 2, \ldots, n) \tag{5.90}$$

Here $n = 2$, $q_1 = h$, and $q_2 = \theta$ and the equations of motion become

$$\begin{aligned} m\left(\ddot{h} + bx_\theta\ddot{\theta}\right) + k_h h &= -L \\ I_P\ddot{\theta} + mbx_\theta\ddot{h} + k_\theta\theta &= M_{\frac{1}{4}} + b\left(\frac{1}{2} + a\right)L \end{aligned} \tag{5.91}$$

5.4.1 Stability Based on Steady-flow Aerodynamics

For the aerodynamics, the steady-flow theory we used in the previous chapter gives

$$\begin{aligned} L &= 2\pi\rho_\infty bU^2\theta \\ M_{\frac{1}{4}} &= 0 \end{aligned} \tag{5.92}$$

where, in accord with thin-airfoil theory, we have taken the lift-curve slope to be 2π. Assuming this representation to be adequate for the time being, we can apply the p method since the aerodynamic loads are specified for arbitrary motion. (We shall later consider more sophisticated aerodynamic theories.)

To simplify the notation, we introduce the uncoupled, natural frequencies at zero airspeed, defined by

$$\omega_h = \sqrt{\frac{k_h}{m}} \qquad \omega_\theta = \sqrt{\frac{k_\theta}{I_P}} \tag{5.93}$$

Substituting Eqs. (5.92) into Eqs. (5.91), making use of the definitions in Eqs. (5.93) and rearranging the equations of motion into matrix form, one obtains

$$\begin{bmatrix} mb^2 & mb^2x_\theta \\ mb^2x_\theta & I_P \end{bmatrix} \begin{Bmatrix} \frac{\ddot{h}}{b} \\ \ddot{\theta} \end{Bmatrix} + \begin{bmatrix} mb^2\omega_h^2 & 2\pi\rho_\infty b^2U^2 \\ 0 & I_P\omega_\theta^2 - 2\left(\frac{1}{2} + a\right)\pi\rho_\infty b^2U^2 \end{bmatrix} \begin{Bmatrix} \frac{h}{b} \\ \theta \end{Bmatrix} = \begin{Bmatrix} 0 \\ 0 \end{Bmatrix} \tag{5.94}$$

Note that the first equation has been multiplied through by b and the variable h has been divided by b to make every term in both equations have the same units. We now make the substitutions $h = \overline{h}\exp(\nu t) = \overline{h}\exp(s\omega_\theta t)$ and $\theta = \overline{\theta}\exp(\nu t) = \overline{\theta}\exp(s\omega_\theta t)$ where s is an unknown, dimensionless, complex eigenvalue such that $s = \nu/\omega_\theta$, which gives

$$\begin{bmatrix} mb^2s^2\omega_\theta^2 + mb^2\omega_h^2 & mb^2x_\theta s^2\omega_\theta^2 + 2\pi\rho_\infty b^2U^2 \\ mb^2x_\theta s^2\omega_\theta^2 & I_Ps^2\omega_\theta^2 + I_P\omega_\theta^2 - 2\left(\frac{1}{2} + a\right)\pi\rho_\infty b^2U^2 \end{bmatrix} \begin{Bmatrix} \frac{\overline{h}}{b} \\ \overline{\theta} \end{Bmatrix} = \begin{Bmatrix} 0 \\ 0 \end{Bmatrix} \tag{5.95}$$

Although this eigenvalue problem can be solved as it is written, it is very convenient to introduce dimensionless variables throughout to further simplify the problem. To this end, we let

$$\begin{aligned} r^2 &= \frac{I_P}{mb^2} & \sigma &= \frac{\omega_h}{\omega_\theta} \\ \mu &= \frac{m}{\rho_\infty\pi b^2} & V &= \frac{U}{b\omega_\theta} \end{aligned} \tag{5.96}$$

Here r is the dimensionless radius of gyration of the wing about the reference point P with $r^2 > x_\theta^2$, σ is the ratio of uncoupled bending to torsional frequencies, μ is the mass ratio parameter reflecting the relative importance of the model mass to the mass of the air affected by the model, and V is the dimensionless freestream speed of the air, sometimes called the reduced velocity. The equations then simplify to

$$\begin{bmatrix} s^2+\sigma^2 & s^2x_\theta + \frac{2V^2}{\mu} \\ s^2x_\theta & s^2r^2 + r^2 - \frac{2V^2}{\mu}\left(\frac{1}{2}+a\right) \end{bmatrix} \begin{Bmatrix} \frac{\overline{h}}{b} \\ \overline{\theta} \end{Bmatrix} = \begin{Bmatrix} 0 \\ 0 \end{Bmatrix} \tag{5.97}$$

For a nontrivial solution to exist, the determinant of the coefficient matrix must be set equal to zero. There are two complex conjugate pairs of roots, say $s_1 = (\Gamma_1 \pm i\Omega_1)/\omega_\theta$ and $s_2 = (\Gamma_2 \pm i\Omega_2)/\omega_\theta$. For a given configuration and altitude one must look at the behavior of the complex roots as functions of V and find the smallest value of V to give divergent oscillations in accordance with Table 5.1. That value is $V_F = U_F/(b\omega_\theta)$ where U_F is the flutter speed.

It is noted that one may find the divergence speed by setting $s = 0$ in Eq. (5.97), which leads to setting the coefficient of $\overline{\theta}$ in the $\overline{\theta}$ equation equal to zero and solving the resulting expression for V. This value is the dimensionless divergence speed V_D, given by

$$V_D = \frac{U_D}{b\omega_\theta} = r\sqrt{\frac{\mu}{1+2a}} \tag{5.98}$$

This is the same answer as one would obtain with an analysis similar to those of Chapter 4.

For looking at flutter, we consider a specific configuration defined by $a = -1/5$, $e = -1/10$, $\mu = 20$, $r^2 = 6/25$, and $\sigma = 2/5$. The divergence speed for this configuration is $V_D = 2.828$ (or $U_D = 2.828\, b\, \omega_\theta$). Plots of the imaginary and real parts of the roots versus V are shown in Figs. 5.12 and 5.13, respectively. The negative of Γ is the modal damping, and Ω is the modal frequency. We consider first the imaginary parts, Ω, as shown in Fig. 5.12. When $V = 0$, one expects the two dimensionless frequencies to be near unity and σ for pitching and plunging oscillations, respectively. Even at $V = 0$ these modes are lightly coupled because of the nonzero off-diagonal term x_θ in the mass matrix. As V increases, the frequencies start to approach one another, and their respective mode shapes exhibit increasing coupling between plunge and pitch. Flutter occurs when the two modal frequencies coalesce, at which point the roots become complex conjugate pairs. At this condition, both modes are highly coupled pitch-plunge oscillations. The flutter speed is $V_F = U_F/(b\omega_\theta) = 1.843$, and the flutter frequency is $\Omega_F/\omega_\theta = 0.5568$. The real parts, Γ, are shown in Fig. 5.13 and remain zero until flutter occurs. When flutter occurs, the real part of one of the roots is positive and the other is negative.

Comparing results from the above analysis with experimental data, one finds that a few elements of realism are at least qualitatively captured. For example, the analysis predicts that flutter occurs at some value of $V = V_F < V_D$, which is correct for the specified configuration. Furthermore, it shows a coalescence of the pitching and plunging frequencies as V approaches

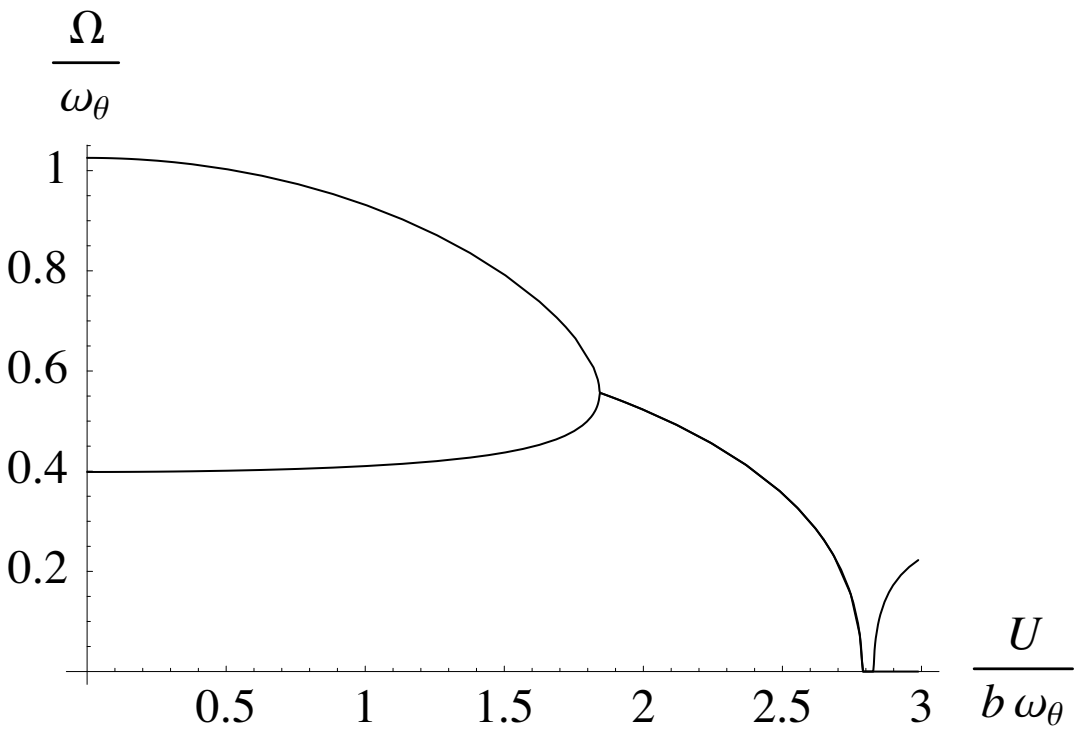

Figure 5.12: Plot of the modal frequency versus V for $a = -1/5$, $e = -1/10$, $\mu = 20$, $r^2 = 6/25$, and $\sigma = 2/5$ (steady-flow theory)

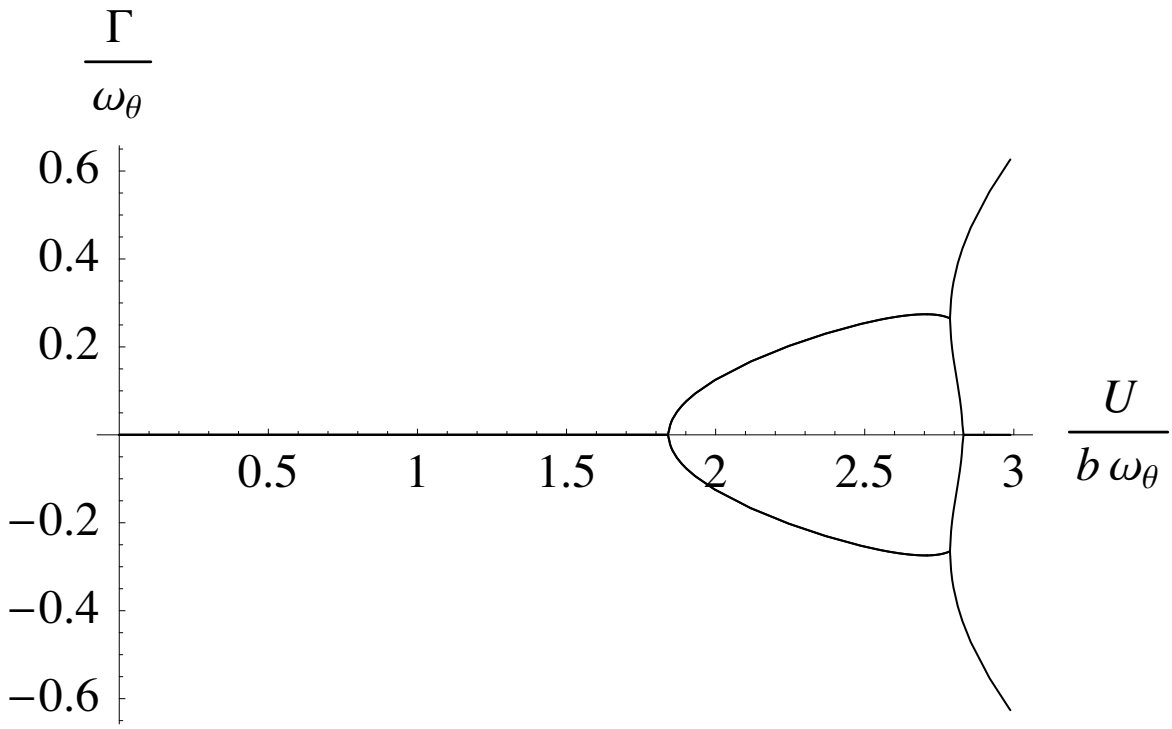

Figure 5.13: Plot of the modal damping versus V for $a = -1/5$, $e = -1/10$, $\mu = 20$, $r^2 = 6/25$, and $\sigma = 2/5$ (steady-flow theory)

V_F, which is not only correct for the specified configuration but is frequently observed in connection with flutter analysis. However, the above analysis is deficient in its ability to accurately predict the flutter speed. Moreover, the damping of all modes below the flutter speed is predicted to be zero, which is known to be incorrect.

The main reason for these deficiencies is that the aerodynamic theory from Chapter 4 was used. Although the aerodynamic theory has obvious deficiencies, such as its linearity and two-dimensionality, a very significant deficiency as far as flutter analysis is concerned is that it neglects unsteady effects, which are in general very important for flutter problems.

5.4.2 Stability Based on Quasi-Steady Aerodynamics

To see the qualitative effects of some of the unsteadiness, we may use quasi-steady aerodynamics, which captures the motion of the airfoil and its effect on the relative wind direction and attendant time dependence of the angle of attack. Because points along the airfoil chordline are plunging (positive down) with speed $\dot{h}$ (plus a small correction for pitching $\dot{\theta}$ which we will for now neglect but pick up later in Section 5.7), the angle of attack is not simply equal to θ at any instant in time. Instead, we approximate the angle of attack as

$$\alpha = \theta + \frac{\dot{h}}{U} \tag{5.99}$$

The second term provides damping in the plunge direction. There is a similar damping term for pitch that we borrow from unsteady aerodynamics and include to provide damping in both degrees of freedom. Thus,

$$\begin{aligned} L &= 2\pi\rho_\infty b U^2 \left(\theta + \frac{\dot{h}}{U}\right) \\ M_{\frac{1}{4}} &= -\pi\rho_\infty b^3 U\dot{\theta} \end{aligned} \tag{5.100}$$

so that Eq. (5.97) becomes

$$\begin{bmatrix} s^2 + \frac{2V}{\mu}s + \sigma^2 & s^2 x_\theta + \frac{2V^2}{\mu} \\ s^2 x_\theta - \left(a + \frac{1}{2}\right)\frac{2V}{\mu}s & s^2 r^2 + \frac{V}{\mu}s + r^2 - \frac{2V^2}{\mu}\left(\frac{1}{2} + a\right) \end{bmatrix} \begin{Bmatrix} \frac{\overline{h}}{b} \\ \theta \end{Bmatrix} = \begin{Bmatrix} 0 \\ 0 \end{Bmatrix} \tag{5.101}$$

This equation has a nontrivial solution only when its determinant goes to zero. The characteristic equation for the determinant is a fourth-order polynomial in s. The imaginary and real parts of the roots obtained from the solution of this equation are shown in Figs. 5.14 and 5.15. The roots for $V = 0$ are again near σ (plunge) and 1 (pitch). The main qualitative difference between these and the results from steady-flow theory are that the modal damping is not zero at speeds below the flutter speed, and one sees that flutter takes place when the real part of s crosses the zero axis. The non-dimensional flutter speed is $V_F = 1.96359$ for the case shown. At a higher speed, the stable root splits into two real roots

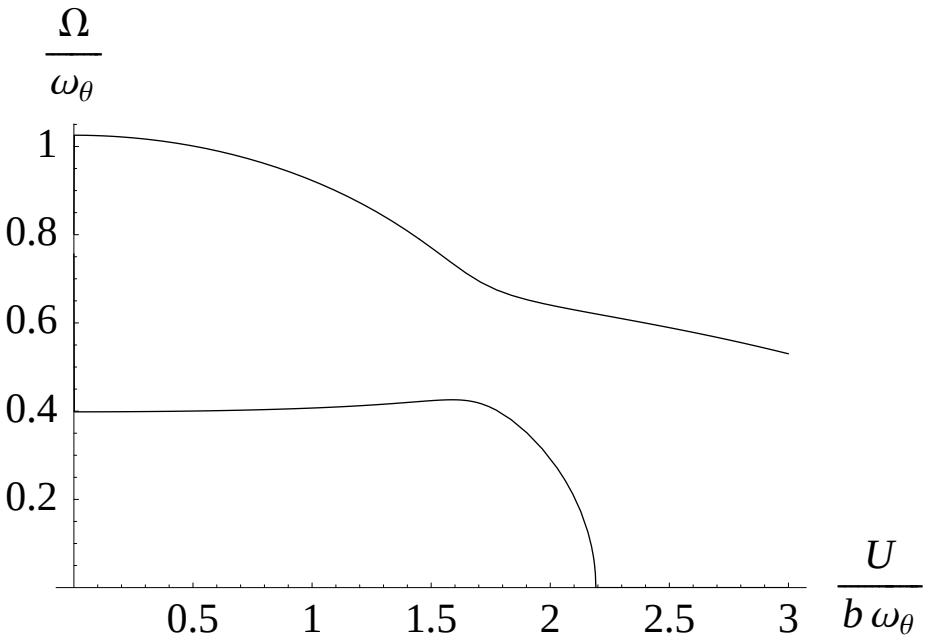

Figure 5.14: Plot of $\Im(s)$, the modal frequency, versus V for $a = -1/5$, $e = -1/10$, $\mu = 20$, $r^2 = 6/25$, and $\sigma = 2/5$ (quasi-steady theory)

when the imaginary value of that root goes to zero at $V = 2.19154$. The non-dimensional divergence speed is still at $V_D = 2\sqrt{2} = 2.82843$, unaffected by the additional terms in the aerodynamics, as expected.

As with typical aeroelastic analyses, below the flutter speed all roots have the form $\nu = \Gamma \pm i\Omega$, $s = (\Gamma \pm i\Omega)/\omega_\theta$ or $p = (\gamma \pm i)k$. At the flutter boundary, all roots but one maintain the same form. That one root becomes pure imaginary, as its real part is zero. At speeds greater than the flutter speed, the one unstable root grows with an exponentially growing amplitude. This is all in accord with the discussion in Section 5.3. The fact that at the flutter boundary all roots are stable except the one neutrally stable root can used to advantage to analyze flutter. This means that all motion damps out except for the root that goes unstable, and at the flutter boundary all motion is simple harmonic.

5.4.3 Motivation for Better Aerodynamic Theory

Although additional realism has been captured by the quasi-steady theory, the theory is still inadequate. The flow is unsteady because of three separate physical reasons, only one of which is addressed so far. First, because of the wing's unsteady motion relative to the air, the relative wind vector is not fixed in space. This is partly dealt with in quasi-steady theory. Second, the airfoil motion disturbs the flow, shedding a vortex at the trailing edge. The downwash from this vortex, in turn, changes the flow that impinges on the airfoil. Third,

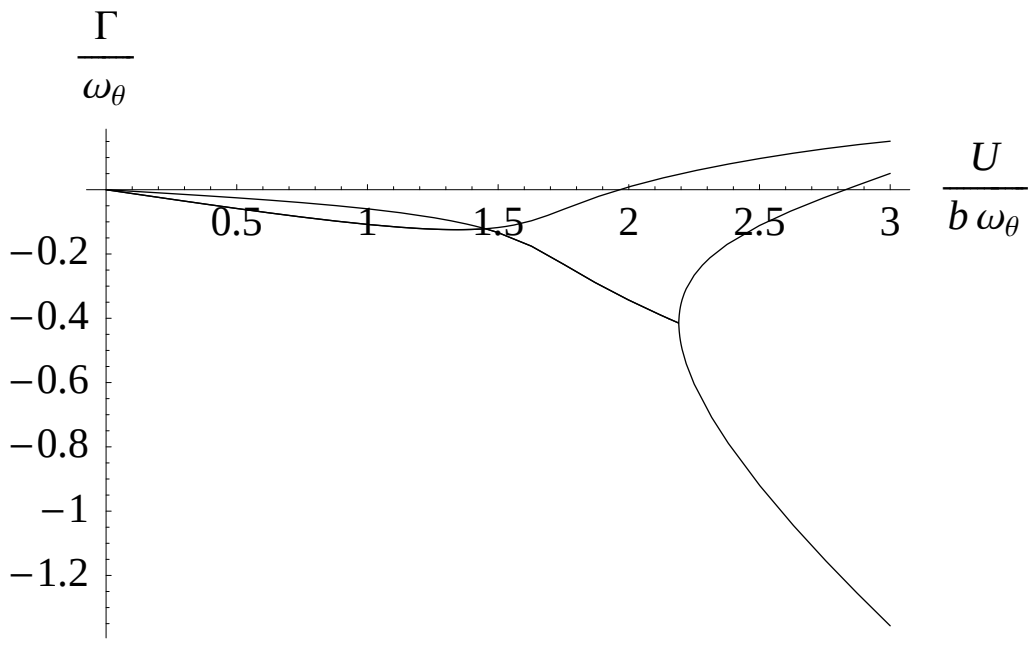

Figure 5.15: Plot of $\Re(s)$, the modal damping, versus V for $a = -1/5$, $e = -1/10$, $\mu = 20$, $r^2 = 6/25$, and $\sigma = 2/5$ (quasi-steady theory)

the motion of the airfoil accelerates air particles near the airfoil surface, thus creating the need to account for the resulting inertial forces (although this "apparent inertia" effect is less significant than that of the shed vorticity). Thus, in order to obtain a more accurate prediction of the flutter speed, it is necessary to include unsteadiness in the aerodynamic theory. This demands a far more sophisticated aerodynamic theory.

Unfortunately, development of unsteady aerodynamic theories is no small undertaking. Unsteady aerodynamic theories can most simply be developed when simple harmonic motion is assumed *a priori*. Although such limited theories cannot be used in the p method of flutter analysis described in Section 5.3, they can be used in classical flutter analysis, described in the next section. As will be seen, classical flutter analysis can predict the flutter speed and flutter frequency, but it cannot predict values of modal damping and frequency away from the flutter condition. To obtain a reasonable sense of modal damping and frequencies at points other than the flutter condition, a couple of approximate schemes will be discussed in Section 5.6.

If these approximations turn out to be inadequate for predicting modal damping and frequencies, one has no choice but to carry out a flutter analysis that does not assume simple harmonic motion, which in turn requires a still more powerful aerodynamic theory. One such approach that fits easily into the framework of Section 5.3 is the finite-state theory of Peters et al. (1995). Such a theory not only facilitates the calculation of subcritical eigenvalues, but since it is a time-domain model it also can be used in control design.

Hence, in the sections to follow, we first look at classical flutter analysis and the approximate techniques associated therewith and then turn to a more detailed discussion of unsteady aerodynamics, including one theory that assumes simple harmonic motion (the Theodorsen theory) and one that does not (the Peters finite-state theory).

5.5 Classical Flutter Analysis

Through the end of the twentieth century, most lifting surface flutter analyses performed in the aircraft industry were based on what is called a "classical flutter analysis" or some derivative thereof. The objective of such an analysis is to determine the flight conditions that correspond to the flutter boundary. It was previously noted that the flutter boundary corresponds to conditions for which one of the modes of motion has a simple harmonic time dependency. Since this is considered to be a stability boundary, it is implied that all modes of motion are convergent (stable) for less critical flight conditions (lower airspeed). Moreover, all modes other than the critical one are convergent at the flutter boundary.

The method of analysis is not based on solving the generalized equations of motion as described in Section 5.3. Rather, it is presumed that the solution involves simple harmonic motion. With such a solution being specified, the equations of motion are then solved for the flight condition(s) that yield such a solution. Whereas in the p method one determines the eigenvalues for a set flight condition, the real parts of which provide the modal damping, it is apparent that classical flutter analysis cannot provide the modal damping for an arbitrary flight condition. Thus, it cannot provide any definitive measure of flutter stability other than the location of the stability boundary. Although this is the primary weakness of such a method, its primary strength is that it needs only the unsteady airloads for simple harmonic motion of the surface, which are more easily and thus more accurately obtained than those for arbitrary motion.

To illustrate classical flutter analysis it is necessary to consider an appropriate representation of unsteady airloads for simple harmonic motion of a lifting surface. Because these oscillatory motions are relatively small in amplitude, it is sufficient to use a linear aerodynamic theory for the computation of these loads. These aerodynamic theories are usually based on linear potential flow theory, which presumes that the motion of the structure is a small perturbation with respect to the freestream speed. For purposes of demonstration it will suffice to consider again the typical section of a two-dimensional lifting surface that is experiencing simultaneous translational and rotational motions, as illustrated in Fig. 5.11. The motion is simple harmonic; thus, h and θ will be represented as

$$\begin{aligned} h(t) &= \overline{h} \exp(i\omega t) \\ \theta(t) &= \overline{\theta} \exp(i\omega t) \end{aligned} \tag{5.102}$$

where ω is the frequency of the motion. Although the h and θ motions are of the same frequency, they are not necessarily in phase. This can be taken into account mathematically

by representing the amplitude $\overline{\theta}$ as a real number and $\overline{h}$ as a complex number. Since a linear aerodynamic theory is to be used the resulting lift, L, and the pitching moment about P, denoted by M where

$$M = M_{\frac{1}{4}} + b\left(\frac{1}{2} + a\right) L \tag{5.103}$$

will also be simple harmonic with frequency ω, so that

$$\begin{aligned} L(t) =& \overline{L}\exp(i\omega t) \\ M(t) =& \overline{M}\exp(i\omega t) \end{aligned} \tag{5.104}$$

The amplitudes of these airloads can be computed as complex, linear functions of the amplitudes of motion as

$$\begin{aligned} \overline{L} =& -\pi\rho_\infty b^3\omega^2\left[\ell_h(k, M_\infty)\frac{\overline{h}}{b} + \ell_\theta(k, M_\infty)\overline{\theta}\right] \\ \overline{M} =& \pi\rho_\infty b^4\omega^2\left[m_h(k, M_\infty)\frac{\overline{h}}{b} + m_\theta(k, M_\infty)\overline{\theta}\right] \end{aligned} \tag{5.105}$$

Here the freestream air density is represented as ρ_∞ and the four complex functions contained in the square brackets represent the dimensionless aerodynamic coefficients for the lift and moment resulting from plunging and pitching. These coefficients are in general functions of the two parameters k and M_∞, where

$$\begin{aligned} k =& \frac{b\omega}{U} \qquad \text{(reduced frequency)} \\ M_\infty =& \frac{U}{c_\infty} \qquad \text{(Mach number)} \end{aligned} \tag{5.106}$$

As in the case of steady airloads, compressibility effects are reflected here by the dependence of the coefficients on M_∞. The reduced frequency parameter k is unique to unsteady flows. This dimensionless frequency parameter is a measure of the unsteadiness of the flow and normally will have a value between zero and unity for conventional flight vehicles. It may also be noted that for any specified values of k and M_∞ each of the coefficients can be written as a complex number. As in the case of $\overline{h}$ relative to $\overline{\theta}$, the fact that lift and pitching moment are complex quantities reflects their phase relationships with respect to the pitch angle (where we can regard $\overline{\theta}$ as a real number for convenience). The speed at which flutter occurs corresponds to specific values of k and M_∞ and must be found by iteration. Examples of how this process can be carried out for one- and two-degree-of-freedom systems are given in this section.

5.5.1 One-Degree-of-Freedom Flutter

To illustrate the application of classical flutter analysis a very simple configuration will be treated first. This example is a one-degree-of-freedom aeroelastic system consisting of a rigid

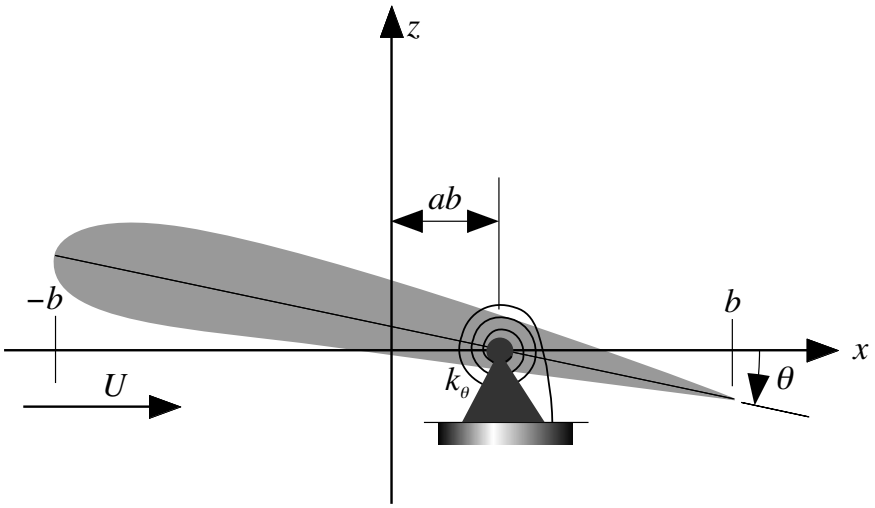

Figure 5.16: Schematic of the airfoil of a two-dimensional wing that is spring-restrained in pitch

two-dimensional wing that is permitted to rotate in pitch about a specified reference point; this is a special case of the typical section configuration in Fig. 5.11 for which the plunge degree of freedom is equal to zero, as depicted in Fig. 5.16. The system equations of motion reduce to one equation that can be written as

$$I_P\ddot{\theta} + k_\theta\theta = M \tag{5.107}$$

To be consistent with classical flutter analysis, the motion of the system will be presumed to be simple harmonic as

$$\theta = \overline{\theta}\exp(i\omega t) \tag{5.108}$$

The aerodynamic pitching moment, M, in the equation of motion is in response to this simple harmonic pitching displacement. As previously discussed this airload can be described by

$$M = \overline{M}\exp(i\omega t) \tag{5.109}$$

where

$$\overline{M} = \pi\rho_\infty b^4\omega^2 m_\theta(k, M_\infty)\overline{\theta} \tag{5.110}$$

Substituting these simple harmonic functions into the equation of motion yields an algebraic relation between the coefficients of $\overline{\theta}$ as

$$k_\theta - \omega^2 I_P = \pi\rho_\infty b^4\omega^2 m_\theta(k, M_\infty) \tag{5.111}$$

Introducing the natural frequency of the system at zero airspeed,

$$\omega_\theta = \sqrt{\frac{k_\theta}{I_P}} \tag{5.112}$$

and rearranging the algebraic relation, one obtains the final equation to be solved for the flight condition at the flutter boundary as

$$\frac{I_P}{\pi\rho_\infty b^4}\left[1-\left(\frac{\omega_\theta}{\omega}\right)^2\right]+m_\theta(k,M_\infty)=0 \tag{5.113}$$

To solve this equation it will be presumed that the configuration parameters I_P, ω_θ, and b are known. The unknown parameters that describe the motion and flight condition are ω, ρ_∞, k, and M_∞. These four unknowns must be determined from the single algebraic equation, Eq. (5.113). Since the aerodynamic coefficient, $m_\theta(k,M_\infty)$, is complex, it can be written as

$$m_\theta(k,M_\infty)=\Re(k,M_\infty)+i\Im(k,M_\infty) \tag{5.114}$$

As a consequence, both the real and imaginary parts of the algebraic relation must be zero, thus providing two real equations to determine the four unknowns. Therefore, two of the unknown parameters should be specified. A fixed altitude will be chosen that specifies the freestream atmospheric density, ρ_∞. The second parameter to be fixed will be the Mach number, which can be given a temporary value of zero. This, of course, implies that the flow is incompressible and the aerodynamic moment coefficient is then only a function of the reduced frequency. The governing algebraic equation can now be written as

$$\frac{I_P}{\pi\rho_\infty b^4}\left[1-\left(\frac{\omega_\theta}{\omega}\right)^2\right]+\Re(k,0)+i\Im(k,0)=0 \tag{5.115}$$

Equating the imaginary part of the left-hand side to zero gives a relation that can be solved for the reduced frequency, k_F, at the flutter boundary.

$$\Im(k_F,0)=0 \tag{5.116}$$

With k_F known $\Re(k_F,0)$ can be numerically evaluated. Equating the real part of the left-hand side to zero now enables the frequency, ω_F, to be determined from

$$\left(\frac{\omega_\theta}{\omega_F}\right)^2=1+\frac{\pi\rho_\infty b^4\Re(k_F,0)}{I_P} \tag{5.117}$$

Now that k_F and ω_F have been determined, it is possible to compute the flutter speed as

$$U_F=\frac{b\omega_F}{k_F} \tag{5.118}$$

The flutter speed determined by the above procedure corresponds to the originally specified altitude and is based on an incompressible representation of the airloads. After this speed has been determined, the speed of sound, c_∞, at the specified altitude can be used to find the flutter Mach number as

$$M_F=\frac{U_F}{c_\infty} \tag{5.119}$$

If this flutter Mach number is sufficiently small to justify the use of incompressible aerodynamics coefficients, then the altitude-speed combination obtained is a point on the flutter boundary. If the flutter Mach number is too high to validate the incompressible approximation, then the entire procedure should be repeated using aerodynamic coefficients that are based on the initially computed flutter Mach number. Using the standard atmospheric model, which relates density and the speed of sound, this iterative scheme will converge to a flight condition on the flutter boundary.

5.5.2 Two-Degree-of-Freedom Flutter

The analysis of multi-degree-of-freedom systems for determination of the flutter boundary can be adequately demonstrated by the simple two-degree-of-freedom configuration of Fig. 5.11. The equations of motion, already derived as Eqs. (5.91), are repeated here

$$\begin{aligned} m\left(\ddot{h}+bx_\theta\ddot{\theta}\right)+k_h h =& -L \\ I_P\ddot{\theta}+mbx_\theta\ddot{h}+k_\theta\theta =& M \end{aligned} \tag{5.120}$$

where, as before,

$$M = M_{\frac{1}{4}} + b\left(\frac{1}{2}+a\right)L \tag{5.121}$$

The next step in classical flutter analysis is to presume that the motion is simple harmonic as represented by

$$\begin{aligned} h =& \overline{h}\exp(i\omega t) \\ \theta =& \overline{\theta}\exp(i\omega t) \end{aligned} \tag{5.122}$$

The corresponding lift and moment can be written as

$$\begin{aligned} L =& \overline{L}\exp(i\omega t) \\ M =& \overline{M}\exp(i\omega t) \end{aligned} \tag{5.123}$$

Substituting these time-dependent functions into the equations of motion, one obtains a pair of algebraic equations for the amplitudes of h and θ of the form

$$\begin{aligned} -\omega^2 m\overline{h}-\omega^2 mbx_\theta\overline{\theta}+m\omega_h^2\overline{h} =& -\overline{L} \\ -\omega^2 mbx_\theta\overline{h}-\omega^2 I_P\overline{\theta}+I_P\omega_\theta^2\overline{\theta} =& \overline{M} \end{aligned} \tag{5.124}$$

where we recall that

$$\begin{aligned} \overline{L} =& -\pi\rho_\infty b^3\omega^2\left[\ell_h\left(k,M_\infty\right)\frac{\overline{h}}{b}+\ell_\theta\left(k,M_\infty\right)\overline{\theta}\right] \\ \overline{M} =& \pi\rho_\infty b^4\omega^2\left[m_h\left(k,M_\infty\right)\frac{\overline{h}}{b}+m_\theta\left(k,M_\infty\right)\overline{\theta}\right] \end{aligned} \tag{5.125}$$

Substituting these lift and moment amplitudes into Eq. (5.124) and rearranging, one obtains a pair of homogeneous, linear, algebraic equations for $\overline{h}$ and $\overline{\theta}$, given by

$$\begin{aligned}\left\{\frac{m}{\pi\rho_\infty b^2}\left[1-\left(\frac{\omega_h}{\omega}\right)^2\right]+\ell_h\left(k,M_\infty\right)\right\}\frac{\overline{h}}{b}+\left[\frac{mx_\theta}{\pi\rho_\infty b^2}+\ell_\theta\left(k,M_\infty\right)\right]\overline{\theta}=0\\ \left[\frac{mx_\theta}{\pi\rho_\infty b^2}+m_h\left(k,M_\infty\right)\right]\frac{\overline{h}}{b}+\left\{\frac{I_P}{\pi\rho_\infty b^4}\left[1-\left(\frac{\omega_\theta}{\omega}\right)^2\right]+m_\theta\left(k,M_\infty\right)\right\}\overline{\theta}=0\end{aligned} \tag{5.126}$$

The coefficients in these equations that involve the inertia terms will be symbolically simplified by defining the dimensionless parameters used earlier, namely

$$\begin{aligned}\mu &= \frac{m}{\pi\rho_\infty b^2} && \text{(mass ratio)}\\ r &= \sqrt{\frac{I_P}{mb^2}} && \text{(mass radius of gyration about } P)\end{aligned} \tag{5.127}$$

Using these parameters allows us to rewrite the above two homogeneous equations in a somewhat simpler way:

$$\begin{aligned}\left\{\mu\left[1-\left(\frac{\omega_h}{\omega}\right)^2\right]+\ell_h\right\}\frac{\overline{h}}{b}+\left(\mu x_\theta+\ell_\theta\right)\overline{\theta}=0\\ \left(\mu x_\theta+m_h\right)\frac{\overline{h}}{b}+\left\{\mu r^2\left[1-\left(\frac{\omega_\theta}{\omega}\right)^2\right]+m_\theta\right\}\overline{\theta}=0\end{aligned} \tag{5.128}$$

The third step in the flutter analysis is to solve these algebraic equations for the flight condition(s) for which the presumed simple harmonic motion is valid. This result will correspond to the flutter boundary. If it is presumed that the configuration parameters m, e, a, I_P, ω_h, ω_θ, and b are known, then the unknown quantities $\overline{h}$, $\overline{\theta}$, ω, ρ_∞, M_∞, and k describe the motion and flight condition. Because Eqs. (5.128) are linear and homogeneous in $\overline{h}/b$ and $\overline{\theta}$, the determinant of their coefficients must be zero for a nontrivial solution for the motion to exist. This condition can be written as

$$\begin{vmatrix}\mu\left[1-\sigma^2\left(\frac{\omega_\theta}{\omega}\right)^2\right]+\ell_h & \mu x_\theta+\ell_\theta\\ \mu x_\theta+m_h & \mu r^2\left[1-\left(\frac{\omega_\theta}{\omega}\right)^2\right]+m_\theta\end{vmatrix}=0 \tag{5.129}$$

The determinant in this relation is called the "flutter determinant." It should be noted that the parameter $\sigma=\omega_h/\omega_\theta$ has been introduced, so that a common term which is explicit in ω is available, namely ω_θ/ω. Thus, expansion of the determinant will yield a quadratic polynomial in the unknown $(\omega_\theta/\omega)^2$.

To complete the solution for the flight condition at the flutter boundary it must be recognized that four unknowns remain: ω_θ/ω, $\mu=m/(\pi\rho_\infty b^2)$, M_∞, and $k=b\omega/U$. The one equation available for their solution is the second-degree polynomial equation from the

determinant. However, because the aerodynamic coefficients are complex quantities, this complex equation represents two real equations, wherein both the real and imaginary parts must be identically zero for a solution to be obtained. This means that two of the four unknowns must be specified. A procedure to solve for and map out the flutter boundary is outlined as follows:

1. Specify an altitude, which fixes the parameter μ.
2. Specify M_∞, say, to be zero.
3. Specify a set of trial k values, say from 0.001 to 1.0.
4. For each value of k (and the specified value of M_∞) calculate the functions ℓ_h, ℓ_θ, m_h and m_θ.
5. Solve the flutter determinant, which is a quadratic equation with complex coefficients, for the values of $(\omega_\theta/\omega)^2$ that correspond to each of the selected values of k. Note that these roots will be complex in general, the real part being an approximation of $(\omega_\theta/\omega)^2$, and the imaginary part being related to the damping of the mode.
6. Interpolate to find the value of k at which the imaginary part of one of the roots becomes zero. This can be done approximately by plotting the imaginary parts of both roots versus k, so that the value of k at which one of the imaginary parts crosses the zero axis can be determined. This value of k then has a corresponding real value of $(\omega_\theta/\omega)^2$, which provides the value of ω.
7. Determine $U = b\omega/k$, and $M_\infty = U/c_\infty$.
8. Repeat steps 3 – 7 with the value of M_∞ obtained in step 7 until converged values are obtained for M_{∞_F}, k_F and U_F for flutter at a given μ.
9. Repeat the whole procedure for various values of μ (an indication of the altitude for a given aircraft) to determine the flutter boundary in terms of, say, altitude versus M_{∞_F}, k_F and U_F.

Step 6 above can also be carried out easily with computerized symbolic manipulation software such as Mathematica™or Maple.™One simply finds the value of k that makes the imaginary part of one of the two roots of the flutter determinant vanish.

5.6 Engineering Solutions for Flutter

It has been noted in the preceding section that the presumption of simple harmonic motion in classical flutter analysis has both advantages and disadvantages. The prime argument for specification of simple harmonic time dependency is, of course, its correspondence to

the stability boundary. Identification of the flight conditions along this boundary requires the execution of a tedious, iterative process such as the one outlined above. This type of solution can be attributed to Theodorsen (1934), who presented the first comprehensive flutter analysis with his development of the unsteady airloads on a two-dimensional wing in an incompressible potential flow.

Although unsteady aerodynamics analyses for simple harmonic motion are not simple to formulate and execute, they are far more tractable than those for oscillatory motions with varying amplitude. Over the years since the work of Theodorsen, numerous unsteady aerodynamic formulations have been developed for simple harmonic motion of lifting surfaces. These techniques have proven to be quite adequate for compressible flows in both the subsonic and supersonic regimes. They have also been developed for three-dimensional surfaces and in some cases with surface-to-surface interaction. This availability of relatively accurate unsteady aerodynamic theories for simple harmonic motion has been the stimulus for further development of flutter analyses beyond that of the classical flutter analysis described in Section 5.5.

There are two other very important considerations of the practicing engineer. The first is to obtain an understanding of the margin of stability at flight conditions in the vicinity of the flutter boundary. The second, and possibly the more important, is to obtain an understanding of the physical mechanism that causes the instability. With these two pieces of information, the engineer can propose design variations that may alleviate or even eliminate the instability. When a suitable unsteady aerodynamic theory is available, the p method can address these considerations. In this section we look at alternative ways that engineers have addressed these problems when unsteady aerodynamic theories that assume simple harmonic motion must be used.

5.6.1 The k Method

Subsequent to Theodorsen's analysis of the flutter problem, numerous schemes were devised to extract the roots of the "flutter determinant" and thus identify the stability boundary. Scanlan and Rosenbaum (1951) presented a brief overview of these techniques as they were offered during the 1940's. It was fairly common to include in the flutter analysis a parameter that simulated the effect of structural damping. Observations at that time indicated that the energy removed per cycle during a simple harmonic oscillation was nearly proportional to the square of the amplitude but independent of the frequency. This behavior can be characterized by a damping force that is proportional to the displacement but in phase with the velocity.

To incorporate this form of structural damping into the analysis of Section 5.5.2, Eqs. (5.120) can be written as

$$\begin{aligned} m\left(\ddot{h} + bx_\theta\ddot{\theta}\right) + k_h h &= -L + D_h \\ I_P\ddot{\theta} + mbx_\theta\ddot{h} + k_\theta\theta &= M + D_\theta \end{aligned} \tag{5.130}$$

where the dissipative structural damping terms are

$$\begin{aligned} D_h =& \overline{D}_h \exp(i\omega t) \\ =& - ig_h m\omega_h^2 \overline{h} \exp(i\omega t) \\ D_\theta =& \overline{D}_\theta \exp(i\omega t) \\ =& - ig_\theta I_P \omega_\theta^2 \overline{\theta} \exp(i\omega t) \end{aligned} \tag{5.131}$$

Proceeding as before, Eqs. (5.128) become

$$\begin{aligned} &\left\{ \mu \left[1 - \left(\frac{\omega_h}{\omega} \right)^2 (1 + ig_h) \right] + \ell_h \right\} \frac{\overline{h}}{b} + (\mu x_\theta + \ell_\theta) \overline{\theta} = 0 \\ &(\mu x_\theta + m_h) \frac{\overline{h}}{b} + \left\{ \mu r^2 \left[1 - \left(\frac{\omega_\theta}{\omega} \right)^2 (1 + ig_\theta) \right] + m_\theta \right\} \overline{\theta} = 0 \end{aligned} \tag{5.132}$$

The damping coefficients g_h and g_θ have representative values from 0.01 to 0.05 depending on the structural configuration. Most early analysts who incorporated this type of structural damping model into their flutter analyses specified the coefficient values *a priori* with the intention of improving the accuracy of their results.

It was Scanlan and Rosenbaum (1948) who suggested that the damping coefficients be treated as unknown together with ω. In this instance the subscripts on g can be removed. Writing $\sigma = \omega_h/\omega_\theta$ as before, and introducing

$$Z = \left(\frac{\omega_\theta}{\omega} \right)^2 (1 + ig) \tag{5.133}$$

one obtains the flutter determinant as

$$\begin{vmatrix} \mu (1 - \sigma^2 Z) + \ell_h & \mu x_\theta + \ell_\theta \\ \mu x_\theta + m_h & \mu r^2 (1 - Z) + m_\theta \end{vmatrix} = 0 \tag{5.134}$$

which is a quadratic equation in Z. The two unknowns of this quadratic equation are complex, denoted by

$$Z_{1,2} = \left(\frac{\omega_\theta}{\omega_{1,2}} \right)^2 (1 + ig_{1,2}) \tag{5.135}$$

The computational strategy for solving Eq. (5.134) proceeds in a manner similar to the one outlined for Eq. (5.129). The primary differences are that (a) no iteration on k is required and (b) the numerical results consist of two pairs of real numbers, (ω_1, g_1) and (ω_2, g_2), which can be plotted versus airspeed as either $U/(b\omega_\theta)$ or "reduced velocity" $1/k$.

Plots of the damping coefficient versus airspeed can indicate the margin of stability at conditions near the flutter boundary, where $g = 0$. These plots proved to be of such significance that the technique of incorporating the unknown structural damping was initially called the "U-g method," which is more indicative that it presumes simple harmonic motion

throughout. The numerical values of g_i that are obtained for each k can only be interpreted as the required damping (of the specified form) to achieve simple harmonic motion at frequency ω_i. Because this damping does not really exist and has been introduced as an artifice to produce the desired motion, it is truly artificial structural damping.

The plots of frequency versus airspeed in conjunction with the damping plots can in many cases provide an indication of the physical mechanism that leads to the instability. The values of frequency along the $U = 0$ axis correspond to the coupled modes of the original structural dynamic system. As the airspeed increases the individual behavior or interaction of these roots can indicate the transfer of energy from one mode to another. Such observations could suggest a way to delay the onset of the instability. To confirm identification of the modes of motion for any specified reduced frequency, it is only necessary to substitute the corresponding eigenvalues, ω_i and g_i, back into the homogeneous equations of motion to compute the associated eigenvector $(\overline{h}/b, \overline{\theta})$. Since this is a complex number, it can provide the magnitude and phase of the original deflections h and θ.

5.6.2 The p-k Method

Although the k method provides significant advantages to the practicing aeroelastician, it is a mathematically improper formulation. The impropriety of imposing simple harmonic motion with the introduction of artificial damping has precipitated many heated discussions throughout the industry. It has been argued that for conditions other than the $g = 0$ case the frequency and damping characteristics do not correctly represent the system behavior. As a result design changes that are based on these characteristics can lead to expensive and potentially dangerous results.

In 1971 Hassig presented definitive numerical results that clearly indicated that the k method of flutter analysis can exhibit an improper coupling among the modes of motion. His presentation utilized a simple form of unsteady aerodynamics in a k method analysis, and then he compared the results with those from a p method analysis.

To illustrate the p method in such a way that direct comparison with the other methods is facilitated, the general solution to the homogeneous modal equations of motion given by Eqs. (5.62) can be written in terms of a dimensionless time, $\tau = Ut/b$, as

$$\xi_i(\tau) = \overline{\xi}_i \exp(p\tau) \tag{5.136}$$

Substitution of this expression into Eqs. (5.61) yields $n + 1$ linear, homogeneous equations for the $\overline{\xi}_i$s which can be written in matrix form as

$$\left[p^2[\,M\,] + \frac{b^2}{U^2}[\,M\,][\,\omega^2\,] - \rho_\infty[A(p)]\right]\{\overline{\xi}\} = 0 \tag{5.137}$$

where it is noted that $[\,M\,]$ and $[\,\omega^2\,]$ are diagonal matrices with elements M_1, M_2, ..., M_n and ω_1^2, ω_2^2, ..., ω_n^2, respectively; n is the number of degrees of freedom; and the unsteady

aerodynamic matrix is expressed as

$$[A(p)] = p^2[c] + p[b] + [a] \tag{5.138}$$

where the matrices $[a]$, $[b]$, and $[c]$ are the same as those found in Eq. (5.63). Again, for a non-trivial solution of the generalized coordinate amplitudes, the determinant of the coefficient matrix in Eq. (5.137) must be zero, so that

$$\left| p^2[\grave{} M \acute{}] + \frac{b^2}{U^2}[\grave{} M \acute{}][\grave{} \omega^2 \acute{}] - \rho_\infty [A(p)] \right| = 0 \tag{5.139}$$

For a given speed and altitude this flutter determinant can be solved for p. The result will typically yield $n+1$ complex conjugate pairs, represented as

$$p = \gamma k \pm ik \tag{5.140}$$

where k is the reduced frequency of Eqs. (5.106), and γ is the rate of decay, given by

$$\gamma = \frac{1}{2\pi} \ln \left(\frac{a_{n+1}}{a_n} \right) \tag{5.141}$$

and where a_n and a_{n+1} represent the amplitudes of successive cycles.

Application of the k method to this modal representation can be readily achieved by letting $p = ik$ in the preceding formulation. This yields a flutter determinant comparable to Eq. (5.139) as

$$\left| -k^2[\grave{} M \acute{}] + \frac{b^2}{U^2}[\grave{} M \acute{}][\grave{} \omega^2 \acute{}] - \rho_\infty [A(ik)] \right| = 0 \tag{5.142}$$

At selected values of reduced frequency and altitude, Eq. (5.142) can be solved for the complex roots of b^2/U^2, denoted by $\lambda_r + i\lambda_i$. These roots may be interpreted as

$$\lambda_r + i\lambda_i = \left(\frac{b^2}{U^2} \right) (1 + ig) \tag{5.143}$$

where g is the structural damping required to sustain simple harmonic motion. This structural damping parameter can be related to the rate of decay parameter of the p method as

$$g \cong 2\gamma \tag{5.144}$$

This is a good approximation for small damping as in the case of flight vehicles.

Another important aspect in making any correlation between the p and k methods is the matter of adequate inclusion of compressibility effects in the unsteady aerodynamic terms. In the p method the flutter determinant is solved for selected combinations of speed and altitude. Consequently, the appropriate Mach number can be used for the aerodynamic terms at the outset of the computation. In contrast, the k method preselects combinations of

reduced frequency and altitude. As a result of then computing the airspeed as an unknown, λ_r, the Mach number cannot be accurately specified. The result is that an iterative process similar to the one in Section 5.5 must be conducted to ensure that compressibility effects are adequately incorporated in the k method.

Hassig applied the p and k methods of flutter analysis to a realistic aircraft configuration. By incorporating the same unsteady aerodynamic representation in each analysis he was able to make a valid comparison of the results. His observations are typified by Fig. 5.17 (which is his Fig. 1). It can be noted from this figure that not only is the modal coupling wrongly predicted by the k method; but, more important, the wrong mode is predicted to become unstable. The only consistently valid result between the two analyses is that of the flutter speed for which $g = \gamma = 0$. In spite of the inconsistent modal coupling exhibited by the k method, it does permit the use of simple harmonic modeling of the unsteady aerodynamic terms. As previously mentioned the accuracy of simple harmonic airload predictions far exceeds the accuracy of airload predictions for transient motions. It is for this reason that a compromise between the two models has been suggested.

The p-k method is such a compromise. It is based on conducting a p method type of analysis with the restriction that the unsteady aerodynamics matrix is for simple harmonic motion. Using an estimated value of k in computing $[A(ik)]$, one finds the flutter determinant to be

$$\left| p^2[\grave{} M \acute{}] + \frac{b^2}{U^2}[\grave{} M \acute{}][\grave{} \omega^2 \acute{}] - \rho_\infty [A(ik)] \right| = 0 \tag{5.145}$$

Given a set of initial guesses for k, say $k_0 = b\omega_i/U$ for the i^{th} root, this equation can be solved for p. This typically yields a set of complex conjugate pairs of roots, the number of which corresponds to the number of degrees of freedom in the structural model. For one of the roots, denoting the initial solution as

$$k_1 = |\Im(p)| \qquad \gamma_1 = \frac{\Re(p)}{k_1} \tag{5.146}$$

one can compute $[A(ik_1)]$. Using this new matrix in Eq. (5.145) leads to another set of p's, so that

$$k_2 = |\Im(p)| \qquad \gamma_2 = \frac{\Re(p)}{k_2} \tag{5.147}$$

Continual updating of the aerodynamic matrix in this way provides an iterative scheme that is convergent for each of the roots, negative γ being a measure of the modal damping. The earliest presentation of this technique was offered by Irwin and Guyett in 1965.

Hassig applied the p-k method to the configuration of Fig. 5.17. As illustrated by Fig. 5.18 (which is his Fig. 2), the p-k method appears to yield approximately the same result as the p method. This, of course, simply validates the convergence of the scheme. Its greatest advantage is that it can utilize airloads which have been formulated for simple harmonic motion. Another comparison offered by Hassig was between the widely used k method and the p-k method for a horizontal stabilizer/elevator configuration. This example of a strongly

coupled system provided the results given in Fig. 5.19 (which is his Fig. 3). Here again, as in the k versus p comparison of Fig. 5.17, widely differing conclusions can be drawn regarding the modal coupling. In addition to the easily interpreted frequency and damping plots versus airspeed for strongly coupled systems, a second advantage is offered by the p-k method regarding computational effort. The k method requires numerous computer runs at constant density to ensure matching the Mach number with airspeed and altitude. The p-k method does not have this requirement.

The accuracy of the p-k method depends on the level of damping in any particular mode. It is left as an exercise to the reader (see Problem 15) to show that the p-k method damping is only a good approximation for the damping in lightly damped modes. Fortunately, these are the modes about which we care the most.

5.7 Unsteady Aerodynamics

In Section 5.4, flutter analysis was conducted using an aerodynamic theory for steady flow. The lift and pitching moment used were functions only of the instantaneous pitch angle, θ. Fung (1955) suggested a simple experiment to demonstrate that things are not that simple: Attempt to rapidly move a stick in a straight line through water and notice the results. In the wake of the stick there is a vortex pattern, with vortices being shed alternately from each side of the stick. This shedding of vortices induces a periodic force perpendicular to the stick's line of motion, causing the stick to tend to wobble back and forth in your hand. A similar phenomenon happens with the motion of a lifting surface through a fluid and must be accounted for in unsteady aerodynamic theories.

In a more complete unsteady aerodynamic theory, the lift and pitching moment consist of two parts from two physically different phenomena: noncirculatory and circulatory effects. Noncirculatory effects, also called apparent mass and inertia effects, are generated when the wing motion has a nonzero acceleration. It has to then carry with it a part of the air surrounding it. That air has finite mass, which leads to inertial forces opposing its acceleration.

Circulatory effects are generally more important for aircraft wings. Indeed, in steady flight it is the circulatory lift that keeps the aircraft aloft. Vortices are an integral part of the process of generation of circulatory lift. Basically, there is a difference in the velocities on the upper and lower surfaces of an airfoil. Such a velocity profile can be represented as a constant velocity flow plus a vortex. In a dynamic situation, the strength of the vortex (i.e., the circulation) is changing with time. However, when circulatory forces of steady-flow theories depend only on the instantaneous pitch angle, this is an indication that they do not include the effects of the vortices shed into the wake. For example, contrast strip theory, which does not include the effect of the shed vorticity, with lifting line theory, which does.

Restricting our discussion to two dimensions and potential flow, we recall an implication of the Helmholtz theorem: the total vorticity will always vanish within any closed curve surrounding a particular set of fluid particles. Thus, if some clockwise vorticity develops

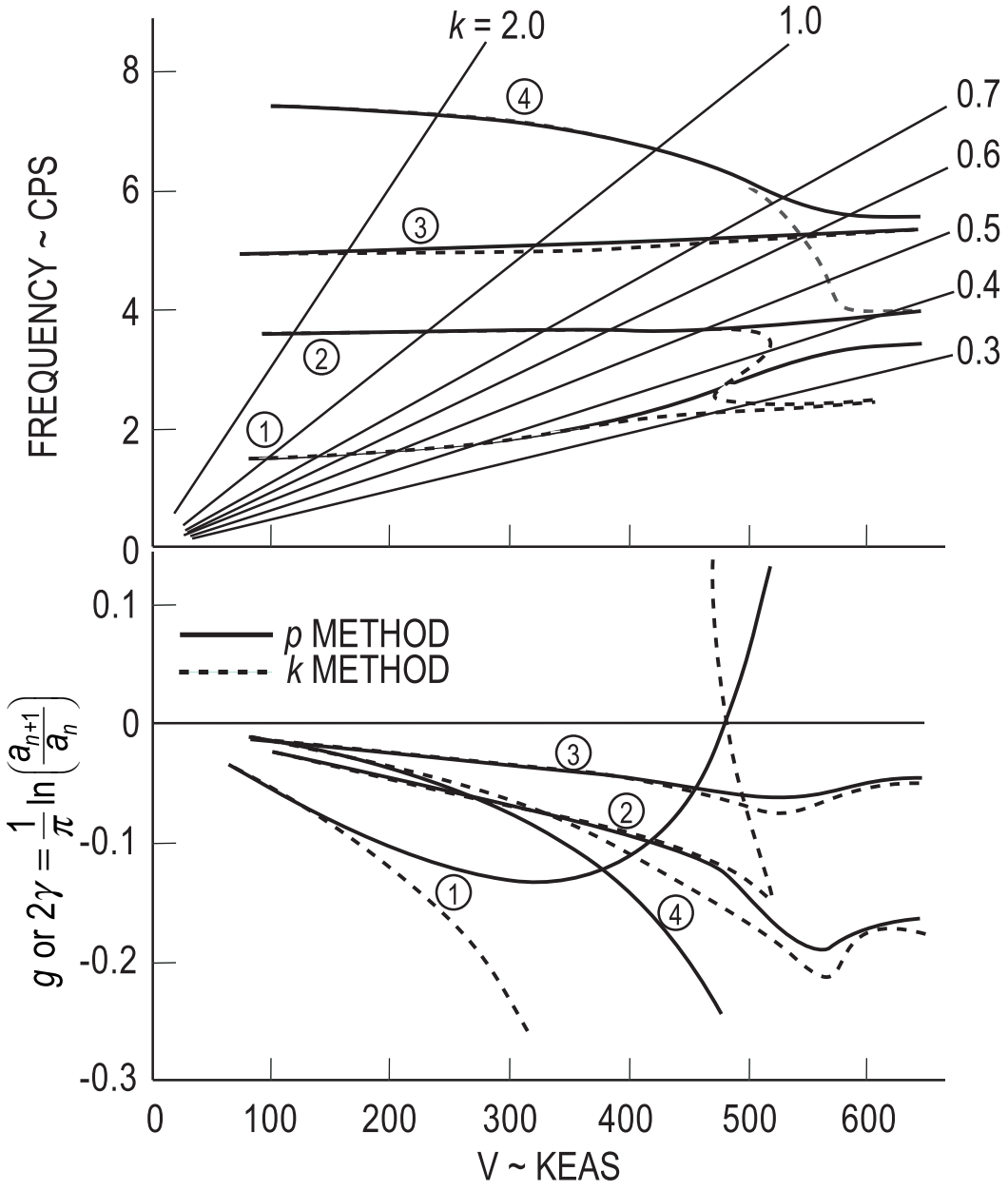

Figure 5.17: Comparison between p and k methods of flutter analysis for a twin-jet transport airplane [from Hassig (1971) Fig. 1, used by permission]

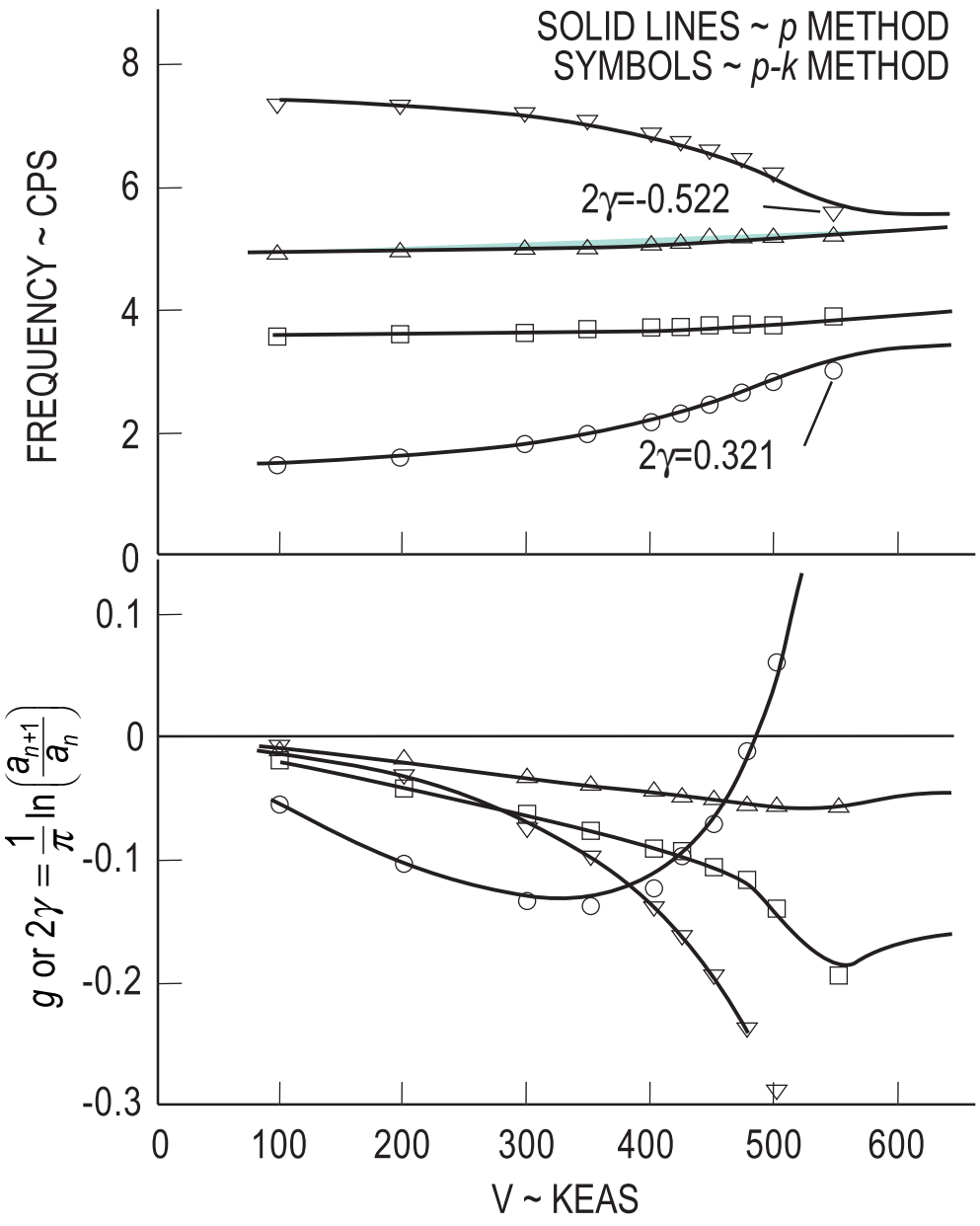

Figure 5.18: Comparison between p and p-k methods of flutter analysis for a twin-jet transport airplane [from Hassig (1971) Fig. 2, used by permission]

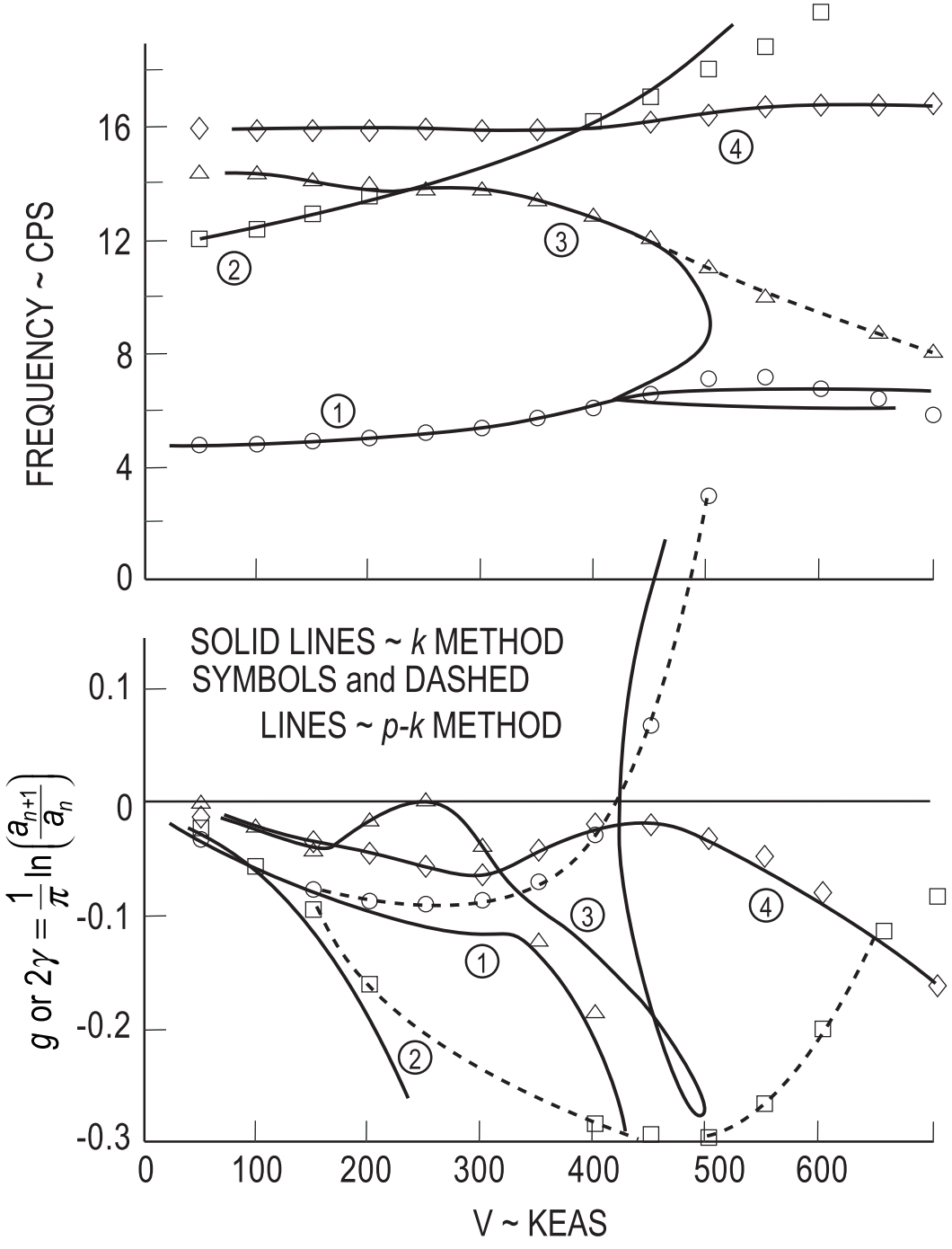

Figure 5.19: Comparison between p-k and k methods of flutter analysis for a horizontal stabilizer with elevator [from Hassig (1971) Fig. 3, used by permission]

about the airfoil, a counterclockwise vortex of the same strength has to be shed into the flow. As it moves along this shed vortex changes the flow field by inducing an unsteady flow back onto the airfoil. This behavior is a function of the strength of the shed vortex and its distance away from the airfoil. Thus, accounting for the effect of shed vorticity is in general a very complex undertaking and would necessitate knowledge of each and every vortex shed in the flow. However, if one assumes that the vortices shed in the flow move with the flow, then one can estimate the effect of these vortices.

In this section we will present two types of unsteady aerodynamic theories, both of which are based on potential flow theory and take into account the effects of shed vorticity. The simpler theory is appropriate for classical flutter analysis as well as for the k and p-k methods. The other is a finite-state theory cast in the time domain, appropriate for time-domain analysis as well as for eigen-analysis in the form of the p method.

5.7.1 Theodorsen's Unsteady Thin-Airfoil Theory

Theodorsen (1934) derived a theory of unsteady aerodynamics for a thin airfoil undergoing small oscillations in incompressible flow. The lift contains both circulatory and noncirculatory terms, whereas the pitching moment about the quarter-chord is entirely noncirculatory. According to Theodorsen's theory, the lift and pitching moment are given by

$$\begin{aligned} L &= 2\pi\rho_\infty UbC(k)\left[\dot{h}+U\theta+b\left(\frac{1}{2}-a\right)\dot{\theta}\right]+\pi\rho_\infty b^2\left(\ddot{h}+U\dot{\theta}-ba\ddot{\theta}\right) \\ M_{\frac{1}{4}} &= -\pi\rho_\infty b^3\left[\frac{1}{2}\ddot{h}+U\dot{\theta}+b\left(\frac{1}{8}-\frac{a}{2}\right)\ddot{\theta}\right] \end{aligned} \tag{5.148}$$

where the generalized forces are given in Eqs. (5.89). The function $C(k)$ is a complex-valued function of the reduced frequency k, given by

$$C(k)=\frac{H_1^{(2)}(k)}{H_1^{(2)}(k)+iH_0^{(2)}(k)} \tag{5.149}$$

where $H_n^{(2)}(k)$ are Hankel functions of the second kind, which can be expressed in terms of Bessel functions of the first and second kind, respectively, as

$$H_n^{(2)}(k)=J_n(k)-iY_n(k) \tag{5.150}$$

The function $C(k)=F(k)+iG(k)$ is called Theodorsen's function and is plotted in Figs. 5.20 and 5.21. Note that $C(k)$ is real and equal to unity for the steady case (i.e., for $k=0$). As k increases, one finds that the imaginary part increases in magnitude while the real part decreases. As k tends to infinity, $C(k)$ approaches 1/2. However, for practical situations k does not exceed values of the order of unity. Hence, the plot in Fig. 5.20 only extends to $k=1$. The large k behavior is shown in Fig. 5.21. When any harmonic function is multiplied by $C(k)$, its magnitude is reduced and a phase lag is introduced.

A few things are noteworthy concerning Eqs. (5.148). First, in Theodorsen's theory the lift-curve slope is equal to 2π. Thus, the first of the two terms in the lift is the circulatory lift without the effect of shed vortices multiplied by $C(k)$. The multiplication by $C(k)$ is a consequence of the theory having taken into account the effect of shed vorticity. The second term in the lift as well as the pitching moment are noncirculatory, depending on the acceleration and angular acceleration of the airfoil. The circulatory lift is the more significant of the two terms in the lift.

For steady flow the circulatory lift is linear in the angle of attack, but for unsteady flow there is no single angle of attack since the flow direction varies along the chordline as the result of the induced flow. However, just so we can discuss the concept for unsteady flow, it is possible to introduce a so-called effective angle of attack. For simple harmonic motion it can be inferred from Theodorsen's theory that an effective angle of attack is

$$\alpha = C(k)\left[\theta + \frac{\dot{h}}{U} + \frac{b}{U}\left(\frac{1}{2} - a\right)\dot{\theta}\right] \tag{5.151}$$

As we will show in Section 5.7.2 by comparison with the finite-state aerodynamic model introduced therein, α, is the angle of attack measured at the three-quarter chord based on an averaged value of the induced flow. Recall that in steady-flow aerodynamics, the angle of attack is the pitch angle θ. Here, however, α depends on θ as well as on $\dot{h}$, $\dot{\theta}$, and k. Because of these additional terms and because of the behavior of $C(k)$, we expect changes in magnitude and phase between θ and α carrying over into changes in the magnitude and phase of the lift and pitching moment relative to that of θ. Indeed, the function $C(k)$ is sometimes called the lift-deficiency function because it reduces the magnitude of unsteady lift relative to steady lift. It also introduces an important phase shift between the peak values of pitching oscillations and corresponding oscillations in lift and pitching moment. An approximation of Theodorsen theory in which $C(k)$ is set equal to unity is called a "quasi-steady" thin-airfoil theory. Such an approximation has value only for cases in which k is restricted to be very small.

Theodorsen's theory may be used in classical flutter analysis. There the reduced frequency of flutter is not known *a priori*. One can find k at the flutter condition using the method described in Section 5.5. Theodorsen's theory may also be used in the k and p-k methods, as described in Sections 5.6.1 and 5.6.2, respectively.

5.7.2 Finite-State Unsteady Thin-Airfoil Theory of Peters et al.

Although the Theodorsen theory is an excellent choice for classical flutter analysis, there are situations in which an alternative approach is needed. First, frequently one needs to calculate the modal damping in subcritical flight conditions. Second, there is a growing interest in the active control of flutter, and design of controllers requires that the system be represented in state-space form. To meet these requirements, one needs to represent the actual aerodynamic loads (which are in the frequency domain in Theodorsen's theory) in

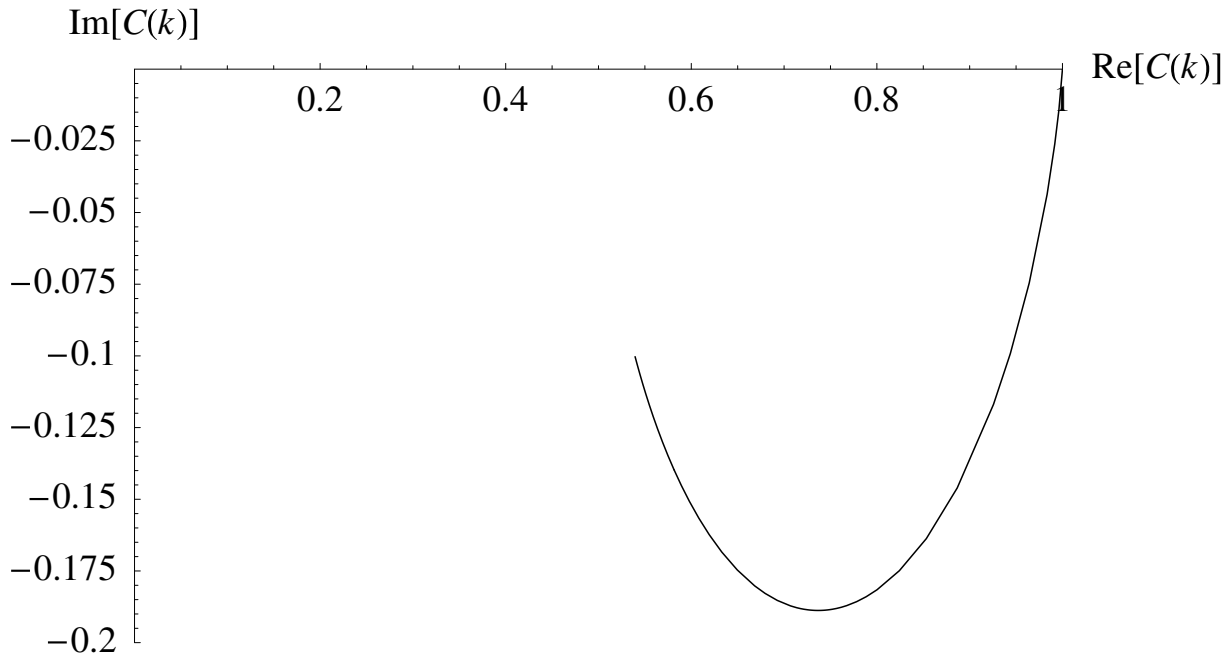

Figure 5.20: Plot of the real and imaginary parts of $C(k)$ for k varying from zero, where $C(k) = 1$, to unity

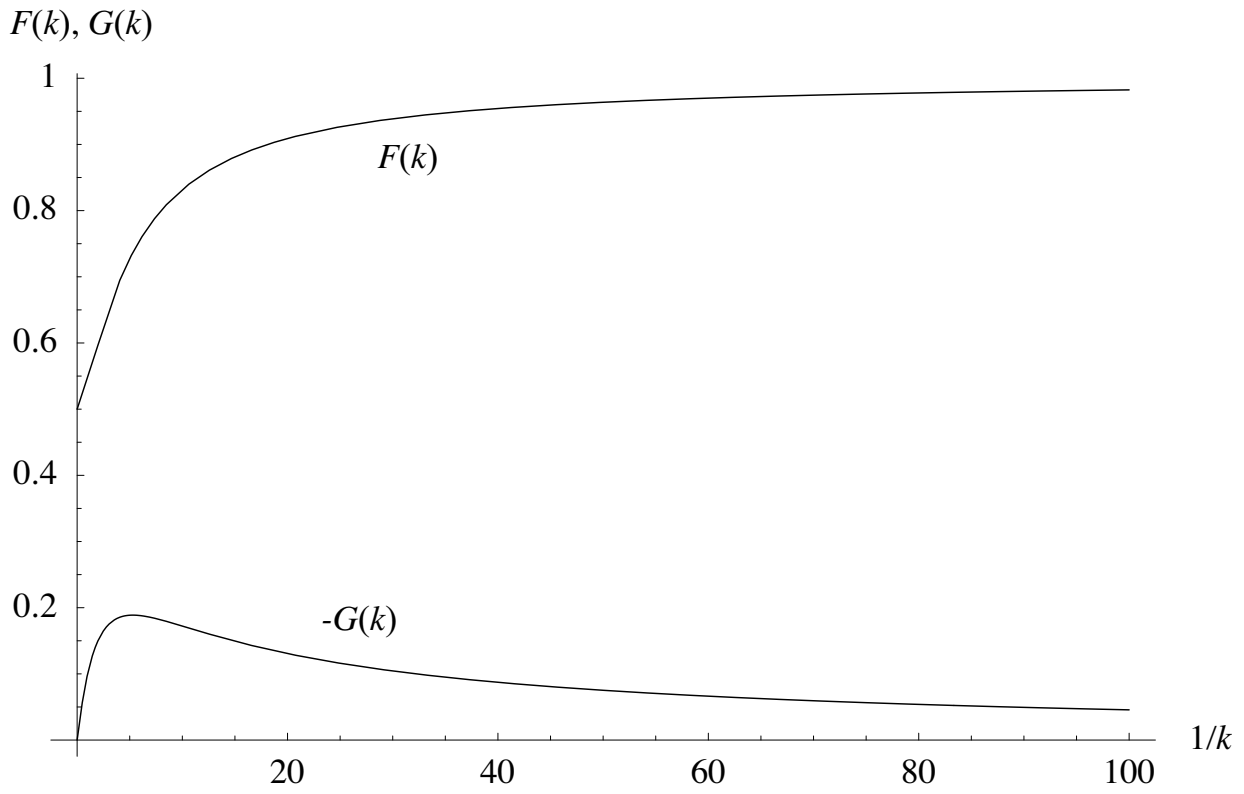

Figure 5.21: Plot of the real and imaginary parts of $C(k)$ versus $1/k$

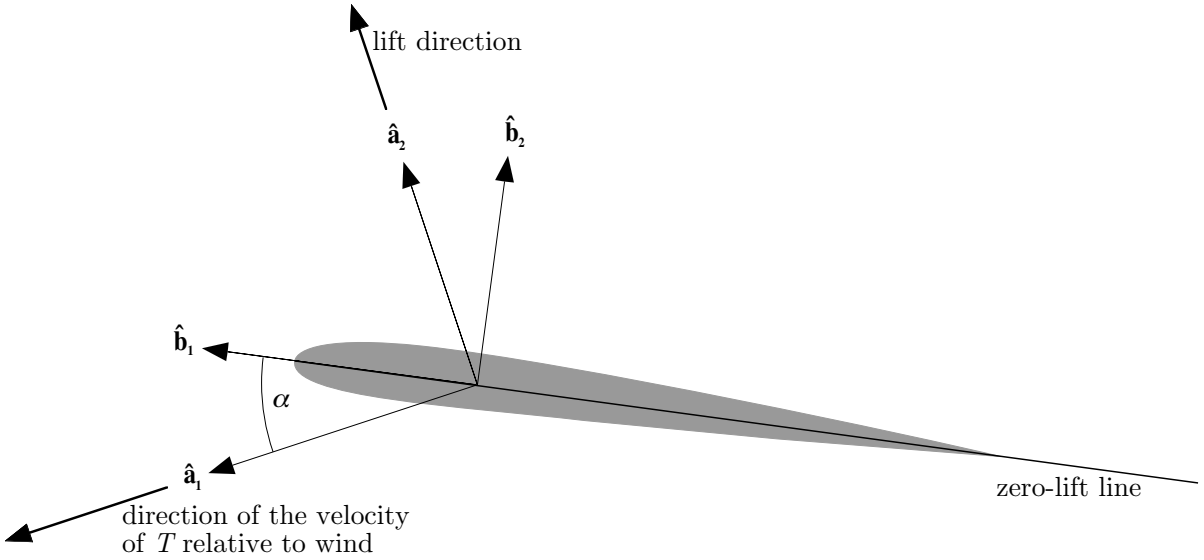

Figure 5.22: Schematic showing geometry of the zero-lift line, relative wind, and lift directions

terms of time-domain differential equations. Finite-state theories approximate the actual infinite-state aerodynamic model to within engineering accuracy. One such approach is the finite-state, induced-flow theory for inviscid, incompressible flow of Peters et al.

Consider a typical section of a rigid, symmetric wing, shown in Fig. 5.11, and the additional vectorial directions defined in Fig. 5.22. To begin the presentation of this theory, we first relate the three sets of unit vectors:

1. a set fixed in the inertial frame, $\hat{\mathbf{i}}_1$ and $\hat{\mathbf{i}}_2$, such that the air is flowing at velocity $-U\hat{\mathbf{i}}_1$,

2. a set fixed in the wing, $\hat{\mathbf{b}}_1$ and $\hat{\mathbf{b}}_2$, with $\hat{\mathbf{b}}_1$ directed along the zero-lift line toward the leading edge and $\hat{\mathbf{b}}_2$ perpendicular to $\hat{\mathbf{b}}_1$,

3. a set $\hat{\mathbf{a}}_1$ and $\hat{\mathbf{a}}_2$ associated with the local relative wind vector at the three-quarter chord, such that $\hat{\mathbf{a}}_1$ is along the relative wind vector and $\hat{\mathbf{a}}_2$ is perpendicular to it, in the assumed direction of the lift.

The relationships among these unit vectors can be simply stated as

$$\begin{Bmatrix} \hat{\mathbf{b}}_1 \\ \hat{\mathbf{b}}_2 \end{Bmatrix} = \begin{bmatrix} \cos(\theta) & \sin(\theta) \\ -\sin(\theta) & \cos(\theta) \end{bmatrix} \begin{Bmatrix} \hat{\mathbf{i}}_1 \\ \hat{\mathbf{i}}_2 \end{Bmatrix} \tag{5.152}$$

and

$$\begin{Bmatrix} \hat{\mathbf{a}}_1 \\ \hat{\mathbf{a}}_2 \end{Bmatrix} = \begin{bmatrix} \cos(\alpha) & -\sin(\alpha) \\ \sin(\alpha) & \cos(\alpha) \end{bmatrix} \begin{Bmatrix} \hat{\mathbf{b}}_1 \\ \hat{\mathbf{b}}_2 \end{Bmatrix} \tag{5.153}$$

and $\hat{\mathbf{i}}_3 = \hat{\mathbf{a}}_3 = \hat{\mathbf{b}}_3 = \hat{\mathbf{b}}_1 \times \hat{\mathbf{b}}_2$.

Induced-flow theories approximate the effects of shed vortices based on changes they cause in the flow field near the airfoil. Thus, the velocity field near the airfoil consists of the freestream velocity plus an additional component to account for the induced flow. Although the induced flow varies throughout the flow field, we will approximate its value near the airfoil as an average value along the chordline. Thus, the local inertial wind velocity is written approximately as $-U\hat{\mathbf{i}}_1 - \lambda_0\hat{\mathbf{b}}_2$ where λ_0 is the average induced flow (perpendicular to the airfoil zero-lift line). According to classical thin-airfoil theory, one should calculate the angle of attack using the instantaneous relative wind velocity vector as calculated at T. To represent the relative wind velocity vector at T, one can write the relative wind vector (i.e., the velocity of the wing with respect to the air) as $W\hat{\mathbf{a}}_1$ and set it equal to the inertial velocity of T minus the inertial air velocity, that is,

$$\begin{aligned} W\hat{\mathbf{a}}_1 &= \mathbf{v}_T - (-U\hat{\mathbf{i}}_1 - \lambda_0\hat{\mathbf{b}}_2) \\ &= \mathbf{v}_T + U\hat{\mathbf{i}}_1 + \lambda_0\hat{\mathbf{b}}_2 \end{aligned} \tag{5.154}$$

where $\mathbf{v}_T$ is the inertial velocity of the three-quarter chord, given by

$$\mathbf{v}_T = \mathbf{v}_P + \dot{\theta}\hat{\mathbf{b}}_3 \times \mathbf{r}_{PT} \tag{5.155}$$

and $\mathbf{r}_{PT}$ is the position vector from P to T. From Fig. 5.11 one finds that

$$\mathbf{r}_{PT} = \left[\frac{b}{2} + (1+a)b - 2b\right]\hat{\mathbf{b}}_1 = b\left(a - \frac{1}{2}\right)\hat{\mathbf{b}}_1 \tag{5.156}$$

Thus,

$$\mathbf{v}_T = \mathbf{v}_P + \dot{\theta}\hat{\mathbf{b}}_3 \times b\left(a - \frac{1}{2}\right)\hat{\mathbf{b}}_1 \tag{5.157}$$

The inertial velocity of the reference point P is

$$\mathbf{v}_P = -\dot{h}\hat{\mathbf{i}}_2 \tag{5.158}$$

while $\dot{\theta}\hat{\mathbf{b}}_3$ is the inertial angular velocity of the wing. Carrying out the cross product in Eq. (5.157), one obtains

$$\mathbf{v}_T = -\dot{h}\hat{\mathbf{i}}_2 + b\dot{\theta}\left(a - \frac{1}{2}\right)\hat{\mathbf{b}}_2 \tag{5.159}$$

so that the relative wind can be written as

$$W\hat{\mathbf{a}}_1 = U\hat{\mathbf{i}}_1 - \dot{h}\hat{\mathbf{i}}_2 + \left[b\dot{\theta}\left(a - \frac{1}{2}\right) + \lambda_0\right]\hat{\mathbf{b}}_2 \tag{5.160}$$

Alternatively, one may write the relative wind in terms of its components along $\hat{\mathbf{b}}_1$ and $\hat{\mathbf{b}}_2$, that is,

$$W\hat{\mathbf{a}}_1 = W\cos(\alpha)\hat{\mathbf{b}}_1 - W\sin(\alpha)\hat{\mathbf{b}}_2 \tag{5.161}$$

where α is given by (see Fig. 5.22)

$$\tan(\alpha) = -\frac{\hat{\mathbf{a}}_1 \cdot \hat{\mathbf{b}}_2}{\hat{\mathbf{a}}_1 \cdot \hat{\mathbf{b}}_1} \tag{5.162}$$

Using Eq. (5.160), one finds that

$$\begin{aligned} W\hat{\mathbf{a}}_1 \cdot \hat{\mathbf{b}}_1 &= U\cos(\theta) - \dot{h}\sin(\theta) \\ W\hat{\mathbf{a}}_1 \cdot \hat{\mathbf{b}}_2 &= -U\sin(\theta) - \dot{h}\cos(\theta) + b\left(a - \frac{1}{2}\right)\dot{\theta} + \lambda_0 \end{aligned} \tag{5.163}$$

Assuming small angles, one may now show that

$$\begin{aligned} \alpha &= \theta + \frac{\dot{h}}{U} + \frac{b}{U}\left(\frac{1}{2} - a\right)\dot{\theta} - \frac{\lambda_0}{U} \\ W &= U + \text{ higher-order terms} \end{aligned} \tag{5.164}$$

According to this derivation, α is an effective angle of attack based on the relative wind vector at the three-quarter chord, which, in turn, is based on the average value of the induced flow λ_0 over the wing chordline. Note that α is *not* equal to the pitch angle θ. Because of the motion of the wing and the induced flow field, the relative wind direction is not fixed in inertial space. Therefore, the effective angle of attack depends on the pitch rate, on the plunge velocity, and on the induced flow. Moreover, the lift is assumed to be perpendicular to the relative wind vector. This assumption is adequate for the calculation of lift and pitching moment, which are both first-order in the motion variables. However, sufficiently rapid plunge motion (as in the flapping wings of an insect) can result in a value of α that is not small, and one would need to make "small but finite" angle assumptions to calculate the drag (or propulsive force equal to negative drag) one could encounter in such situations.

The total lift and moment expressions including the noncirculatory forces are

$$\begin{aligned} L &= \pi\rho_\infty b^2\left(\ddot{h} + U\dot{\theta} - ba\ddot{\theta}\right) + 2\pi\rho_\infty Ub\left[\dot{h} + U\theta + b\left(\frac{1}{2} - a\right)\dot{\theta} - \lambda_0\right] \\ M_{\frac{1}{4}} &= -\pi\rho_\infty b^3\left[\frac{1}{2}\ddot{h} + U\dot{\theta} + b\left(\frac{1}{8} - \frac{a}{2}\right)\ddot{\theta}\right] \end{aligned} \tag{5.165}$$

Note the similarity between Eqs. (5.165) and (5.148). In particular, by studying the circulatory lift in both lift equations, one then can see the basis for identifying α, calculated as in the first of Eqs. (5.164), with the expression in Eq. (5.151).

The lift and pitching moment are then used to form the generalized forces from Eqs. (5.89) and are, in turn, used in the structural equations, Eqs. (5.91). Even so, these two equations are incomplete, having more than two unknowns. The induced flow velocity λ_0 needs to be expressed in terms of the airfoil motion. The induced-flow theory of Peters et al. does just that, representing the average induced flow λ_0 in terms of N induced-flow states $\lambda_1, \lambda_2, \ldots, \lambda_N$ as

$$\lambda_0 \approx \frac{1}{2}\sum_{n=1}^{N} b_n \lambda_n \tag{5.166}$$

where the b_n are found by least-squares method. The induced-flow dynamics are then derived from the assumption that the shed vortices stay in the plane of the airfoil and travel downstream with the same velocity as the flow. Introducing a column matrix $\{\lambda\}$ containing the values of λ_n, one can write the set of N first-order ordinary differential equations governing $\{\lambda\}$ as

$$[A]\left\{\dot{\lambda}\right\} + \frac{U}{b}\{\lambda\} = \{c\}\left[\ddot{h} + U\dot{\theta} + b\left(\frac{1}{2} - a\right)\ddot{\theta}\right] \tag{5.167}$$

where the matrices $[A]$ and $\{c\}$ can be derived for a user-defined number of induced-flow states. The expressions of the matrices used above are given for N finite states as

$$[A] = [D] + \{d\}\{b\}^T + \{c\}\{d\}^T + \frac{1}{2}\{c\}\{b\}^T \tag{5.168}$$

where

$$\begin{aligned} D_{nm} &= \tfrac{1}{2n} && n = m+1 \\ &= -\tfrac{1}{2n} && n = m-1 \\ &= 0 && n \neq m \pm 1 \end{aligned} \tag{5.169}$$

$$\begin{aligned} b_n &= (-1)^{n-1}\tfrac{(N+n-1)!}{(N-n-1)!}\tfrac{1}{(n!)^2} && n \neq N \\ &= (-1)^{n-1} && n = N \end{aligned} \tag{5.170}$$

$$\begin{aligned} d_n &= \tfrac{1}{2} && n = 1 \\ &= 0 && n \neq 1 \end{aligned} \tag{5.171}$$

and

$$c_n = \frac{2}{n} \tag{5.172}$$

The resulting aeroelastic model is in the time domain, in contrast to classical flutter analysis, which is in the frequency domain (see Section 5.5). Thus, it can be used for flutter analysis by the p method as well as in the design of control systems to alleviate flutter.

Results using the finite-state, induced-flow model (i.e., Eqs. 5.167 and 5.91 with generalized forces given by Eqs. 5.89 with lift and pitching moment given by Eqs. 5.165) for the problem analyzed previously in Section 5.4 (recall that $a = -1/5$, $e = -1/10$, $\mu = 20$, $r^2 = 6/25$, and $\sigma = 2/5$) are given here. These results are based on use of $N = 6$ induced

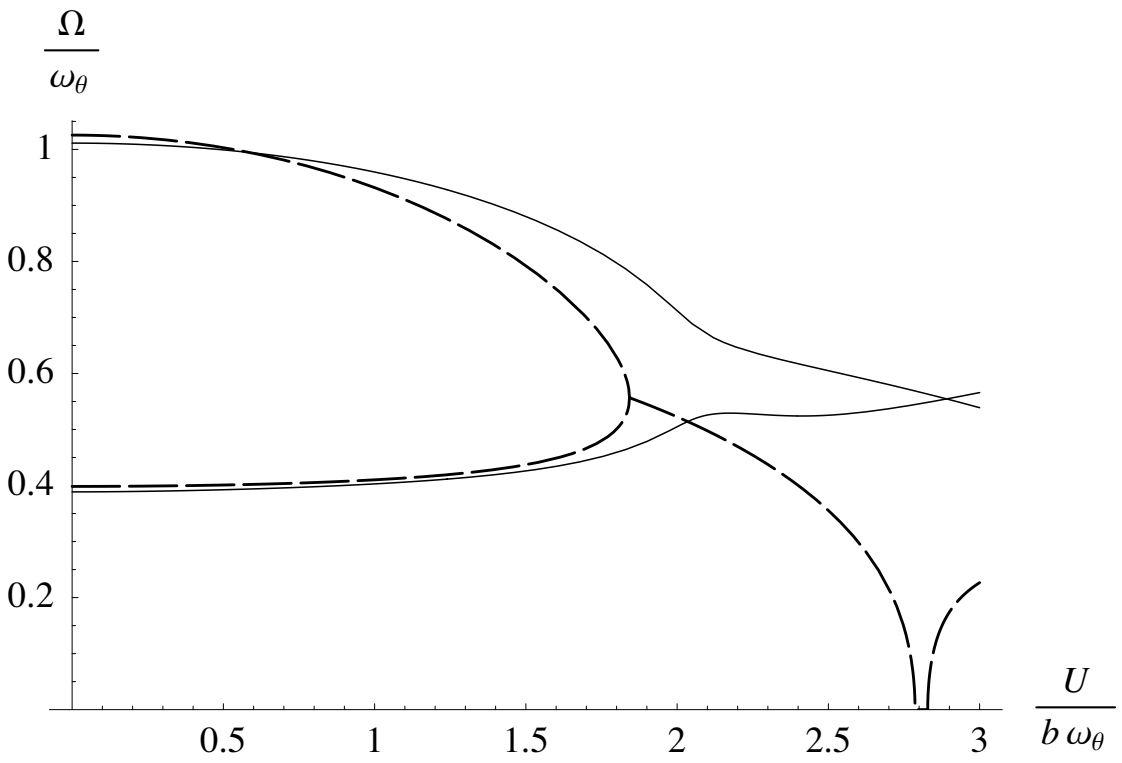

Figure 5.23: Plot of the modal frequency versus $U/(b\omega_\theta)$ for $a = -1/5$, $e = -1/10$, $\mu = 20$, $r^2 = 6/25$, and $\sigma = 2/5$; solid lines: p method, aerodynamics of Peters et al.; dashed lines: steady flow aerodynamics

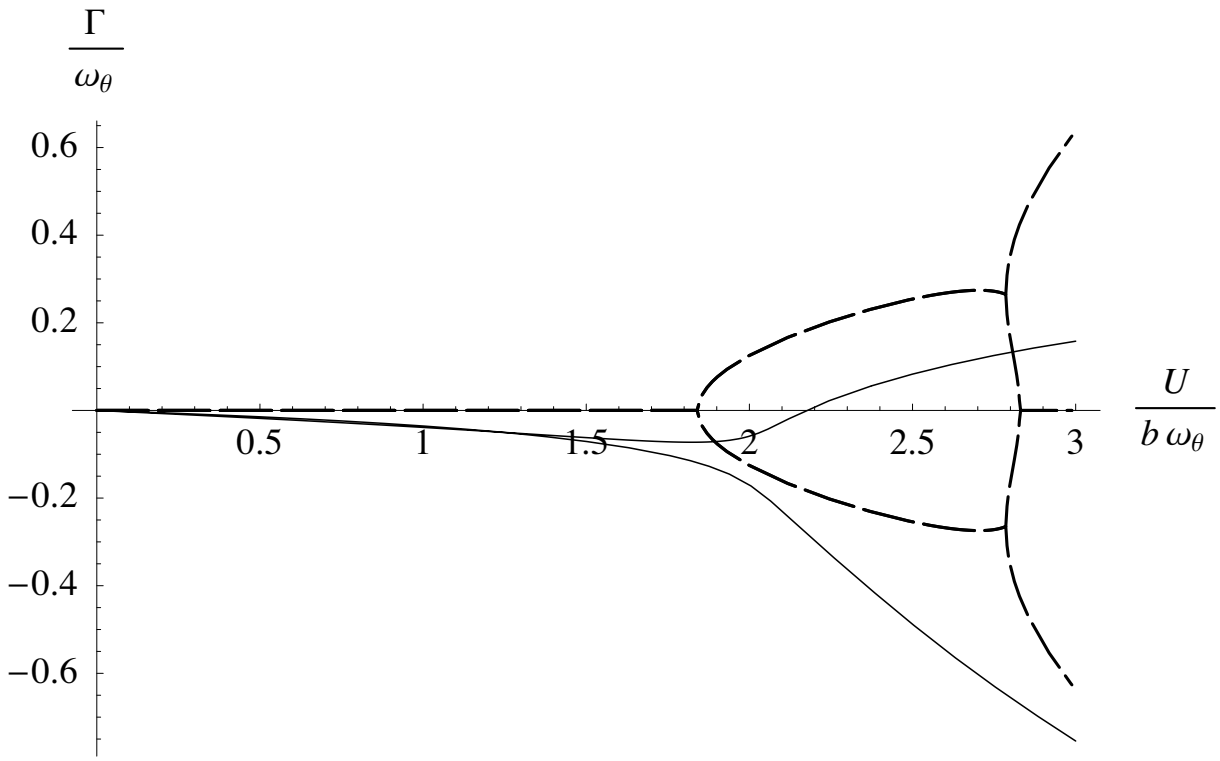

Figure 5.24: Plot of the modal damping versus $U/(b\omega_\theta)$ for $a = -1/5$, $e = -1/10$, $\mu = 20$, $r^2 = 6/25$, and $\sigma = 2/5$; solid lines: p method, aerodynamics of Peters et al.; dashed lines: steady flow aerodynamics

flow states. The frequency and damping results are shown in Figs. 5.23 and 5.24, respectively. As before, a frequency coalescence is observed near where one of the modes goes unstable. The flutter speed obtained is $V_F = U_F/(b\omega_\theta) = 2.165$, and the flutter frequency is $\Omega_F/\omega_\theta = 0.6545$. Although this value of the flutter speed is close to that observed previously using the simpler theory, the unsteady theory produces complex roots for all $V \neq 0$, so that there is modal damping in all the modes below the flutter speed. The equations contain damping terms proportional to the velocity that account for the initial increase in damping. At higher velocities, however, the destabilizing circulatory term (the nonsymmetric term in the stiffness matrix that also is present in the steady-flow theory) overcomes the damping caused by the unsteady terms, resulting in flutter.

It is left to the reader as an exercise to show the equivalence of the theory of Peters et al. and Theodorsen's theory; see Problem 17.

5.7.3 Alternative Unsteady Thin-Airfoil Theory

An alternative form of unsteady aerodynamic theory suitable for rapid maneuvers and gust entry can be cast in terms of an integro-differential form, suitable for very high reduced frequencies ($k > 10$). For this theory one has

$$\begin{aligned} L =& \pi\rho_\infty b^2 \left(\ddot{h} + U\dot{\theta} - ba\ddot{\theta}\right) + 2\pi\rho_\infty Ub\left\{\left[\dot{h} + U\theta + b\left(\frac{1}{2} - a\right)\dot{\theta}\right]_{t=0}\phi(\tau)\right. \\ &\left. + \int_0^\tau \phi(\tau-\sigma)\left[\dot{h} + U\theta + b\left(\frac{1}{2} - a\right)\dot{\theta}\right]d\sigma\right\} \\ M_{\frac{1}{4}} =& -\pi\rho_\infty b^3\left[\frac{1}{2}\ddot{h} + U\dot{\theta} + b\left(\frac{1}{8} - \frac{a}{2}\right)\ddot{\theta}\right] \end{aligned} \tag{5.173}$$

where $\tau = Ut/b$, the nondimensional time. The pitching moment and the first term of the lift are made up of apparent mass terms, and the second and third terms of the lift are Duhamel convolution integrals, with the Wagner function for an indicial angle of attack, given by

$$\phi(\tau) = \frac{2}{\pi}\int_0^\infty \frac{F(k)}{k}\sin(k\tau)\,dk \approx \frac{\tau+2}{\tau+4} \tag{5.174}$$

which amounts to the Fourier transform of $C(\tau)$ and follows the lift change due to a unit step change in the angle of attack. The memory effect is in the integration terms.

The quasi-steady assumption of $\phi(\tau) = 1$ is tantamount to having lift change instantaneously. Then the lift and moment become

$$\begin{aligned} L =& \pi\rho_\infty b^2 \left(\ddot{h} + U\dot{\theta} - ba\ddot{\theta}\right) + 2\pi\rho_\infty Ub\left[\dot{h} + U\theta + b\left(\frac{1}{2} - a\right)\dot{\theta}\right] \\ M_{\frac{1}{4}} =& -\pi\rho_\infty b^3\left[\frac{1}{2}\ddot{h} + U\dot{\theta} + b\left(\frac{1}{8} - \frac{a}{2}\right)\ddot{\theta}\right] \end{aligned} \tag{5.175}$$

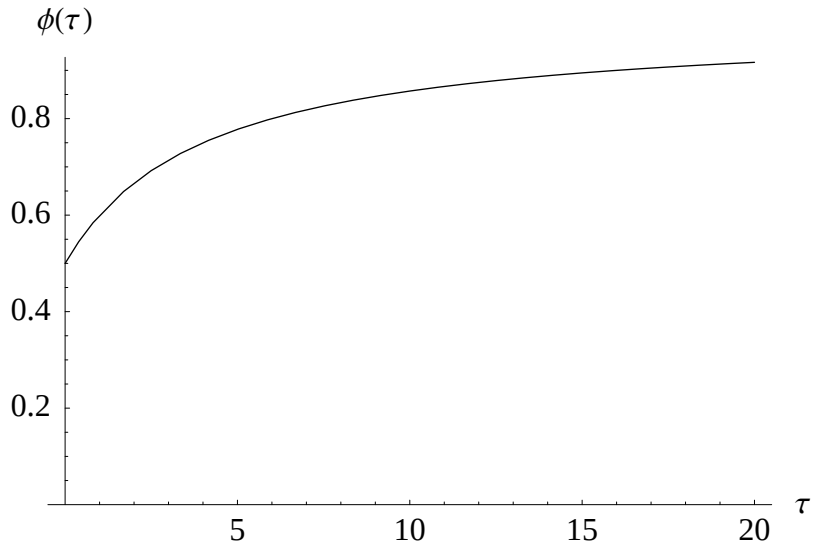

Figure 5.25: Wagner function

5.8 Flutter Prediction via Assumed Modes

As previously noted, in industry it is now typical to use the finite element method as a means to realistically represent aircraft structural dynamics. Although it is certainly possible to conduct full finite element flutter analyses, flutter analysis based on a truncated set of the modes of the stucture is still very helpful and relatively simple; and for those reasons alone it is often done. In this section we show how such an analysis can be done within the framework of the Ritz method, already established in Section 2.7.

Let us consider an unswept wing that is modeled as a beam of length ℓ. For the structural model, we adopt the same notation as we used in chapter 4. Thus, for a beam with bending rigidity EI and torsional rigidity GJ, the strain energy becomes

$$U = \frac{1}{2}\int_0^\ell \left[EI\left(\frac{\partial^2 w}{\partial y^2}\right)^2 + GJ\left(\frac{\partial \theta}{\partial y}\right)^2 \right] dy \tag{5.176}$$

To obtain the kinetic energy, we first consider the airfoil section shown in Fig. 5.26. Denoting the mass per unit volume of the material by ρ and noting that the velocity of a typical point within the cross-sectional plane is

$$\mathbf{v} = z\frac{\partial \theta}{\partial t}\hat{\mathbf{i}} + \left(\frac{\partial w}{\partial t} - x\frac{\partial \theta}{\partial t}\right)\hat{\mathbf{k}} \tag{5.177}$$

where $\hat{\mathbf{i}}$ and $\hat{\mathbf{k}}$ are unit vectors in the x and z directions, respectively, one can write the

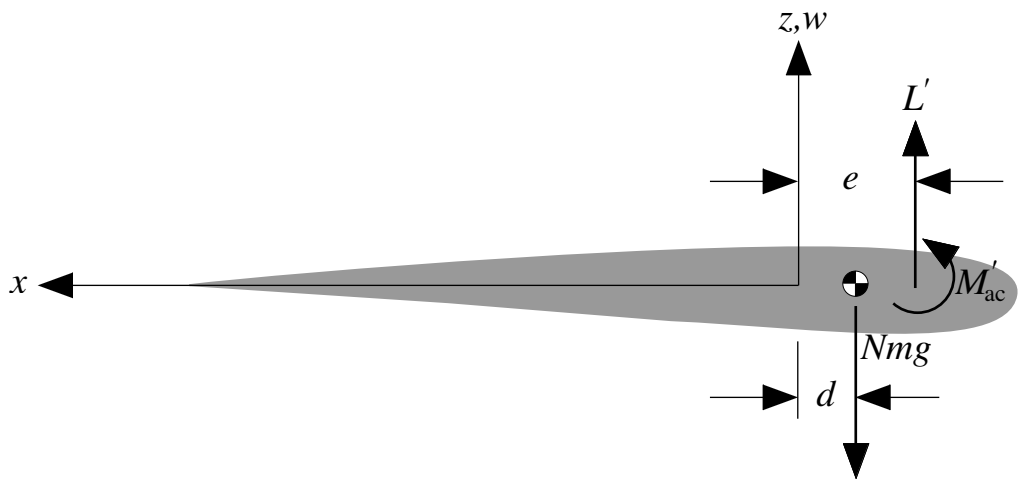

Figure 5.26: Cross section of spanwise uniform lifting surface

kinetic energy as

$$K = \frac{1}{2}\int_0^\ell \iint_A \rho \left[\left(\frac{\partial w}{\partial t} - x\frac{\partial \theta}{\partial t} \right)^2 + z^2 \left(\frac{\partial \theta}{\partial t} \right)^2 \right] dx\, dz\, dy \tag{5.178}$$

Straightforward evaluation of the cross-sectional integrals yields

$$K = \frac{1}{2}\int_0^\ell \left[m\left(\frac{\partial w}{\partial t} \right)^2 + 2md\frac{\partial w}{\partial t}\frac{\partial \theta}{\partial t} + mb^2r^2 \left(\frac{\partial \theta}{\partial t} \right)^2 \right] dy \tag{5.179}$$

where m is the mass per unit length, d is the offset of the mass centroid from the elastic axis (positive when the mass centroid is toward the leading edge), and br is the cross-sectional mass radius of gyration about the elastic axis.

Finally, one needs the virtual work of the aerodynamic forces, which can be written as

$$\overline{\delta W} = \int_0^\ell \left[L'\delta w + \left(M'_{\text{ac}} + eL' \right) \delta\theta \right] dy \tag{5.180}$$

where, as before, L' and M'_{ac} are the distributed lift and pitching moment per unit length of the wing.

Owing to longstanding conventions in the literature of unsteady aerodynamics, this notation is not compatible with what we have used so far in this chapter. Thus, we rewrite

these three expressions (i.e., strain energy, kinetic energy, and virtual work) in terms of the notation of this chapter. In particular, one can show that the following replacements can be made for the notation used in Fig. 4.12:

$$\begin{aligned} d &\rightarrow -bx_\theta \\ e &\rightarrow \left(\frac{1}{2}+a\right)b \\ L' &\rightarrow L' \\ M'_{\text{ac}} &\rightarrow M'_{\frac{1}{4}} \end{aligned}$$

Thus, the strain energy is unchanged from above. The kinetic energy becomes

$$K = \frac{1}{2}\int_0^\ell \left[m\left(\frac{\partial w}{\partial t}\right)^2 - 2mbx_\theta \frac{\partial w}{\partial t}\frac{\partial \theta}{\partial t} + mb^2r^2\left(\frac{\partial \theta}{\partial t}\right)^2 \right] dy \tag{5.181}$$

and the virtual work becomes

$$\overline{\delta W} = \int_0^\ell \left\{ L'\delta w + \left[M'_{\frac{1}{4}} + \left(\frac{1}{2}+a\right)bL' \right]\delta\theta \right\} dy \tag{5.182}$$

A reasonable choice for the assumed modes is the set of uncoupled free-vibration modes of the wing for bending and torsion, such that

$$\begin{aligned} w(y,t) &= \sum_{i=1}^{N_w} \eta_i(t)\Psi_i(y) \\ \theta(y,t) &= \sum_{i=1}^{N_\theta} \phi_i(t)\Theta_i(y) \end{aligned} \tag{5.183}$$

where N_w and N_θ are the numbers of modes used to represent bending and torsion, respectively; η_i and ϕ_i are the generalized coordinates associated with bending and torsion, respectively; and Ψ_i and Θ_i are the bending and torsion mode shapes, respectively. Here Θ_i is given by

$$\Theta_i = \sqrt{2}\sin(\gamma_i y) \tag{5.184}$$

where

$$\gamma_i = \frac{\pi\left(i-\frac{1}{2}\right)}{\ell} \tag{5.185}$$

and, according to Eq. (2.93), Ψ_i is given as

$$\Psi_i = \cosh(\alpha_i y) - \cos(\alpha_i y) - \beta_i[\sinh(\alpha_i y) - \sin(\alpha_i y)] \tag{5.186}$$

with α_i and β_i as given in Table 2.1.

The next step in the application of the Ritz method is to spatially discretize the strain energy, kinetic energy, and virtual work expressions. Because of orthogonality of the assumed modes, the strain energy simplifies to

$$U = \frac{1}{2}\left[\frac{EI}{\ell^3}\sum_{i=1}^{N_w}(\alpha_i\ell)^4\eta_i^2 + \frac{GJ}{\ell}\sum_{i=1}^{N_\theta}(\gamma_i\ell)^2\phi_i^2\right] \tag{5.187}$$

The kinetic energy is also considerably simplified because of the orthogonality of the assumed modes and can be written as

$$K = \frac{m\ell}{2}\left(\sum_{i=1}^{N_w}\dot{\eta}_i^2 + b^2r^2\sum_{i=1}^{N_\theta}\dot{\phi}_i^2 - 2bx_\theta\sum_{i=1}^{N_\theta}\sum_{j=1}^{N_w}A_{ij}\dot{\phi}_i\dot{\eta}_j\right) \tag{5.188}$$

where

$$A_{ij} = \frac{1}{\ell}\int_0^\ell \Theta_i\Psi_j dy \qquad i = 1, 2, \ldots, N_\theta \qquad j = 1, 2, \ldots, N_w \tag{5.189}$$

Note the inertial coupling between bending and torsion modes reflected by the term involving A_{ij}.

The virtual work expression can be used to identify the generalized forces

$$\overline{\delta W} = \sum_{i=1}^{N_w}\Xi_{w_i}\delta\eta_i + \sum_{i=1}^{N_\theta}\Xi_{\theta_i}\delta\phi_i \tag{5.190}$$

Thus,

$$\begin{aligned}\Xi_{w_i} &= \int_0^\ell \Psi_i L'\,dy \\ \Xi_{\theta_i} &= \int_0^\ell \Theta_i\left[M'_{\frac{1}{4}} + \left(\frac{1}{2}+a\right)bL'\right]dy\end{aligned} \tag{5.191}$$

where expressions for L' and $M'_{\frac{1}{4}}$ can be found by taking expressions for L and $M_{\frac{1}{4}}$ in Eqs. (5.148) or (5.165) and replacing h with $-w$ and dots with partial derivatives with respect to time. This we carry out for illustrative purposes using Theodorsen theory, for which

$$\begin{aligned}L' &= 2\pi\rho_\infty UbC(k)\left[U\theta - \frac{\partial w}{\partial t} + b\left(\frac{1}{2}-a\right)\frac{\partial\theta}{\partial t}\right] + \pi\rho_\infty b^2\left(U\frac{\partial\theta}{\partial t} - \frac{\partial^2 w}{\partial t^2} - ba\frac{\partial^2\theta}{\partial t^2}\right) \\ M'_{\frac{1}{4}} &= -\pi\rho_\infty b^3\left[U\frac{\partial\theta}{\partial t} - \frac{1}{2}\frac{\partial^2 w}{\partial t^2} + b\left(\frac{1}{8}-\frac{a}{2}\right)\frac{\partial^2\theta}{\partial t^2}\right]\end{aligned} \tag{5.192}$$

Substituting Eqs. (5.183) into Eqs. (5.192), one obtains expressions for the generalized forces

that can be easily put into matrix form:

$$\begin{Bmatrix}\Xi_w\\ \Xi_\theta\end{Bmatrix} = -\pi\rho_\infty b^2\ell \begin{bmatrix}[\,`1\,] & ba[A]^T\\ ba[A] & b^2\left(a^2+\frac{1}{8}\right)[\,`1\,]\end{bmatrix}\begin{Bmatrix}\ddot{\eta}\\ \ddot{\phi}\end{Bmatrix} - \pi\rho_\infty bU\ell \begin{bmatrix}2C(k)[\,`1\,] & -b\left[1+2\left(\frac{1}{2}-a\right)C(k)\right][A]^T\\ 2b\left(\frac{1}{2}+a\right)C(k)[A] & b^2\left(\frac{1}{2}-a\right)\left[1-2\left(\frac{1}{2}+a\right)C(k)\right][\,`1\,]\end{bmatrix}\begin{Bmatrix}\dot{\eta}\\ \dot{\phi}\end{Bmatrix} - \pi\rho_\infty bU^2\ell \begin{bmatrix}[0] & -2C(k)[A]^T\\ [0] & -b(1+2a)C(k)[\,`1\,]\end{bmatrix}\begin{Bmatrix}\eta\\ \phi\end{Bmatrix} \tag{5.193}$$

where $[\,`1\,]$ denotes an identity matrix and [0] denotes a matrix of zeros. Because of limitations inherent in the derivation of Theodorsen's theory, this expression for the generalized forces is valid only for simple harmonic motion.

All that now remains in the application of the Ritz method is to invoke Lagrange's equations to get the generalized equations of motion, which can be written in matrix form as

$$m\ell \begin{bmatrix}[\,`1\,] & -bx_\theta[A]^T\\ -bx_\theta[A] & b^2r^2[\,`1\,]\end{bmatrix}\begin{Bmatrix}\ddot{\eta}\\ \ddot{\phi}\end{Bmatrix} + \begin{bmatrix}\frac{EI}{\ell^3}[\,`B\,] & [0]\\ [0] & \frac{GJ}{\ell}[\,`T\,]\end{bmatrix}\begin{Bmatrix}\eta\\ \phi\end{Bmatrix} = \begin{Bmatrix}\Xi_w\\ \Xi_\theta\end{Bmatrix} \tag{5.194}$$

where elements of the diagonal matrices $[\,`B\,]$ and $[\,`T\,]$ are given by

$$\begin{aligned} B_{ii} &= (\alpha_i\ell)^4\\ T_{ii} &= (\gamma_i\ell)^2\end{aligned} \tag{5.195}$$

The appearance of diagonal matrices $[\,`B\,]$ and $[\,`T\,]$ in the stiffness matrix and the appearances of $[\,`1\,]$ in the mass matrix and generalized forces are due to our choice of basis functions that are orthogonal. Such a choice is not necessary, but it does simplify the discretized equations.

Following the methodology of classical flutter analysis in Section 5.5, one sets

$$\begin{aligned}\eta(t) &= \overline{\eta}\exp(i\omega t)\\ \phi(t) &= \overline{\phi}\exp(i\omega t)\end{aligned} \tag{5.196}$$

where ω is the frequency of the simple harmonic motion. This leads to a flutter determinant that can be solved by following steps similar to those outlined in Section 5.5, the only difference being that there are now more degrees of freedom if either N_w or N_θ exceeds unity.

Let us consider the case in which $N_w = N_\theta = 1$. If we introduce dimensionless constants similar to those in Section 5.5, the equations of motion can be put in the form of Eqs. (5.128), that is,

$$\begin{aligned}&\left\{\mu\left[1-\left(\frac{\omega_w}{\omega}\right)^2\right]+\ell_w\right\}\frac{\overline{\eta}_1}{b} + (-\mu x_\theta+\ell_\theta)A_{11}\overline{\theta} = 0\\ &(-\mu x_\theta+m_w)A_{11}\frac{\overline{\eta}_1}{b} + \left\{\mu r^2\left[1-\left(\frac{\omega_\theta}{\omega}\right)^2\right]+m_\theta\right\}\overline{\theta} = 0\end{aligned} \tag{5.197}$$

Here ℓ_w, ℓ_θ, m_w, and m_θ are defined in a manner similar to the quantities on the right-hand side of Eqs. (5.105) with the loads from Theodorsen theory

$$\begin{aligned}
\ell_w &= 1 - \frac{2iC(k)}{k} \\
\ell_\theta &= a + \frac{i}{k}\left[1 + 2\left(\frac{1}{2} - a\right)C(k)\right] + \frac{2C(k)}{k^2} \\
m_w &= a - \frac{2i\left(\frac{1}{2} + a\right)C(k)}{k} \\
m_\theta &= a^2 + \frac{1}{8} - \frac{\left(\frac{1}{2} - a\right)\left[1 - 2\left(\frac{1}{2} + a\right)C(k)\right]i}{k} + \frac{2\left(\frac{1}{2} + a\right)C(k)}{k^2}
\end{aligned} \tag{5.198}$$

and the fundamental bending and torsion frequencies are

$$\begin{aligned}
\omega_w &= (\alpha_1 \ell)^2 \sqrt{\frac{EI}{m\ell^4}} \\
\omega_\theta &= \frac{\pi}{2}\sqrt{\frac{GJ}{mb^2 r^2 \ell^2}}
\end{aligned} \tag{5.199}$$

Finally, the constant $A_{11} = 0.958641$. It is clear that these equations are in the same form as the ones solved earlier for the typical section and that the influence of wing flexibility for this simplest two-mode case only enters in a minor way, namely, to adjust the coupling terms by a factor of less than 5%. However, because of the relatively complex manner in which this coupling term enters the evaluated flutter determinant, this small change can alter the flutter speed by a more significant amount.

This analysis does not include the effects of material damping. An empirical term, motivated by experimental results, can be added to the stiffness matrix $[K]$ that is proportional to the stiffness matrix and is of the form $ig[K]$. Such a term is thus 90° out of phase with displacement and in phase with velocity. It depends on the amplitude of the motion but not on the frequency. Values of g range between 0.01 and 0.03.

The main purpose of this example is to demonstrate how the tools already presented can be used to conduct a flutter analysis of a flexible wing. Addition of higher modes can certainly affect the results, as can such things as spanwise variations in the mass and stiffness properties, concentrated masses and inertias along the wing, and structural damping. Incorporation of these additional features into the analysis would serve to make the analysis more suitable for realistic flutter calculations. However, to fully capture the realism afforded by these and other important considerations, such as aircraft with delta-wing configurations or very low aspect ratio wings, a full finite element analysis would be necessary. Even in such cases it is typical that flutter analyses based on assumed modes give the analyst a reasonably good idea of the mechanisms of instability. Moreover, the full finite element method can be used to obtain a realistic set of assumed modes that could, in turn, be used in a Ritz analysis similar to that above.

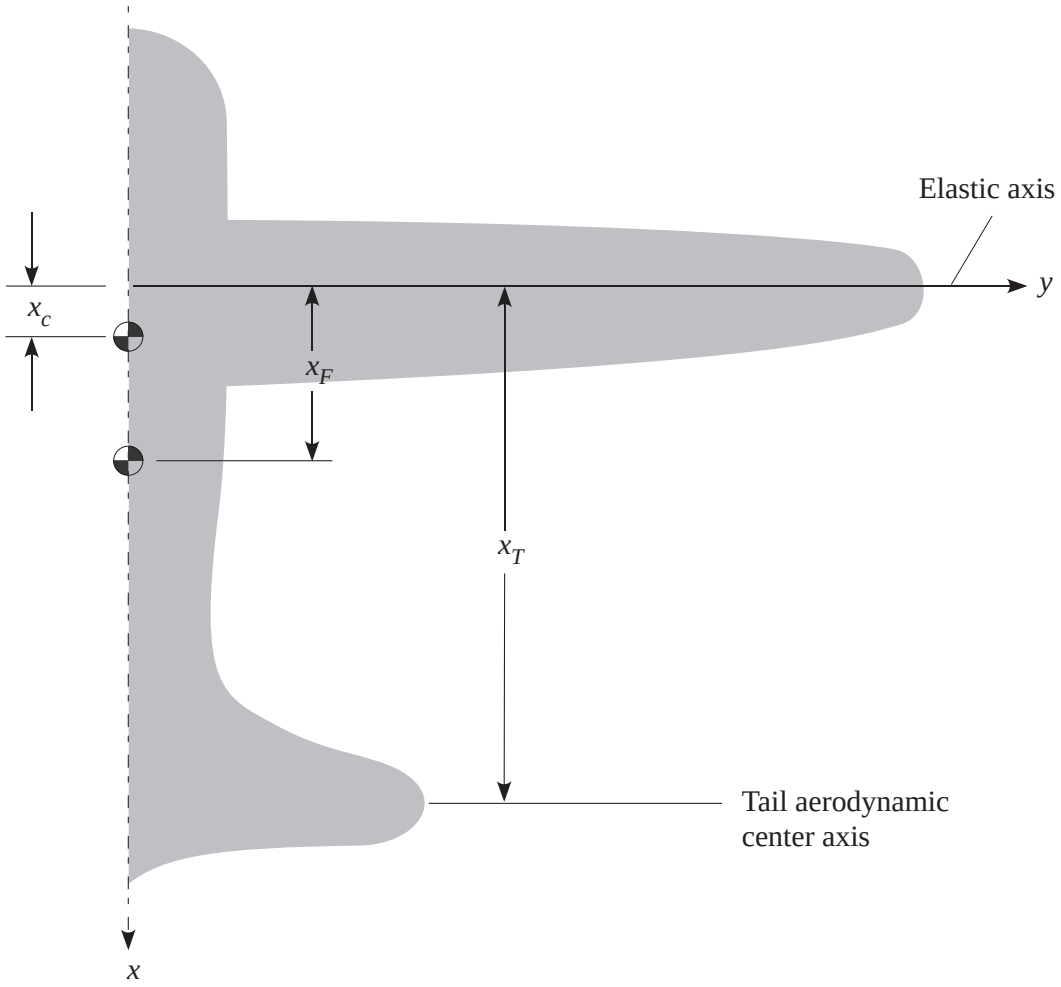

Figure 5.27: Schematic of aircraft for flutter analysis

5.9 Flutter of an Aircraft with Unswept Wings

We can take the equations of the last section and augment them with degrees of freedom for the aircraft rigid-body modes. A schematic of a complete aircraft is shown in Fig. 5.27, except that we do not make use of the elevator. Assuming the fuselage and tail section are very stiff, one can ignore the elastic modes thereof. It is sufficient for our purposes to consider only one elastic bending mode and one elastic torsion mode for the wing, assumed here to be uniform. To illustrate the incorporation of rigid-body modes into the analysis, we

alter the series above as follows:

$$\begin{aligned} w &= \sum_{i=1}^{4} \xi_i W_i \\ \theta &= \sum_{i=1}^{4} \xi_i Q_i \end{aligned} \tag{5.200}$$

where

$$\begin{array}{ll} W_1 = 1 & Q_1 = 0 \\ W_2 = x_c & Q_2 = 1 \\ W_3 = \Psi_1 & Q_3 = 0 \\ W_4 = 0 & Q_4 = \Theta_1 \end{array} \tag{5.201}$$

From this the natures of the two rigid-body degrees of freedom are revealed, with ξ_1 being the translation of the aircraft measured at the aircraft center of mass, and ξ_2 being a rotation about the aircraft center of mass. As a result, the strain energy is written instead as

$$U = \frac{1}{2} \{\xi\}^T \begin{bmatrix} 0 & 0 & 0 & 0 \\ 0 & 0 & 0 & 0 \\ 0 & 0 & \frac{EI(\alpha_1 \ell)^4}{\ell^3} & 0 \\ 0 & 0 & 0 & \frac{GJ(\gamma_1 \ell)^2}{\ell} \end{bmatrix} \{\xi\} \tag{5.202}$$

where $\{\xi\}$ is a column matrix containing the generalized coordinates ξ_i for i =1, 2, 3, 4.

The kinetic energy is more challenging. Here we need to regard the fuselage and tail as one rigid body and also take into account the rigid-body motion of the wings. The aircraft center of mass is located a distance x_c behind the wing elastic axis, and the fuselage center of mass is a distance x_F behind the wing elastic axis. We introduce x_* as the length coordinate along the x axis measured from the aircraft center of mass. Therefore, the velocity of points along the x_* axis is

$$\mathbf{v}_F = (\dot{\xi}_1 - x_* \dot{\xi}_2) \hat{\mathbf{k}} \tag{5.203}$$

Denoting the fuselage mass per unit length along x_* as m_*, we note that

$$\int_F m_* dx_* = M_F (x_F - x_c) \tag{5.204}$$

so that twice the kinetic energy of half the fuselage becomes

$$2K_F = \frac{M_F \dot{\xi}_1^2}{2} - (x_F - x_c) M_F \dot{\xi}_1 \dot{\xi}_2 + \frac{I_F \dot{\xi}_2^2}{2} \tag{5.205}$$

Because of the symmetry we use the "2" on the left hand side to indicate that we only need half the fuselage contribution. Here the fuselage mass is denoted by M_F, the fuselage moment of inertia about the aircraft mass center is I_F, and K_F is the kinetic energy of half

the fuselage. To get the wing contribution we first note that the velocity of a point anywhere within a wing cross section can be written as

$$\mathbf{v}_w = z\left(\dot{\xi}_2 + \dot{\theta}_e\right)\hat{\mathbf{i}} + \left[\dot{\xi}_1 + \dot{w}_e + x_c\dot{\xi}_2 - x\left(\dot{\xi}_2 + \dot{\theta}_e\right)\right]\hat{\mathbf{k}} \tag{5.206}$$

with the subscript e being the elastic terms that make up w and θ and the dots in $\dot{w}$ and $\dot{\theta}$ are partial derivatives with respect to t. This is equivalent to replacing w with $\dot{\xi}_1 + \dot{w}_e + x_c\dot{\xi}_2 - x\left(\dot{\xi}_2 + \dot{\theta}_e\right)$ and θ with $\dot{\xi}_2 + \dot{\theta}_e$ in Eqs. (5.192). Thus, the wing kinetic energy may be written as

$$K_w = \frac{1}{2}\int_0^\ell \left[m\left(\dot{\xi}_1 + \dot{w}_e + x_c\dot{\xi}_2\right)^2 + 2md\left(\dot{\xi}_2 + \dot{\theta}_e\right)\left(\dot{\xi}_1 + \dot{w}_e + x_c\dot{\xi}_2\right) + \rho I_p\left(\dot{\xi}_2 + \dot{\theta}_e\right)^2\right] dy \tag{5.207}$$

or

$$K_w = \frac{1}{2}\int_0^\ell \left\{\dot{\xi}\right\}^T \begin{bmatrix} m & (x_c+d)m & m\Psi_1 & md\Theta_1 \\ (x_c+d)m & \rho I_p + (2x_cd + x_c^2)m & (x_c+d)m\Psi_1 & (\rho I_p + mdx_c)\Theta_1 \\ m\Psi_1 & (x_c+d)m\Psi_1 & m\Psi_1^2 & md\Psi_1\Theta_1 \\ md\Theta_1 & (\rho I_p + mdx_c)\Theta_1 & md\Psi_1\Theta_1 & \rho I_p\Theta_1^2 \end{bmatrix} \left\{\dot{\xi}\right\} dy \tag{5.208}$$

with ρI_p the mass polar moment of inertia of the cross section. We can rewrite this in terms of integrated wing properties, such as its mass

$$M_w = \int_0^\ell m dy \tag{5.209}$$

its moment of inertia

$$I_w = \int_0^\ell \rho I_p dy \tag{5.210}$$

and the following integrals

$$\begin{array}{lll} S_w = \int_0^\ell md\,dy & A_w = \int_0^\ell m\Psi_1\,dy & B_w = \int_0^\ell md\,\Theta_1\,dy \\ C_w = \int_0^\ell md\Psi_1\,dy & D_w = \int_0^\ell \rho I_p\Theta_1\,dy & E_w = \int_0^\ell m\Psi_1^2\,dy \\ F_w = \int_0^\ell md\Psi_1\Theta_1\,dy & G_w = \int_0^\ell \rho I_p\Theta_1^2\,dy & \end{array} \tag{5.211}$$

so that

$$K_w = \frac{1}{2}\left\{\dot{\xi}\right\}^T \begin{bmatrix} M_w & S_w + x_cM_w & A_w & B_w \\ S_w + x_cM_w & I_w + 2x_cS_w + x_c^2M_w & C_w + x_cA_w & D_w + x_cB_w \\ A_w & C_w + x_cA_w & E_w & F_w \\ B_w & D_w + x_cB_w & F_w & G_w \end{bmatrix} \left\{\dot{\xi}\right\} \tag{5.212}$$

and the total kinetic energy is

$$K = \frac{1}{2}\left\{\dot{\xi}\right\}^T \begin{bmatrix} \frac{1}{2}M_F + M_w & \frac{1}{2}M_F(x_c - x_F) + S_w + x_c M_w & A_w & B_w \\ \frac{1}{2}M_F(x_c - x_F) + S_w + x_c M_w & \frac{1}{2}I_F + I_w + 2x_c S_w + x_c^2 M_w & C_w + x_c A_w & D_w + x_c B_w \\ A_w & C_w + x_c A_w & E_w & F_w \\ B_w & D_w + x_c B_w & F_w & G_w \end{bmatrix} \left\{\dot{\xi}\right\} \tag{5.213}$$

The virtual work is altered because of the presence of rigid-body modes. The virtual displacement at the aerodynamic center is written as

$$\overline{\delta \mathbf{r}}_{\text{ac}} = \left[\delta\xi_1 + \delta w_e + x_c\delta\xi_2 - b\left(\frac{1}{2} + a\right)(\delta\xi_2 + \delta\theta_e)\right]\hat{\mathbf{k}} \tag{5.214}$$

Thus, the virtual work contribution for the wing is

$$\overline{\delta W}_w = \int_0^\ell \left\{L'\left[\delta\xi_1 + \delta w_e + x_c\delta\xi_2 - b\left(\frac{1}{2} + a\right)(\delta\xi_2 + \delta\theta_e)\right] + M'_{\frac{1}{4}}(\delta\xi_2 + \delta\theta_e)\right\} dy \tag{5.215}$$

The virtual work is also changed because of the presence of the tail. For this addition, we need the virtual displacement of the tail, given by

$$\overline{\delta \mathbf{r}}_T = (\delta\xi_1 - x_T\delta\xi_2)\hat{\mathbf{k}} \tag{5.216}$$

so that the virtual work contributed by the tail is given by

$$\overline{\delta W}_T = \int_0^{\ell_T} \left[L_T(\delta\xi_1 - x_T\delta\xi_2) + M_T\delta\xi_2\right] dy \tag{5.217}$$

The generalized force is $\Xi_i = \partial(\overline{\delta W})/\partial(\delta\xi_i)$ for i =1, 2, 3, 4. From these expressions, one can form the generalized force in terms of matrices, such that

$$\{\Xi\} = \pi\rho_\infty \int_0^{L_\alpha} [\overline{c}]\, dy \left\{\ddot{\xi}\right\} + \pi U\rho_\infty \int_0^{L_\alpha} \left[\overline{b}\right] dy \left\{\dot{\xi}\right\} + 2\pi U^2 C(k)\rho_\infty \int_0^{L_\alpha} [\overline{a}]\, dy \{\xi\} \tag{5.218}$$

where the length over which one integrates, L_α is ℓ for the wing and ℓ_T for the tail and the integrands depend on whether the contribution is from the wing or tail. The contribution of the wing to $[\overline{c}]$ can be written as

$$[\overline{c}_w] = b^2 \begin{bmatrix} -1 & -ab - x_c & -\Psi_1 & -ab\Theta_1 \\ b(1+a) - x_c & \frac{[8a(1+a)-1]b^2 + 8(b-x_c)x_c}{8} & (b + ab - x_c)\Psi_1 & \frac{b\{[8a(1+a)-1]b - 8ax_c\}\Theta_1}{8} \\ -\Psi_1 & -(ab + x_c)\Psi_1 & -\Psi_1^2 & -ab\Theta_1\Psi_1 \\ (1+a)b\Theta_1 & \frac{b\{[8a(1+a)-1]b + 8(1+a)x_c\}\Theta_1}{8} & (1+a)b\Theta_1\Psi_1 & \frac{[8a(1+a)-1]b^2\Theta_1^2}{8} \end{bmatrix} \tag{5.219}$$

The contribution of the wing to $[\overline{b}]$ is

$$[\overline{b}_w] = b^2[\overline{b}_{w_1}] + bC(k)[\overline{b}_{w_2}] \tag{5.220}$$

with

$$[\overline{b}_{w_1}] = \begin{bmatrix} 0 & 1 & 0 & \Theta_1 \\ 0 & x_c - b\left(a+\frac{3}{2}\right) & 0 & x_c - b\left(a+\frac{3}{2}\right)\Theta_1 \\ 0 & \Psi_1 & 0 & \Theta_1\Psi_1 \\ 0 & -b\left(a+\frac{3}{2}\right)\Theta_1 & 0 & -b\left(a+\frac{3}{2}\right)\Theta_1^2 \end{bmatrix} \tag{5.221}$$

and

$$[\overline{b}_{w_2}] = \begin{bmatrix} -2 & b(1-2a)-2x_c & -2\Psi_1 & b(1-2a)\Theta_1 \\ b(1+2a)-2x_c & \frac{[b(1+2a)-2x_c][(2a-1)b+2x_c]}{2} & [b(1+2a)-2x_c]\Psi_1 & \frac{(2a-1)b(b+2ab-2x_c)\Theta_1}{2} \\ -2\Psi_1 & [b(1-2a)-2x_c]\Psi_1 & -2{\Psi_1}^2 & (1-2a)b\Theta_1\Psi_1 \\ (1+2a)b\Theta_1 & \frac{(1+2a)b[(2a-1)b+2x_c]\Theta_1}{2} & (1+2a)b\Theta_1\Psi_1 & \frac{\left(4a^2-1\right)b^2\Theta_1^2}{2} \end{bmatrix} \tag{5.222}$$

The contribution of the wing to $[\overline{a}]$ is

$$[\overline{a}_w] = b\begin{bmatrix} 0 & 1 & 0 & \Theta_1 \\ 0 & x_c - b\left(a+\frac{1}{2}\right) & 0 & \left[x_c - b\left(a+\frac{1}{2}\right)\right]\Theta_1 \\ 0 & \Psi_1 & 0 & \Theta_1\Psi_1 \\ 0 & -b\left(a+\frac{1}{2}\right)\Theta_1 & 0 & -b\left(a+\frac{1}{2}\right)\Theta_1^2 \end{bmatrix} \tag{5.223}$$

The contribution of the tail is a bit simpler, since only rigid body degrees of freedom are involved. The semi-chord of the tail is denoted as b_T, the value of a is taking to be -1/2 (placing the reference line at the quarter chord) and the lift and pitching moment may be written as in Eqs. (5.192) with w replaced by $\xi_1 + x_T\xi_2$ and θ by ξ_2. Thus, the contribution of the tail to $[\overline{c}]$ can be written as

$$[\overline{c}_T] = b_T^2\begin{bmatrix} -1 & \frac{b_T}{2} - x_T & 0 & 0 \\ \frac{b_T}{2} - x_T & (b_T - x_T)x_T - \frac{3b_T^2}{8} & 0 & 0 \\ 0 & 0 & 0 & 0 \\ 0 & 0 & 0 & 0 \end{bmatrix} \tag{5.224}$$

The contribution of the tail to $[\overline{b}]$ can be written as

$$[\overline{b}_T] = b_T\begin{bmatrix} -2C(k) & b_T + 2C(k)(b_T - x_T) & 0 & 0 \\ -2C(k)x_T & -(b_T - x_T)[b_T - 2C(k)x_T] & 0 & 0 \\ 0 & 0 & 0 & 0 \\ 0 & 0 & 0 & 0 \end{bmatrix} \tag{5.225}$$

Finally, the contribution of the tail to $[\overline{a}]$ can be written as

$$[\overline{a}_T] = b_T\begin{bmatrix} 0 & 1 & 0 & 0 \\ 0 & x_T & 0 & 0 \\ 0 & 0 & 0 & 0 \\ 0 & 0 & 0 & 0 \end{bmatrix} \tag{5.226}$$

To solve these equations, one must invoke the classical flutter solution technique or use the k method, both of which rely on the assumption of simple harmonic motion with $\{\xi(t)\} = \left\{\hat{\xi}\right\} \exp(i\omega t)$. The reduced frequency must be defined in terms of reference values of the semi-chord. That is, $k = b_r\omega/U$ where b_r is a reference value of the semi-chord for the wing or the tail. For the k method, the governing equations will take the form

$$-\omega^2 [M] \left\{\hat{\xi}\right\} + [K] \left\{\hat{\xi}\right\} = \rho_\infty \omega^2 [A] \left\{\hat{\xi}\right\} \tag{5.227}$$

with $\pi\omega^2 [A]$ being all the aerodynamic terms from the generalized forces, and the matrix $[A]$ is complex. Now adding the artificial damping one obtains

$$[[M] + \rho_\infty [A] - Z [K]] \left\{\hat{\xi}\right\} = \{0\} \tag{5.228}$$

where

$$Z = \frac{1 + ig}{\omega^2} \tag{5.229}$$

The form of Eq. (5.228) becomes

$$\begin{bmatrix} B_{rr} & B_{re} \\ B_{er} & B_{ee} \end{bmatrix} \left\{\begin{matrix} \hat{\xi}_r \\ \hat{\xi}_e \end{matrix}\right\} = Z \begin{bmatrix} 0 & 0 \\ 0 & K_{ee} \end{bmatrix} \left\{\begin{matrix} \hat{\xi}_r \\ \hat{\xi}_e \end{matrix}\right\} \tag{5.230}$$

This is an eigenvalue problem, but the matrix on the right-hand side is singular. However,

$$[B_{rr}] \left\{\hat{\xi}_r\right\} + [B_{re}] \left\{\hat{\xi}_e\right\} = 0 \tag{5.231}$$

so that

$$\left\{\hat{\xi}_r\right\} = -[B_{rr}]^{-1} [B_{re}] \left\{\hat{\xi}_e\right\} \tag{5.232}$$

and

$$\left[[B_{ee}] - [B_{er}] [B_{rr}]^{-1} [B_{re}]\right] \left\{\hat{\xi}_e\right\} = Z [K_{ee}] \left\{\hat{\xi}_e\right\} \tag{5.233}$$

which is now a standard eigenvalue problem.

Thus, the problem reduces to a matrix, the size of which depends on the number of assumed elastic modes. The solution procedure is the same as without rigid-body modes. A similar situation would be found with the p method.

Additional configuration parameters that are of interest include sweep and stores. The procedure used in static aeroelasticity to incorporate sweep effects will also work for flutter. Just as sweep increases divergence speed, it also increases flutter speed. The increase is nominally between $1/\cos\Lambda$ and $1/\cos\sqrt{\Lambda}$ for small sweep angles; see Fig. 5.28.

It has been confirmed by wind-tunnel tests that such features as nacelles, stores, and tip pods definitely change flutter boundaries. There are three primary effects. First, the added mass has the effect of reducing natural frequencies (both bending and torsion). Second, the

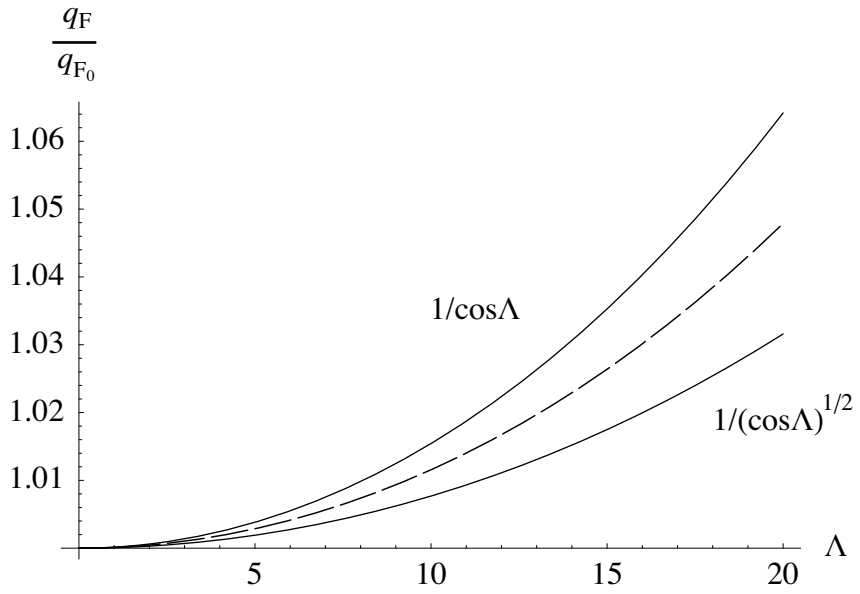

Figure 5.28: Nominal increase in flutter speed with sweep back

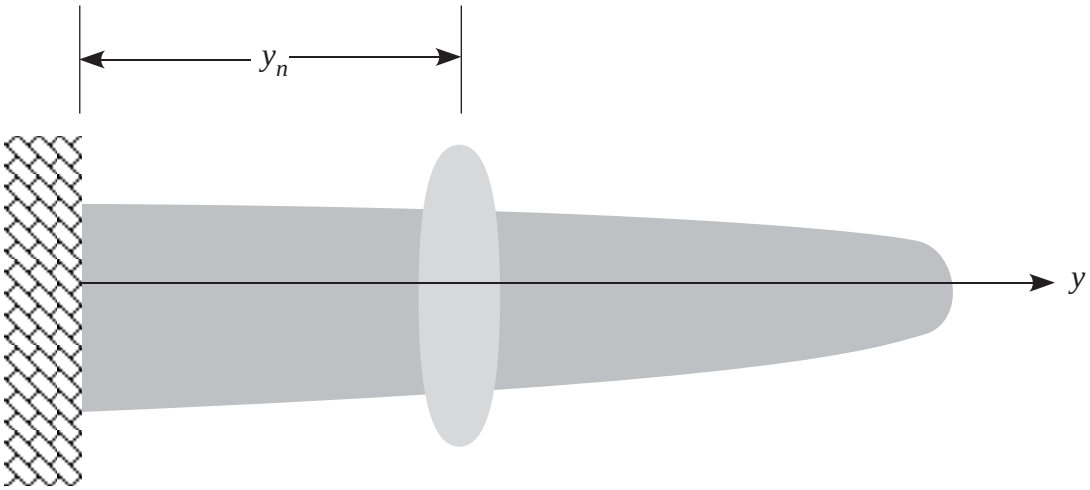

Figure 5.29: Top view of a nacelle on a wing

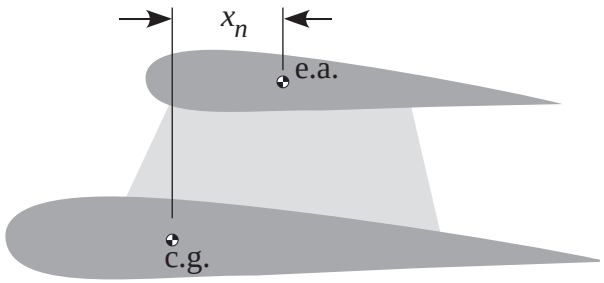

Figure 5.30: Side view of a nacelle on a wing

mass center of the wing moves so that the motion is shifted. Finally, there is an influence of aerodynamics due to flow interactions and drag.

One may describe a nacelle or a bomb in terms of the variables x_n and y_n, shown in Figs. 5.29 and 5.30. Moving the nacelle along the wing can have either a stabilizing or destabilizing effect, as depicted in Fig. 5.31. Moving the nacelle forward has a stabilizing effect, a typical pattern of which is shown in Fig. 5.32.

Another configuration variable that can influence flutter is the deflection of an aileron or control surface. This entails adding one degree of freedom to the complete aircraft model above, ξ_5, the aileron deflection. Rather than being prescribed, we now consider it as an unknown function of time. We can write the displacement of points along the wing section as

$$w(x,y,t) = \sum_{i=1}^{4}(W_i + xQ_i)\xi_i(t) + \langle x - x_k \rangle \, \xi_5(t) \tag{5.234}$$

where the last term, similar to the way the delta wing was treated, only applies over the wing where the aileron exists. The angle brackets mean that the term is only non-zero when $x > x_k$ (Macauley brackets), where x_k is the location along the airfoil chordline of the aileron hinge.

The kinetic energy is

$$K = K_{\text{old}} + \frac{1}{2}\left\{\dot{\xi}\right\}^T \begin{bmatrix} 0 & 0 & 0 & 0 & m_{15} \\ 0 & 0 & 0 & 0 & m_{25} \\ 0 & 0 & 0 & 0 & m_{35} \\ 0 & 0 & 0 & 0 & m_{45} \\ m_{15} & m_{25} & m_{35} & m_{45} & m_{55} \end{bmatrix} \frac{1}{2}\left\{\dot{\xi}\right\} \tag{5.235}$$

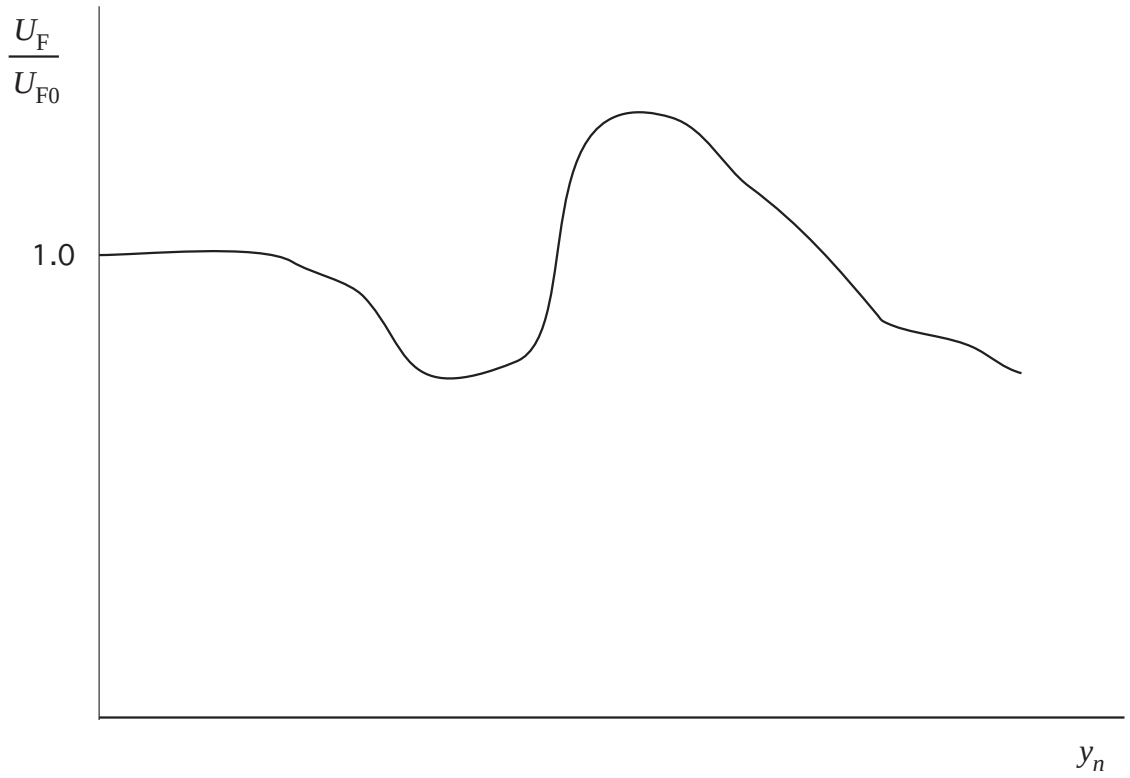

Figure 5.31: Flutter speed versus position along wing

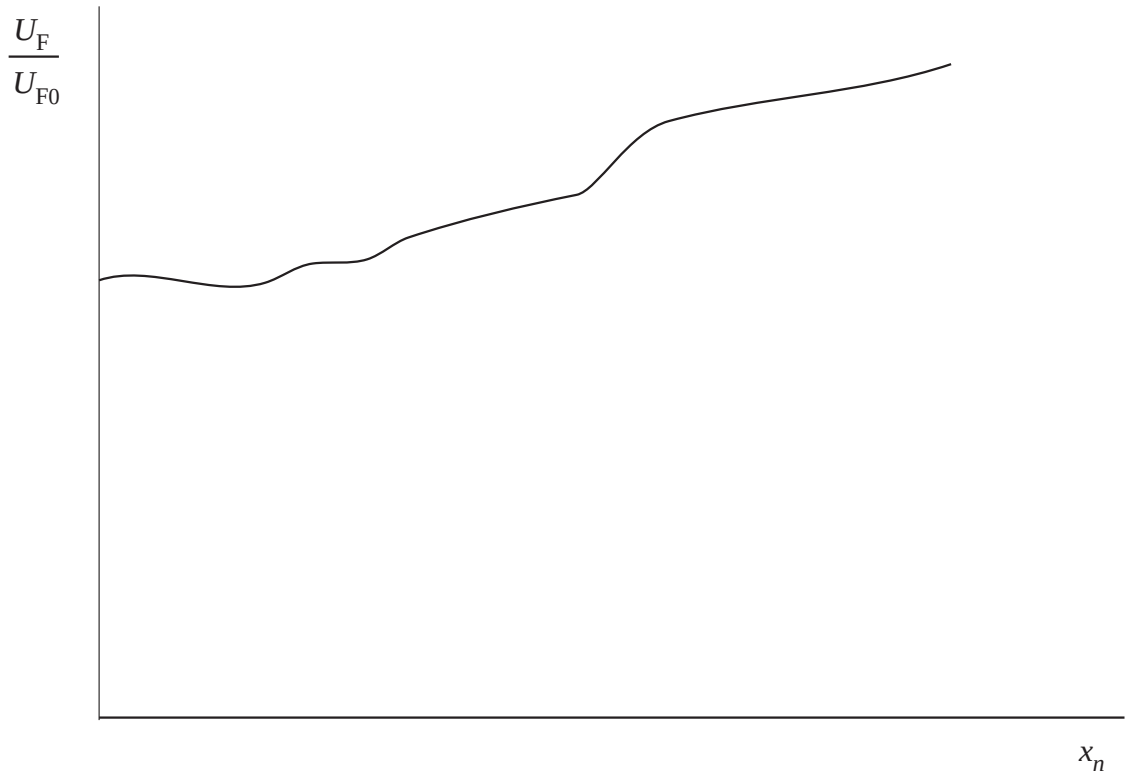

Figure 5.32: Flutter speed versus fore/aft position

where K_{old} is the kinetic energy from Eq. (5.213) and

$$\begin{aligned} m_{i5} &= \int_0^\ell \int_{\text{l.e.}}^{\text{t.e.}} m(x,y)\left[W_i + xQ_i\right]\langle x - x_k\rangle\, dxdy \quad i = 1,2,3,4 \\ &= \int_0^\ell \int_{\text{l.e.}}^{\text{t.e.}} m(x,y)\left\{W_i\langle x - x_k\rangle + Q_i\left[\langle x - x_k\rangle^2 + x_k\langle x - x_k\rangle\right]\right\} dxdy \quad i = 1,2,3,4 \\ m_{55} &= \int_0^\ell \int_{\text{l.e.}}^{\text{t.e.}} m(x,y)\langle x - x_k\rangle^2\, dxdy \end{aligned} \tag{5.236}$$

Introducing

$$\begin{aligned} S_\beta(y) &= \int_{\text{l.e.}}^{\text{t.e.}} m(x,y)\langle x - x_k\rangle\, dx \\ I_\beta(y) &= \int_{\text{l.e.}}^{\text{t.e.}} m(x,y)\langle x - x_k\rangle^2\, dx \end{aligned} \tag{5.237}$$

one may write

$$\begin{aligned} m_{i5} &= \int_0^\ell \left\{S_\beta(y)W_i + \left[I_\beta(y) + x_k S_\beta(y)\right]Q_i\right\} dy \\ m_{55} &= \int_0^\ell I_\beta(y)dy \end{aligned} \tag{5.238}$$

The strain energy changes only a bit:

$$U = U_{\text{old}} + \frac{1}{2}\{\xi\}^T \begin{bmatrix} 0 & 0 & 0 & 0 & 0 \\ 0 & 0 & 0 & 0 & 0 \\ 0 & 0 & 0 & 0 & 0 \\ 0 & 0 & 0 & 0 & 0 \\ 0 & 0 & 0 & 0 & k_{55} \end{bmatrix} \frac{1}{2}\{\xi\} \tag{5.239}$$

where U_{old} is the strain energy from Eq. (5.202).

The aerodynamics changes by the need to incorporate terms involving δ, $\dot{\delta}$, and $\ddot{\delta}$, which in classical flutter analysis amounts to adding complex coefficients to $\overline{\delta}$ in equations such as Eqs. (5.105).

Results from a flutter analysis with three modes typically have the form of Fig. 5.33. The aileron mode typically goes unstable and then becomes stable again. This is generally a "mild flutter" in that a small amount of structural damping will overpower it. Other remedies include increasing the control system stiffness, changing the mass balance S_β of the aileron, and reducing the mass coupling terms m_{i5} for $i = 1$, 2, 3, and 4.

Other parts of the aircraft besides wings and control surfaces can exhibit flutter. Flutter also can take place involving other modes, such as antisymmetric modes (recalling that we analyzed only the symmetric case). Consider the antisymmetric behavior of the aircraft.

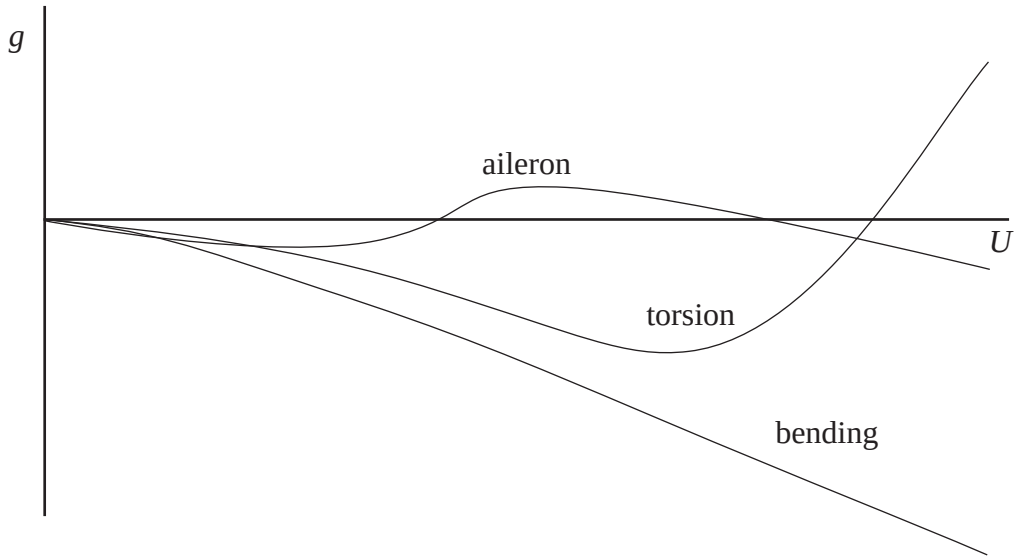

Figure 5.33: Typical behavior of g for bending, torsion, and aileron modes

One may let ξ_1 be the rigid-body roll degree of freedom, ξ_2 the first wing bending mode, ξ_3 the first wing torsion mode, and ξ_4 the aileron mode.

There is the possibility of an instability of the aft fuselage and tail, such that ξ_1 is the first aft bending mode of the aft fuselage/tail, ξ_2 is the first bending of the horizontal tail, and ξ_3 is the first torsion of the horizontal tail. Another instability of the aft fuselage portion involves ξ_1 as the rigid-body pitch of the aircraft, ξ_2 is the first fuselage torsion mode, ξ_3 is the first bending mode of the horizontal tail, ξ_4 is the first torsion of the horizontal tail, and ξ_5 is the horizontal tail aileron deflection.

Specific parts of an aircraft can be analyzed separately, and 20 – 25 modes are typically needed to analyze the flutter of a full aircraft. It is necessary to identify possible couplings between modes of one component with another.

5.10 Flutter Boundary Characteristics

The preceding sections have described procedures for the determination of the flutter boundary in terms of altitude, speed and Mach number. For a standard atmosphere any two of these conditions is sufficient to describe the flight condition. The final flutter boundary is usually presented in terms of a dimensionless flutter speed as $U_F/(b\omega_\theta)$. This parameter is similar to the reciprocal of reduced frequency and is called the reduced velocity. A useful presentation of this reduced flutter speed as a function of the mass ratio, $\mu = m/(\pi\rho_\infty b^2)$, is illustrated in Fig. 5.34. It is immediately apparent that the flutter speed increases in a nearly linear fashion with increasing mass ratio. This result can be interpreted in either of two ways. For a given configuration, variations in μ would correspond to changes in atmo-

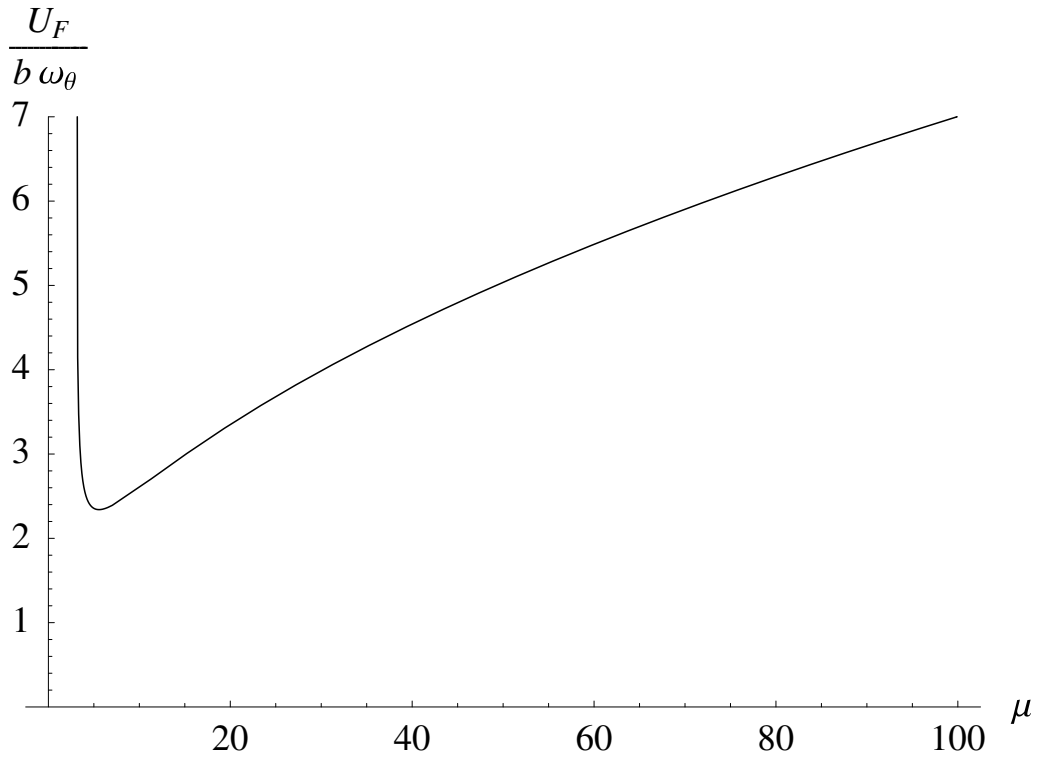

Figure 5.34: Plot of dimensionless flutter speed versus mass ratio for the case $\sigma = 1/\sqrt{10}$, $r = 1/2$, $x_\theta = 0$, and $a = -3/10$

Vehicle Type	$\mu = \frac{m}{\pi\rho_\infty b^2}$
Gliders and Ultralights	5 – 15
General Aviation	10 – 20
Commercial Transports	15 – 30
Attack Aircraft	25 – 55
Helicopter Blades	65 – 110

Table 5.2: Variation of mass ratio for typical vehicle types

spheric density and thus altitude. In such a case the mass ratio increases with increasing altitude. This implies that any flight vehicle is more susceptible to aeroelastic flutter at low altitudes than it is at higher ones.

A second interpretation of the mass ratio is related to its numerical value for any fixed altitude. The value of μ will depend on the type of flight vehicle as reflected by its mass per unit span, m. Table 5.2 gives some vehicle configurations and typical mass ratio values for atmospheric densities between sea level and 10,000 ft.

The flutter boundary is very sensitive to the dimensionless parameters. In Fig. 5.35, for example, one sees a dramatic change in the flutter speed versus the frequency ratio $\sigma = \omega_h/\omega_\theta$. The significant drop in the flutter speed for $x_\theta = 0.2$ around $\sigma = 1.4$ is of utmost practical importance. There are certain frequency ratios at which the flutter speed becomes very small, depending on the values of the other parameters. This dip will be observed in the plot of flutter speed versus frequency ratio for the wings of most high-performance aircraft, which have relatively large mass ratios and positive static unbalances. The chordwise offsets also have a strong influence on the flutter speed, as seen in Fig. 5.36. Indeed, a small change in the mass center location can lead to a large increase in the flutter speed. The mass center location, e, cannot be changed without simultaneously changing the dimensionless radius of gyration, r, but the relative change in the flutter speed for a small percentage change in the former is more than for a similar percentage change in the latter. These facts have led to a concept of mass balancing wings to alleviate flutter, similar to the way control surfaces are mass balanced. If the center of mass is moved forward of the reference point, the flutter speed is generally relatively high. Unfortunately, however, this is not easily accomplished, but fortunately a large change is not usually needed to ensure safety. It is noted that care must be exercised in examining changes in other parameters caused by such changes in the mass distribution. For example, the torsional frequency may be altered significantly in the process of changing the radius of gyration. Finally, we note that the flutter frequency for bending-torsion flutter is somewhere in between ω_h and ω_θ, where normally $\sigma < 1$. However, situations do arise in which the flutter frequency may exceed ω_θ.

It is important to note there are some combinations of the chordwise offset parameters e and a for which the present simplified theories indicate flutter is not possible. Bisplinghoff, Ashley, and Halfman (1955) classify the effects of the chordwise offsets e and a in terms of

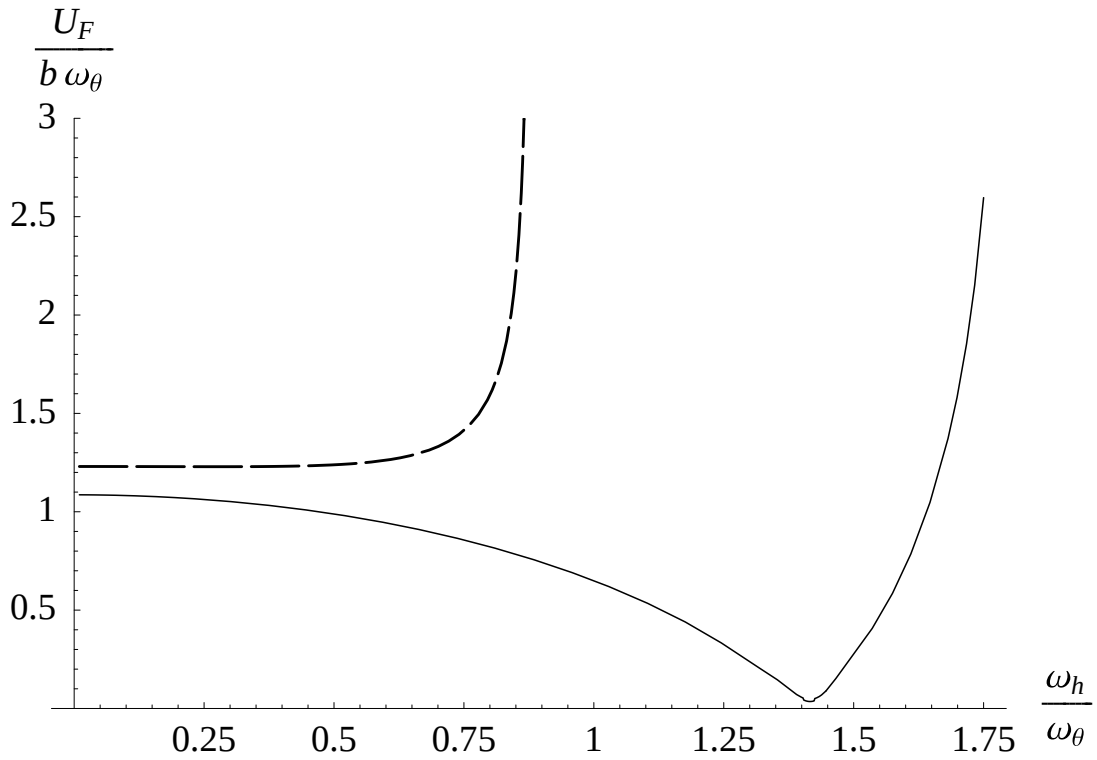

Figure 5.35: Plot of dimensionless flutter speed versus frequency ratio for the case $\mu = 3$, $r = 1/2$ and $a = -1/5$ where the solid line is for $x_\theta = 0.2$ and the dashed line is for $x_\theta = 0.1$

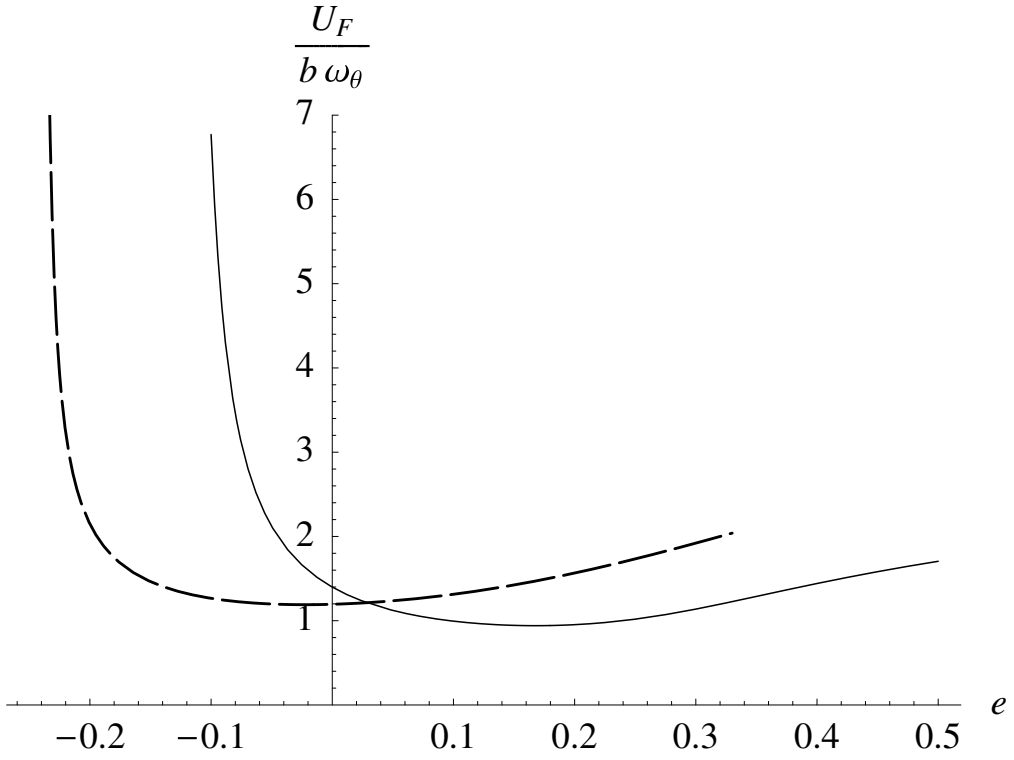

Figure 5.36: Plot of dimensionless flutter speed versus e for the case $\mu = 10$, $\sigma = 1/\sqrt{2}$, and $r = 1/2$; the solid line is for $a = 0$ and the dashed line is for $a = 0.2$

small and large σ. For small σ, they note that flutter can only happen when the mass center is behind the quarter-chord (i.e., when $e > -1/2$) and thus it cannot happen when $e \leq -1/2$. For large σ, flutter can only happen when the elastic axis is in front of the quarter-chord (i.e., when $a < -1/2$) and thus it cannot happen when $a \geq -1/2$. Moreover, for the typical section model in combination with the aerodynamic models presented herein, flutter does not appear to happen for any combination of σ and r when the mass centroid, elastic axis, and aerodynamic center all coincide (i.e., when $e = a = -1/2$). Even if this prediction of the analysis is correct, practically speaking, it is very difficult to achieve coincidence of these points in wing design. Remember, however, that all these statements are made with respect to simplified models. One needs to analyze real wings in a design setting using powerful tools, such as NASTRAN or ASTROS. Indeed, bending-torsion flutter is a very complicated phenomenon, and it seems to defy all our attempts at generalization. Additional discussion of these phenomena, along with a large body of solution plots, can be found in Bisplinghoff, Ashley, and Halfman (1955).

Additional insight may be gained by taking the flutter speed calculated from quasi-steady theory in Section 5.4.2, which may be ascertained from the Routh-Hurwitz stability criteria in closed form. These formulae are long and complex, but they may be reduced to a simpler form by assuming that $\mu > 10$ and that $\sigma^2 < 1/10$, yielding

$$V_F = \frac{U_F}{b\omega_\theta} \approx \frac{r\sqrt{\mu}\sqrt{1 + x_\theta\,(1 + 2\,a + 2\,x_\theta)}}{\sqrt{1 + 2\,a + 2\,x_\theta}\sqrt{1 + 2\,r^2 + (1 + 2\,a)\;x_\theta}} \tag{5.240}$$

From this one can determine that the flutter speed increases if r or μ increase and when x_θ decreases. If the flight vehicle flies in the transonic regime, there may be a dip in the flutter speed when plotted against the Mach number caused by shock effects. The flutter speed is usually increased in industry by (a) increasing by r (increasing the polar moment of inertia), (b) ω_θ (usually by increasing torsional stiffness), (c) adjusting the mass balance to try to drive x_θ to zero, and (d) adding damping or servo-controls to the system.

The final flutter boundary can be presented in numerous ways for any given flight vehicle. The manner in which it is illustrated depends on the engineering purpose it is intended to serve. One possible presentation of the flutter boundary is to superpose it on the vehicle's flight envelope. A typical flight envelope for a Mach 2 attack aircraft is illustrated in Fig. 5.37 with two flutter boundaries indicated by the curves marked "No. 1" and "No. 2." The shaded region above the flutter boundaries, being at higher altitudes, corresponds to stable flight conditions; below the boundaries flutter will be experienced. Flutter boundary no. 1 indicates that for a portion of the intended flight envelope, the vehicle will experience flutter. It should be noted that these conditions of instability correspond to a flight Mach number near unity (transonic flow) and high dynamic pressure. This observation can be generalized by saying that a flight vehicle is more susceptible to aeroelastic flutter for conditions of (1) lower altitude, (2) transonic flow, and (3) higher dynamic pressure.

If it is determined that the vehicle will experience flutter in any portion of its intended flight envelope, it is necessary to make appropriate design changes to eliminate the instability

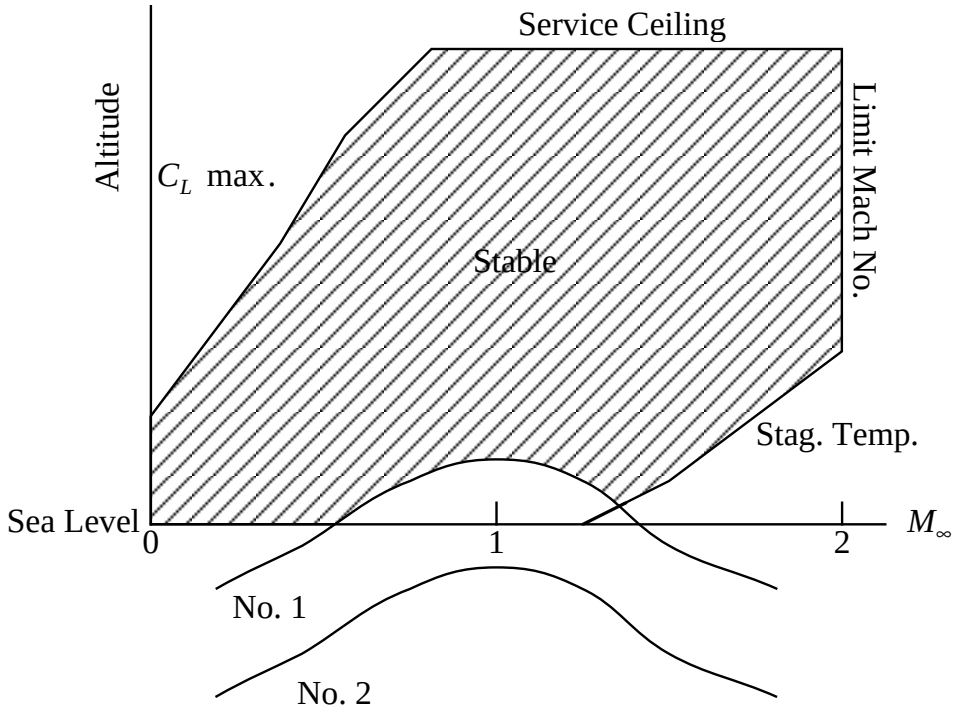

Figure 5.37: Flight envelope for typical Mach 2 fighter

for such conditions. These changes may involve alteration of the inertial, elastic or aerodynamic properties of the configuration. Many times small variations in all three provide the best compromise. Flutter boundary no. 2 is indicative of a flutter-safe vehicle. Note that at the minimum altitude transonic condition there appears to be a safety margin with respect to flutter instability. All flight vehicle specifications require such a safety factor, which is generally called the "flutter margin." Most specifications require that the margin be 15% over the limit equivalent airspeed. In other words the minimum flutter speed at sea level should not be less that 1.15 times the airspeed for the maximum expected dynamic pressure as evaluated at sea level. The process generally requires analysis, wind-tunnel testing of models, ground vibration tests (to determine the natural frequencies), full-scale wind-tunnel tests where appropriate and possible, and flight testing.

5.11 Dynamic Response and Transient Stresses

Even if a flight vehicle is stable, it can be rendered unsafe for flight because of transient stresses that induce fatigue in key components. Moreover, transient responses to gusts and other unsteady loads can make the aircraft ride unpleasant or the pilot's duties far more involved and thus less safe. In this section we consider a few of the more well known dynamic response problems encountered in aircraft.

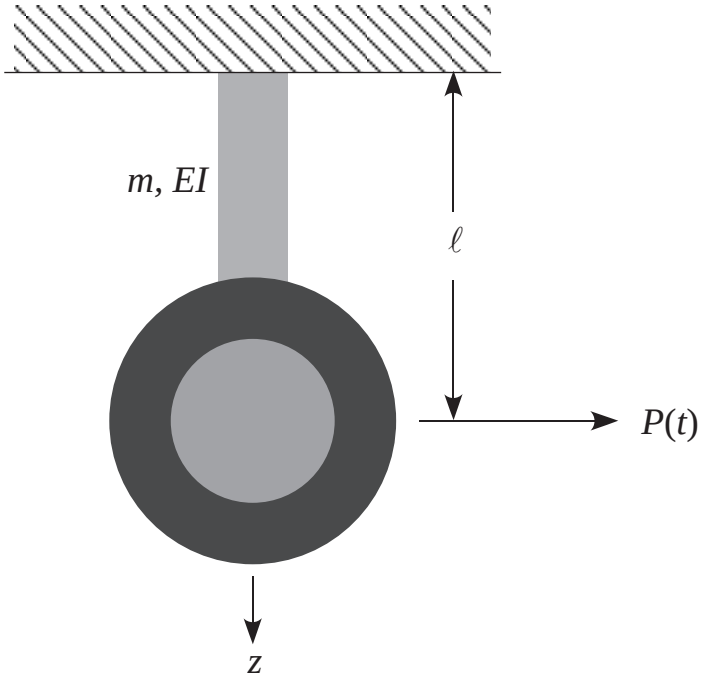

Figure 5.38: Schematic of flexible landing gear undergoing time-dependent force

5.11.1 Landing Gear

Consider the landing gear depicted in Fig. 5.38. Given the approximation of an impulsive load

$$P(t) = \begin{cases} P_m \sin(\Omega t) & t \leq \frac{\pi}{\Omega} \\ 0 & t \geq \frac{\pi}{\Omega} \end{cases} \tag{5.241}$$

where the larger the value of Ω, the more nearly the load approaches a true impulse. If the strut is assumed to be rigid, the moment at the root of the strut can be computed directly as

$$M_{\text{root}} = \ell P(t) \tag{5.242}$$

which follows the force trend, as expected.

In reality, the strut is not rigid, but is flexible and will vibrate under the load. Let's use a modal approximation to analyze the behavior. Let

$$v(z,t) = \sum_{i=1}^{N} \xi_i(t)\psi_i(z) \tag{5.243}$$

where $\psi_i(z)$ are the free-vibration bending modes for a clamped-free beam; see section 2.2.4. Assuming the strut to be uniform and ignoring the mass of the wheel, the kinetic energy is thus

$$K = \frac{m\ell}{2} \left\{\dot{\xi}\right\}^T [\,`1`\,] \left\{\dot{\xi}\right\} \tag{5.244}$$

and the strain energy is

$$U = \frac{EI}{2\ell^3} \{\xi\}^T [\grave{}\, \alpha^4 \,\acute{}] \{\xi\} \tag{5.245}$$

where the elements of the diagonal matrix $[\grave{}\, \alpha^4 \,\acute{}]$ are the separation constants, such that the natural frequencies are given by

$$\omega_i^2 = \frac{EI\alpha_i^4}{m} \tag{5.246}$$

The separation constants α_i are given in Table 2.1. The virtual work of the applied load is

$$\overline{\delta W} = \{\delta\xi\}^T \psi_i(\ell) = 2 \{\delta\xi\}^T (-1)^{i+1} \tag{5.247}$$

With all the above in place, the equations of motion are

$$\left\{\ddot{\xi}\right\} + [\grave{}\, \omega^2 \,\acute{}] \{\xi\} = \frac{2P(t)}{m\ell} \begin{Bmatrix} 1 \\ -1 \\ 1 \\ \vdots \end{Bmatrix} \tag{5.248}$$

This is a set of uncoupled equations, the i^{th} of which is

$$\ddot{\xi}_i + \omega_i^2 \xi_i = \frac{2P(t)(-1)^{i+1}}{m\ell} \tag{5.249}$$

Assuming the strut to be at rest at $t = 0$, we find that

$$\xi_i(0) = \dot{\xi}_i(0) = 0 \tag{5.250}$$

Therefore the solution can be split into two parts:

$$\begin{array}{lll} \xi_i = & A_i \sin(\omega_i t) + B_i \cos(\omega_i t) + C_i \sin(\Omega t) & t \le \frac{\pi}{\Omega} \\ \xi_i = & D_i \sin(\omega_i t) + E_i \cos(\omega_i t) & t \ge \frac{\pi}{\Omega} \end{array} \tag{5.251}$$

with the solution and its first time derivative being continuous at $t = \pi/\Omega$.

First we note that $\xi_i(0) = 0 = B_i$. Next, because $\dot{\xi}_i(0) = 0$ one finds that

$$\dot{\xi}_i(0) = 0 = \omega_i A_i + \Omega C_i \tag{5.252}$$

so that

$$C_i = -\frac{\omega_i A_i}{\Omega} \tag{5.253}$$

Thus, for the first time interval we have

$$\xi_i = A_i \left[\sin(\omega_i t) - \frac{\omega_i}{\Omega} \sin(\Omega t)\right] \tag{5.254}$$

Finally, we can find A_i by substituting back into the governing differential equation:

$$\ddot{\xi}_i + \omega_i^2 \xi_i = A_i \left(\Omega\omega_i - \frac{\omega_i^3}{\Omega} \right) \sin(\Omega t) = \frac{2P_m \sin(\Omega t)(-1)^{i+1}}{m\ell} \tag{5.255}$$

so that

$$A_i = \frac{2P_m(-1)^{i+1}\Omega}{m\ell\omega_i \left(\Omega^2 - \omega_i^2\right)} \tag{5.256}$$

and

$$\xi_i = \frac{2P_m(-1)^{i+1}\Omega}{m\ell\omega_i \left(\Omega^2 - \omega_i^2\right)} \left[\sin(\omega_i t) - \frac{\omega_i}{\Omega} \sin(\Omega t) \right] \qquad t \le \frac{\pi}{\Omega} \tag{5.257}$$

At the start of the second interval

$$\begin{aligned} \xi\left(\frac{\pi}{\Omega}\right) =& \frac{2P_m\Omega(-1)^{i+1}}{m\ell\omega_i \left(\Omega^2 - \omega_i^2\right)} \sin\left(\frac{\pi\omega_i}{\Omega}\right) = D_i \sin\left(\frac{\pi\omega_i}{\Omega}\right) + E_i \cos\left(\frac{\pi\omega_i}{\Omega}\right) \\ \dot{\xi}\left(\frac{\pi}{\Omega}\right) =& \frac{2P_m\Omega(-1)^{i+1}}{m\ell \left(\Omega^2 - \omega_i^2\right)} \left[1 + \cos\left(\frac{\pi\omega_i}{\Omega}\right) \right] = \omega_i D_i \cos\left(\frac{\pi\omega_i}{\Omega}\right) - \omega_i E_i \sin\left(\frac{\pi\omega_i}{\Omega}\right) \end{aligned} \tag{5.258}$$

the solution of which yields

$$\begin{aligned} D_i =& \frac{2P_m\Omega(-1)^{i+1}}{m\ell\omega_i \left(\Omega^2 - \omega_i^2\right)} \left[1 + \cos\left(\frac{\pi\omega_i}{\Omega}\right) \right] \\ E_i =& -\frac{2P_m\Omega(-1)^{i+1}}{m\ell\omega_i \left(\Omega^2 - \omega_i^2\right)} \sin\left(\frac{\pi\omega_i}{\Omega}\right) \end{aligned} \tag{5.259}$$

Putting this all together for the second interval, we can write

$$\xi_i = \frac{2P_m\Omega(-1)^{i+1}}{m\ell\omega_i \left(\Omega^2 - \omega_i^2\right)} \left\{ \sin(\omega_i t) + \sin\left[\omega_i \left(t - \frac{\pi}{\Omega} \right) \right] \right\} \qquad t \ge \frac{\pi}{\Omega} \tag{5.260}$$

For both intervals, it can be seen that the response contributed by higher modes may be less significant because of the presence of ω_i in the denominator. However, when the frequency of the pulse Ω is close to one of the natural frequencies, the influence of that mode may be accentuated. When the frequency of the pulse (Ω) is smaller than the first mode frequency, then only a few modes are needed. When it is much larger, as in an actual impulse, many modes may be required.

To look at the influence of the higher modes, let's consider the displacement at the lower end of the gear, which can be written as

$$v(\ell, t) = 2 \sum_{i=1}^{N} \xi_i(t)(-1)^{i+1} \tag{5.261}$$

We will consider three cases: a "quasi-static" load with $\Omega = 0.5\omega_1$, a "dynamic" load with $\Omega = 10\omega_1$, and a "quasi-impulsive" case with $\Omega = 25\omega_1$. Note that $\omega_2 = 6.26689\omega_1$,

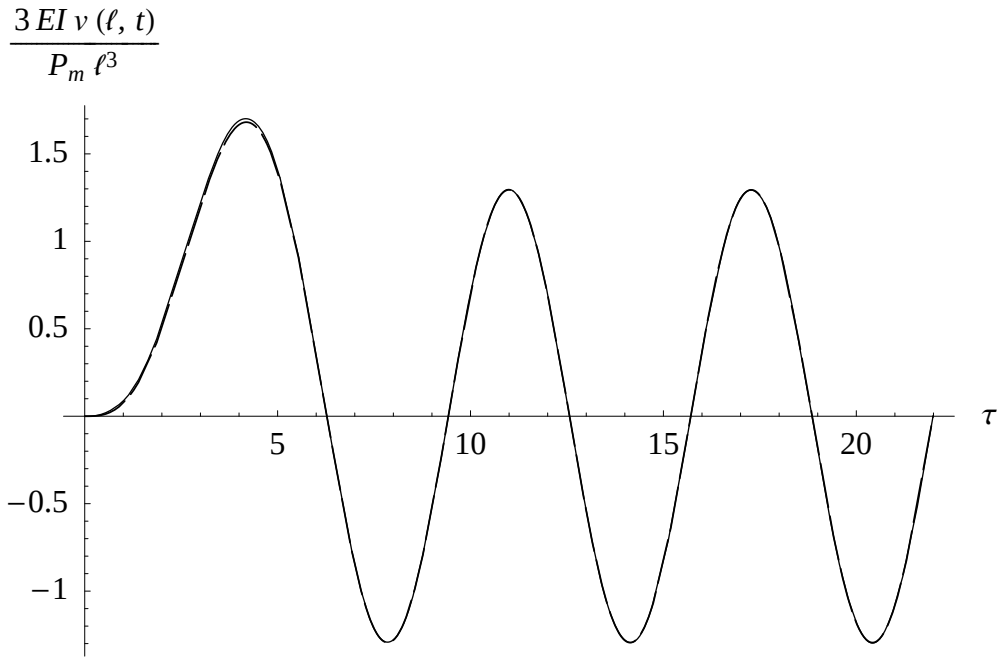

Figure 5.39: Normalized displacement $v(\ell, \tau)$ for the response of a landing gear to a quasi-static sinusoidal pulse with $\Omega = 0.5\omega_1$; one mode (dashes), two modes (solid line)

$\omega_3 = 17.5475\omega_1$, and $\omega_4 = 34.3861\omega_1$. The dynamic case has Ω between the second and third natural frequencies, and the quasi-impulsive case has Ω larger than the third natural frequency. We will look at the tip displacement and the bending moment at the root end.

First let's consider the quasi-static case for which $\Omega = 0.5\omega_1$. The tip displacements, normalized by the static value of $P_m\ell^3/(3\,EI)$ and obtained from using one and two modes, are shown in Fig. 5.39 versus nondimensional time $\tau = \omega_1 t$. For this value of Ω it is clear that the result for one mode is sufficient for plotting accuracy. The maximum error for two modes is less than 0.005 (considering seven modes as the exact value), considerably less than the smallest error that can be seen on the plot. Notice that the peaks in the displacement versus time curve are larger than the static value, especially for the first one which overshoots by nearly 70%.

For the dynamic case, with $\Omega = 10\omega_1$, the results for two and three modes are shown in Fig. 5.40. The maximum error for the two-mode result is within 0.005. For the quasi-impulsive case, $\Omega = 25\omega_1$. Results for two and three modes are shown in Fig. 5.41. Again, the maximum error for the two-mode case is around 0.005. These plots give the impression that dynamic response, even to a quasi-impulsive load, is a matter of a few modes. For complex structures, it is generally true that a relatively small numbers modes will suffice for the displacement response to a dynamic load while a more would be required for modeling impact loading.

It is not usually the displacement that designers care about, however. It is instead the

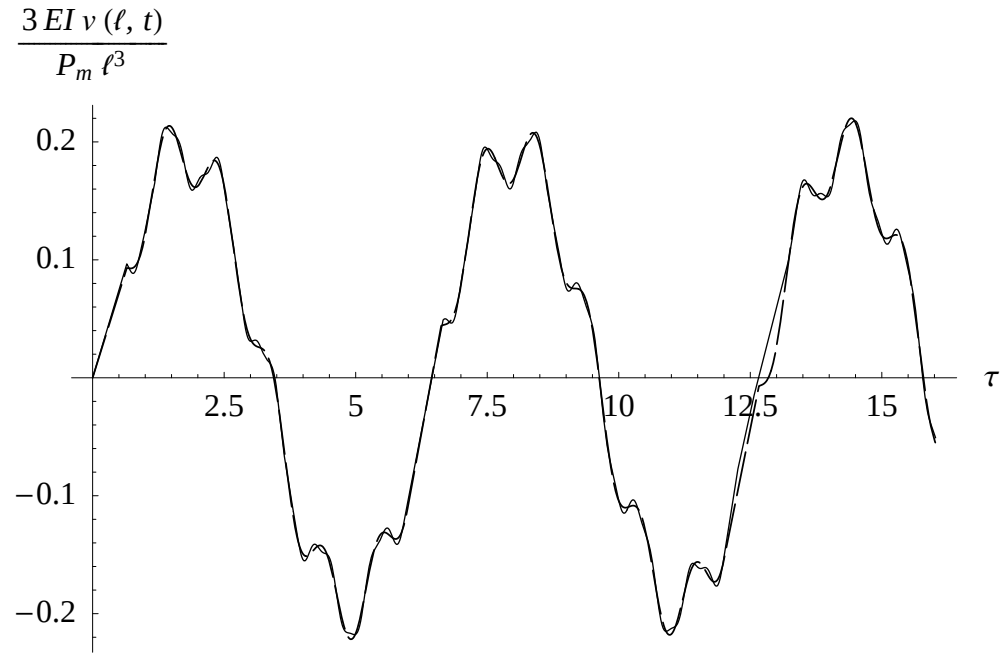

Figure 5.40: Normalized displacement $v(\ell, \tau)$ for the response of a landing gear to a dynamic sinusoidal pulse with $\Omega = 10\omega_1$; two modes (dashes), three modes (solid line)

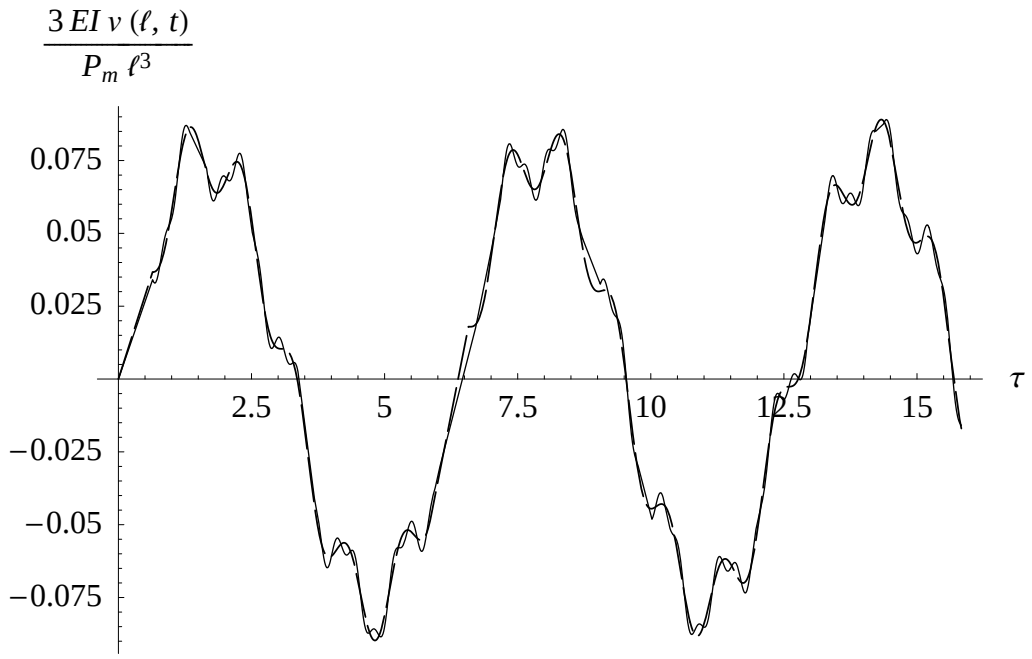

Figure 5.41: Normalized displacement $v(\ell, \tau)$ for the response of a landing gear to a quasi-impulsive sinusoidal pulse with $\Omega = 25\omega_1$; two modes (dashes), three modes (solid line)

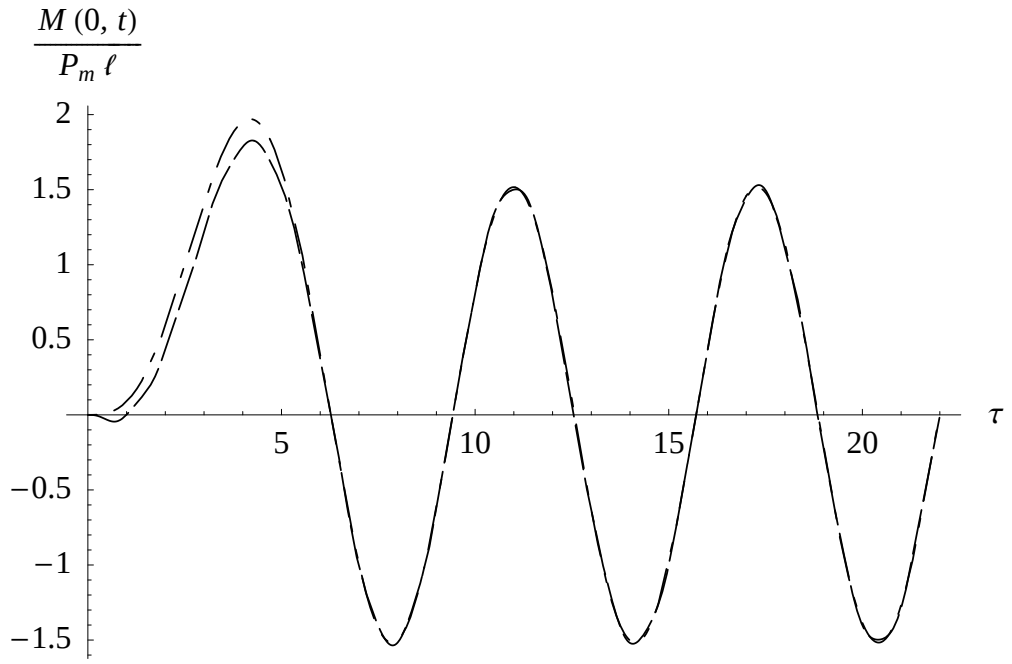

Figure 5.42: Modal displacement method approximation (i.e. by differentiation of mode shape) of root bending moment on strut subjected to a quasi-static sinusoidal pulse with $\Omega = 0.5\omega_1$; one mode (dashed line), two modes (solid line)

maximum stress that they need to know. For a strut modeled as a beam this would be calculated from the root bending moment. The bending moment at the root of the strut can be calculated in two different ways. First, the most straightforward way is to write

$$M(0,t) = EI \sum_{i=1}^{N} \xi_i(t) \psi_i''(0) \tag{5.262}$$

where $\psi_i''(0) = 2\alpha_i^2$, so that

$$M(0,t) = 2EI \sum_{i=1}^{N} \xi_i(t) \alpha_i^2 = 2\sqrt{EI\, m} \sum_{i=1}^{N} \omega_i \xi_i(t) \tag{5.263}$$

The method is called the "mode displacement method" or MDM. Because the generalized coordinates are multiplied by α_i^2 which is proportional to ω_i, this will generally mean convergence at a more sluggish rate than one obtains for the tip displacement.

To illustrate the relative convergence properties of the MDM, we consider the root bending moment normalized by its peak static value $P_m \ell$. In Fig. 5.42 the results for one and two modes are plotted. Clearly there is a larger error than was the case for the displacement. To achieve a result that is converged, at least four or five modes are needed. In Fig. 5.43 the

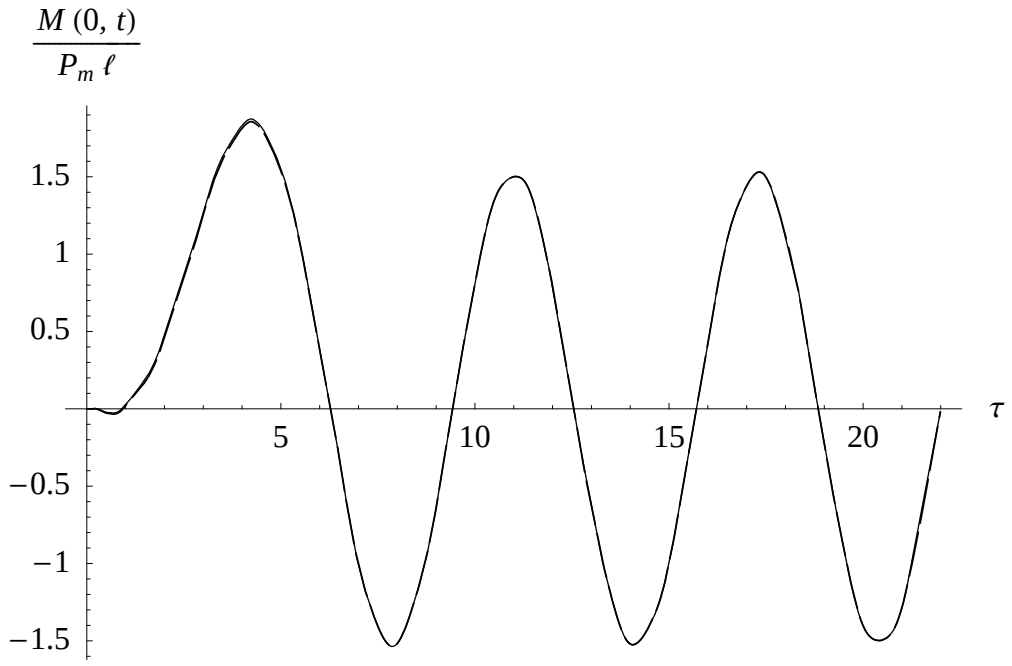

Figure 5.43: Modal displacement method approximation (i.e. by differentiation of mode shape) of root bending moment on strut subjected to a quasi-static sinusoidal pulse with $\Omega = 0.5\omega_1$; four-mode result (dashed line), five-mode result (solid line)

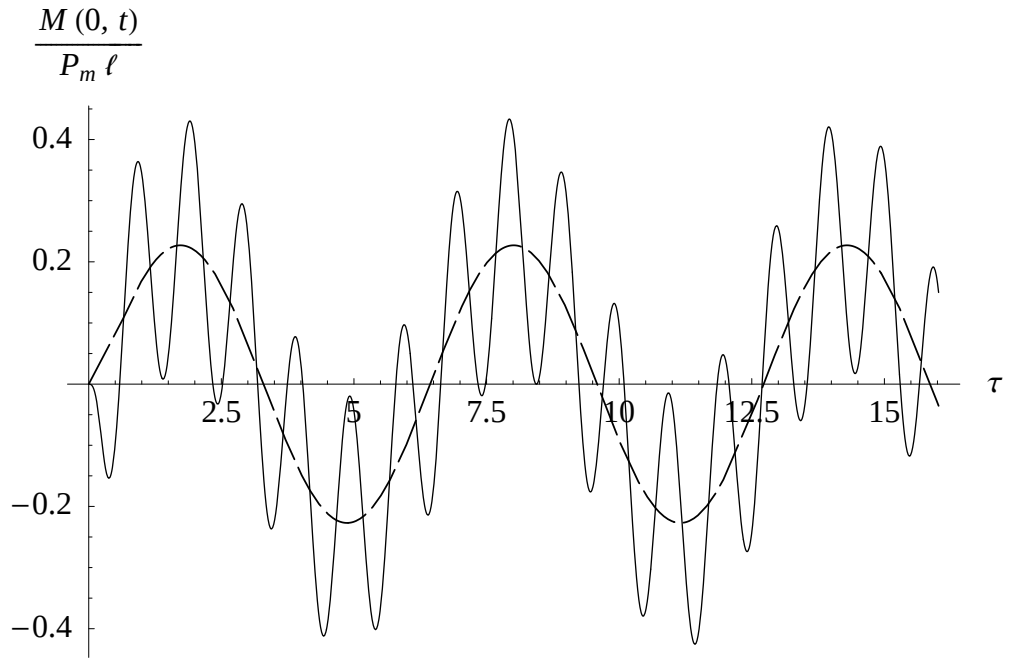

Figure 5.44: Modal displacement method approximation (i.e. by differentiation of mode shape) of root bending moment on strut subjected to a dynamic sinusoidal pulse with $\Omega = 10\omega_1$; one mode (dashed line), two modes (solid line)

results for four and five modes are plotted, with the five-mode result having a maximum error of about 0.06. Clearly to get the stresses, a significant increase in the number of modes is required for the quasi-static case. With four modes, the result is mostly converged; however, near the initial time there are some irregularities. The reason for the inaccuracy stems from the differentiation of the mode shape twice.

Looking now at performance of the MDM for a dynamic sinusoidal pulse, results for one and two modes are presented in Fig. 5.44 while those for four and five modes are in Fig. 5.45. One sees that the error is quite large for a one-mode approximation. The results for five modes have a maximum error of 0.06, but the maximum error with six modes is larger. Results for the quasi-impulsive case are similar, as shown in Figs. 5.46 and 5.47, where the maximum error for five modes is about 0.01. Clearly, if one needs to know the bending stress at the root of the strut, it may require a lot of modes.

An alternative approach to the MDM is the integrate the applied and inertial loads along the beam, referred to as the "force summation method" (FSM).[1] This method relies on integration, which does not introduce error to the same extent as differentiation. To get at this we integrate the beam equation twice (see Eq. 2.185) while enforcing the boundary

[1]Sometimes this method is referred to as the "mode acceleration method." Actually, the mode acceleration method is not the same thing, though it is closely related. This will be discussed further below.

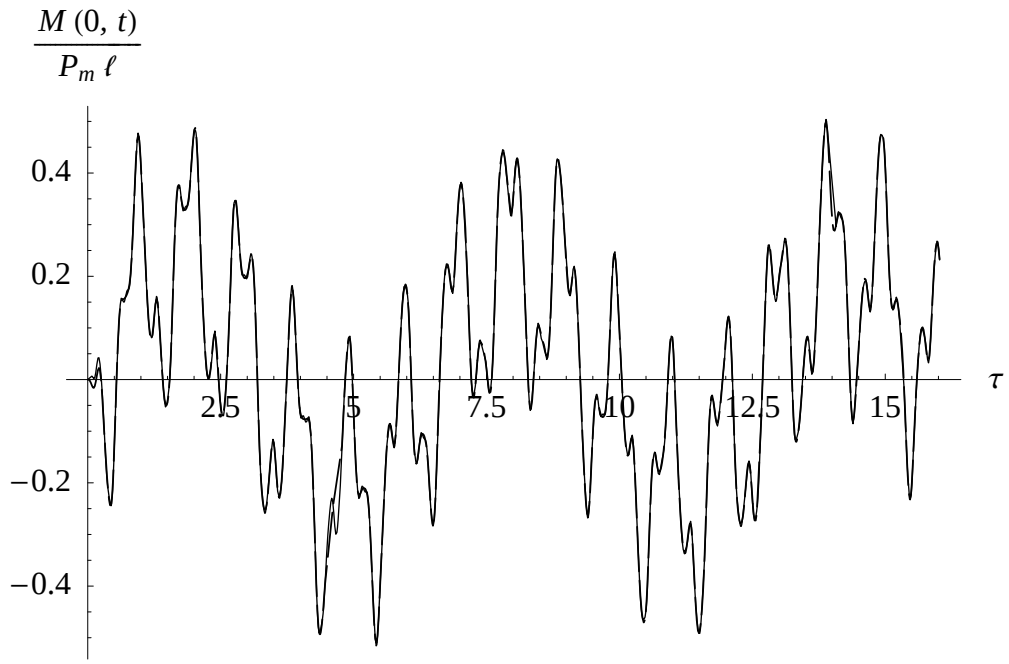

Figure 5.45: Modal displacement method approximation (i.e. by differentiation of mode shape) of root bending moment on strut subjected to a dynamic sinusoidal pulse with $\Omega = 10\omega_1$; four modes (dashed line), five modes (solid line)

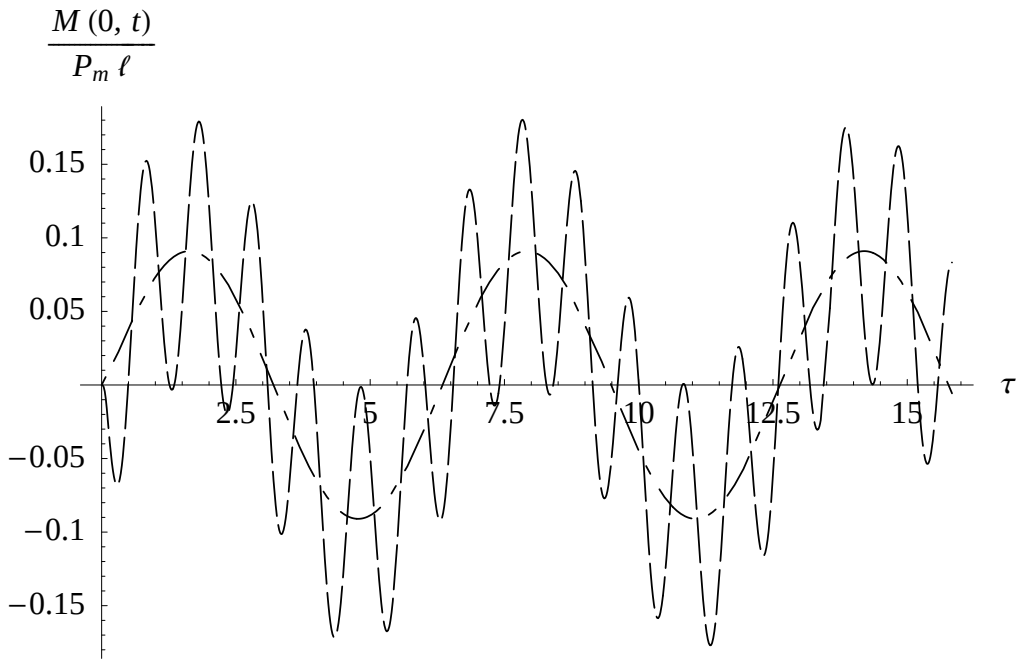

Figure 5.46: Modal displacement method approximation (i.e. by differentiation of mode shape) of root bending moment on strut subjected to a quasi-impulsive sinusoidal pulse with $\Omega = 25\omega_1$; one mode (dashed line), two modes (solid line)

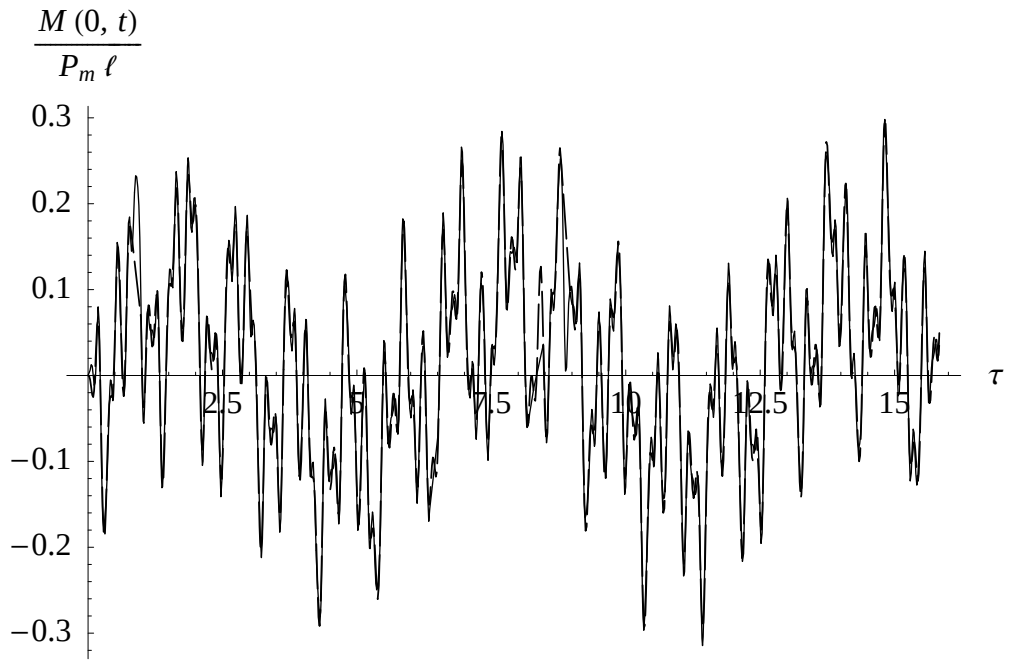

Figure 5.47: Modal displacement method approximation (i.e. by differentiation of mode shape) of root bending moment on strut subjected to a quasi-impulsive sinusoidal pulse with $\Omega = 25\omega_1$; four modes (dashed line), five modes (solid line)

conditions, obtaining

$$\begin{aligned} EI\frac{\partial^2 v}{\partial z^2} =& P(t)(\ell - z) - \int_z^\ell (z-\zeta)\left[f(\zeta,t) - m\frac{\partial^2 v(\zeta,t)}{\partial t^2}\right] d\zeta \qquad t \le \frac{\pi}{\Omega} \\ =& -\int_z^\ell (z-\zeta)\left[f(\zeta,t) - m\frac{\partial^2 v(\zeta,t)}{\partial t^2}\right] d\zeta \qquad t \ge \frac{\pi}{\Omega} \end{aligned} \tag{5.264}$$

Here the distributed applied load $f(z,t)$ is zero, and the moment at the root becomes

$$\begin{aligned} M(0,t) =& \ell P(t) - \int_0^\ell z\, m\, \frac{\partial^2 v}{\partial t^2} dz \qquad t \le \frac{\pi}{\Omega} \\ =& -\int_0^\ell z\, m\, \frac{\partial^2 v}{\partial t^2} dz \qquad t \ge \frac{\pi}{\Omega} \end{aligned} \tag{5.265}$$

Substitution of the modal approximation into this expression gives

$$\begin{aligned} M(0,t) =& \ell P(t) - m\sum_{i=1}^N \ddot{\xi}_i \int_0^\ell z\, \psi_i\, dz \qquad t \le \frac{\pi}{\Omega} \\ =& -m\sum_{i=1}^N \ddot{\xi}_i \int_0^\ell z\, \psi_i\, dz \qquad t \ge \frac{\pi}{\Omega} \end{aligned} \tag{5.266}$$

where the integral can be written as

$$\begin{aligned} \int_0^\ell z\, \psi_i\, dz =& \frac{1}{\alpha_i^4}\int_0^\ell z\, \psi_i'''' dz \\ =& \frac{1}{\alpha_i^4}\left(\cancelto{0}{z\psi_i'''\Big|_0^\ell} - \int_0^\ell \psi_i''' dz\right) \\ =& \frac{\psi_i''(0)}{\alpha_i^4} = \frac{2}{\alpha_i^2} \end{aligned} \tag{5.267}$$

so that

$$\begin{aligned} M(0,t) =& \ell P(t) - 2m\sum_{i=1}^N \frac{\ddot{\xi}_i}{\alpha_i^2} \qquad t \le \frac{\pi}{\Omega} \\ =& -2m\sum_{i=1}^N \frac{\ddot{\xi}_i}{\alpha_i^2} \qquad t \ge \frac{\pi}{\Omega} \end{aligned} \tag{5.268}$$

Comparing this expression with Eq. (5.263), one sees that the α_i, which increases with i, appears in the numerator to the second power in Eq. (5.263) whereas it appears in the denominator to the second power in Eq. (5.268). Thus, the integration of applied and inertial loads should converge faster for most problems.

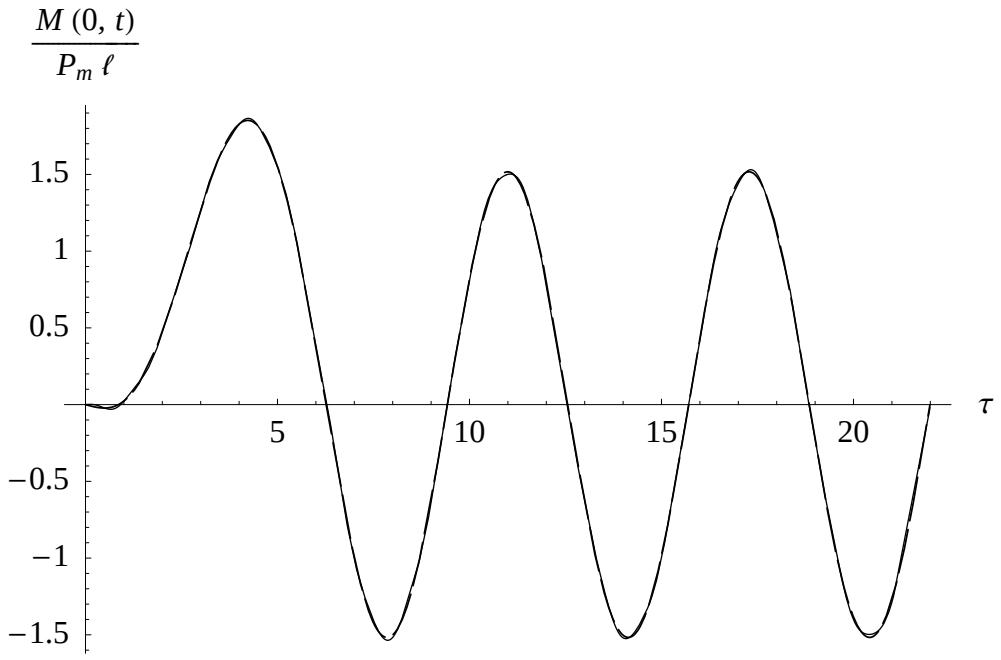

Figure 5.48: Force summation method approximation of root bending moment on strut subjected to a quasi-static sinusoidal pulse with $\Omega = 0.5\omega_1$; one mode (dashed line), two modes (solid line)

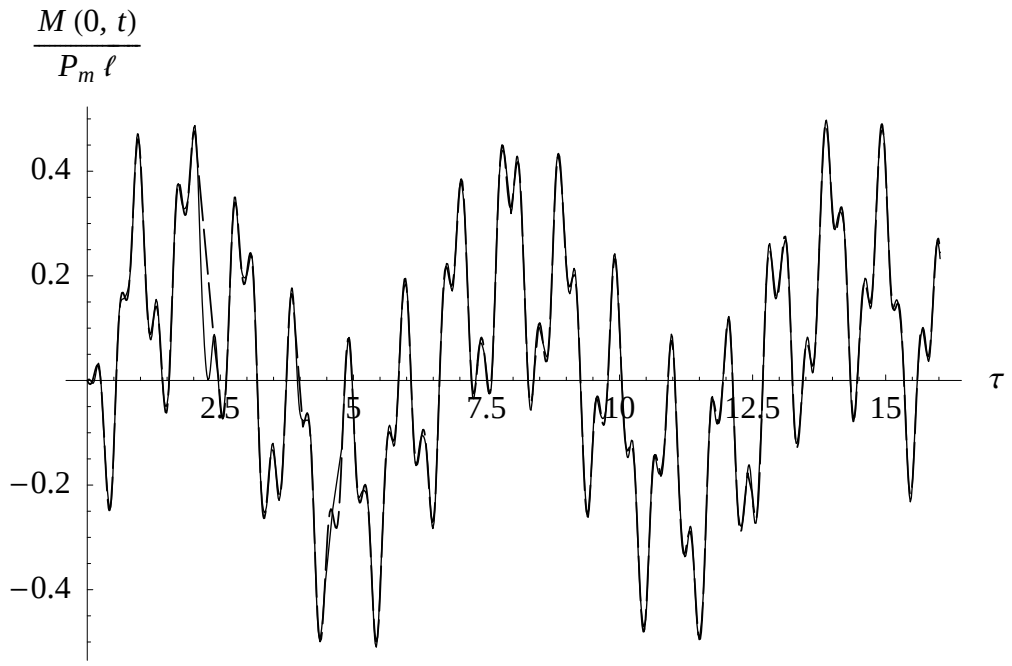

Figure 5.49: Force summation method method approximation of root bending moment on strut subjected to a dynamic sinusoidal pulse with $\Omega = 10\omega_1$; three modes (dashed line), four modes (solid line)

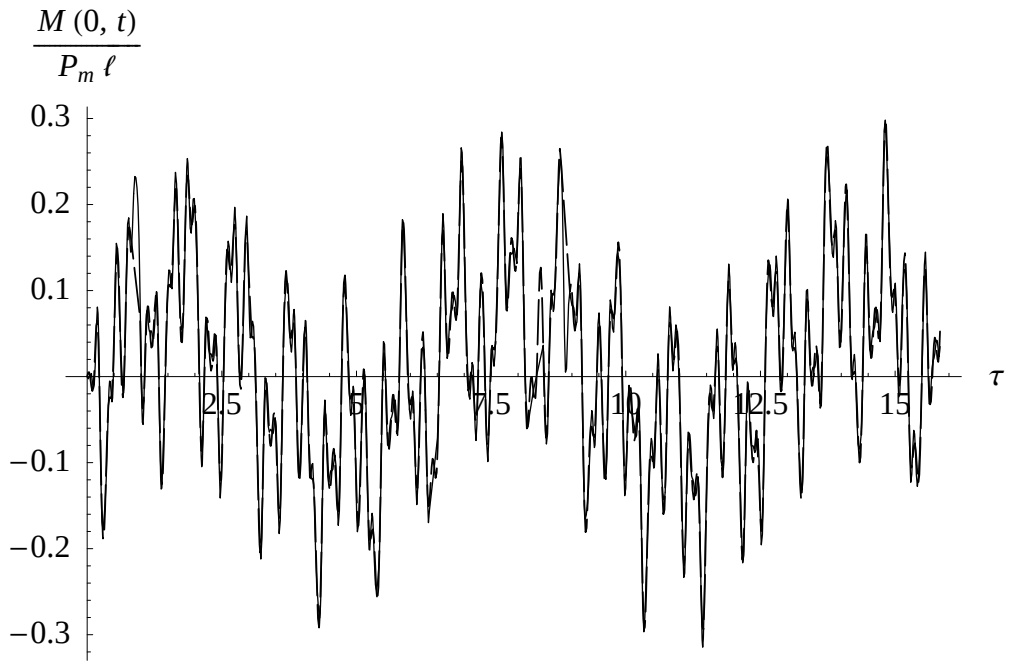

Figure 5.50: Force summation method method approximation of root bending moment on strut subjected to a quasi-impulsive sinusoidal pulse with $\Omega = 25\omega_1$; four modes (dashed line), five modes (solid line)

To illustrate that it does indeed converge more rapidly, let us again consider the three cases of sinusoidal loads. First, for the quasi-static case, results for the FSM with one and two modes are shown in Fig. 5.48. The maximum error with only two modes is about 0.002. For the dynamic case, results are shown in Fig. 5.49 for three and four modes. For the quasi-impulsive case, results are shown in Fig. 5.50 for four and five modes. For the dynamic case, the maximum error for four modes is about 0.01, while for the quasi-impulsive case the maximum error for the five mode case is 0.05. Although more modes are required than for the quasi-static case, one may say that for a given number of modes the FSM results generally are more accurate than their MDM counterparts for dynamic and quasi-impulsive loads. Alternatively, one may say that for comparable accuracy, generally fewer modes are required for FSM than for MDM.

We can also gain some additional insight regarding the failure of using the moment we would have gotten from assuming the strut to be rigid. Note the first term of Eq. (5.268) is the normalized bending moment from ignoring all deformation. The second term gives the correction, and this correction cannot be ignored. The inclusion of the vibratory contribution to the loads results in a large dynamic overshoot (note the peaks in Fig. 5.48, for example). A few modes using FSM is frequently sufficient for the problem at hand in the "quasi-static regime" where $\Omega < \omega_1$. When we have $\Omega >> \omega_1$ we can have a truly dynamic or quasi-impulsive situation requiring more modes. When we are modeling actual impact, we may need still more modes to capture the response.

It is important to note that there is another approach, which in the literature is known as the mode-acceleration method (MAM). In this method, one writes the displacement as a quasi-static term plus a modal summation. For our strut problem, this means that instead of Eq. (5.243) we write

$$v(x,t) = \overline{v}(x)\sin(\Omega t) + \sum_{i=1}^{N} q_i(t)\psi_i(x) \tag{5.269}$$

Here $\overline{v}(x)$ is the static shape under the load P_m, which satisfies

$$(EI\overline{v}'')'' = P_m \langle x - \ell + \epsilon \rangle_{-1} \tag{5.270}$$

where we have made use of the Macauley bracket notation to represent the concentrated force near the end of the beam, with ϵ as a small positive constant that we will take as zero in the limit. The generalized coordinates are here denoted by q_i only to distinguish them from ξ_i of Eq. (5.243). Let us start with the partial differential equation of motion

$$\frac{\partial^2}{\partial x^2}\left(EI\frac{\partial^2 v}{\partial x^2}\right) + \frac{\partial^2 v}{\partial t^2} = f(x,t) \tag{5.271}$$

We can now express the applied load term for $t \leq \pi/\Omega$ as

$$f(x,t) = P_m \langle x - \ell + \epsilon \rangle_{-1} \sin(\Omega t) \tag{5.272}$$

Substitution of Eq. (5.269) into Eq. (5.271), one finds that

$$\begin{aligned}(EI\overline{v}'')''\sin(\Omega t)+\sum_{i=1}^{N}\left[q_i\left(EI\psi_i''\right)''+\ddot{q}_i\psi_i\right]-m\Omega^2\overline{v}\sin(\Omega t)\\ =P_m\left\langle x-\ell+\epsilon\right\rangle_{-1}\sin(\Omega t)\end{aligned}\tag{5.273}$$

Clearly, the right-hand side term is cancelled by the first term on the left-hand side. Multiplying the remaining terms by $\psi_j dx$ and integrating both sides from 0 to ℓ, one finds that

$$\sum_{i=1}^{N}\int_0^\ell\left(EI\psi_i''\psi_j''q_i+m\psi_i\psi_j\ddot{q}_i\right)dx=\Omega^2\sin(\Omega t)\int_0^\ell m\overline{v}\psi_j dx\tag{5.274}$$

Making use of orthogonality of the assumed mode shapes, we can simplify this to

$$M_i\left(\ddot{q}_i+\omega_i^2q_i\right)=\Omega^2\sin(\Omega t)\int_0^\ell m\overline{v}\psi_i dx\qquad t\le\pi/\Omega\tag{5.275}$$

These are the same generalized equations of motion as before (see Eq. 5.249) except with an altered right-hand side. For a uniform beam, the right hand side can be simplified and the equation written as

$$\ddot{q}_i+\omega_i^2q_i=2(-1)^{i+1}\frac{\Omega^2}{\omega_i^2}\frac{P(t)}{m\ell}\tag{5.276}$$

The generalized force of the standard method (Eq. 5.249) is here multiplied by Ω^2/ω_i^2. Thus, this generalized force attenuates much more rapidly as i increases. We thus expect this method to converge more rapidly than the standard approach. The reason for this improvement stems from the fact that *we are only using the series to represent the difference between the quasi-static deflection under the load and the actual deflection; we are not having to represent the quasi-static deflection by the modal series because we can write it in closed form.*

The solution for q_i can be found in a manner similar to the way ξ_i was found above in Eqs. (5.257) and (5.260). The corresponding solutions are

$$\begin{aligned}q_i=&\frac{2P_m(-1)^{i+1}\Omega}{m\ell\omega_i\left(\Omega^2-\omega_i^2\right)}\left[\frac{\Omega}{\omega_i}\sin(\Omega t)-\sin(\omega_i t)\right]\qquad t\le\frac{\pi}{\Omega}\\ q_i=&\frac{2P_m\Omega(-1)^{i+1}}{m\ell\omega_i\left(\Omega^2-\omega_i^2\right)}\left\{\sin(\omega_i t)+\sin\left[\omega_i\left(t-\frac{\pi}{\Omega}\right)\right]\right\}\qquad t\ge\frac{\pi}{\Omega}\end{aligned}\tag{5.277}$$

To close the loop, one can show that the moment calculated from

$$M(x,t)=EI\frac{\partial^2v}{\partial x^2}\tag{5.278}$$

with v given as in Eq. (5.269) is *exactly* the same as moment calculated by FSM in Eq. (5.268). In other words, if one starts with the standard modal summation approach, in which $v(x,t)$

is assumed to be in the form of Eq. (5.243), one finds the generalized coordinates ξ_i as in Eqs. (5.257) and (5.260). These are in turn used to find the moment from FSM, Eq. (5.268). Then, if we take that moment and use it to find $v(x,t)$, viz.,

$$v = \int_0^x \int_0^\eta \frac{M(\zeta,t)}{EI(\zeta)} d\zeta d\eta \tag{5.279}$$

the result is the same as one would obtain by applying the MAM.

The MAM results for displacement only show modest improvement relative to those of the standard modal summation approach, which performs quite well anyway. The displacement error from using the MAM with only one mode is less than 0.003 for the quasi-static case, about the same as two modes with the standard modal summation method. Using two modes the error for the dynamic case is less than 0.004. Finally, using two modes for the quasi-impulsive case the error is less than 0.005. These are comparable, though slightly less, than their standard modal summation counterparts.

5.11.2 Unrestrained Elastic Airplane

Now let us consider the more general problem of a flexible airplane, though we will focus on determining the loads on the wings. As we've shown before, the generalized equations of motion for the entire aircraft will have the form

$$\ddot{\xi}_i + \omega_i^2 \xi_i = \frac{\Xi_i}{M_i} \tag{5.280}$$

where the total generalized force from the applied force $f(y,t)$ on a wing, for example, is given by

$$\Xi_i(t) = \int_0^\ell f(y,t)\psi_i(y) dy \tag{5.281}$$

and ψ_i is the i^{th} mode shape. The applied force can be further broken down as

$$f = f^{\text{D}} + f^{\text{M}} \tag{5.282}$$

Thus, the generalized force can also be broken down in a similar manner and can be written in terms of Ξ^{D}, forces caused by disturbances such as a gust or known maneuver, and Ξ^{M}, forces caused by the motion of the aircraft in response to the known disturbance, viz.,

$$\Xi_i = \Xi_i^{\text{D}}(t) + \Xi_i^{\text{M}}(\xi_1, \xi_2, \ldots, \dot{\xi}_1, \dot{\xi}_2, \ldots, \ddot{\xi}_1, \ddot{\xi}_2, \ldots) \tag{5.283}$$

Note that Ξ^{D} is typically a nonhomogeneous term, while, for example,

$$\{\Xi^{\text{M}}\} = \rho_\infty [a] \{\xi\} + \rho_\infty \frac{b}{U} [b] \left\{\dot{\xi}\right\} + \rho_\infty \frac{b^2}{U^2} [c] \left\{\ddot{\xi}\right\} \tag{5.284}$$

is homogeneous. Note that if $\{\Xi^{\mathrm{M}}\} = 0$, the equations decouple and if $\{\Xi^{\mathrm{D}}\} = 0$ the equations are homogeneous as in a flutter problem. If $\{\Xi^{\mathrm{M}}\} \neq 0$, the equations are uncoupled structurally but coupled aerodynamically.

If $\{\Xi^{\mathrm{M}}\} = 0$, the equations can be time-marched (or solved analytically in some cases). On the other hand, if $\{\Xi^{\mathrm{M}}\} \neq 0$, simple problems may be solved by Laplace transform, while in general numerical integration is needed.

We now turn to seeing how the MDM and FSM methods apply in this type of analysis. For FSM, we must decompose the forces caused disturbances, motion, and inertial forces, so that

$$f^{\mathrm{T}} = f^{\mathrm{D}} + f^{\mathrm{M}} + f^{\mathrm{I}} \tag{5.285}$$

where for a wing represented as a beam $f^{\mathrm{I}} = -m\frac{\partial^2 w}{\partial y^2}$. If the aircraft is fairly stiff, we can use a modal representation, so that

$$w(y,t) = \sum_i \psi_i(y)\xi_i(t) \tag{5.286}$$

and

$$f^{\mathrm{T}} = f^{\mathrm{D}} - \sum_{i=-1}^{0} m\psi_i(y)\ddot{\xi}_i(t) - \sum_{i=1}^{N} m\psi_i(y)\ddot{\xi}_i(t) + f^{\mathrm{M}} \tag{5.287}$$

where the first two terms may be referred to as pseudo-static forces while the last two involve elastic, vibratory motion. The negative and zero index on the summation refers, as before, to rigid-body modes while the positive index refers to the elastic modes.

The bending moment on the wing is then

$$M(y,t) = \int_y^\ell \left[f^{\mathrm{D}} - \sum_{i=-1}^{0} m\psi_i(\eta)\ddot{\xi}_i(t) - \sum_{i=1}^{N} m\psi_i(\eta)\ddot{\xi}_i(t) + f^{\mathrm{M}} \right] (\eta - y)d\eta \tag{5.288}$$

which, when evaluated at the root where $y = 0$, can be written as

$$\begin{aligned} M(0,t) =& \int_0^\ell \left[f^{\mathrm{D}} - \sum_{i=-1}^{0} m\psi_i(y)\ddot{\xi}_i(t) - \sum_{i=1}^{N} m\psi_i(y)\ddot{\xi}_i(t) + f^{\mathrm{M}} \right] ydy \\ =& C^{\mathrm{D}} - \sum_{i=-1}^{0} B_i\ddot{\xi}_i(t) - \sum_{i=1}^{N} B_i\ddot{\xi}_i(t) + C^{\mathrm{M}}(\xi, \dot{\xi}, \ddot{\xi}) \end{aligned} \tag{5.289}$$

Applying the above landing gear strut implementation for the MDM to the wing, one obtains

$$M(0,t) = EI \sum_{i=1}^{N} \psi_i''(0)\xi_i \tag{5.290}$$

This involves differentiation. However, there is another way to cast the problem in terms of the MDM. Recall that the eigenmodes are obtained from the equation

$$\frac{d^2}{dy^2}\left(EI\frac{d^2\psi_i}{dy^2}\right) - \omega_i^2 m\psi_i = 0 \tag{5.291}$$

The equation governing the forced response can be written as

$$f^{\mathrm{T}} = \sum_{i=1}^{N}\frac{d^2}{dy^2}\left(EI\frac{d^2\psi_i}{dy^2}\right) = \sum_{i=1}^{N}\omega_i^2 m(y)\psi_i(y)\xi_i(t) \tag{5.292}$$

The summation only covers the elastic modes because the frequencies associated with the rigid-body modes are zero. The bending moment is then

$$M(0,t) = \int_0^\ell y f^{\mathrm{T}} dy = \sum_{i=1}^{N}\omega_i^2 B_i\xi_i \tag{5.293}$$

It can easily be shown that the two MDM implementations give identical results. Thus, as with the landing gear strut, there are really only two distinct methods (MDM and FSM) to be compared. The predicted results for the bending moment (or most any stress component) resemble those for the strut; namely, the dynamic (i.e. the actual) result overshoots the quasi-static behavior by an amount that can be significant, e.g., a factor of 50% – 200%. A quasi-static estimate of the stress, then, could be way off.

For the MDM we have Eq. (5.293). Using the generalized equations of motion, $\omega_i^2\xi_i$ for an arbitrary elastic mode (which is all there is in Eq. 5.293) can be written as

$$\omega_i^2\xi_i = \frac{\Xi_i^{\mathrm{D}}}{M_i} + \frac{\Xi_i^{\mathrm{M}}}{M_i} - \ddot{\xi}_i \tag{5.294}$$

so that

$$M(0,t) = \sum_{i=1}^{N} B_i\frac{\Xi_i^{\mathrm{D}}}{M_i} - \sum_{i=1}^{N} B_i\ddot{\xi}_i + \sum_{i=1}^{N} B_i\frac{\Xi_i^{\mathrm{M}}}{M_i} \tag{5.295}$$

For the FSM, recall that

$$M(0,t) = C^{\mathrm{D}} - \sum_{i=-1}^{0} B_i\ddot{\xi}_i - \sum_{i=1}^{N} B_i\ddot{\xi}_i + C^{\mathrm{M}} \tag{5.296}$$

But the generalized equation of motion for a rigid-body mode shows that

$$\ddot{\xi}_i = \frac{\Xi_i^{\mathrm{D}}}{M_i} + \frac{\Xi_i^{\mathrm{M}}}{M_i} \tag{5.297}$$

so that

$$M(0,t) = C^{\mathrm{D}} - \sum_{i=-1}^{0} B_i \frac{\Xi_i^{\mathrm{D}}}{M_i} - \sum_{i=-1}^{0} B_i \frac{\Xi_i^{\mathrm{M}}}{M_i} + C^{\mathrm{M}} - \sum_{i=1}^{N} B_i \ddot{\xi}_i \tag{5.298}$$

A direct comparison is now possible. Writing both results, underlining certain terms will illuminate the similarities and differences. The nonunderlined terms will be for the vibratory portions, the single-underlined ones for the motion terms, and the double-underlined ones for the disturbance, so that

$$\begin{array}{lrcl} M(0,t) = & -\sum_{i=1}^{N} B_i \ddot{\xi}_i & + \underline{\sum_{i=1}^{N} B_i \frac{\Xi_i^{\mathrm{M}}}{M_i}} & + \underline{\underline{\sum_{i=1}^{N} B_i \frac{\Xi_i^{\mathrm{D}}}{M_i}}} \quad \text{MDM} \\ M(0,t) = & -\sum_{i=1}^{N} B_i \ddot{\xi}_i & + \underline{C^{\mathrm{M}} - \sum_{i=-1}^{0} B_i \frac{\Xi_i^{\mathrm{M}}}{M_i}} & + \underline{\underline{C^{\mathrm{D}} - \sum_{i=-1}^{0} B_i \frac{\Xi_i^{\mathrm{D}}}{M_i}}} \quad \text{FSM} \end{array} \tag{5.299}$$

The vibratory portions are approximate and identical between the two methods. FSM draws its strength from the fact that the disturbance and motion terms are exact while with MDM these are only approximate.

Finally, it should be noted that these methods can be used to also compute other structural load transients, such as the shear force and twisting moment, which contribute to calculation of other stress components. The shear force along the wing can be written as

$$V(y,t) = -\int_{y}^{\ell} f^{\mathrm{T}}(\eta) d\eta \tag{5.300}$$

while the twisting moment can be written as

$$T(y,t) = -\int_{y}^{\ell} t^{\mathrm{T}}(\eta) d\eta \tag{5.301}$$

where t^{T} is the total of distributed applied and inertial twisting moment about the wing elastic axis. If the wing is plate-like, then the twisting moment might be written as

$$T(y,t) = \int_{y}^{\ell} \int_{\mathrm{L.E.}}^{\mathrm{T.E.}} x f^{\mathrm{T}} dx dy \tag{5.302}$$

where f^{T} is here the force per unit area.

5.11.3 Gust Response

Consider the response of an aircraft to a discrete gust. This evaluation is important for heavily-loaded transport aircraft, for example, because a gust can cause the wings to reach their maximum load limits. We are going to look at the response to both "sharp-edged" and "discrete" gusts.

Response to a Sharp-edged Gust

A sharp-edged gust is represented as a step change in the vertical velocity of the air encountered by a flying aircraft. For an aircraft of mass M_{T} in straight and level flight, where the vertical velocity is zero, this amounts to a step change in the angle of attack. Looking at this in the most simplistic manner, assume that the aircraft is rigid, that the gust velocity is the gust velocity w_g multiplied by a unit step function, and that the lift responds instantaneously. Thus, assuming the change in angle of attack is a small angle, the change in lift can be modeled as

$$\Delta L = q_\infty S C_{\ell\alpha} \Delta\alpha = q_\infty S C_{\ell\alpha} \frac{w_g}{U} \tag{5.303}$$

The vertical acceleration caused by the gust can then be written as

$$\ddot{z} = \frac{\Delta L}{M_{\text{T}}} \tag{5.304}$$

so that the incremental load factor is

$$\Delta N = \frac{\Delta L}{M_{\text{T}} g} = \frac{\ddot{z}}{g} \tag{5.305}$$

Substituting Eq. (5.303), the total weight W_{T} for $M_{\text{T}} g$, and the definition of q_∞ into this relation, one finds that

$$\begin{aligned} \Delta N =& \frac{1}{2} \rho_\infty U^2 S C_{\ell\alpha} \frac{w_g}{U W_{\text{T}}} \\ =& \frac{\rho_\infty U C_{\ell\alpha} w_g}{2 \frac{W_{\text{T}}}{S}} \end{aligned} \tag{5.306}$$

where the fraction in the denominator can be identified the wing loading per unit area. This is a conservative case. Usually no gust is really sharp-edged, the lift buildup is not really instantaneous, and no aircraft is rigid.

An empirical alleviation factor is sometimes used, such that

$$\Delta N = K_g \frac{\rho_\infty U C_{\ell\alpha} w_g}{2 \frac{W_{\text{T}}}{S}} \tag{5.307}$$

where $0.6 \leq K_g \leq 0.9$. It is better to refine the analysis to account for the last two of the three assumptions.

First, let us consider unsteady aerodynamics. For 2-D incompressible flow, recall Eqs. (5.173) with

$$\begin{aligned} L_{\text{ea}} =& L \\ M_{\text{ea}} =& M_{\frac{1}{4}} + b \left(a + \frac{1}{2} \right) L \end{aligned} \tag{5.308}$$

and the Wagner function as shown in Fig. 5.25. Consider an initial condition beginning at rest, so that

$$L = \pi\rho_\infty b^2\left(\ddot{h} + U\dot{\theta} - ba\ddot{\theta}\right) + 2\pi\rho_\infty Ub\int_0^\tau \phi(\tau-\sigma)\left[\dot{h} + U\theta + b\left(\frac{1}{2}-a\right)\dot{\theta}\right]d\sigma \quad (5.309)$$

This is a convolution integral where the Wagner function ϕ describes the lift buildup from a step change in angle of attack. Note that based on the definition of the nondimensional time τ and the approximate formula $\phi(\tau) = (\tau+2)/(\tau+4)$ shows that after about 36 semi-chords of travel the lift builds up to within 5% of the steady-state value.

We can also base the model explicitly on a step gust, so that

$$L = 2\pi\rho_\infty Ub\left[w_g(0)\psi(\tau) + \int_0^\tau \frac{dw_g}{d\sigma}\psi\left(\tau-\sigma\right)\right]d\sigma \quad (5.310)$$

also a convolution integral. Here σ is a dummy non-dimensional time variable and ψ is the Kussner function, the lift caused by a step change in gust velocity. The Kussner function requires about the same time as the Wagner function to build up to the steady state value.

When the quasi-steady approximation is used, $\phi(\tau) = \psi(\tau) = 1$, so that

$$\begin{aligned} L =& \pi\rho_\infty b^2\left(\ddot{h} + U\dot{\theta} - ba\ddot{\theta}\right) + 2\pi\rho_\infty Ub\left[\dot{h} + U\theta + b\left(\frac{1}{2}-a\right)\dot{\theta}\right] \\ L =& 2\pi\rho_\infty Ubw_g(t) \end{aligned} \quad (5.311)$$

Response to a Discrete Gust

Consider now a "discrete" gust, represented as

$$w_g = \frac{w_{\max}}{2}\left[1 - \cos\left(\frac{2\pi x}{x_g}\right)\right] \quad (5.312)$$

pictured in Fig. **??**. At $t = 0$ the aircraft is flying straight and level, so it sees the gust velocity as w_g when $0 \le t \le x_g/U$ and zero otherwise. We will model the aircraft using a modal approach with

$$\begin{aligned} w(x,y,t) &= \sum_{i=-1}^{N}\left[\psi_i(y) + x\phi_i(y)\right]\xi_i(t) \\ \theta(x,y,t) &= \sum_{i=-1}^{N}\phi_i(y)\xi_i(t) \end{aligned} \quad (5.313)$$

where the modes ψ_i and ϕ_i include both rigid and elastic modes for the wing. Recalling the previous development, we can write the generalized forces as

$$\Xi_i = \Xi_i^{\mathrm{D}} + \Xi_i^{\mathrm{M}} \quad (5.314)$$

where the explicit gust terms go under the category of disturbance (the superscript D) and the motion of the aircraft caused by the gust go under the category of motion terms (the superscript M). The generalized forces will include some homogeneous terms and some nonhomogeneous terms. The homogeneous ones can be put on the left-hand side, while the nonhomogeneous terms become forcing functions. The resulting equations can be put in the form

$$\left[M + C^A\right]\left\{\ddot{\xi}\right\} + \left[C^B\right]\left\{\dot{\xi}\right\} + \int_0^\tau \left[C^C\right]\left\{\ddot{\xi}\right\}\phi(\tau-\sigma)d\sigma + \int_0^\tau \left[C^D\right]\left\{\dot{\xi}\right\}\phi(\tau-\sigma)d\sigma = \left\{\Xi^G\right\} \tag{5.315}$$

where the term on the right-hand side is a known function of time. This is a system of coupled integro-differential equations in time, the solution of which can be accomplished in terms of numerical methods or Laplace transforms. Once w is known, one can compute the accelerations and bending moment.

Typical results involve a significant overshoot relative to the results for the rigid case where the dynamic overstress may be large at the wing tip (of the order of 2).

5.12 Epilogue

In this chapter we have considered the general problem of dynamic aeroelasticity, emphasizing lifting-surface flutter but considering also dynamic loads and gust response analysis. Several types of flutter analysis have been presented, including the p method, classical flutter analysis, the k method, and the p-k method. The application of classical flutter analysis to discrete one- and two-degree-of-freedom wind-tunnel models has been presented. The student has been exposed to Theodorsen's unsteady thin-airfoil theory along with the more modern finite-state thin-airfoil theory of Peters et al. Application of the assumed modes method to construct a flutter analysis of a flexible wing has been demonstrated as well. Some of the important parameters of the flutter problem have been discussed, along with current design practice. For dynamic loads, the modal displacement and force summation methods are compared for a simple problem and show the overall superiority of the latter for accuracy and computational efficiency. Finally, the methodology for setting up gust response analysis has been presented.

With a good understanding of the material presented herein, the student should be sufficiently equipped to apply these fundamentals to the design of flight vehicles. Moreover, with appropriate graduate-level studies beyond the scope of material presented herein, the student will be able conduct research in the exciting field of aeroelasticity. Current research topics are quite diverse. With the increase in the sophistication of controls technology, it has become more and more common to attack flutter problems by active control of flaps or other flight control surfaces. These so-called flutter suppression systems provide alternatives to costly design changes. One type of system for which flutter suppression systems are an excellent choice is a military aircraft that must carry weapons as stores. These aircraft must

be free of flutter within their flight envelope for several different configurations. Sometimes avoidance of flutter by design changes is simply beyond the capability of the designer for such complex systems. There is also research to determine in flight when a flutter boundary is being approached. This could be of great value for situations in which damage had altered the properties of the aircraft structure, perhaps unknown to the pilot, thus shifting the flutter (or divergence) boundary and making the aircraft unsafe to operate within its original flight envelope. Other current problems of interest to aeroelasticians include improved analysis methodology for prediction of flutter, gust response, and limit-cycle oscillations; design of control systems to improve gust response and limit-cycle oscillations; and incorporation of aeroelastic analyses at an earlier stage of aircraft design. Finally, current research must challenge the overall perception of aeroelasticians as being reactionary because we step in at the latter stages of the design process for aircraft systems and announce that there is a flutter or divergence problem. Instead, aeroelasticians must come to the place where we influence the design process, leading quite possibly to improved designs that actually take advantage of the aircraft's inherent flexibility. An example of such a philosophy is the Air Force/NASA Active Aeroelastic Wing program (extending roughly from the late 1980's until 2005). Although the program did not succeed in producing a post-reversal design, it did achieve superior roll rates by making use of wing flexibility.

Problems

1. Compute the flutter speed for the incompressible, one-degree-of-freedom flutter problem with

$$m_\theta = \frac{i-2}{k} - 10i$$
$$I_P = 50\pi\rho_\infty b^4 \qquad \omega_\theta = 10 \text{ Hz} \qquad b = 0.5 \text{ ft}$$

   ans.: $U_F = 405.6$ ft/sec

2. According to Theodorsen's theory, the circulatory lift is proportional to a quantity that, for simple harmonic motion, can be shown to be equal to the effective angle of attack given by

$$\alpha = C(k)\left[\theta + \frac{\dot{h}}{U} + \frac{b}{U}\left(\frac{1}{2} - a\right)\dot{\theta}\right]$$

   For $a = -1/2$ and simple harmonic motion such that $\overline{\theta} = 1$ and $\overline{h} = bz\left[\cos(\phi) + i\sin(\phi)\right]$, plot α as a function of time for five periods for the following four cases:

   (a) $z = 0.1$; $\phi = 0°$; $k = 0.01$

   (b) $z = 0.1$; $\phi = 0°$; $k = 1.0$

   (c) $z = 0.1$; $\phi = 90°$; $k = 1.0$

   (d) $z = 0.5$; $\phi = 90°$; $k = 1.0$

   Comment on the behavior of α for increasing k, changing the phase angle from 0° to 90°, and increasing the plunge magnitude. You may approximate Theodorsen's function as

$$C(k) = \frac{0.01365 + 0.2808ik - \frac{k^2}{2}}{0.01365 + 0.3455ik - k^2}$$

3. Show that the coefficients used in a classical flutter analysis, if based on Theodorsen's theory, are

$$\ell_h = 1 - \frac{2iC(k)}{k}$$
$$\ell_\theta = -a - \frac{i}{k} - \frac{2C(k)}{k^2} - \frac{2i\left(\frac{1}{2} - a\right)C(k)}{k}$$
$$m_h = -a + \frac{2i\left(\frac{1}{2} + a\right)C(k)}{k}$$
$$m_\theta = \frac{1}{8} + a^2 - \frac{i\left(\frac{1}{2} - a\right)}{k} + \frac{2\left(\frac{1}{2} + a\right)C(k)}{k^2} + \frac{2i\left(\frac{1}{4} - a^2\right)C(k)}{k}$$

4. Consider a wing in incompressible flow with freestream speed U and pivoted about its leading edge. The pitch motion is spring restrained with spring constant $k_\theta = I_P\omega_\theta^2$. Use the exact $C(k)$ and

   (a) determine the flutter speed and flutter frequency for $I_P = 2500\pi\rho_\infty b^4$;

(b) determine the minimum possible flutter speed and flutter frequency.

ans.: (a) $U_F = 28.2279\, b\omega_\theta$ and $\omega_F = 1.13879\, \omega_\theta$; (b) $U_F = 24.7877\, b\omega_\theta$ and $\omega_F = \omega_\theta$.

5. Consider an incompressible, two-degree-of-freedom flutter problem in which $a = -1/5$, $e = -1/10$, $\mu = 20$, $r^2 = 6/25$, and $\sigma = 2/5$. Compute the flutter speed and the flutter frequency using the classical flutter approach. For the aerodynamic coefficients use those of Theodorsen's theory with $C(k)$ approximated as in Problem 2.

   ans.: $U_F = 2.170\ b\omega_\theta$ and $\omega_F = 0.6443\ \omega_\theta$.

6. Consider an incompressible, flutter problem for a *flexible wing* in which $a = -1/5$, $e = -1/10$, $\mu = 20$, $r^2 = 6/25$, and $\sigma = 2/5$. Consider a two-degree-of-freedom case in which there is one elastic mode for each of the deformation variables. Compute the flutter speed and the flutter frequency using the classical flutter approach using Theodorsen's theory with the exact $C(k)$.

   ans.: $U_F = 2.228\ b\omega_\theta$ and $\omega_F = 0.6368\ \omega_\theta$.

7. Consider an incompressible, two-degree-of-freedom flutter problem in which $a = -1/5$, $\mu = 3$, and $r = 1/2$. Compute the flutter speed and flutter frequency for two cases $x_\theta = e - a = 1/5$ and $x_\theta = e - a = 1/10$, and let $\sigma = 0.2$, 0.4, 0.6, 0.8, and 1.0. Use the classical flutter approach, and for the aerodynamic coefficients use those of Theodorsen's theory with $C(k)$ approximated as in Problem 2. Compare with the results in Fig. 5.35.

8. Set up the complete set of equations for flutter analysis by the p method using the unsteady aerodynamic theory of Peters et al. (1995), nondimensionalizing Eqs. (5.167) and redefining λ_i as $b\omega_\theta\lambda_i$.

9. Write a computer program using MATLAB™or Mathematica™to set up the solution of the equations derived in Problem 8.

10. Using the computer program written in Problem 9, solve for the dimensionless flutter speed and flutter frequency for an incompressible, two-degree-of-freedom flutter problem in which $a = -1/3$, $e = -1/10$, $\mu = 50$, $r = 2/5$, and $\sigma = 2/5$.

    ans.: $U_F = 2.807\ b\omega_\theta$ and $\omega_F = 0.5952\ \omega_\theta$.

11. Write a computer program using MATLAB™or Mathematica™to set up the solution of a two-degree-of-freedom flutter problem using the k method.

12. Use the computer program written in Problem 11 to solve a flutter problem in which $a = -1/5$, $e = -1/10$, $\mu = 20$, $r^2 = 6/25$, and $\sigma = 2/5$. Plot the values of $\omega_{1,2}/\omega_\theta$ and g versus $U/(b\omega_\theta)$ and compare your results with the quantities plotted in Figs. 5.23 and 5.24. Noting how the quantities plotted in these two sets of figures are different, comment on the similarities and differences you observe in these plots and why those differences are there. Finally, explain why your predicted flutter speed is the same as that determined by the classical method.

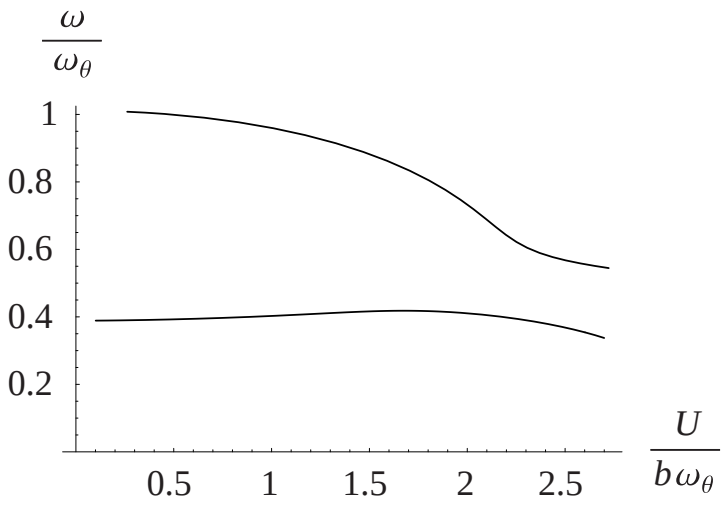

Figure 5.51: Plot of $\omega_{1,2}/\omega_\theta$ versus $U/(b\omega_\theta)$ using the k method and Theodorsen aerodynamics with $a = -1/5$, $e = -1/10$, $\mu = 20$, $r^2 = 6/25$, and $\sigma = 2/5$

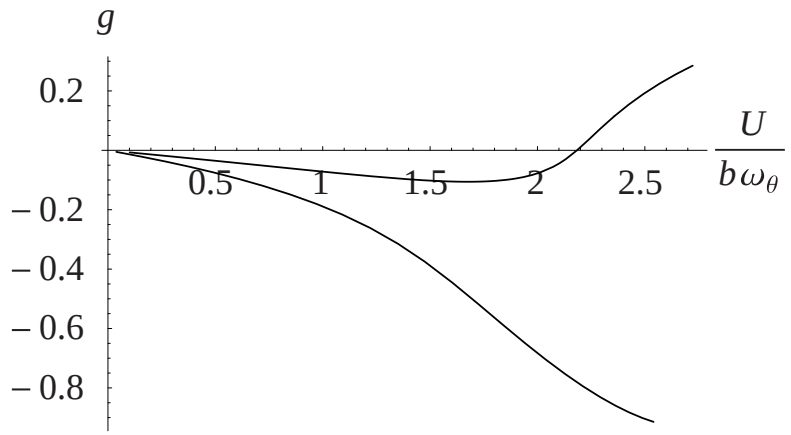

Figure 5.52: Plot of g versus $U/(b\omega_\theta)$ using the k method and Theodorsen aerodynamics with $a = -1/5$, $e = -1/10$, $\mu = 20$, $r^2 = 6/25$, and $\sigma = 2/5$

ans.: See Figs. 5.51 and 5.52.

13. Show that the flutter determinant for the p-k method applied to the typical section using Theodorsen aerodynamics can be expressed as

$$\begin{vmatrix} p^2 + \frac{\sigma^2}{V^2} - \frac{k^2}{\mu} + \frac{2ikC(k)}{\mu} & \frac{p^2\mu x_\theta + k(i+ak) + [2+ik(1-2a)]C(k)}{\mu} \\ \frac{p^2\mu x_\theta + ak^2 - ik(1+2a)C(k)}{\mu} & \frac{8\mu r^2\left(p^2+\frac{1}{V^2}\right) + 4i(1+2a)[2i-k(1-2a)]C(k) - k[k-4i+8a(i+ak)]}{8\mu} \end{vmatrix}$$

14. Write a computer program using MATLAB™or Mathematica™to set up the solution of a two-degree-of-freedom flutter problem using the p-k method and Theodorsen aerodynamics.

15. Use the computer program written in Problem 14 to solve a flutter problem in which $a = -1/5$, $e = -1/10$, $\mu = 20$, $r^2 = 6/25$, and $\sigma = 2/5$. Plot the values of the estimates of $\Omega_{1,2}/\omega_\theta$ and $\Gamma_{1,2}/\omega_\theta$ versus $U/(b\omega_\theta)$ and compare your results with the quantities plotted in Figs. 5.23 and 5.24. Explain why the estimated damping from the p-k method sometimes differs from that of the p method.

ans.: See Figs. 5.53 and 5.54.

16. Write a computer program using MATLAB™or Mathematica™to set up the solution of a two-degree-of-freedom flutter problem using the p-k method and the aerodynamics of Peters et al.

17. Using the computer programs of Problems 14 and 16, show that the p-k method yields the same results regardless of whether one uses Theodorsen theory or the aerodynamic theory of Peters et al., assuming a sufficiently large number of inflow states is used in the latter. You may do this for the case $a = -1/5$, $e = -1/10$, $\mu = 20$, $r^2 = 6/25$, and $\sigma = 2/5$. What does this imply about the two theories?

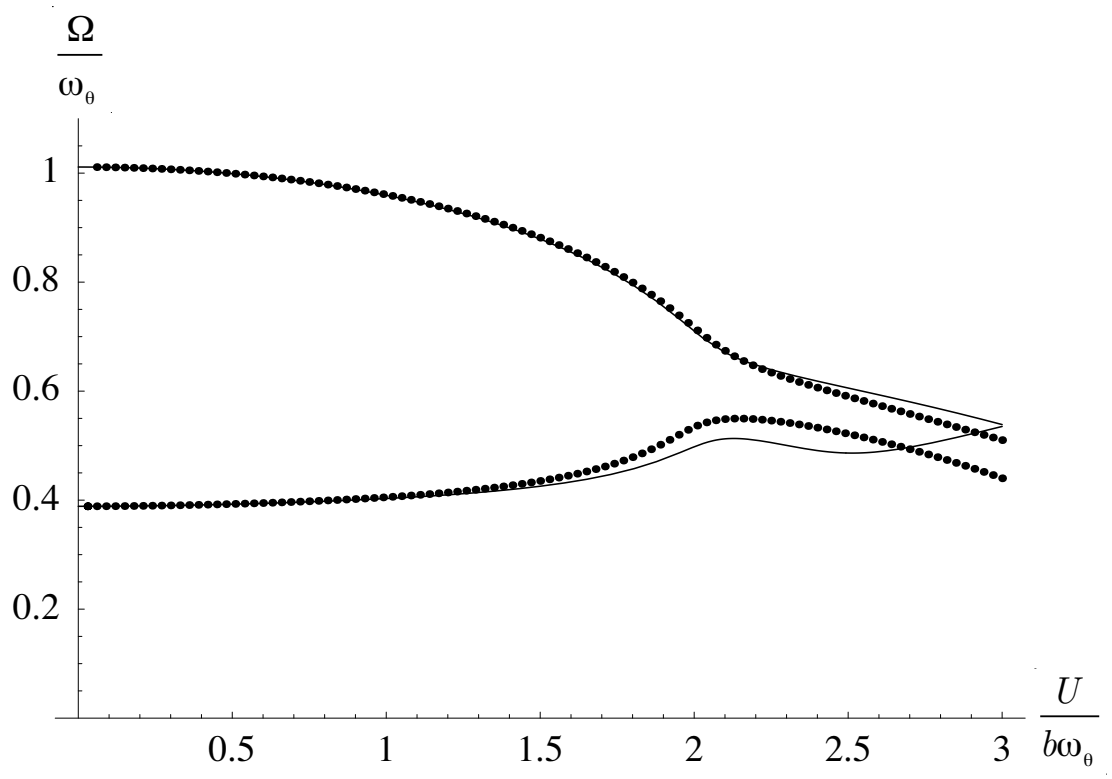

Figure 5.53: Plot of estimated value of $\Omega_{1,2}/\omega_\theta$ versus $U/(b\omega_\theta)$ using the p-k method with Theodorsen aerodynamics (symbols) and the p method with the aerodynamics of Peters et al. (lines) for $a = -1/5$, $e = -1/10$, $\mu = 20$, $r^2 = 6/25$, and $\sigma = 2/5$

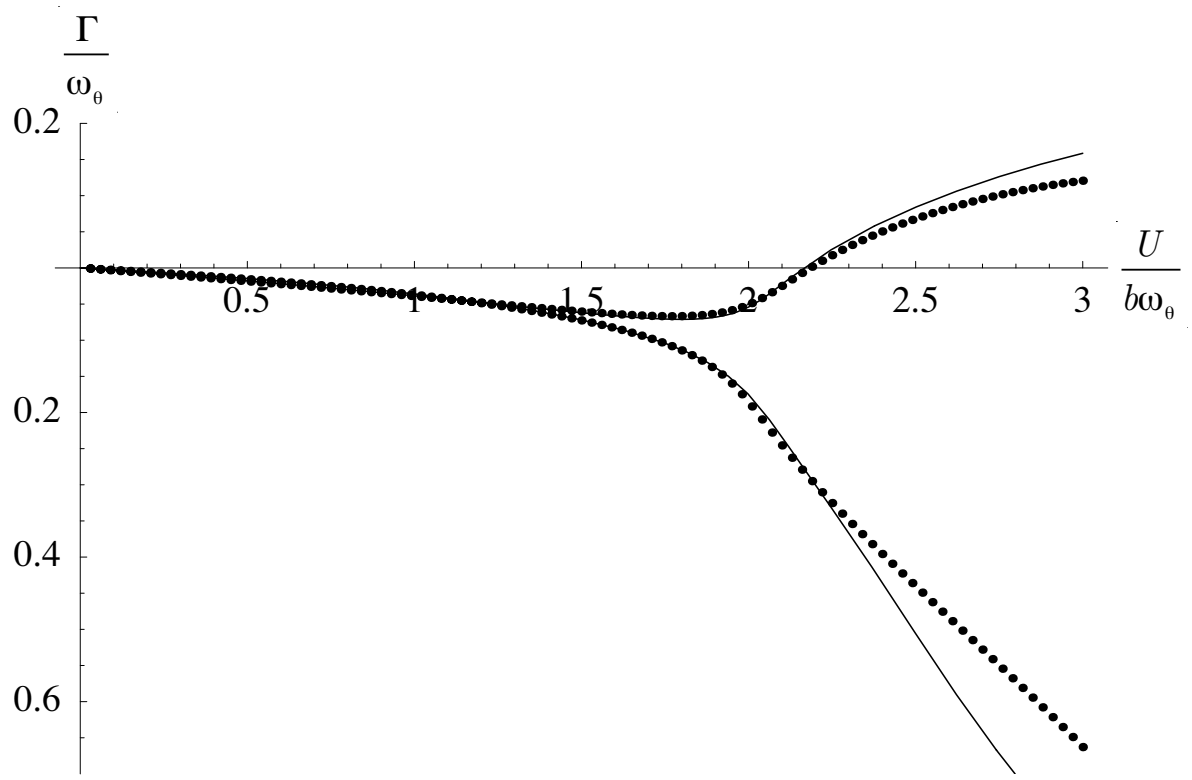

Figure 5.54: Plot of estimated value of $\Gamma_{1,2}/\omega_\theta$ versus $U/(b\omega_\theta)$ using the p-k method with Theodorsen aerodynamics (symbols) and the p method with the aerodynamics of Peters et al. (lines) for $a = -1/5$, $e = -1/10$, $\mu = 20$, $r^2 = 6/25$, and $\sigma = 2/5$

BIBLIOGRAPHY

1. Abramson, H. N., *An Introduction to the Dynamics of Airplanes*, Ronald Press Co., 1958 (reprinted by Dover).

2. Anon., "Manual on Aeroelasticity," six volumes by NATO Advisory Group for Aeronautical Research and Development, 1956 – 1970.

3. Bisplinghoff, R. L. and H. Ashley, *Principles of Aeroelasticity*, John Wiley and Sons, Inc., 1962 (reprinted by Dover).

4. Bisplinghoff, R. L., H. Ashley and R. L. Halfman, *Aeroelasticity*, Addison-Wesley Publishing Co., Inc., 1955.

5. Bolotin, V. V., *Nonconservative Problems of the Theory of Elastic Stability*, Pergamon Press, New York, 1963.

6. Bolotin, V. V., *Dynamic Stability of Elastic Systems*, Holden-Day, Inc., San Francisco, 1964.

7. Collar, A. R., "The First Fifty Years of Aeroelasticity," *Aerospace*, Vol. 5 (Paper No. 545), February 1978, pp. 12 – 20.

8. Diederich, F. W. and B. Budiansky, "Divergence of Swept Wings," NACA TN 1680, 1948.

9. Dowell, E. H., *Aeroelasticity of Plates and Shells*, Noordhoff International Publishing, 1975.

10. Dowell, E. H., E. F. Crawley, H. C. Curtiss, Jr., D. A. Peters, R. H. Scanlan and F. Sisto, *A Modern Course in Aeroelasticity*, 3rd ed., Kluwer Academic Publishers, 1995.

11. Freberg, C. R. and E. N. Kemler, *Aircraft Vibration and Flutter*, John Wiley and Sons, Inc., 1944.

12. Fung, Y. C., *An Introduction to the Theory of Aeroelasticity*, John Wiley and Sons, Inc., 1955 (reprinted by Dover).

13. Garrick, I. E. and W. H. Reed III, "Historical Development of Aircraft Flutter," *J. Aircraft*, Vol. 18, No. 11, Nov. 1981, pp. 897 – 912.

14. Hassig, H. J., "An Approximate True Damping Solution of the Flutter Equation by Determinant Iteration," *Journal of Aircraft*, Vol. 8, No. 11, Nov. 1971, pp. 885 – 889.

15. Irwin, C. A. K. and P. R. Guyett, "The Subcritical Response and Flutter of a Swept Wing Model," Tech. Rept. 65186, Aug. 1965, Royal Aircraft Establishment, Farnborough, UK.

16. Love, A. E. H., *Mathematical Theory of Elasticity*, 4th edition, Dover Publications, New York, 1944, Chapters 18 and 19.

17. Peters, D. A., S. Karunamoorthy and W.-M. Cao, "Finite State Induced Flow Models; Part I: Two-Dimensional Thin Airfoil," *Journal of Aircraft*, Vol. 32, No. 2, Mar.-Apr. 1995, pp. 313 – 322.

18. Scanlan, R. H. and R. Rosenbaum, "Outline of an Acceptable Method of Vibration and Flutter Analysis for a Conventional Airplane," *CAA Aviation Safety Release 302*, Oct. 1948.

19. Scanlan, R. H. and R. Rosenbaum, *Introduction to the Study of Aircraft Vibration and Flutter*, The MacMillan Co., 1951 (reprinted by Dover).

20. Theodorsen, T., *General Theory of Aerodynamic Instability and the Mechanism of Flutter*, NACA TR 496, 1934.

21. Weisshaar, T. A. "Divergence of Forward Swept Composite Wings," *Journal of Aircraft*, Vol. 17, No. 6, June 1980, pp. 442 – 448.

APPENDIX A: LAGRANGE'S EQUATION

A.1 Introduction

When we wish to use Newton's Laws to write the equations of motion of a particle or a system of particles we must be careful to include all the forces of the system. The Lagrangean form of the equations of motion that we shall proceed to derive has the advantage that we can ignore all forces that do no work (e.g., forces at frictionless pins, forces at a point of rolling contact, forces at frictionless guides, and forces in inextensible connections). In the case of conservative systems (systems for which the total energy remains constant) the Lagrangean method gives us an automatic procedure for obtaining the equations of motion provided only that we can write the kinetic and potential energies of the system.

A.2 Degrees of Freedom

Before proceeding to develop the Lagrange equations we must characterize our dynamical systems on some systematic way. The most important property of this sort for our present purpose is the number of independent coordinates that we must know to completely specify the position or configuration of our system. We say that a system has n degrees of freedom if exactly n coordinates serve to completely define its configuration.

Example 1

A free particle in space has three degrees of freedom since we must know three coordinates, x, y, z, for example, to locate it.

Example 2

A wheel that rolls without slipping on a straight track has one degree of freedom since either the distance from some base point or the total angle of rotation will enable us to locate it completely.

A.3 Generalized Coordinates

We usually think of coordinates as lengths or angles. However, any set of parameters that enable us to uniquely specify the configuration of the system can serve as coordinates. When we generalize the meaning of the term in this manner, we call these new quantities generalized coordinates.

Example 3

Consider a bar rotating in a plane about a point O. The angle of rotation with respect to some base line suggests itself as an obvious coordinate for specifying the position of the bar. However, the area swept over by the bar would do equally well and could therefore be used as a generalized coordinate.

If a system has n degrees of freedom, then n generalized coordinates are necessary and sufficient to determine its configuration.

A.4 Lagrange's Equations

In deriving these equations we shall consider systems having two degrees of freedom and hence are completely defined by two generalized coordinates q_1 and q_2. However, the results are easily extended to systems having any number of degrees of freedom.

Suppose our system is made up of n particles. For each particle we can write by Newton's Second Law

$$\begin{aligned} M_i\ddot{x}_i &= X_i \\ M_i\ddot{y}_i &= Y_i \\ M_i\ddot{z}_i &= Z_i \end{aligned} \tag{A.1}$$

where x_i, y_i, z_i are the rectangular Cartesian coordinates of the i^{th} particle, M_i is its mass, and X_i, Y_i, Z_i are the resultants of all forces acting on it in the x, y, and z directions, respectively.

If we multiply both sides of Eqs. (A.1) by δx_i, δy_i, and δz_i, respectively, and add the equations we have

$$M_i\left(\ddot{x}_i\delta x_i + \ddot{y}_i\delta y_i + \ddot{z}_i\delta z_i\right) = X_i\delta x_i + Y_i\delta y_i + Z_i\delta z_i \tag{A.2}$$

The right-hand side of this equation represents the work done by all the forces acting on the i^{th} particle during the virtual displacements δx_i, δy_i, and δz_i. Hence forces that do no work do not contribute to the right-hand side of Eq. (A.2) and may be omitted from the equation. To obtain the corresponding equation for the whole system, we sum both sides of Eq. (A.2) for all particles. Thus

$$\sum_{i=1}^{n} M_i\left(\ddot{x}_i\delta x_i + \ddot{y}_i\delta y_i + \ddot{z}_i\delta z_i\right) = \sum_{i=1}^{n}\left(X_i\delta x_i + Y_i\delta y_i + Z_i\delta z_i\right) \tag{A.3}$$

Now because our system is completely located in space if we know the two generalized coordinates q_1 and q_2, we must be able to write x_i, y_i, and z_i as well as their increments δx_i, δy_i, and δz_i as functions of q_1 and q_2. Hence,

$$\begin{aligned} x_i =& x_i(q_1, q_2) \\ y_i =& y_i(q_1, q_2) \\ z_i =& z_i(q_1, q_2) \end{aligned} \tag{A.4}$$

Differentiating Eq. (A.4) with respect to time gives

$$\begin{aligned} \dot{x}_i =& \frac{\partial x_i}{\partial q_1}\dot{q}_1 + \frac{\partial x_i}{\partial q_2}\dot{q}_2 \\ \dot{y}_i =& \frac{\partial y_i}{\partial q_1}\dot{q}_1 + \frac{\partial y_i}{\partial q_2}\dot{q}_2 \\ \dot{z}_i =& \frac{\partial z_i}{\partial q_1}\dot{q}_1 + \frac{\partial z_i}{\partial q_2}\dot{q}_2 \end{aligned} \tag{A.5}$$

Similarly,

$$\begin{aligned} \delta x_i =& \frac{\partial x_i}{\partial q_1}\delta q_1 + \frac{\partial x_i}{\partial q_2}\delta q_2 \\ \delta y_i =& \frac{\partial y_i}{\partial q_1}\delta q_1 + \frac{\partial y_i}{\partial q_2}\delta q_2 \\ \delta z_i =& \frac{\partial z_i}{\partial q_1}\delta q_1 + \frac{\partial z_i}{\partial q_2}\delta q_2 \end{aligned} \tag{A.6}$$

If we substitute these into Eq. (A.3) and rearrange the terms we obtain

$$\begin{aligned} &\sum_{i=1}^{n}\left[M_i\left(\ddot{x}_i\frac{\partial x_i}{\partial q_1} + \ddot{y}_i\frac{\partial y_i}{\partial q_1} + \ddot{z}_i\frac{\partial z_i}{\partial q_1}\right)\delta q_1\right. \\ &\quad \left. + M_i\left(\ddot{x}_i\frac{\partial x_i}{\partial q_2} + \ddot{y}_i\frac{\partial y_i}{\partial q_2} + \ddot{z}_i\frac{\partial z_i}{\partial q_2}\right)\delta q_2\right] \\ &= \sum_{i=1}^{n}\left[\left(X_i\frac{\partial x_i}{\partial q_1} + Y_i\frac{\partial y_i}{\partial q_1} + Z_i\frac{\partial z_i}{\partial q_1}\right)\delta q_1\right. \\ &\quad \left. + \left(X_i\frac{\partial x_i}{\partial q_2} + Y_i\frac{\partial y_i}{\partial q_2} + Z_i\frac{\partial z_i}{\partial q_2}\right)\delta q_2\right] \end{aligned} \tag{A.7}$$

From Eq. (A.5) we conclude that since x_i, y_i, and z_i are functions of q_1 and q_2 but not of $\dot{q}_1$ and $\dot{q}_2$

$$\begin{aligned} \frac{\partial \dot{x}_i}{\partial \dot{q}_1} &= \frac{\partial x_i}{\partial q_1} \qquad \frac{\partial \dot{x}_i}{\partial \dot{q}_2} = \frac{\partial x_i}{\partial q_2} \\ \frac{\partial \dot{y}_i}{\partial \dot{q}_1} &= \frac{\partial y_i}{\partial q_1} \qquad \frac{\partial \dot{y}_i}{\partial \dot{q}_2} = \frac{\partial y_i}{\partial q_2} \\ \frac{\partial \dot{z}_i}{\partial \dot{q}_1} &= \frac{\partial z_i}{\partial q_1} \qquad \frac{\partial \dot{z}_i}{\partial \dot{q}_2} = \frac{\partial z_i}{\partial q_2} \end{aligned} \tag{A.8}$$

We substitute these relations into the left-hand side of Eq. (A.7) to obtain

$$\begin{aligned}\sum_{i=1}^{n}\Bigg[&M_i\left(\ddot{x}_i\frac{\partial\dot{x}_i}{\partial\dot{q}_1}+\ddot{y}_i\frac{\partial\dot{y}_i}{\partial\dot{q}_1}+\ddot{z}_i\frac{\partial\dot{z}_i}{\partial\dot{q}_1}\right)\delta q_1\\&+M_i\left(\ddot{x}_i\frac{\partial\dot{x}_i}{\partial\dot{q}_2}+\ddot{y}_i\frac{\partial\dot{y}_i}{\partial\dot{q}_2}+\ddot{z}_i\frac{\partial\dot{z}_i}{\partial\dot{q}_2}\right)\delta q_2\Bigg]\\=\sum_{i=1}^{n}\Bigg[&\left(X_i\frac{\partial x_i}{\partial q_1}+Y_i\frac{\partial y_i}{\partial\dot{q}_1}+Z_i\frac{\partial z_i}{\partial q_1}\right)\delta q_1\\&+\left(X_i\frac{\partial x_i}{\partial q_2}+Y_i\frac{\partial y_i}{\partial q_2}+Z_i\frac{\partial z_i}{\partial q_2}\right)\delta q_2\Bigg]\end{aligned}\tag{A.9}$$

Now let us shift our attack on the problem and consider the kinetic energy of the system. This is

$$K=\frac{1}{2}\sum_{i=1}^{n}M_i\left(\dot{x}_i^2+\dot{y}_i^2+\dot{z}_i^2\right)\tag{A.10}$$

Now calculate $\frac{\partial K}{\partial\dot{q}_1}$ and $\frac{\partial K}{\partial\dot{q}_2}$ to obtain

$$\frac{\partial K}{\partial\dot{q}_1}=\sum_{i=1}^{n}M_i\left(\dot{x}_i\frac{\partial\dot{x}_i}{\partial\dot{q}_1}+\dot{y}_i\frac{\partial\dot{y}_i}{\partial\dot{q}_1}+\dot{z}_i\frac{\partial\dot{z}_i}{\partial\dot{q}_1}\right)\tag{A.11}$$

$$\frac{\partial K}{\partial q_1}=\sum_{i=1}^{n}M_i\left(\dot{x}_i\frac{\partial\dot{x}_i}{\partial q_1}+\dot{y}_i\frac{\partial\dot{y}_i}{\partial q_1}+\dot{z}_i\frac{\partial\dot{z}_i}{\partial q_1}\right)\tag{A.12}$$

We next calculate the time derivative of $\frac{\partial x_i}{\partial q_1}$, for which the chain rule gives

$$\begin{aligned}\frac{d}{dt}\left(\frac{\partial x_i}{\partial q_1}\right)=&\frac{\partial^2 x_i}{\partial q_1^2}\dot{q}_1+\frac{\partial^2 x_i}{\partial q_1\partial q_2}\dot{q}_2\\=&\frac{\partial}{\partial q_1}\left(\frac{\partial x_i}{\partial q_1}\dot{q}_1+\frac{\partial x_i}{\partial q_2}\dot{q}_2\right)\\=&\frac{\partial}{\partial q_1}\left(\dot{x}_i\right)=\frac{\partial\dot{x}_i}{\partial q_1}\end{aligned}\tag{A.13}$$

Since from Eq. (A.8) we have

$$\frac{\partial\dot{x}_i}{\partial\dot{q}_1}=\frac{\partial x_i}{\partial q_1}\tag{A.14}$$

we conclude from Eq. (A.13) that

$$\frac{d}{dt}\left(\frac{\partial x_i}{\partial q_1}\right)=\frac{\partial\dot{x}_i}{\partial q_1}\tag{A.15}$$

The following relations can be proven in a similar manner:

$$\begin{aligned}\frac{d}{dt}\left(\frac{\partial y_i}{\partial q_1}\right) &= \frac{\partial \dot{y}_i}{\partial q_1} \\ \frac{d}{dt}\left(\frac{\partial z_i}{\partial q_1}\right) &= \frac{\partial \dot{z}_i}{\partial q_1}\end{aligned} \tag{A.16}$$

Now let us use Eqs. (A.11), (A.12), (A.15), and (A.16) to calculate the function

$$\frac{d}{dt}\left(\frac{\partial K}{\partial \dot{q}_1}\right) - \frac{\partial K}{\partial q_1} \tag{A.17}$$

for which the result is

$$\begin{aligned}\frac{d}{dt}\left(\frac{\partial K}{\partial \dot{q}_1}\right) - \frac{\partial K}{\partial q_1} =& \sum_{i=1}^{n} M_i \left(\ddot{x}_i \frac{\partial \dot{x}_i}{\partial \dot{q}_1} + \ddot{y}_i \frac{\partial \dot{y}_i}{\partial \dot{q}_1} + \ddot{z}_i \frac{\partial \dot{z}_i}{\partial \dot{q}_1}\right) \\ &+ \sum_{i=1}^{n} M_i \left[\dot{x}_i \frac{d}{dt}\left(\frac{\partial \dot{x}_i}{\partial \dot{q}_1}\right) + \dot{y}_i \frac{d}{dt}\left(\frac{\partial \dot{y}_i}{\partial \dot{q}_1}\right) + \dot{z}_i \frac{d}{dt}\left(\frac{\partial \dot{z}_i}{\partial \dot{q}_1}\right)\right] \\ &- \sum_{i=1}^{n} M_i \left(\dot{x}_i \frac{\partial \dot{x}_i}{\partial q_1} + \dot{y}_i \frac{\partial \dot{y}_i}{\partial q_1} + \dot{z}_i \frac{\partial \dot{z}_i}{\partial q_1}\right)\end{aligned} \tag{A.18}$$

From Eqs. (A.15) and (A.16) the second and third terms on the right-hand side of Eq. (A.18) are equal and thus cancel leaving

$$\frac{d}{dt}\left(\frac{\partial K}{\partial \dot{q}_1}\right) - \frac{\partial K}{\partial q_1} = \sum_{i=1}^{n} M_i \left(\ddot{x}_i \frac{\partial \dot{x}_i}{\partial \dot{q}_1} + \ddot{y}_i \frac{\partial \dot{y}_i}{\partial \dot{q}_1} + \ddot{z}_i \frac{\partial \dot{z}_i}{\partial \dot{q}_1}\right) \tag{A.19}$$

A similar relation holds for partial derivatives of K with respect to q_2 and $\dot{q}_2$. Hence Eq. (A.9) can be written

$$\begin{aligned}&\left[\frac{d}{dt}\left(\frac{\partial K}{\partial \dot{q}_1}\right) - \frac{\partial K}{\partial q_1}\right]\delta q_1 + \left[\frac{d}{dt}\left(\frac{\partial K}{\partial \dot{q}_2}\right) - \frac{\partial K}{\partial q_2}\right]\delta q_2 \\ &= \sum_{i=1}^{n}\left(X_i \frac{\partial x_i}{\partial q_1} + Y_i \frac{\partial y_i}{\partial q_1} + Z_i \frac{\partial z_i}{\partial q_1}\right)\delta q_1 \\ &+ \sum_{i=1}^{n}\left(X_i \frac{\partial x_i}{\partial q_2} + Y_i \frac{\partial y_i}{\partial q_2} + Z_i \frac{\partial z_i}{\partial q_2}\right)\delta q_2\end{aligned} \tag{A.20}$$

Since q_1 and q_2 are independent coordinates they can be varied arbitrarily. Hence, we can conclude that

$$\begin{aligned}\frac{d}{dt}\left(\frac{\partial K}{\partial \dot{q}_1}\right) - \frac{\partial K}{\partial q_1} &= \sum_{i=1}^{n}\left(X_i \frac{\partial x_i}{\partial q_1} + Y_i \frac{\partial y_i}{\partial q_1} + Z_i \frac{\partial z_i}{\partial q_1}\right) \\ \frac{d}{dt}\left(\frac{\partial K}{\partial \dot{q}_2}\right) - \frac{\partial K}{\partial q_2} &= \sum_{i=1}^{n}\left(X_i \frac{\partial x_i}{\partial q_2} + Y_i \frac{\partial y_i}{\partial q_2} + Z_i \frac{\partial z_i}{\partial q_2}\right)\end{aligned} \tag{A.21}$$

The right-hand side of Eq. (A.20) is the work done by all the forces on the system when the coordinates of the i^{th} particle undergo the small displacement δx_i, δy_i, and δz_i due to changes δq_1 and δq_2 in the generalized coordinates q_1 and q_2. The coefficients of δq_1 and δq_2 are known as the generalized forces Q_1 and Q_2, since they are the quantities by which the variations of the generalized coordinates must be multiplied to calculate the virtual work done by all the forces acting on the system. Hence,

$$\begin{aligned} Q_1 &= \sum_{i=1}^{n} \left(X_i \frac{\partial x_i}{\partial q_1} + Y_i \frac{\partial y_i}{\partial q_1} + Z_i \frac{\partial z_i}{\partial q_1} \right) \\ Q_2 &= \sum_{i=1}^{n} \left(X_i \frac{\partial x_i}{\partial q_2} + Y_i \frac{\partial y_i}{\partial q_2} + Z_i \frac{\partial z_i}{\partial q_2} \right) \end{aligned} \tag{A.22}$$

and Eqs. (A.21) can be written

$$\begin{aligned} \frac{d}{dt}\left(\frac{\partial K}{\partial \dot{q}_1}\right) - \frac{\partial K}{\partial q_1} &= Q_1 \\ \frac{d}{dt}\left(\frac{\partial K}{\partial \dot{q}_2}\right) - \frac{\partial K}{\partial q_2} &= Q_2 \end{aligned} \tag{A.23}$$

This is one form of Lagrange's equations of motion. They apply to any system that is completely described by two and only two generalized coordinates, whether or not the system is conservative. It can be shown by slightly more extended calculation that they apply to systems of any finite number of degrees of freedom.

A.5 Lagrange's Equations for Conservative Systems

If a system is conservative, the work done by the forces can be calculated from the potential energy P. We define the change in potential energy during a small displacement as the negative of the work done by the forces of the system during the displacement. Because $Q_1\delta q_1 + Q_2\delta q_2$ is the work done by the forces, we have

$$\delta P = -Q_1\delta q_1 - Q_2\delta q_2 \tag{A.24}$$

We have emphasized that q_1 and q_2 are independent and, hence, can be varied arbitrarily. If $\delta q_2 = 0$, we have $\delta P = -Q_1\delta q_1$ so that

$$Q_1 = -\frac{\partial P}{\partial q_1} \tag{A.25}$$

Similarly, it can be seen that

$$Q_2 = -\frac{\partial P}{\partial q_2} \tag{A.26}$$

Replacing Q_1 and Q_2 in Eqs. (A.23) by these expressions we have

$$\begin{aligned} \frac{d}{dt}\left(\frac{\partial K}{\partial \dot{q}_1}\right) - \frac{\partial K}{\partial q_1} + \frac{\partial P}{\partial q_1} = 0 \\ \frac{d}{dt}\left(\frac{\partial K}{\partial \dot{q}_2}\right) - \frac{\partial K}{\partial q_2} + \frac{\partial P}{\partial q_2} = 0 \end{aligned} \tag{A.27}$$

These are Lagrange's equations of motion for a conservative system. As before, they hold for systems of any finite number of degrees of freedom.

Example 4

Find the equations of motion of a particle of weight W moving in space under the force of gravity.

Solution: We need three coordinates to describe the position of the particle and can therefore take x, y, z as our generalized coordinates. Taking x and y in the horizontal place and z vertically upward with the origin at the earth's surface and taking the origin as the zero position for potential energy, one obtains

$$\begin{aligned} &K = \frac{W}{2g}\left(\dot{x}^2 + \dot{y}^2 + \dot{z}^2\right) \qquad P = Wz \\ &\frac{\partial K}{\partial \dot{x}} = \frac{W}{g}\dot{x} \qquad \frac{\partial K}{\partial \dot{y}} = \frac{W}{g}\dot{y} \qquad \frac{\partial K}{\partial \dot{z}} = \frac{W}{g}\dot{z} \qquad \frac{\partial K}{\partial x} = \frac{\partial K}{\partial y} = \frac{\partial K}{\partial z} = 0 \\ &\frac{d}{dt}\left(\frac{\partial K}{\partial \dot{x}}\right) = \frac{W}{g}\ddot{x} \qquad \frac{d}{dt}\left(\frac{\partial K}{\partial \dot{y}}\right) = \frac{W}{g}\ddot{y} \qquad \frac{d}{dt}\left(\frac{\partial K}{\partial \dot{z}}\right) = \frac{W}{g}\ddot{z} \\ &\frac{\partial P}{\partial x} = \frac{\partial P}{\partial y} = 0 \qquad \frac{\partial P}{\partial z} = W \end{aligned} \tag{A.28}$$

Hence, Lagrange's equation, Eq. (A.27) gives

$$\frac{W}{g}\ddot{x} = 0 \qquad \frac{W}{g}\ddot{y} = 0 \qquad \frac{W}{g}\ddot{z} + W = 0 \tag{A.29}$$

Of course, these equations are more easily obtainable by the direct application of Newton's Second Law. This example merely illustrates the application of Lagrange's equations for a familiar problem.

Example 5

Find the equation of motion of the sprung weight W sliding on a smooth horizontal plane (see Fig. A.1).

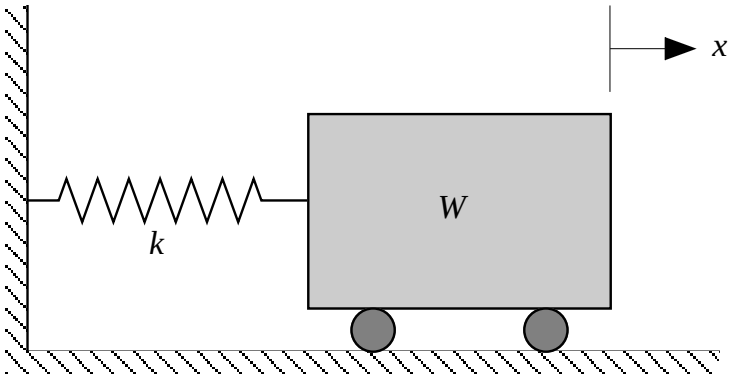

Figure A.1: Schematic for the mechanical system of Example 4

Solution: We may take x as the generalized coordinate and measure it from the equilibrium position. Then

$$\begin{aligned} K &= \frac{W}{2g}\dot{x}^2 & P &= \frac{k}{2}x^2 \\ \frac{\partial K}{\partial \dot{x}} &= \frac{W}{g}\dot{x} & \frac{d}{dt}\left(\frac{\partial K}{\partial \dot{x}}\right) &= \frac{W}{g}\ddot{x} \\ \frac{\partial K}{\partial x} &= 0 & \frac{\partial P}{\partial x} &= kx \end{aligned} \tag{A.30}$$

Lagrange's equation, Eq. (A.27) gives

$$\frac{W}{g}\ddot{x} + kx = 0 \tag{A.31}$$

as the equation of motion.

Example 6

Obtain the equations of motion for the system shown in Fig. A.2. The bar is weightless.

Solution: The coordinates x_1 and x_2 can be taken as generalized coordinates. Take as the zero datum the configuration for which the bar is horizontal and the spring is unstretched. Then

$$\begin{aligned} K &= \frac{W}{2g}\dot{x}_1^2 + \frac{W}{2g}\dot{x}_2^2 & P &= Wx_1 - Wx_2 + \frac{1}{2}k\left(x_2 - x_1\right)^2 \\ \frac{\partial K}{\partial \dot{x}_1} &= \frac{W}{g}\dot{x}_1 & \frac{\partial K}{\partial \dot{x}_2} &= \frac{W}{g}\dot{x}_2 & \frac{\partial K}{\partial x_1} &= \frac{\partial K}{\partial x_2} = 0 \\ \frac{d}{dt}\left(\frac{\partial K}{\partial \dot{x}_1}\right) &= \frac{W}{g}\ddot{x}_1 & \frac{d}{dt}\left(\frac{\partial K}{\partial \dot{x}_2}\right) &= \frac{W}{g}\ddot{x}_2 \\ \frac{\partial P}{\partial x_1} &= W - k\left(x_2 - x_1\right) & \frac{\partial P}{\partial x_2} &= -W + k\left(x_2 - x_1\right) \end{aligned} \tag{A.32}$$

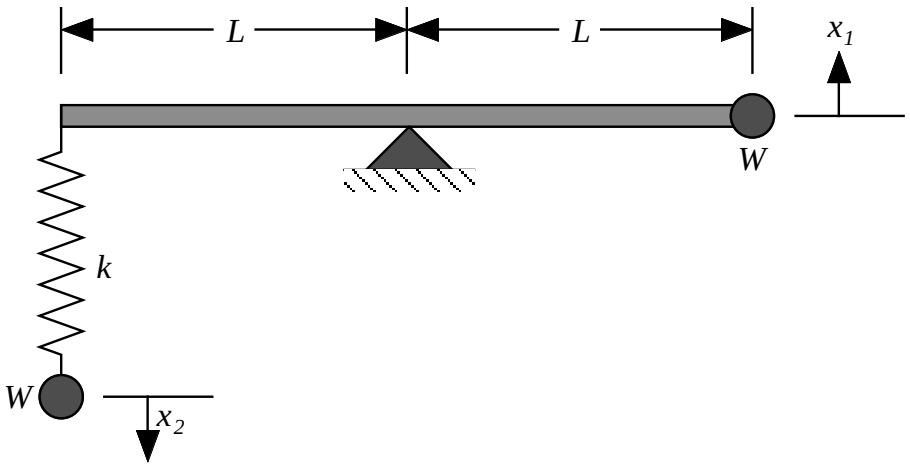

Figure A.2: Schematic for mechanical system of Example 6

The Lagrange equations are

$$\begin{aligned} \frac{W}{g}\ddot{x}_1 + W - k(x_2 - x_1) &= 0 \\ \frac{W}{g}\ddot{x}_2 - W + k(x_2 - x_1) &= 0 \end{aligned} \tag{A.33}$$

This is an example of a two-degree-of-freedom, conservative system.

A.6 Lagrange's Equations for Nonconservative Systems

If the system is nonconservative, then, in general, there will be some forces (conservative) that are derivable from a potential function, $P(q_1, q_2, \ldots)$ and some forces (nonconservative) that are not. Those forces for which a potential function does not exist must be introduced by first determining their virtual work. The coefficient of the virtual displacement δq_i in the virtual work expression is the generalized force, here denoted by Q_i $(i = 1, 2, \ldots)$. In this instance it is convenient to introduce what is called the Lagrangean as

$$L = K - P \tag{A.34}$$

and write the general form of Lagrange's equations as

$$\frac{d}{dt}\left(\frac{\partial L}{\partial \dot{q}_i}\right) - \frac{\partial L}{\partial q_i} = Q_i \qquad (i = 1, 2, \ldots, n) \tag{A.35}$$

Example 7

Rework Example 5 with a dashpot of constant c connected in parallel with the spring.

Solution: The system with a dashpot is nonconservative. Hence, we use Lagrange's equations in form of Eq. (A.35). The kinetic and potential energies are the same as in Example 5. To calculate the Q for the dashpot force, use the definition that Q is the coefficient by which the generalized coordinates must be multiplied to obtain the work done. In any small displacement δx, the work done by the dashpot force $-c\dot{x}$ is $-c\dot{x}\,\delta x$. Hence, $-c\dot{x}$ itself is the generalized force associated with the dashpot. The Lagrangean is

$$L = \frac{W\dot{x}^2}{2g} - \frac{kx^2}{2} \tag{A.36}$$

and

$$Q = -c\dot{x} \tag{A.37}$$

Lagrange's equation then becomes

$$\frac{W}{g}\ddot{x} + kx = -c\dot{x} \tag{A.38}$$